STRATEGIES FOR RAPID SEISMIC HAZARD MITIGATION IN SUSTAINABLE INFRASTRUCTURE SYSTEMS

A Dissertation
Presented to
The Academic Faculty

by

Masahiro Kurata

In Partial Fulfillment
of the Requirements for the Degree
Doctor of Philosophy in the
School of Civil and Environmental Engineering

Georgia Institute of Technology
December 2009

STRATEGIES FOR RAPID SEISMIC HAZARD MITIGATION IN SUSTAINABLE INFRASTRUCTURE SYSTEMS

Approved by:

Dr. Reginald DesRoches, Advisor
School of Civil and Environmental Engineering
Georgia Institute of Technology

Dr. Donald W. White
School of Civil and Environmental Engineering
Georgia Institute of Technology

Dr. Roberto T. Leon
School of Civil and Environmental Engineering
Georgia Institute of Technology

Dr. James I. Craig
School of Aerospace Engineering
Georgia Institute of Technology

Dr. Barry Goodno
School of Civil and Environmental Engineering
Georgia Institute of Technology

Date Approved: [09/14/2009]

I would like to dedicate this work to my family.

ACKNOWLEDGEMENTS

This dissertation has been made with the help of many individuals and I am grateful for their contribution and support. The road left behind this journey has been winded, divided and crossed but has been full of positive experiences upon which I will often reflect with great fondness.

My deepest gratitude is to my co-advisors, Dr. Reginald DesRoches and Dr. Roberto T. Leon, who have shown an undeserved degree of patience. I have been amazingly fortunate to have advisors who gave me the freedom to explore on my own and at the same time the guidance to recover when my steps faltered. Dr. DesRoches taught me how to question thoughts and express ideas. His patience and support helped me overcome many difficult situations and finish this dissertation. Dr. Leon has always been there to listen and give advice. I am deeply grateful to him for the long discussions that helped me sort out the technical details of my work.

I would also like to thank my thesis committee, Dr. Barry Goodno, Dr. Don W. White and Dr. James I. Craig. They have provided encouragement, praise and guidance throughout this process.

Special thanks go to Dr. Laurence Jacobs who cheered and encouraged me throughout this journey. I was very relieved whenever he stopped by our office and created joyful time. I also greatly appreciate his willingness to be my mentor as I taught my first college level class and to give a recommendation for my next position.

I am also grateful to Dr. Masayoshi Nakashima and his research group at Kyoto University for their various forms of support during my experimental study in Japan. I

would like to express my appreciation to Dr. Nakashima, Dr. Hitaka, Dr. Suita, Mr. Shiga, Andres, Mr. Murata, Mr. So, Ms. Furukawa and Ms. Ito.

I am also thankful to the staff at the Georgia Tech, Mike, Andy and Jeremy, who fabricated specimens and maintained the structural lab during my experimental work.

No graduate experience is complete without developing friendships with fellow graduate students. Much of the education I received, both technical and nontechnical, came through long and detailed discussions with office mates and others. I would like to give thanks to Matthew, Tiziano, Curtis, Walter, Jamie, Monique, Benoit, Joan, Ben, Laura, Jason, Takao, Victor, Effe, Cagri, Jazalyn, Niki, Robert, Amal, Chen, Daisuke, and the many other students with whom I have been associated.

I would be remiss if I didn't acknowledge the contribution and support I have received from Aya. Over the years she has expressed confidence in my abilities and supported me unconditionally. My love and appreciation is extended to her.

Most importantly, none of this would have been possible without the love and patience of my family. I would like to express my deepest and most heartfelt gratitude to all of my family members; Shuichi, Kimiko, Kayoko, Kiyomi, Tatsuko, Kuni, Mayuko, Makoto, and Kazune. I dedicate this dissertation to all of them who have been a constant source of love, concern, support and strength all these years.

TABLE OF CONTENTS

LIST OF TABLES

Page

LIST OF FIGURES

Page

SUMMARY

The goal of this study is to design and evaluate economic and rapid seismic retrofit strategies for relatively small rehabilitation projects for steel structures consistent with the tenets of sustainable design. The need to retrofit existing structures in earthquake prone regions may arise directly from the problem of aging and deteriorating conditions, recognition of the vulnerability of existing infrastructure, from updates in seismic code requirements, or changes in building performance objectives. Traditional approaches to seismic hazard mitigation have focused reducing the failure probabilities, consequences from failures, and time to recovery. Such paradigms had been established with little regard to the impact of their rehabilitation measures on the environment and disruptions to occupants. The rapid rehabilitation strategies proposed here have sustainability benefits in terms of providing a more resilient building stock for our communities as well as minimizing environmental and economical impacts and social consequences during the rehabilitation project.

To achieve these goals, a unique approach to design supplemental systems using tension-only elements is proposed. In this design approach undesirable global and local buckling are eliminated. Two rapid rehabilitation strategies are presented. The first is a bracing system consisting of cables and a central energy dissipating device (CORE Damper). The second is a shear wall system with the combined use of thin steel plate and tension-only bracing. Analytical studies using both advanced and simplified models and proof-of-concept testing were carried out for the two devices. The results demonstrated stable, highly efficient performance of the devices under seismic load. Preliminary

applications of the CORE damper to the retrofitting of a braced steel frame showed the ability of the system to minimize soft story failures.

Both techniques can be implemented within a sustainability framework, as these interventions reduce the seismic vulnerability of infrastructure, are low cost, utilize materials and fabrication processes widely available throughout the world, can be handled by unskilled labor and carried out with minimal disruptions to the environment. The approach taken in this study can provide a road map for future development of sustainability-based rehabilitation strategies.

CHAPTER 1

INTRODUCTION

1.1 Defining the Problem

During the past five decades, natural hazards have caused ever increasing loss of human lives, disruptions of economic activity, destruction of civil infrastructure, and environmental damage. The chart in Figure 1.1 presents the overall losses and insured losses adjusted to present US dollar values in 2009, where the trend curves illustrate the increase in losses from great natural catastrophes since 1950. In line with the United Nations definitions, natural catastrophes are classified as great if the affected region's ability to help itself is clearly overstretched and superregional or international assistance is required: when there are thousands of fatalities, when hundreds of thousands of people are left homeless, and/or when overall losses considering the economic circumstances of the country concerned and/or insured losses are of exceptional proportions [Munich Re, 2009]. Four catastrophes satisfied this definition in 2008 [Table 1.1]: the winter damage in China, the earthquake in Sichuan (China), Cyclone Nargis in Myanmar and Hurricane Ike in the Caribbean and the United States. The escalation of severe disasters around the world is tied to population increase, demographic shifts to urban regions, climate change and aging infrastructure systems, and threatens the sustainable development of modern societies through large direct and indirect impacts [ISDR, 2002]. Specific examples of this include:

- Least developed countries are more vulnerable to natural hazards. They are subject to the highest rates of population growth, which is projected to double in less than 30 years [UN, 2009]. Disaster risk increases if the exposure of people and assets to natural hazards increases faster than countries can strengthen their risk-reducing capacities by putting policy, institutions, legislation, planning and regulatory frameworks in place.
- Countries with large populations exposed to severe natural hazards account for a very large proportion of global disaster risk. For example, 75% of global flood mortality risk is concentrated in only three countries: Bangladesh, China and India [UN, 2009].
- Urbanization is increasing at an unprecedented scale. Rapid economic and urban development can lead to a growing concentration of people and economic assets in hazard prone cities. Half of the world population now lives in cities, and within two decades, nearly 60 per cent of the world's population will be urban dwellers [UN-Habitat, 2008]; many of these (e.g. Tokyo, San Francisco, Los Angeles, Miami, Houston, Tai Pei, Istanbul, Mexico City, Lisbon, Beijing, Hong Kong, Mumbai, Calcutta, San Paulo) are located in zones subjected to earthquakes and hurricanes.
- Climate change is expected to lead to the changes in sea water levels and climate patterns. Currently 10% of the world's total population (over 600 million people) and 13% of its urban population (over 360 million people) live on the 2% of the world's land area that is less than 10 meters above sea level, known as the Low Elevation Coastal Zone 11 [Satterthwaite, 2007]. There are clear risks associated

with increased flooding and storm surges, exacerbated by sea level rise, and risk for increased earthquake damage in these areas due to poor and liquefiable soils.

- The American Society of Civil Engineers report, America's infrastructure 2009, noted that the average grade for America's infrastructure is a D and estimated the 5-year investment needed to bring our infrastructure up to the appropriate standard is $2.2 trillion [ASCE, 2009].
- Indirect economic losses of business interruption and market share following the downtime after a disaster are another emerging issue. Gordon *et al.* computed the business interruption effects from the 1994 Northridge earthquake to be 22-32 percent of losses from total structural damage [Gordon, 1998]. Toyoda recently re-estimated the indirect economic loss of the Kobe earthquake from 1995 to 2007 as 14 trillion yen (152 billion US dollars), a figure substantially higher than the estimated total direct loss of 10 trillion yen (109 billion US dollars) [Toyoda, 2008].
- Almost fifteen years after the Kobe earthquake devastated the facilities of one of the country's primary ports, the equipment and harbor facilities have all been rebuilt and modernized, yet the market share of the Port of Kobe has dropped significantly from pre-earthquake revenues; the volume of container cargo handled had only reached 81.8% of the pre-earthquake levels in 2006 and Kobe had dropped from the 6th largest container port in the world to the 35th largest one [Kobe City, 2008].

These examples argue for a much more holistic approach to disaster mitigation. One component of this effort, at the core of the research discussed herein, is an emphasis

on sustainable seismic retrofits to large stocks of existing infrastructure. In this context, sustainability is defined as interventions that require relatively low economic investments, materials and fabrication processes widely available throughout the world, can be handled by unskilled labor and carried out with minimal disruptions to the environment.

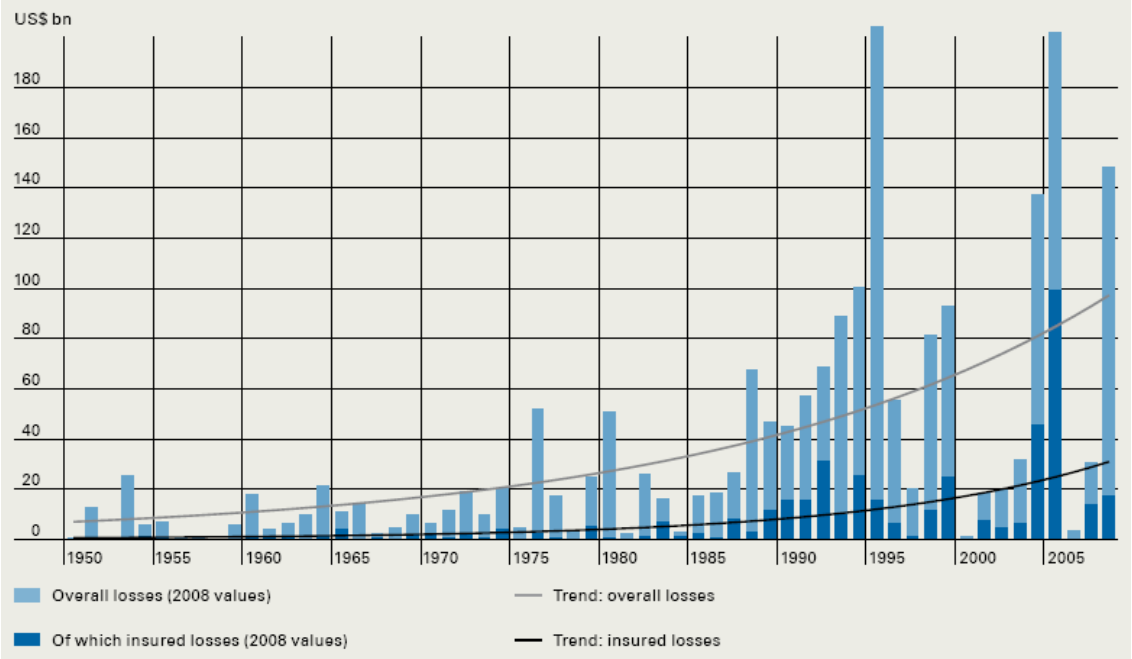

Figure 1.1: Great natural catastrophes 1950-2008, losses with trend [Munich Re, 2008]

Table 1.1: Great natural catastrophes 2008

Date	Region	Loss event	Fatalities	Overall losses (US$ m)
Jan. 10-Feb. 13	China	Winter damage	129	21,000
May 2-5	Myanmar	Cyclone Nargis	85,000	4,000
May 12	China	Earthquake	70,000	85,000
Sept. 7-14	Caribbean, USA	Hurricane Ike	168	38,000

1.2 Seismic Hazard Mitigation

Society in disaster-plagued areas is responsible for monitoring the condition of their civil infrastructure systems and, if needed, for rebuilding or repairing them for continuous usage. For vulnerable existing buildings, structural collapse poses the greatest threat to life in a severe earthquake event, as highlighted by the recent 2005 Pakistan, 2003 Iran and 2008 China earthquake; The NY Times reported that an official figure released by Chinese officials on the number of casualties among children caused by the 2008 Sichuan (Wenchuan) earthquake as 5,335 who had been either killed or remain missing, while another 546 were left disabled. Controversy continues over the alleged poor construction standards that led to school collapses where many children were trapped [NY Times, 2008]. "Schools, hospitals and other critical infrastructure need to be systematically upgraded and retrofitted in earthquake prone areas if we want to save live. There are still too many poorly designed and constructed buildings in earthquake-prone areas, and too many people dying because of it." said Salvano Briceño, Director of the UN secretariat of the International Strategy for Disaster Reduction, who was in Pakistan for the International Conference on School Safety (2008, Islamabad) right after the China earthquake [UN/ISDR, 2008]. Vulnerability to earthquakes is still a primary cause of death during disasters. The need to retrofit in earthquake prone regions may arise directly from the problem of aging infrastructure, recognition of the vulnerability of existing infrastructure, from updates in seismic code requirements, or changes in building performance objectives. Choosing a method of protection against structural collapse for a seismically inadequate building requires a number of critical decisions by building owners. The primary decision is whether to replace or upgrade the

existing structure. If replacement of the building is chosen, new construction is carried out according to the latest seismic codes. Otherwise, the structure should be retrofitted with the latest applicable standards, such as ASCE 41 [ASCE/SEI 2006]. ASCE 41, Seismic Rehabilitation of Existing Buildings, describes the latest generation of performance-based seismic rehabilitation methodologies. An adequate seismic design under such methodologies requires that a structure yields and experiences damage without collapse under the maximum credible event. The addition of seismic isolation, supplemental bracing, concrete or steel shear walls, and damping devices are among the techniques that have been successfully implemented into existing buildings. A large number of supplemental energy-dissipating systems and rehabilitation techniques have been proposed for steel structures since the late 1990's, motivated mainly by the severe damage observed in both the 1994 Northridge and 1995 Kobe earthquakes [Bertero *et al.*, 1994; AIJ Reconnaissance, 1995; FEMA Interim, 1997; Nakashima *et al.*, 1998].

1.3 Opportunities for Sustainability in Seismic Hazard Mitigation

Traditional approaches to seismic hazard mitigation have focused on the resilience of infrastructure systems; reduced failure probabilities, reduced consequences from failures, and reduced time to recovery [e.g., Bruneau, 2003, 2006]. Engineers in urban areas have established such paradigms with seemingly limitless natural resources, and with little regard to the impact of their rehabilitation measures on the environment, and local disruption. Davidson *et al.* noted that the next generation of engineers must be able to design with a narrowing and diminishing set of natural resources for a wider variety and greater number of end users [Davidson *et al.*, 2007]. For instance, a cost-benefit assessment based on such traditional approaches may suggest to building owners

a complete reconstruction of a vulnerable building as the best approach to reduce the vulnerability to seismic hazard. However, the use of a significant quantity of new materials for construction, with their associated energy and gas emission costs, and the impact on the heavy construction equipment on the environment and community may, in fact, not be the most sustainable solution. The main reason why the cost for rehabilitation can exceeds the cost for rebuilding is the increase in the non-construction costs such as architectural demolition and refinishing, engineering fees (for higher level analyses), occupants' relocation and permit, and material testing and legal fees [FEMA 1994]. For instance, the costs of repairing of pre-Northridge type steel connections, which are susceptible to brittle failure and fail qualification in current seismic guidelines, is estimated to exceed $20,000 per connection (the inspection alone might cost $1,500) [Mosallam, 1999]. Researchers have developed cost-effective alternative designs to reinforce such connections, e.g., reduced beam section, welding haunches, and bolting brackets. The main cost reduction anticipated are related to indirect costs such as tenant

Figure 1.2: Seismic retrofit of the Administration Building, San Francisco State University, installation of prefabricated column-joint assembly [Kouyoumdjian, 1999]

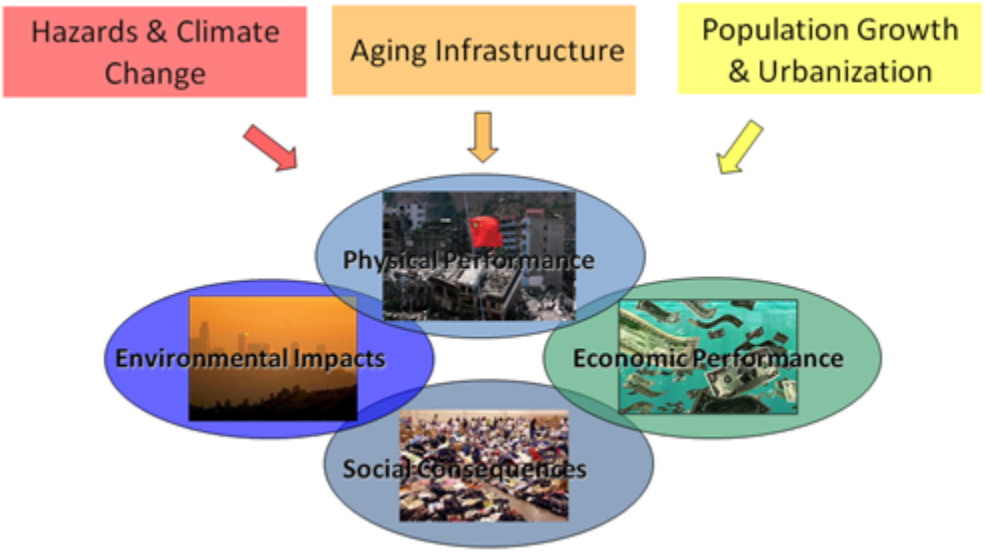

Figure 1.3: Sustainable infrastructure system [DesRoches, 2009]

disruption in occupied buildings and in dealing with safety issues: relocation of occupants or overnight work fees due to noise and fire safety, or fire usage permit [AISC, 1999]. Another rehabilitation scheme to reduce disruption is to utilize a structural steel moment-resisting frame placed on the exterior of a building, e.g. a case for the Administration Building at San Francisco State University [Figure 1.2]. By limiting story drifts to small amounts, the costly reinforcing of existing columns and joints was avoided. This approach permitted continued used of the building during construction and required no changes to the interior of the building [Newman, 2001]. Such a scheme becomes cost-effective when the extra land needed to allow for both the placing of scaffolding and use of heavy construction equipment is available. These examples indicate that the development of innovative seismic hazard mitigation technology involve due consideration of environmental, economic and social impacts could make rehabilitation more competitive to rebuilding. Moreover, the current trend for eco-friendly, green engineering is an opportunity for today's structural engineers to consider the links

between vulnerability to disasters and the development of new paradigms for retrofit based on system-based, holistic thinking [Figure 1.3]. Some of the key ideas to be addressed for the sustainable rehabilitation of infrastructure systems include due consideration of environmental impacts, life-cycle costs, resource depletions, and social consequences.

The development of rehabilitation strategies which are rapid and aimed at relatively small rehabilitation projects is proposed in this thesis. Current rehabilitation strategies are intended for general-size rehabilitation projects, mostly multi-story mixed-use buildings, and are not necessarily optimal for small-size projects. Rapid rehabilitation strategies have sustainability benefits in terms of providing a more resilient building stock for the community as well as minimizing environmental and economical impacts and social consequences during the rehabilitation project. Such rapid rehabilitation strategies are also suitable for a multi-staged incremental seismic rehabilitation strategy proposed by FEMA [Figure 1.4; FEMA, 2002 and 2003], where a series of discretized actions can be made to coincide with regularly scheduled building repairs, and maintenance or capital improvement so that both investment and losses due to business interruptions are minimized.

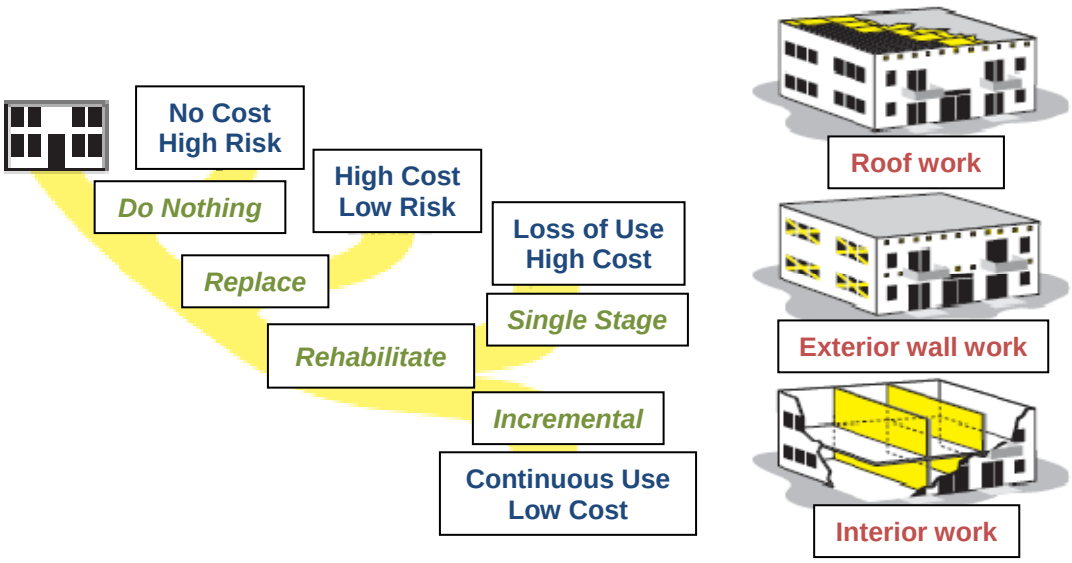

Figure 1.4: Idea of incremental seismic rehabilitation by FEMA (left) option for seismic risk reduction (right) schematic integration opportunity [adapted from FEMA 2002]

1.4 Scope and Objectives

A goal of this study is to design and evaluate two innovative, rapid rehabilitation strategies for low to mid-rise steel buildings consistent with the following tenets of sustainable design. The systems must:

- result in robust and resilient buildings,
- be efficient in the use of materials, with minimal energy requirements and emissions,
- be able to achieve its goals with only minor on-site construction and disruption to existing non-structural elements,
- require minimal modification to existing structural elements, and
- require little maintenance (low life-cycle cost, easy to replace)

To achieve these goals, a unique approach to designing supplemental systems using tension-only elements is proposed. The targets of these strategies are relatively

small rehabilitation projects for steel structures where deficiencies arise from a change in design load (e.g., update of seismic category, change of usage, climate change), existence of non-compact sections, existence of structural irregularities (e.g., structure with a weak or soft story, structure with torsional irregularity), or lack of redundancy. By taking the tension-only approach, designers do not need to worry about undesirable global or local buckling. This means that designers do not need to seek compact sections for supplemental elements with limited strength demand; the compactness limitation sometimes leads to overdesign of supplemental elements. Since elements can be slender, systems constructed with tension-only elements are scalable and adjustable in size. Thanks to the ease of installation, supplemental systems become economical. The key benefits of the tension-only design approach are:

- Elimination of undesirable global and local buckling,
- Rational implementation of an strict capacity design (over-strength is known or capped)
- Scalable and adaptable to many bay geometries
- Use of simple connection
- Rapid and adjustable installation
- Economical and efficient solution

Following the proposed tension-only approach, two rapid rehabilitation strategies are presented. The first is a cable bracing system consisting of tension only cables and a central energy dissipating device. In this device, cables are always in tension and thus begin to carry load immediately after a deformation reversal (no slack), resulting in stable, bi-linear behavior. The second is a shear wall system with the combined use of a

thin steel plate shear wall and tension-only bracing. The thin steel plate shear wall resists deformation by forming a tension field after an onset of global shear buckling.

This dissertation presents the work completed for the development of the proposed systems: verification of the concepts by initial analyses, development of design procedures, prototype designs, proof-of-concept testing, and design modifications.

1.5 Dissertation Outline

The content of the dissertation is organized into the following chapters:

- **CHAPTER 2** introduces an innovative cable bracing geometry with a Couples Resisting Damper (CORE Damper). The chapter presents the validation of the system through static analyses, the prototype design and finite element analyses of the CORE Damper, the dynamic behavior of the prototype system, and the introduction and static analyses of modified geometry with Nickel-Titanium shape memory alloys for the addition of re-centering capability.

- **CHAPTER 3** presents the proof-of-concept testing of the prototype for the cable bracing system. The chapter reports the performance of a full-scale specimen under quasi-static cyclic loading.

- **CHAPTER 4** demonstrates the upgrading of seismically deficient steel frames using the “Cable Bracing-CORE Damper System”. The responses of an original and upgraded building subjected to near and far field ground motions are examined.

- **CHAPTER 5** introduces a new type of steel shear wall system for seismic rehabilitation, referred to as "Narrow Steel Plate Shear Wall with Tension-Only Bracing (NPSW-TB)". The chapter presents the design approach and design flowchart for the NPSW-TB system. The performance of a prototype as well as the scaled system for a proof-of-concept testing is evaluated by static pushover analyses.

- **CHAPTER 6** presents the proof-of-concept test results of the NPSW-TB system which is a part of research collaboration program with Kyoto University in Japan. Two scaled systems, with and without tension-only bracing, were tested to evaluate the effect of the bracing on global and local behaviors.

- **CHAPTER 7** provides a summary and conclusion of the research. Discussion on the impacts of the work and suggestions for future research on sustainable seismic rehabilitation strategy are also made.

CHAPTER 2

CABLE BRACING-COUPLE RESISTING DAMPER (CORE DAMPER) SYSTEM

2.1 Introduction

Concentrically Braced Frames (CBFs) have long been recognized as a practical and economical solution for the control of lateral deformation [e.g., Constantinou, 1993, 1998; Tremblay, 2003]. When bracing elements are designed as compact to exhibit sufficient compression strength, CBFs provides a stable ductile behavior under severe lateral cyclic loading. This system, known as "Tension-Compression" CBF has been favored by building codes based on numbers of analytical and experimental studies [e.g., Martinez-Rueda, 2002; Black, 2004]. Compared to this, CBF with non-compact or slender bracing elements, known as "Tension-only" CBF exhibits extremely pinched hysteresis behavior during strong earthquake, is permitted only in Ordinarily Concentrated Brace Frame (OCBF) with x-bracing configuration; but not for K, V, and inverted V configurations in the current seismic guideline in U.S. [AISC, 2007].

The retrofit and strengthening of smaller structures can be addressed effectively through the addition of structural elements such as cross-braces. However, for many such structures it is not possible to either follow a strict capacity design approach or find small members with the required compactness criteria to withstand large cyclic load reversals; the compactness limitation sometimes leads to overdesign of supplemental elements. In these situations, a bracing system with tension-only elements such as cables

or tension-rods and incorporating an energy dissipater with reliable strength and stiffness characteristics is an attractive alternative. By taking the tension-only approach, designers do not need to worry about undesirable global buckling, which means, designers do not need to seek compact sections for supplemental elements with limited strength demand. Connections on tension-only elements to existing frame are simple, rapid and adjustable [see Figure 2.1 for example connections].

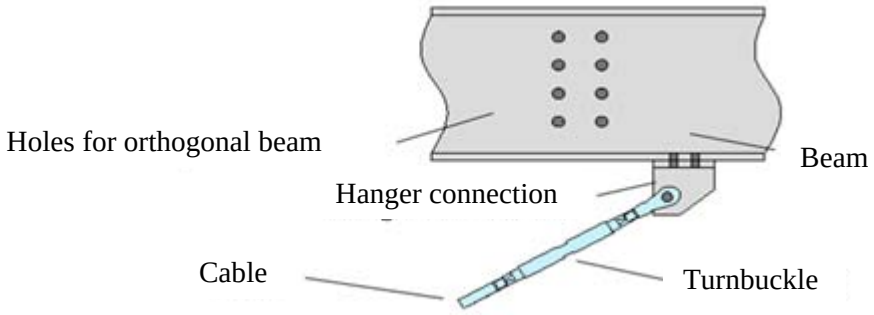

Fig 2.1(a):

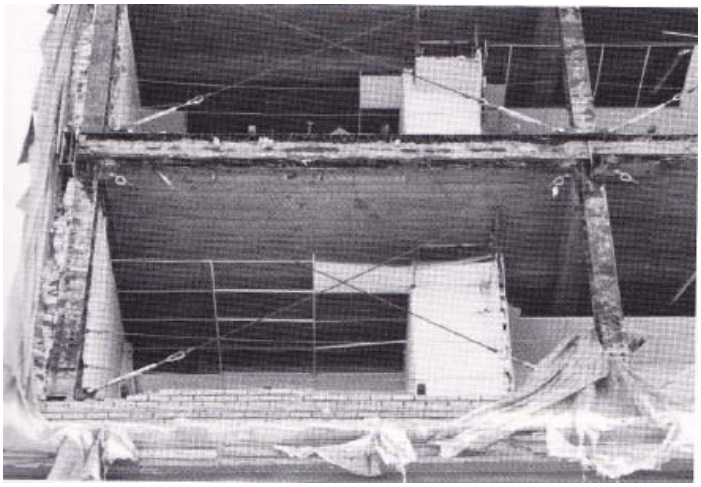

Fig 2.1(b):

Figure 2.1: Example connections of tension-only elements (a) adjustable hanger connection with turn buckle (b) temporary support after Loma Prieta earthquake [SEAOC, 1989]

A tension-only system, defined as a system where selected key elements remain always in tension under cyclic lateral loading, can provide stable bi-linear hysteresis if used in conjunction with an appropriate energy dissipating device [Martinez-Rueda, 2002]. Such systems are not new. Pall (1982, 1983) proposed a friction device with a slip joint for a cross bracing and an inverted V-bracing [Figure 2.2(a)]. Anagnostides *et al*. (1989) proposed a new type of friction device for a tension-only cross-bracing system [Figure 2.2(b)]. Mualla and Bellev (2002) conducted dynamic tests of a scaled steel frame with friction damper devices installed in an inverted cable V-bracing system [Figure 2.2(c)]. These systems utilize friction-based damper devices where friction force is introduced by preloading of steel plates with high strength bolts. The surface of the steel plates is normally coated by special friction lining materials to achieve a good hysteretic response where the slipping force is predictable and remains unchanged during the required number of cyclic loading. The design of the friction-based device should account for the creep of the surface materials as well as relaxation of high strength bolts to minimize the long term degradation of friction force. Previous tests indicated that devices based on rotational friction give more consistent hysteresis loops than those based on linear sliding friction where significant damage was observed after the tests on the steel plates and friction material as a result of scuffing between the two surfaces [Anagnostides, 1989]. Recent application of the friction-based device in real building can be found in Chang *et al*. (2006).

An example of previously proposed systems which do not use friction-based dampers is a system proposed by Phocas and Pocanschi (2003). This system utilized the energy dissipating mechanism of the bending and yielding of mild steel plates whose

performance is independent from the surface condition of materials and remains unchanged for years. In their system, diagonals of the system are fixed at the bottom of the columns and are able to move at the top corners of the frame through rotations of the connecting eccentric discs [Figure 2.2(d)]. In this geometry, attention should be paid to the condition of the top of column which needs to sustain a brace force doubled by the pulley mechanism used.

The cable cross bracing system developed by the author has a unique geometry and provides stable energy dissipation until very large deformations are reached by taking advantage of permanent rotations in a central energy dissipating device. This system basically consists of eight eccentrically connected elastic cables and a Couples Resisting Damper (CORE Damper). Similar to previously developed metallic yielding devices [Whittaker, 1991; Tsai ,1993; Xia and Hanson, 1992; Fierro and Perry, 1993], the CORE Damper developed herein dissipates energy through the bending and yielding of mild steel plates and does not require periodical maintenance. In order to achieve stable hysteretic behavior and allow for easy replacement after a major seismic event, the connections in regions of anticipated maximum ductility are designed using high strength bolted connections to avoid potential brittle weld failures.

The concept of the proposed bracing system was first validated in nonlinear static cyclic analyses in the OpenSEES platform [Mazzoni *et al*., 2009]. The analyses provided the approximate strength demand, required deformation capacity, and optimal shape for the central energy dissipating device (CORE Damper). The details of the CORE Damper were carefully refined through simulations using the general purpose finite element analysis program ABAQUS as a design tool. The dynamic behavior of the proposed

system under high strain rates was also examined to see the effect of high speed loading on the local and global performance of the system.

As a secondary objective, the addition of re-centering capability to the existing bracing system was considered. Here, the re-centering system is specifically intended to reduce the residual deformation at critical sections of existing buildings. The fundamentals of the re-centering system are similar to the original system, except that cables are connected only in one diagonal rather than in a cross bracing geometry. By simply adding extra cables made of shape memory alloy (NITINOL) to the same diagonal in the base system, the system can be upgraded to a re-centering system. The concept of the re-centering system was validated through non-linear static cyclic analyses in the OpenSEES platform.

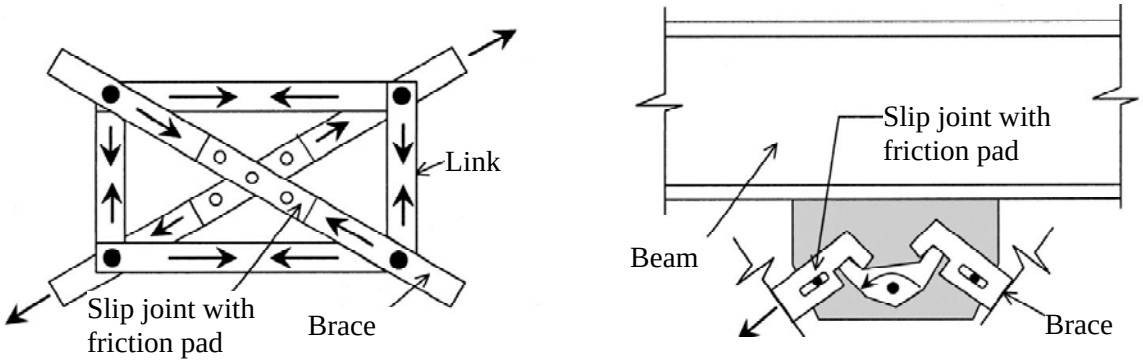

Fig 2.2(a):

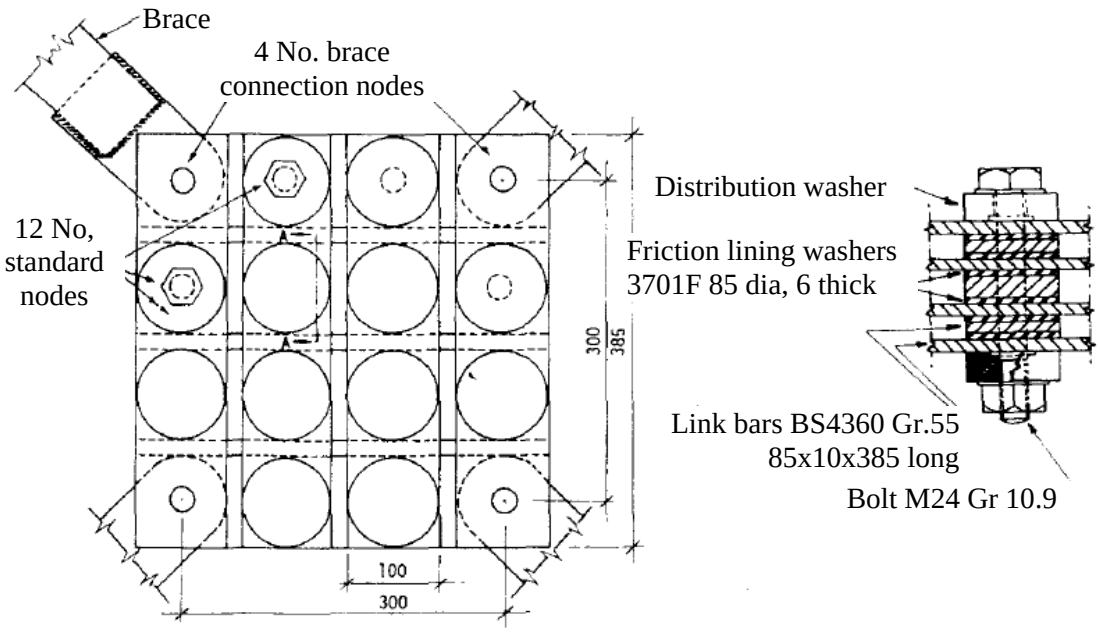

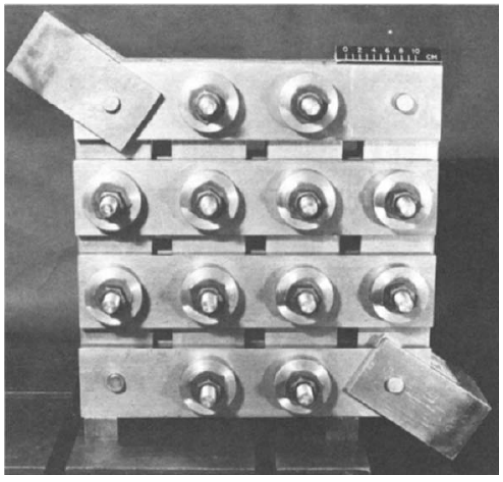

Fig 2.2(b):

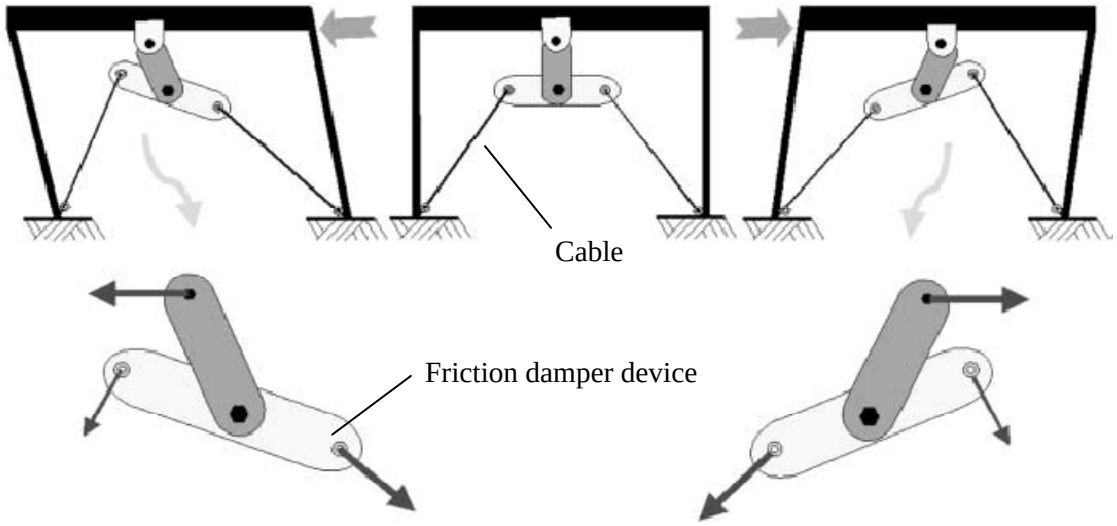

Fig 2.2(c):

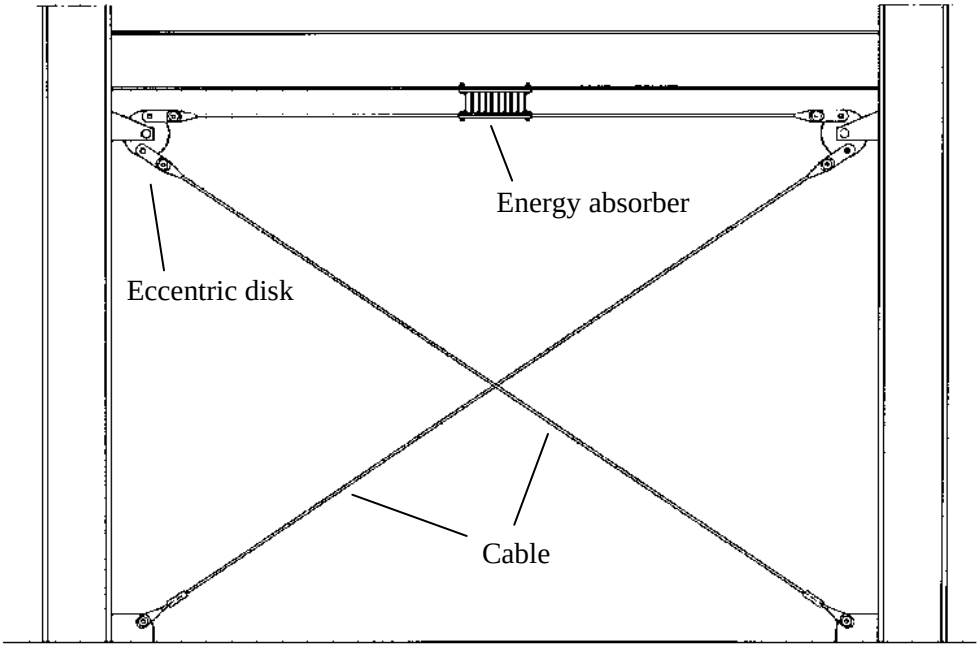

Fig 2.2(d):

Figure 2.2: Example tension-only cable bracing mechanism proposed in past (a) friction device [Pall, 1983] (b) friction device [Anagnostides, 1989] (c) friction device [Mualla and Bellev, 2002] (d) hysteretic damper system with eccentric disc [Phocas and Pocanschi, 2003]

2.2 Geometry of Proposed System

The proposed system consists of eight eccentrically connected elastic cables and a Couples Resisting Damper (CORE Damper) [Figure 2.3(a)]. The damper consists basically of two front and back rigid elements connected by a rotational spring with bi-linear hysteresis. When the earthquake load deforms the originally weak moment frame, four cables in tension begin to resist the deformation and rotate the front and back rigid plates in opposite directions while tied together by a rotational spring [Figure 2.3(b)]. Note that the other four cables, which connect across the shortened diagonal, are not slack when the loading direction changes because of the permanent rotation of the rigid elements. As shown in Figure 2.3(c), the other cables start to resist load when unloading curve crosses the zero force threshold, resulting in a system that exhibits bi-linear load displacement behavior instead of the typical slip type curve associated with tension-only diagonal systems.

Figure 2.4 illustrates the two key kinematic characteristics of the proposed geometry. One characteristic is the extension/shortening of the diagonals of the overall frame. The other characteristic is the elongation/shortening of cables caused by the local rotation of a rigid element. The proposed system utilizes the interaction of these two phenomena effectively and eliminates the any shortening or slack in cables; the possible slack in the cables connecting the shortened diagonal is eliminated by the geometric elongation caused by the rotation of the central device.

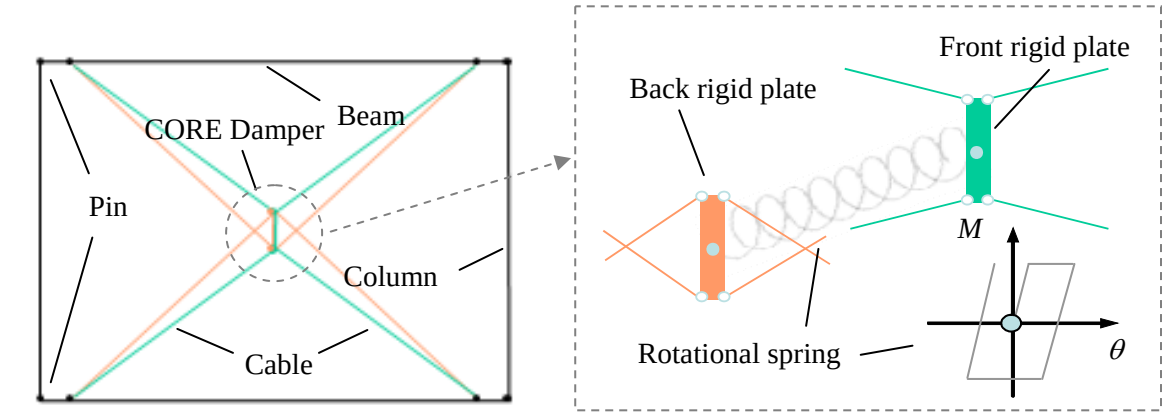

Fig 2.3(a):

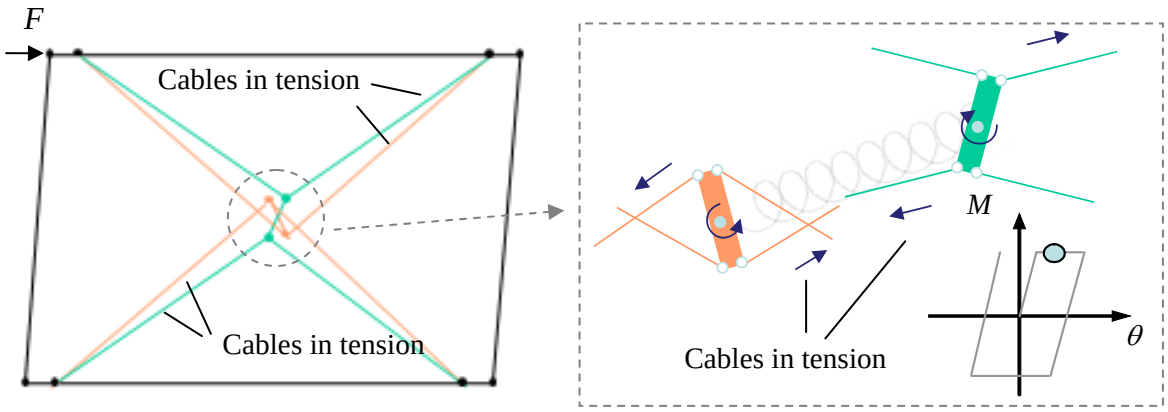

Fig 2.3(b):

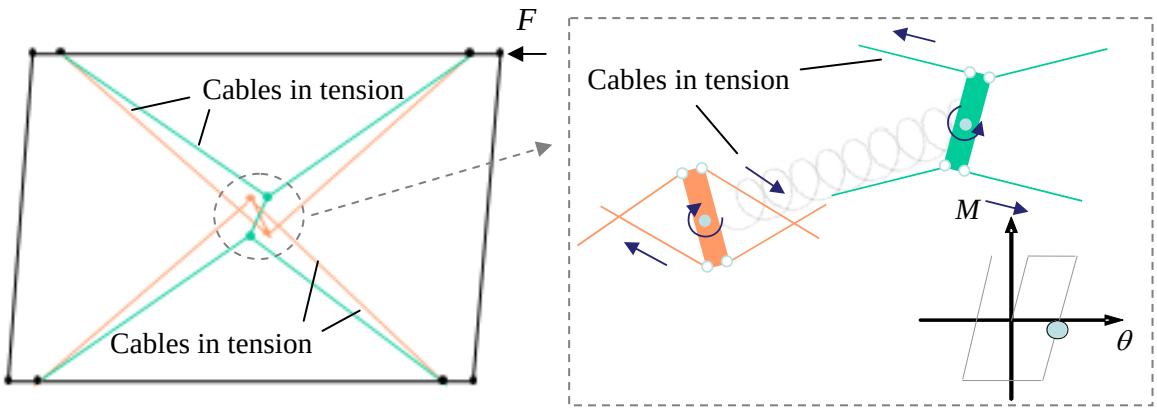

Fig 2.3(c):

Figure 2.3: Concept of cable cross bracing with CORE Damper (a) initial phase; analysis model (left), central energy dissipater (right) (b) loading phase (c) unloading phase

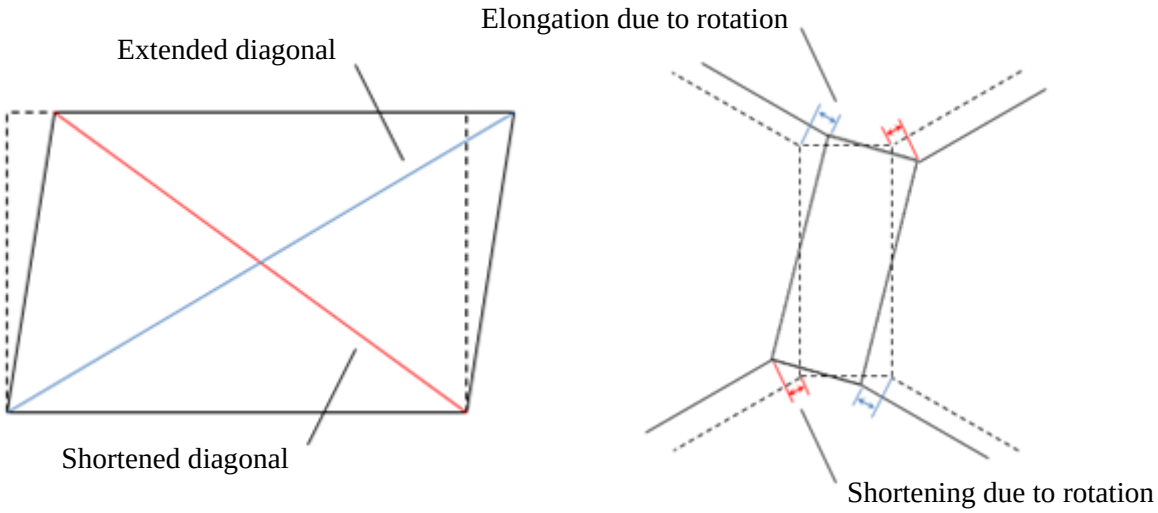

Figure 2.4: Kinematic characteristics and resulting deformations in cables

2.3 Preliminary Analyses

Analysis Model Description

Schematics of an analytical model constructed in OpenSEES [Mazzoni, 2009] are shown Figure 2.5(a). The proposed cable bracing-CORE Damper system is installed into a portal frame with four pins assumed at its corners. The dimension of the portal frame is 5280mm x 7280mm measured at center of beams and columns, which represents a multi-purpose testing system at the Structural Laboratory of the Georgia Institute of Technology that was used for the full-scale tests [Chapter 3]. Beams and columns are modeled using the *nonlinearBeamColumn* element with nominal material properties corresponding to A36 mild steel. Pin connections are modeled by restricting translational degrees-of-freedom in two nodes at the same location using the *equalDOF* command. Cables are modeled as co-rotational elastic truss elements connected to elastic beams and rigid elements of the central device. The elastic stiffness of a cable is taken as 70% of a

comparable steel section based on literature data; see, for example, [Costello, 1999]. In the central device [Figure 2.5(b)], the rotational spring connecting the center nodes of the front and back rigid elements is modeled by coupling the translational DOFs and assigning a *zerolength* element with bi-linear hysteresis for the rotational DOF. The rigid elements are modeled using *elasticBeamColumn* elements with very large stiffness.

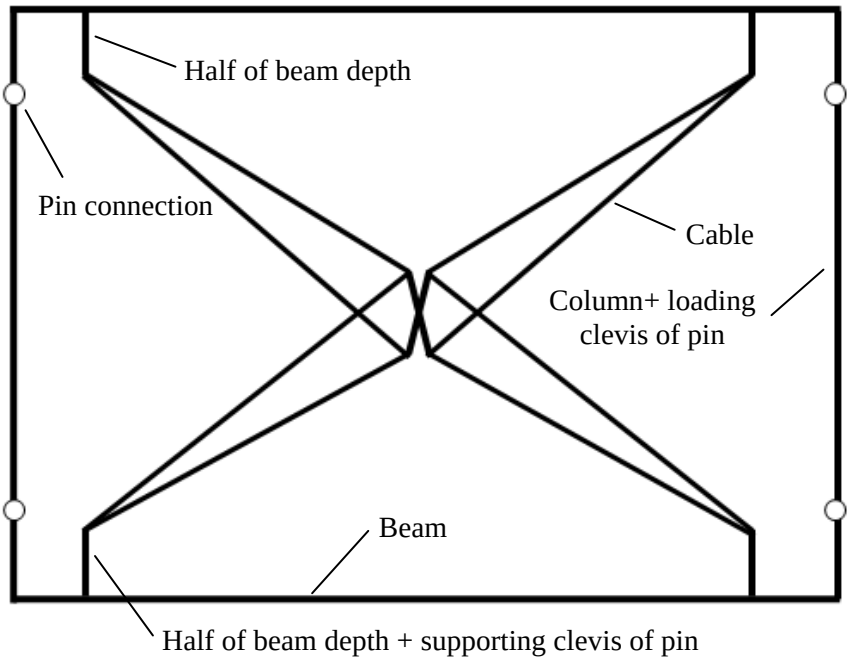

Fig 2.5(a):

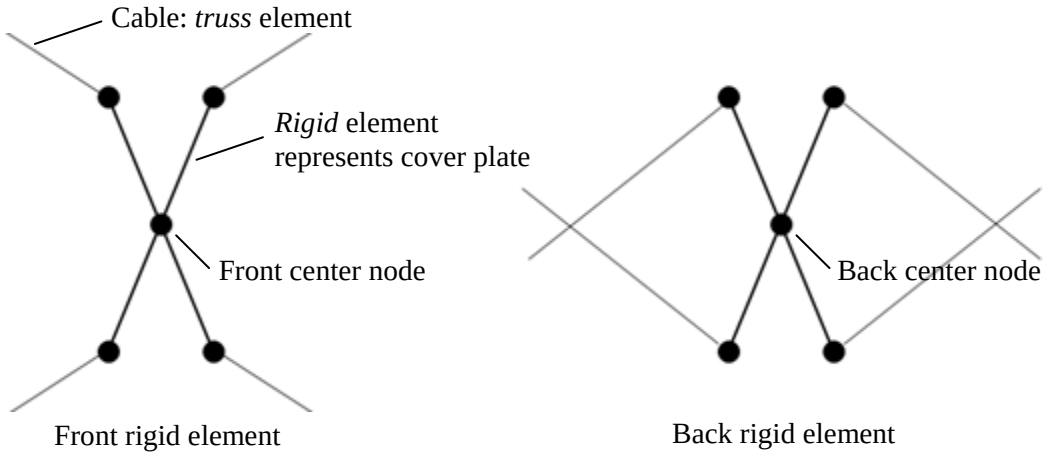

Fig 2.5(b):

Figure 2.5: Analysis model (a) overall system (b) simplified CORE Damper model

Preliminary Analyses Results

Figure 2.6 shows the results from the preliminary non-linear static analysis of the proposed system. In the analysis, an arbitrary bi-linear hysteresis behavior was implemented for the rotational spring. One cycle of 3% story drift amplitude, which is 1.5 times larger than the required deformation capacity for braced frames in the current seismic design guidelines, was applied to the model frame [NEHRP, 2004]. The results showed that if the rotational spring could deliver a stable bi-linear curve, then the behavior of the entire subassemblage, as characterized by its force vs. story drift curve, was also stable and bi-linear. The deformation of cables in compression was limited even under large deformations, thanks to the permanent rotation in the CORE Damper [Figure 2.6(c)]. As the plots indicate, the cables in either one of two diagonals always carry tension force at any points in one loading cycle [Figure 2.6(d)].

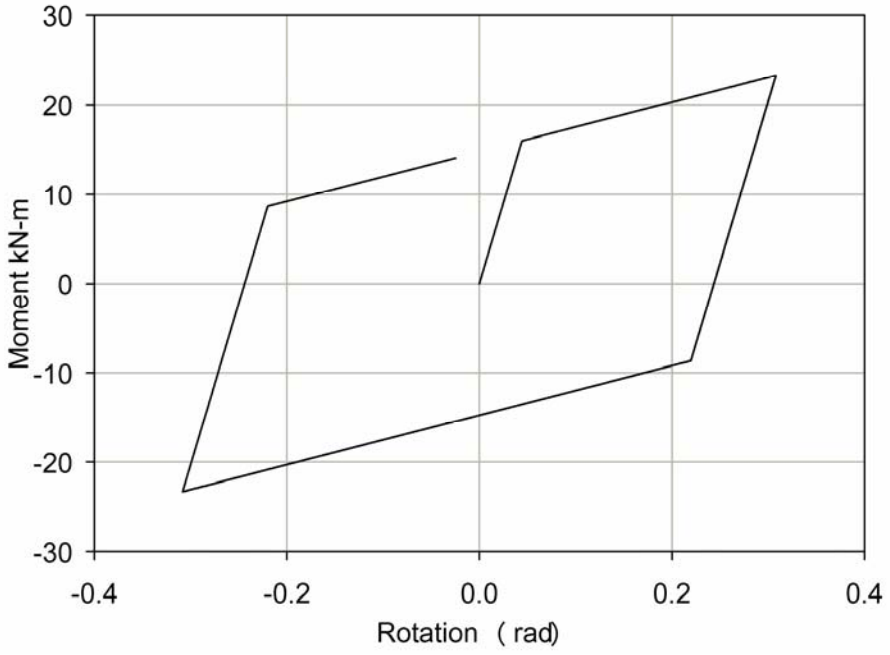

Fig 2.6(a):

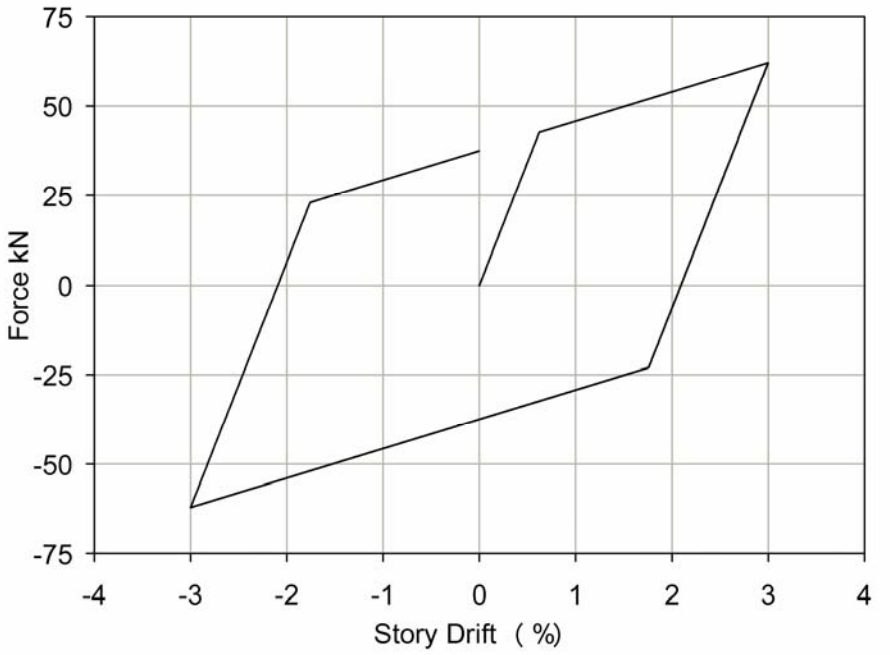

Fig 2.6(b):

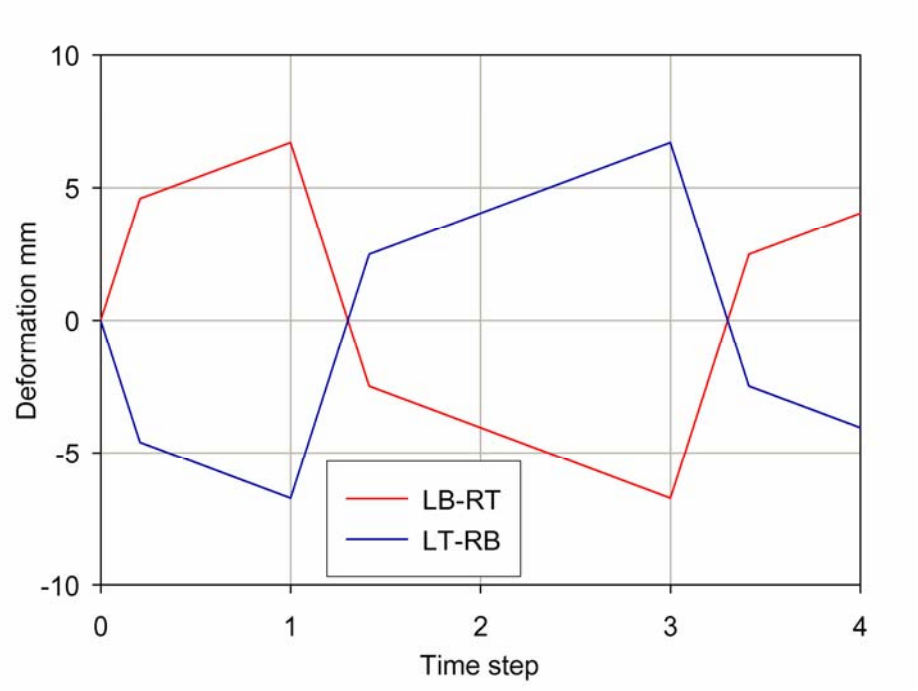

Fig 2.6(c):

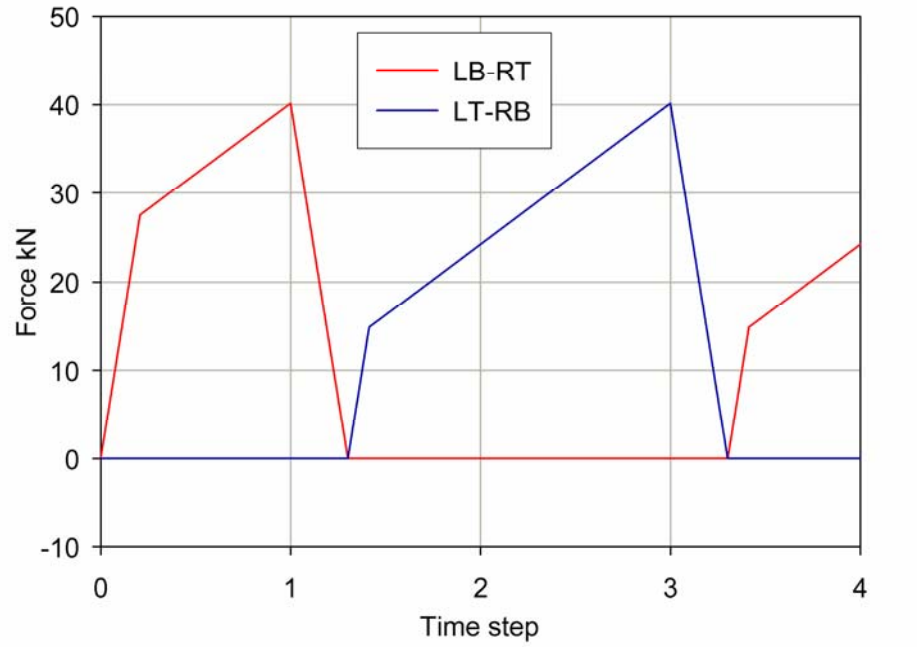

Fig 2.6(d):

Figure 2.6: Preliminary OpenSEES analysis (a) rotational spring hysteresis (b) system base shear (c) cable deformation hysteresis (d) cable force hysteresis

Optimal Shape of CORE Damper

Using this analysis model, a parametric study was conducted to determine an approximate optimal shape for the CORE Damper. The main parameter studied was the aspect ratio of the rigid element to which the cables are connected. For these studies, the diagonal length of the rigid element was fixed. Figure 2.7(a) shows the maximum rotation demands for the damper with various aspect ratios during the cyclic loading at 3% story drift amplitude. The rotation demand is smallest when the aspect ratio is between 1 and 2 and gradually increases at aspect ratios greater than 2. The relationship between base shear and rotation of the spring was linear [Figure 2.7(b)]. This indicated that the stiffness of the system can be controlled by the aspect ratio of the rigid elements.

By setting the initial performance goal of the prototype to be a stable and ductile behavior under very large story drifts, it is concluded that the best shape for the rigid element is either a square or slight oblong in order to limit rotational demand.

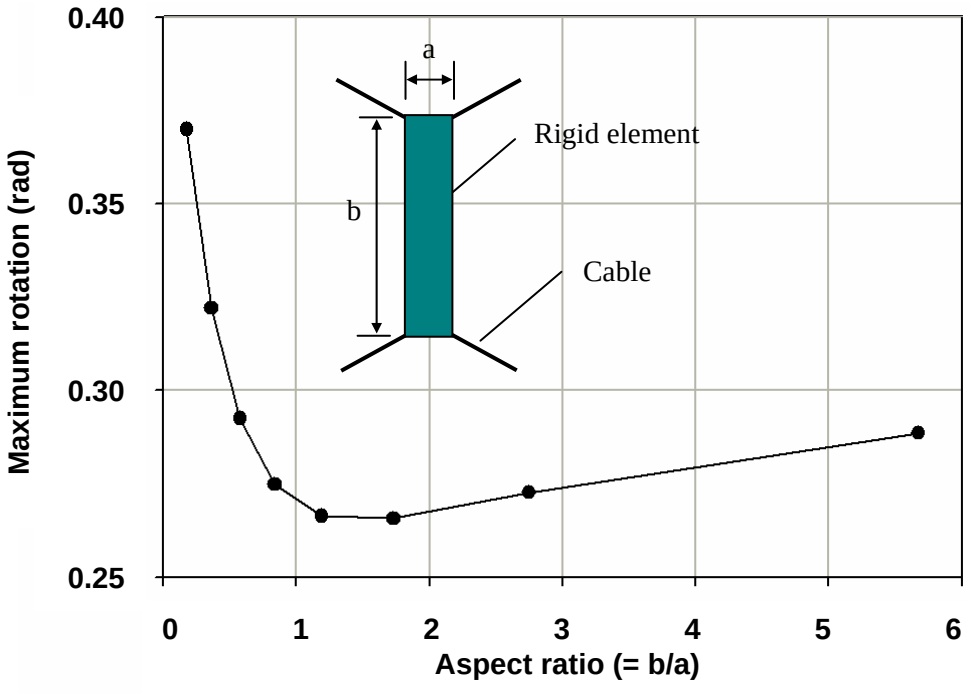

Fig 2.7(a):

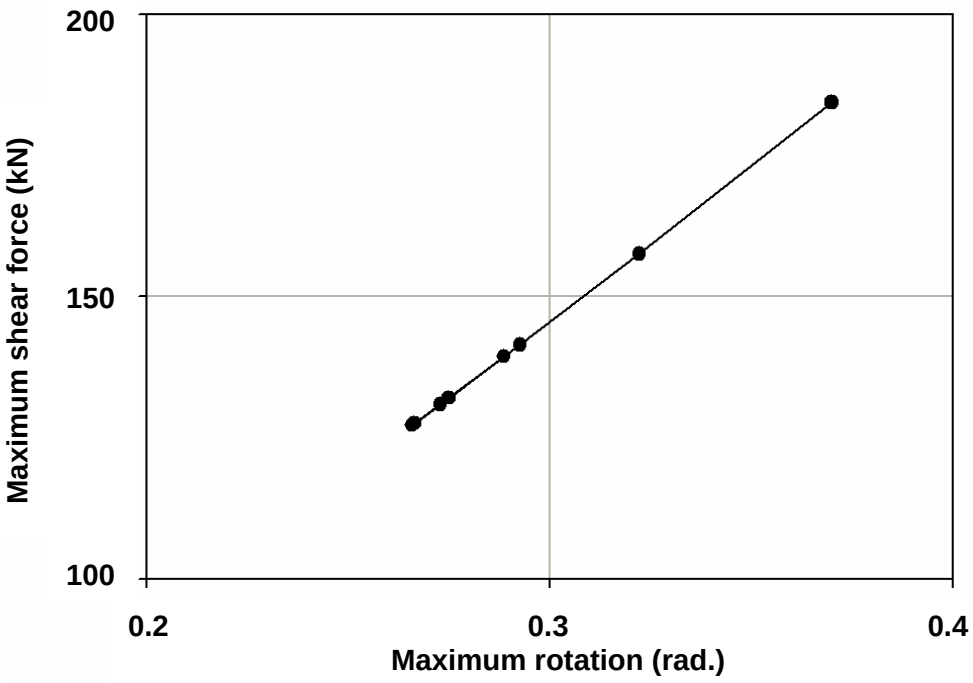

Fig 2.7(b):

Figure 2.7: Parametric studies to geometry of CORE Damper (a) aspect ratio vs. maximum rotation (b) base shear vs. rotation

2.4 Design of CORE Damper

Geometry and Dimension of CORE Damper

The Couples Resisting Damper (CORE Damper) for the proposed cable system was optimized by using a general purpose finite element analysis program, ABAQUS [Dassault Systems 2008]. Figure 2.8 shows the geometry of a prototype with a performance goal of achieving a stable hysteresis curve up to 0.3 to 0.4 radians of rotation. The dimension of the prototype is shown in Appendix A. The prototype CORE Damper has dimensions of 152mm x 760mm x 152mm and is compact and is light enough (65kg) to be carried by two construction workers with a small wheelbarrow or similar moving device. It is also possible to assemble it on site since all the components are connected through high-strength bolts; turnbuckles can be provided in the cables to make all necessary geometric adjustments. The plastic deformation of the device is limited only to the steel plate energy absorber (SPEA) which is replaceable after a major earthquake event. The assembly of the CORE Damper proceeds as follows. First, a hollow steel section (HSS) is placed between two SPEAs (Gr. 36 mild steel) and a post tensioning force is applied to the outer surface of the SPEAs by high strength rods. This subassembly is then connected to the cover plates (Gr. 50 mild steel) with high strength bolts; these bolts are not pre-tensioned. To prevent the development of undesirable axial forces in the SPEA, these bolts are allowed to slip along a long slotted hole.

Figure 2.9 illustrates the free-body-diagram of the main components of the prototype. In this figure, the top and bottom cover plates are shown in their deformed condition, while the middle subassembly is shown in its undeformed condition. In the schematics, the dotted arrows indicate the forces acting between the bottom cover plate

and the middle assembly, while the solid arrows indicate the forces between the top cover plate and the middle assembly. In this device, the torsional moment induced by the rotation of the top and bottom rigid steel plates is resisted by the bending moment of two lozenge steel plates. Each end of these plates is transversely connected to the top and bottom rigid plates, respectively. The lozenge shapes of these Steel Plate Energy Absorbers (SPEAs) have two objectives. One is to avoid the SPEAs placed in parallel from touching each other even under severe deformations. The other is to achieve a uniformly distributed stress over the length of the plates to avoid developing a severe kink at its center connection. In this respect, its concept is similar to the ADAS and TADAS elements [Whittaker 1991; Tsai 1993]. Unlike these common energy dissipating plates, the SPEAs in this energy dissipater are free of welds and do not require that welding be limited to locations far from the regions with anticipated maximum ductility demands.

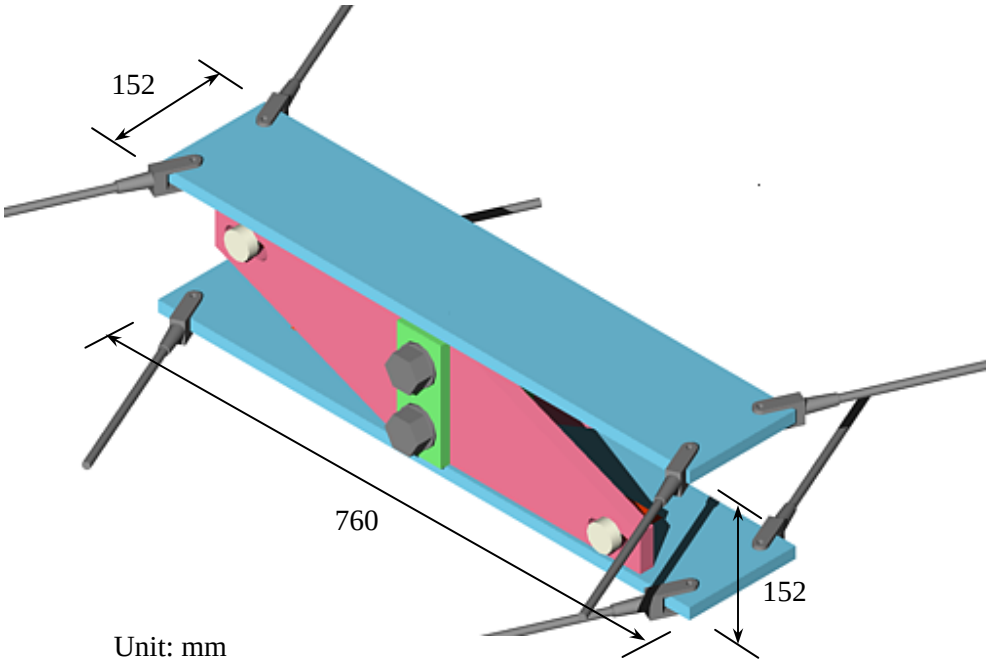

Fig 2.8(a):

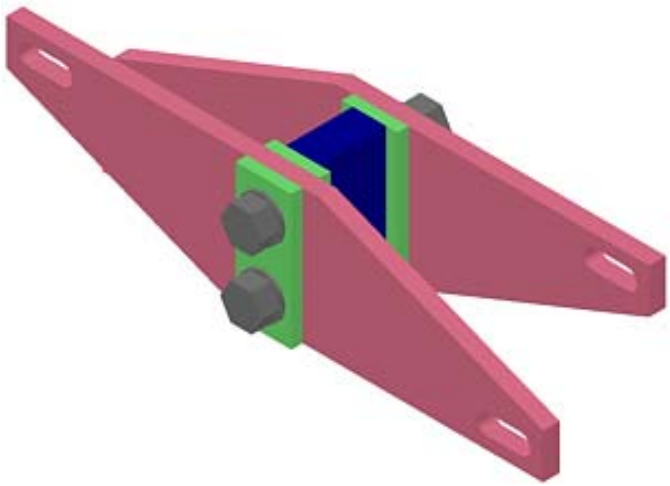

Fig 2.8(b):

Fig 2.8(c):

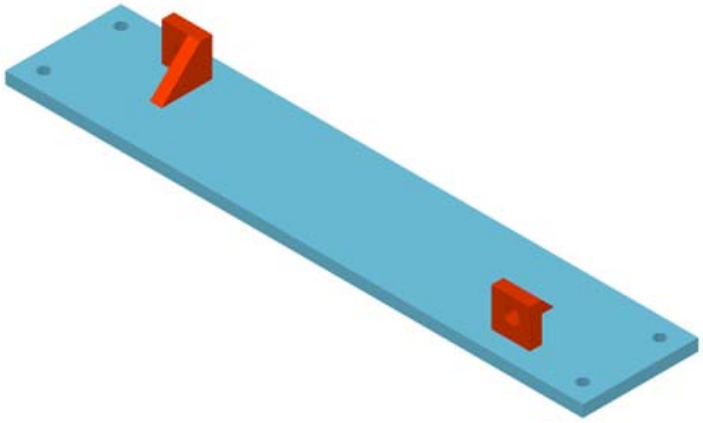

Fig 2.8(d):

Figure 2.8: Assemblage and components of CORE Damper (a) isometric view with cover plates (b) isometric view without cover plate (c) steel plate energy absorber (Gr. 36) (d) steel cover plate with bolts (Gr. 50)

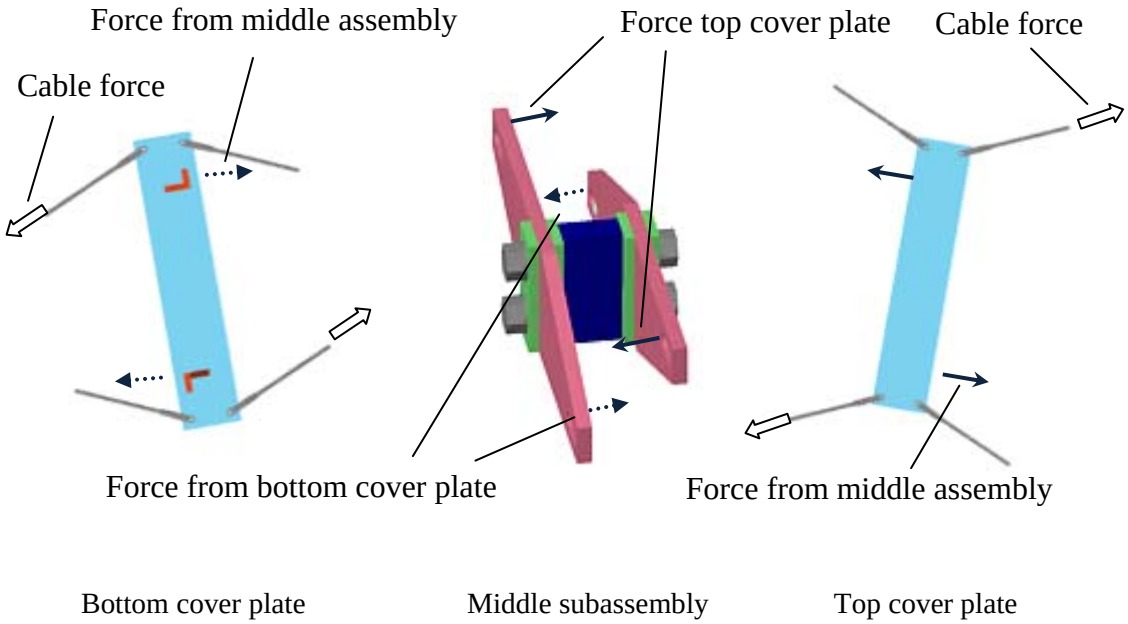

Figure 2.9: Free-body-diagram of CORE Damper

FE Analysis Model

The analysis model of the CORE Damper consists of two cover plates, two steel plate energy absorbers (SPEA) and four rectangular steel plate washers [Figure 2.10]. In the analysis, high strength bolts and annular washers are modeled as a part of the cover plate. Instead of modeling a steel HSS and high strength rods, the movements of the plate washers placed inside of the SPEAs are fixed and a uniform pressure is applied to the outer surface of the plate washers placed outside of the SPEAs. The cyclic loading is applied to two loading points, RP-1 and RP-2, each of which is rigidly constrained to the outer surface of top and bottom cover plates. Eight-node linear brick elements with reduced integral (C3D8R) and hourglass control are used for the SPEAs and the middle part of the cover plates. Four-node linear tetrahedron elements (C3D4) and six-node linear triangular prism elements (C3D6) are used for the part around the bolted connections of the cover plates and bolts. The material properties of the SPEAs and plate washers are bi-linear with yield strength of 269MPa, obtained from tensile coupon tests for a proof-of-concept test reported in Chapter 3. The material properties of the cover plates are assumed to be bi-linear with yield strength of 345MPa. Bolts are assumed to be elastic.

Slip motion is allowed between high strength bolts and SPEAs and between steel plate washers and SPEAs utilizing a contact element feature in ABAQUS. For the contact element, a surface-to-surface discretization method is used since it provides more accurate stress and pressure results than node-to-surface discretization when the surface geometry is reasonably well represented by the contact surfaces. The tracking approach is a finite-sliding simulation. The tangent behavior of the contact properties is formulated

by a penalty method with the static coefficient of friction assumed as 0.3. The penalty method is a stiff approximation of a hard contact. In the normal direction, an augmented Lagrange method is used with separation allowed after contact. The augmented Lagrange method uses the same kind of stiff approximation as the penalty method, but also uses augmentation iterations to improve the accuracy of the approximation [Dassault Systems 2008].

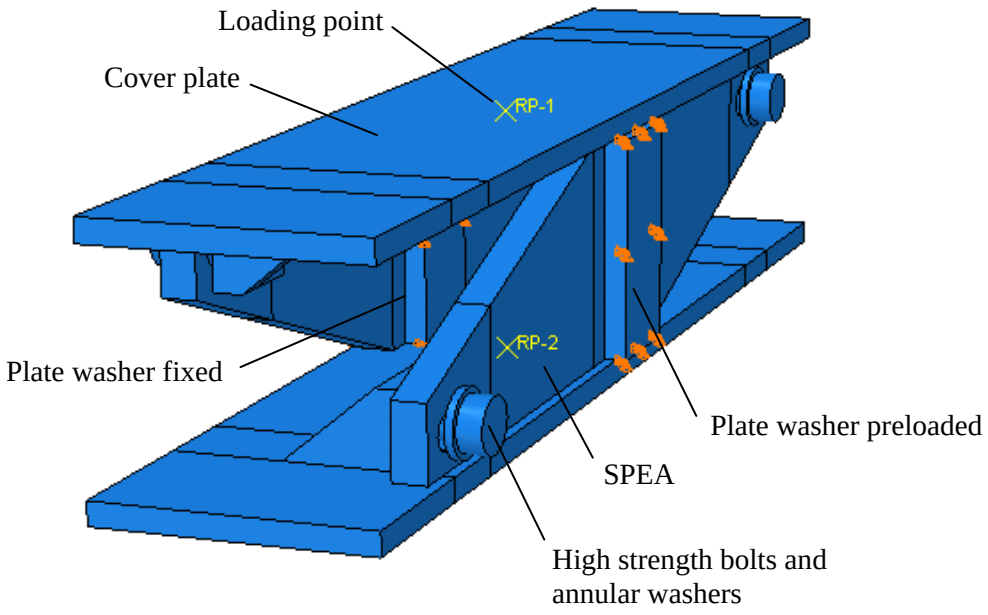

Figure 2.10: Finite element analysis model

FE Analysis Results

Typical deformed shapes of the CORE Damper obtained from finite element analyses are presented in Figure 2.11. Two different deformation modes of the CORE Damper were defined. In the outward deformation mode [Figure 2.11(a)], the front cover plate rotates clockwise and the SPEAs deform outward. In the inward deformation mode [Figure 2.11(b)], the front cover plate rotates counterclockwise and the SPEAs deform inward. For illustrative purposes, the deformed shape is also shown without cover plates

and HSS. In these analyses, a cyclic rotation is applied to the top and bottom cover plates with the amplitude of 0.18 rad. The relative rotation between the two plates is 0.36 rad., which corresponds to the deformation when a bracing system is subjected to 3% story drift in a preliminary OpenSEES analysis.

Figure 2.12 shows the overall behavior the CORE Damper during one cycle of static loading. In the hysteresis curve, the solid line corresponds to the moment versus rotation curve of the CORE Damper when deformation is applied first to the outward direction. The dotted line corresponds to that when deformation is applied first to the inward direction. In both cases, the CORE Damper yields approximately at 0.6% story drift (0.072rad) and shows post-yielding stiffness slightly higher in the outward direction as compared to the inward direction, primarily because of the bolt slip at the loading point of the SPEA. The von Mises stress contours for the SPEA [Figure 2.13] shows that the stress distributes uniformly in the center part of plate without severe stress concentrations. In the figures, stress is also high in the loading area around the long slotted holes. Under large deformations, the stress exceeds the yield stress of 269MPa at the most part of the SPEA. Figure 2.14 shows the equivalent plastic strain (PEEQ) in SPEAs. A large amount of plastic strain is accumulated in the center part of the SPEAs during cyclic loading. The part subjected to plastic deformation gradually increases as the loading proceeds. The plots also indicated that the plastic strain on the outer surface of the SPEAs is larger than that on the inner surface.

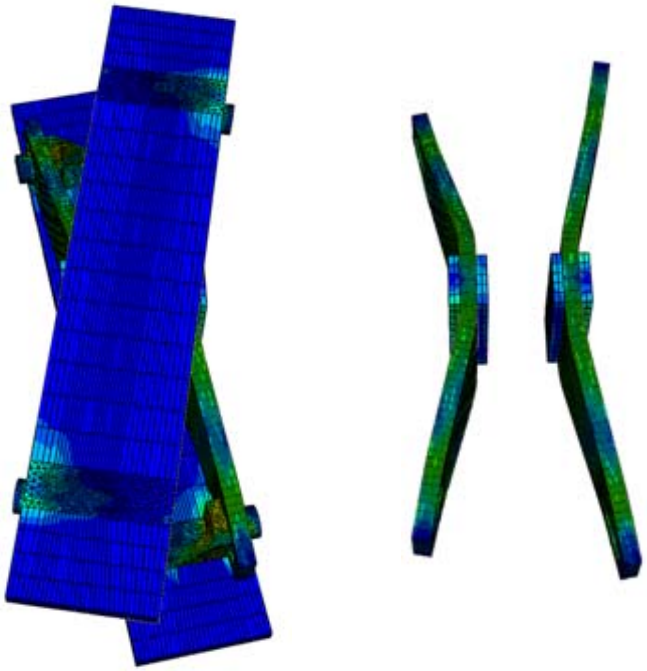

Fig 2.11(a):

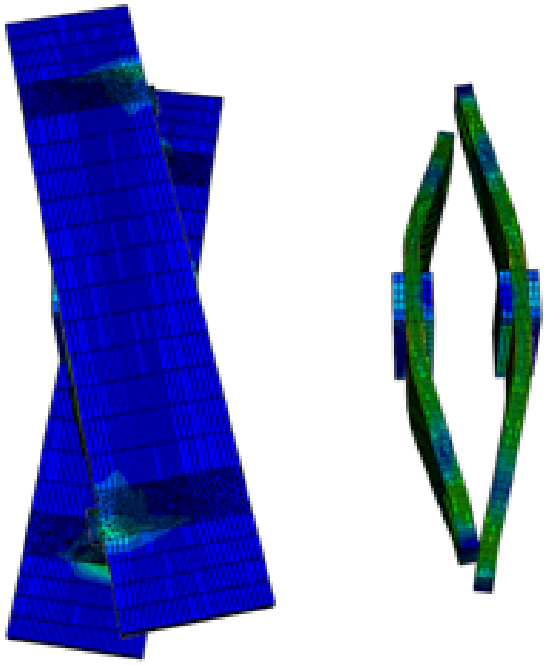

Fig 2.11(b):

Figure 2.11: Deformed shape of CORE Damper at 3% drift (a) outward deformation mode w/t and w/o cover plate (b) inward deformation mode w/t and w/o cover plate

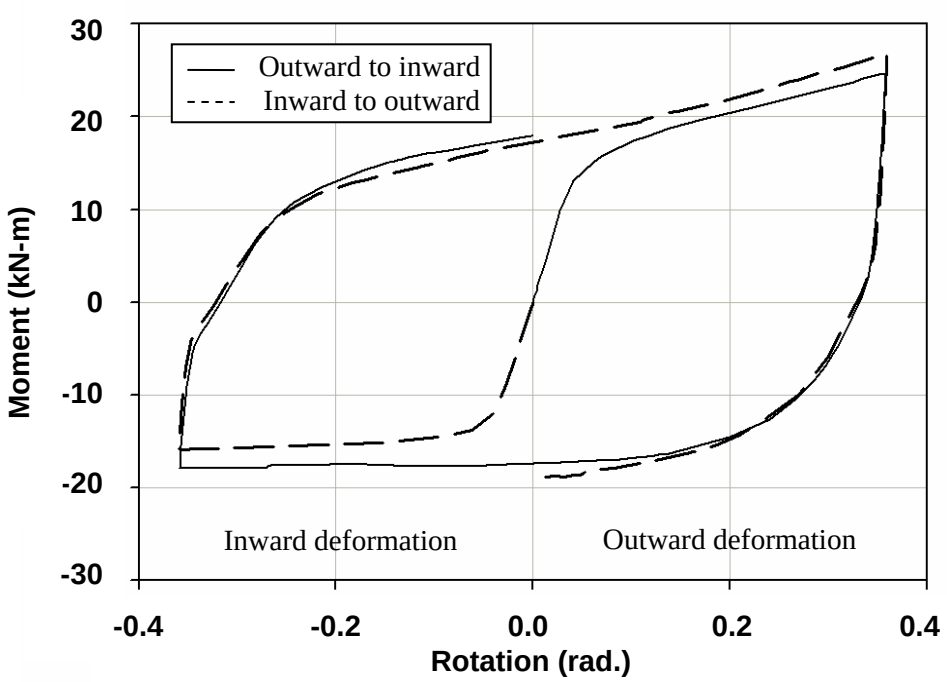

Figure 2.12: Hysteresis behavior of CORE Damper

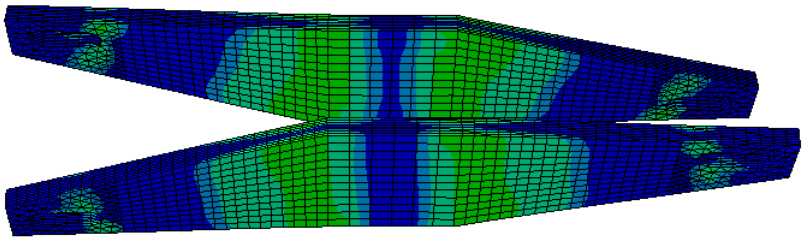

Fig 2.13(a):

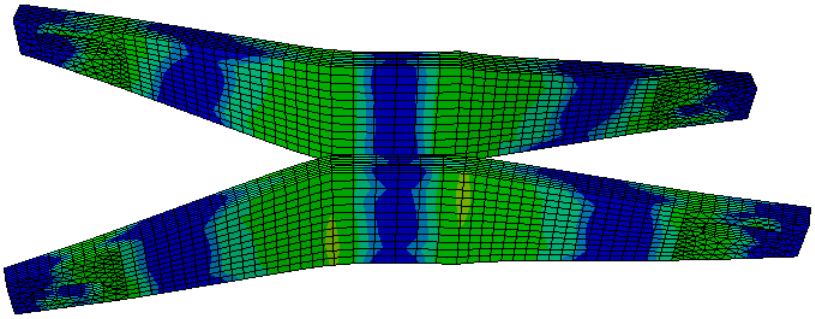

Fig 2.13(b):

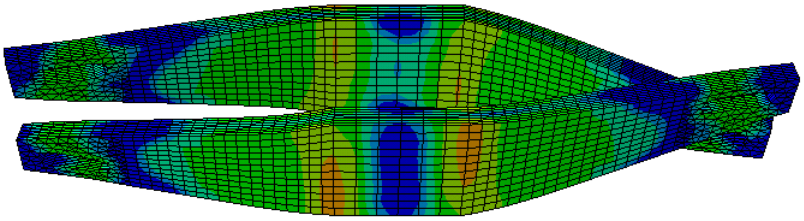

Fig 2.13(c):

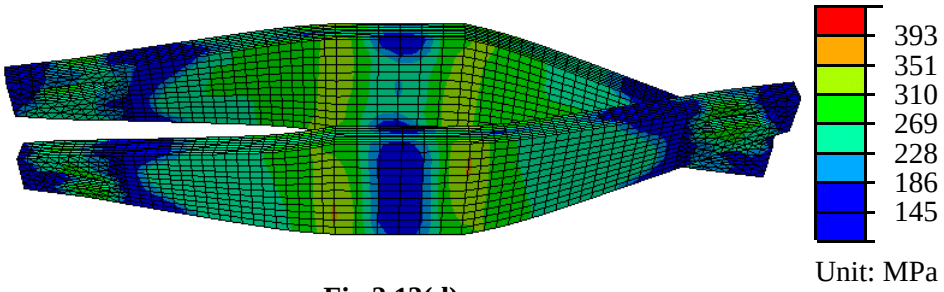

Fig 2.13(d):

Figure 2.13: Sequence of von Mises stress contour in SPEA during outward to inward cyclic loading (a) yielding at 0.072rad, outward (b) max outward deformation at 0.36rad (c) max inward deformation at -0.36rad (d) residual stress

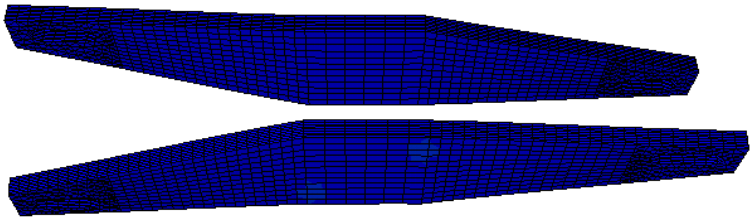

Fig 2.14(a):

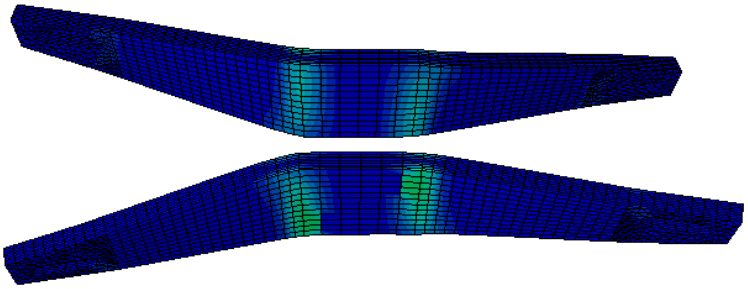

Fig 2.14(b):

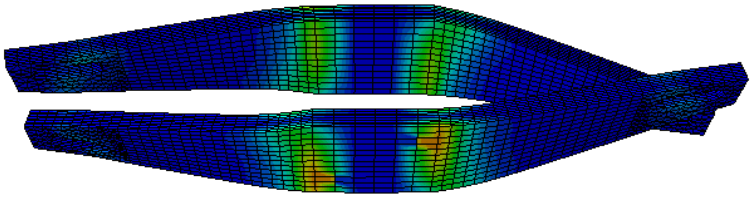

Fig 2.14(c):

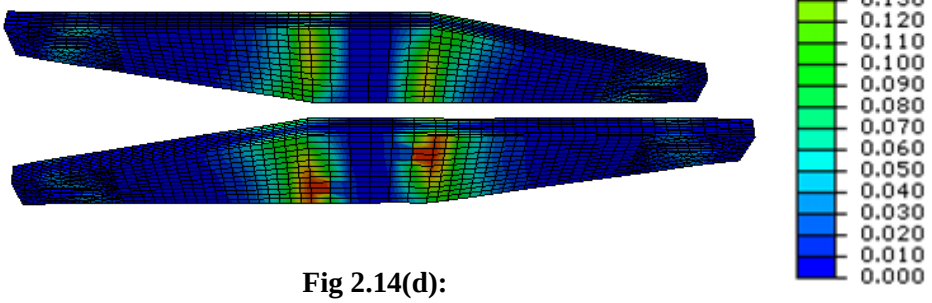

Fig 2.14(d):

Figure 2.14: Sequence of equivalent plastic strain (PEEQ) in SPEA during outward to inward cyclic loading (a) yielding at 0.072rad, outward (b) max outward deformation at 0.36rad (c) max inward deformation at -0.36rad (d) residual strain

2.5 Dynamic Behavior of "Cable Bracing-CORE Damper System"

Introduction

In the proposed bracing system, the cables resisting frame deformations switch when the direction of loading changes. When the movement of the CORE Damper starts to lag the movement of the framing, some slackness starts to occur in the cables. The effect of this phenomenon on global behavior was investigated by forcing the frame to vibrate at a very high speed. Nonlinear dynamic analyses of the proposed bracing system under sinusoidal cyclic loading with various frequencies were carried out.

When the cables become slack, they might be subjected to impact type loading when the loading reverses. The effect of impact loading in inelastic tension-only concentrically braced steel frames (TOCBF) had been experimentally studied in Canada [Tremblay, 1996; Filiatrault, 1998]. The study revealed that the sudden increase of tensile force in steel braces in TOCBF is limited by the yield strength of steel and this hysteresis effect attenuates the impact forces on the connections and other structural elements. The increase of tensile force is mainly caused by the increase of the yielding strength of steel under high strain rate loading. Although their conclusion is intended only for the TOCBF systems, it indicates that, in the proposed system, the yielding of the CORE Damper should attenuate the impact loading into cables and their connections to the frame. The selection of the cables should be carefully done since cables are still vulnerable against severe impact loading as it can lead to 'bird-caging', where outer strands separate form a core in a permanent manner [Costello, 1990].

The study presented here deals with the effect of the movement of the CORE Damper in the local cable forces and the global behavior of the system but does not

directly deal with the issue of the impact loading. For the study of such issues, carefully planned full-scale experiments under dynamic loading or on a large shake table are highly recommended.

Analysis Model

The hysteresis curve of the CORE Damper used in FE analysis was implemented into the analysis model developed for the preliminary static analyses [Figure 2.5 and Figure 2.12]. To account for the dynamic behavior, the real weight of the prototype of the damper is divided by the gravitational acceleration and added to the center nodes of the damper as nodal mass. The weights of the cables are negligible and ignored. The sinusoidal displacement history applied to the center of the top beam has a magnitude of 1% story drift. The frequency of the sine wave is incremented from 0.1 Hz to 4Hz. Numerical damping is not considered for the analyses.

Analysis Results

The effects of dynamic loading become noticeable when the frequency of sine wave reaches 1Hz [Figure 2.15(a)]. In the hysteresis curve, the effects of dynamic load, which is defined here as a higher mode shaking of the CORE Damper, is seen when cables carry a small tension force and/or the speed of loading is high at zero displacement. The shaking of the damper attenuates as cables start to carry higher tension force.

The effects become severe as the speed of loading increases [Figure 2.15(b)]. Until the hysteresis force reaches the point where the CORE damper yields, the higher frequency force vibrations evident in the hysteresis curve remain at similar amplitudes.

In the post yielding range, the vibration attenuates rapidly as the force is limited by the yield strength of the damper.

Table 2.1 is a summary of the increase in the maximum system force and the maximum cable force. As the hysteresis curve indicates, the increments in forces are limited until the frequency of 1Hz and become noticeable for higher frequencies. In general, the effects of dynamic loading are larger in the local cable forces than in the global system behavior.

The analysis results indicate that the effects of vibration of the central device are very limited under very high speed loading since the effect is attenuated by the yielding of the CORE Damper which is consistent with the experimental results of tension only bracings under impact loading reported by Tremblay [Tremblay, 1996].

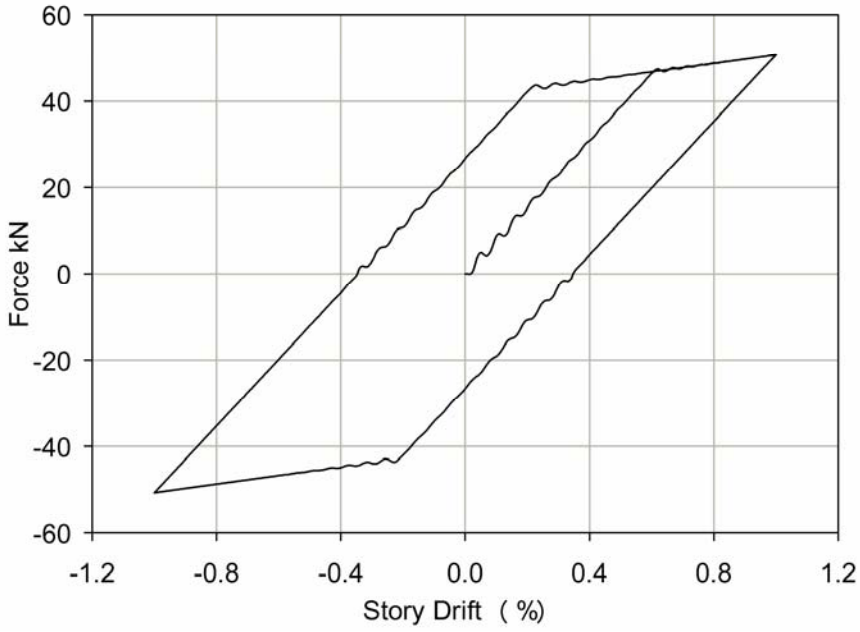

Fig 2.15(a):

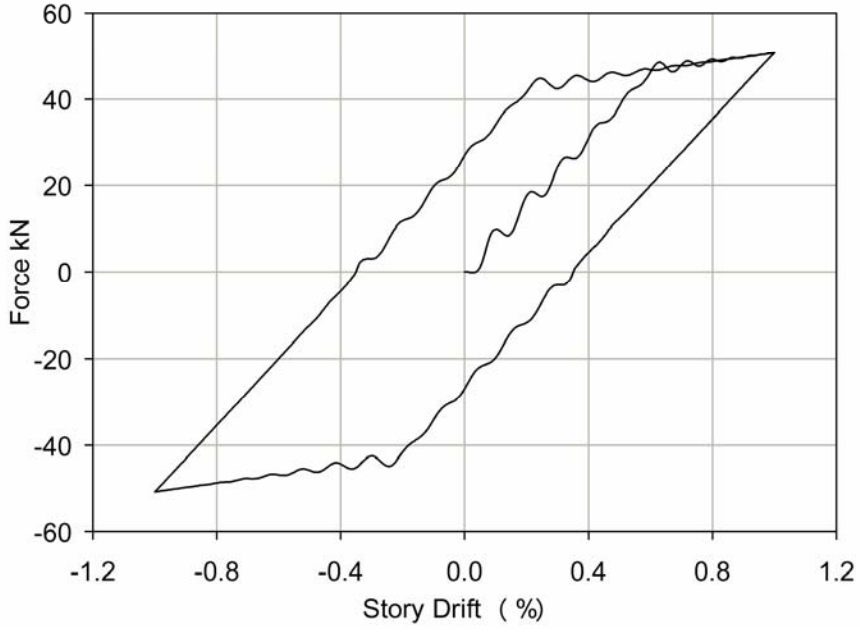

Fig 2.15(b):

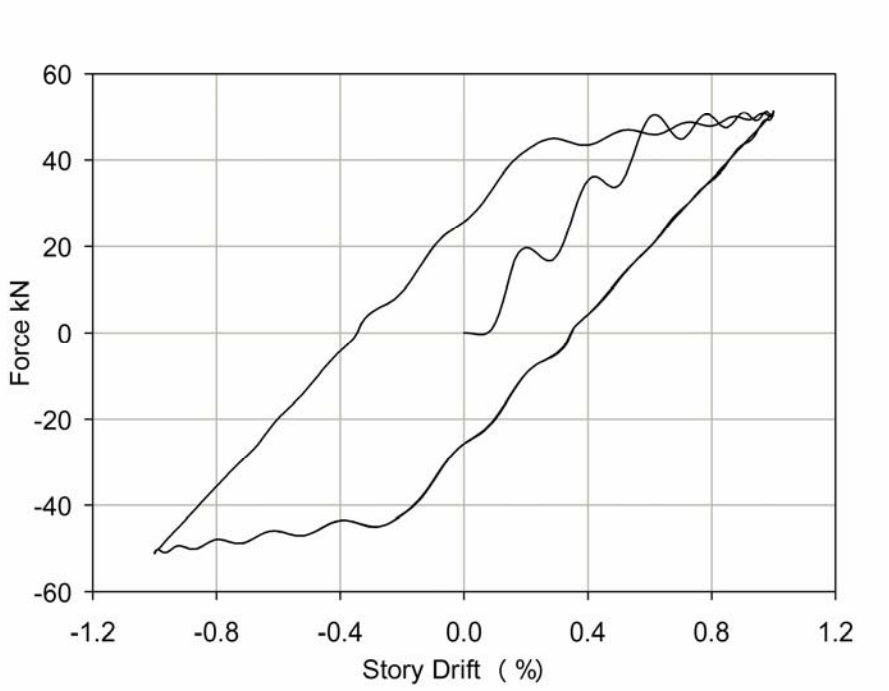

Fig 2.15(c):

Figure 2.15: Hysteresis under high frequency loading (a) 1Hz sine wave (b) 2Hz sine wave (c) 4Hz sine wave

Table 2.1: Dynamic effect in forces

Frequency of sine wave	*Max. shear force of system*	*Shear force increment from 0.001Hz*	*Max. cable force*	*Cable force increment from 0.001Hz*
Hz	kN	%	kN	%
0.001	11.40		29.80	
0.5	11.40	0	29.81	0.034
1.0	11.40	0	29.83	0.101
2.0	11.41	0.088	29.97	0.570
4.0	11.56	1.4	30.79	3.32

2.6 Re-Centering Bracing System

Background

For a special rehabilitation case where rapid repair/rehabilitation is necessary to minimize downtime in a building, an addition of re-centering capability has the benefit of reducing residual deformation as well as reducing the repair time for a particular story or bay in an existing building. Figure 2.16 shows the previously proposed re-centering systems which utilize post-tensioning forces of steel tendons [Ricles *et al.*, 2002; Christopoulos *et al.*, 2008.] These systems typically have hysteresis curves where the unloading curve returns to the origin. Other types of the re-centering system includes the system shown in Figure 2.16 which utilizes the unique pseudoelastic properties of nickel-titanium-based shape memory alloys (NITINOL) as a source of re-centering force [McCormick *et al*., 2007a and 2007b]. A cable made of numbers of NIINOL wires posses a pseudoelastic behavior up to 6% strain without residual strain when load is removed.

Here, a re-centering system with tension-only elements is considered specifically for the reduction of residual deformation at critical sections of existing buildings. This study analytically demonstrates the upgrading of an existing building whose primary lateral loading system is a tension-only bracing system with a slip-type hysteresis behavior. The re-centering capability is realized by the simple addition of NITINOL cables. The performance of the proposed system is evaluated through a nonlinear static analysis in the OpenSEES platform.

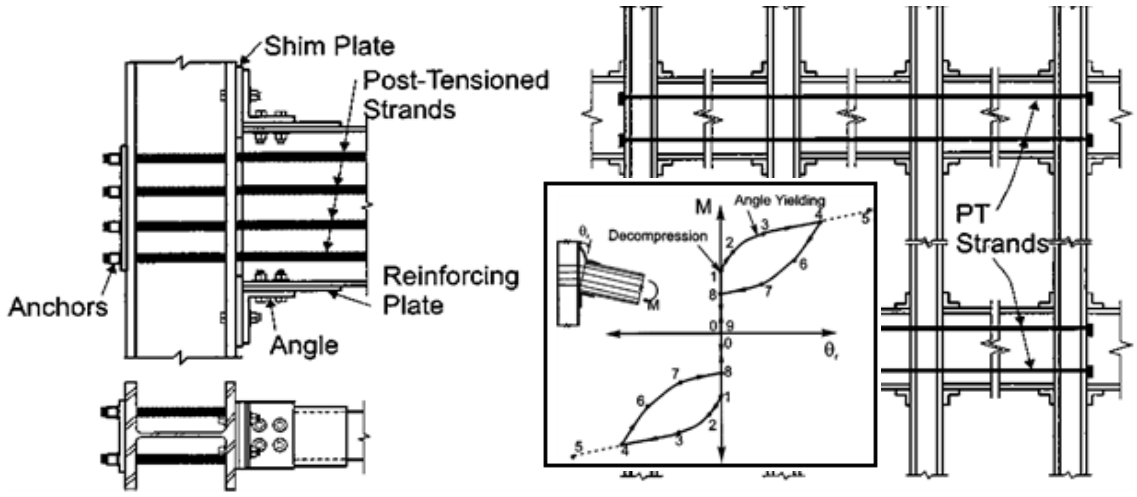

Fig 2.16(a):

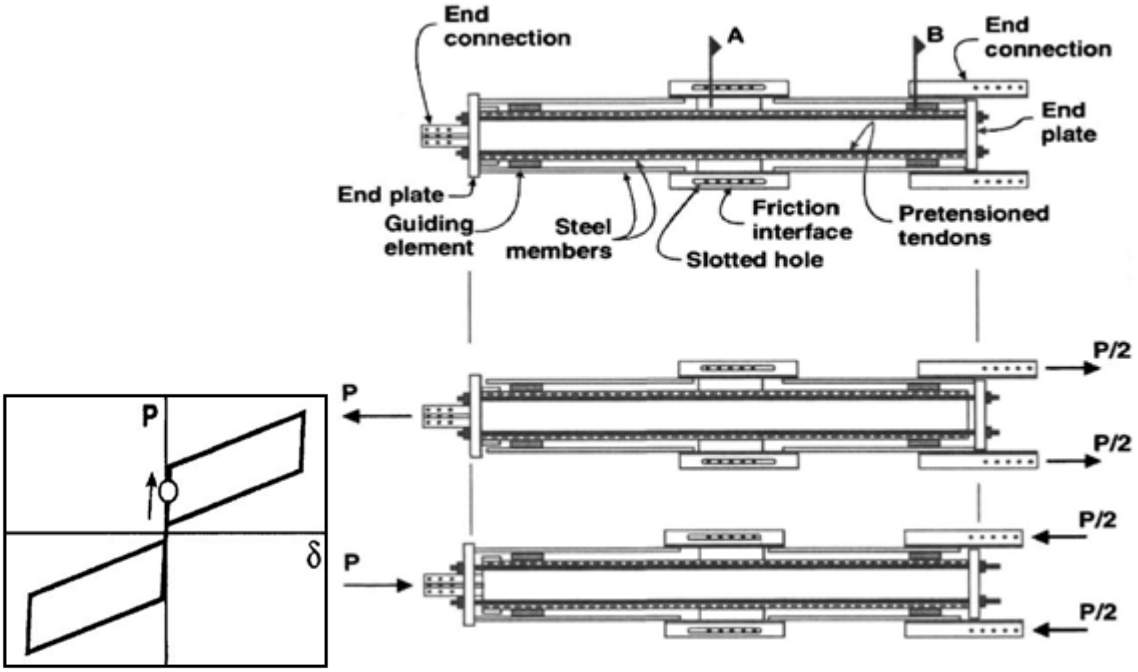

Fig 2.16(b):

Figure 2.16: Self-centering systems with post-tensioning force (a) self-centering system [Ricles *et al.*, 2002] (b) self-centering energy dissipative bracing [Christopoulos *et al.*, 2008]

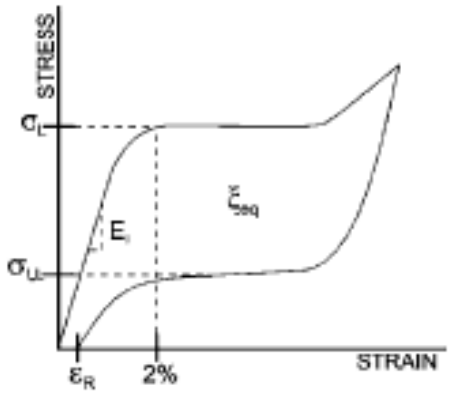

Fig 2.17(a):

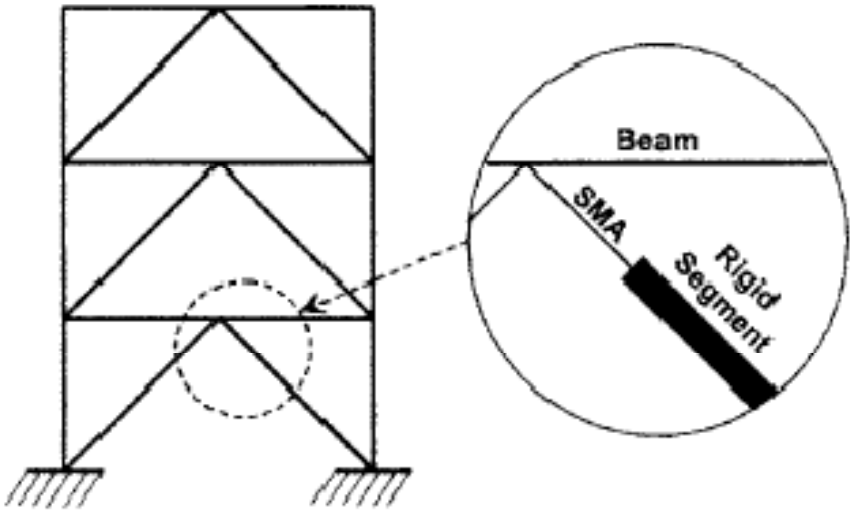

Fig 2.17(b):

Figure 2.17: Self-centering capacity with NITINOL (a) pseudoelastic force-strain curve (b) CBSF with NITINOL [McCormick, 2007]

Geometry

The proposed system is a variant of the CORE Damper bracing system, with steel cables and NITINOL cables placed in parallel. The geometry of the CORE Damper system is adopted for the example study although the approach is widely applicable to other type of tension-only bracing systems. Figure 2.18 shows the system configuration and the conceptual system behavior. The base system is similar to the CORE Damper system except that cables are connected only in one diagonal. Thus, the base system shows slip type behavior once the rotational spring yields. The NITINOL cables generate re-centering forces when the damper device exhibits a permanent deformation and the resultant system has the combined behavior of these two systems. The NITINOL cables are used in series with steel cables so that the resulting cable has larger stiffness and deformation is efficiently concentrated in NITINOL cables. The location where the NITINOL cables are connected in the center device is defined by a preliminary analysis as distance between the connections of the NITINOL cables become one third of the length of the rigid element.

In the system, the total area of NITINOL cables added is less than half of the area of steel cables and the strength and stiffness of the system are mainly those of steel cables. The contribution of the NITINOL cables becomes significant when the systems experiences large deformations and yielding of the rotational spring. The NITINOL cables contribute to system behavior in two main ways. One is the re-centering force generated from its unique pseudoelastic property and the other is the elastic stiffness when the base system loses its initial stiffness because of sagging in the steel cables.

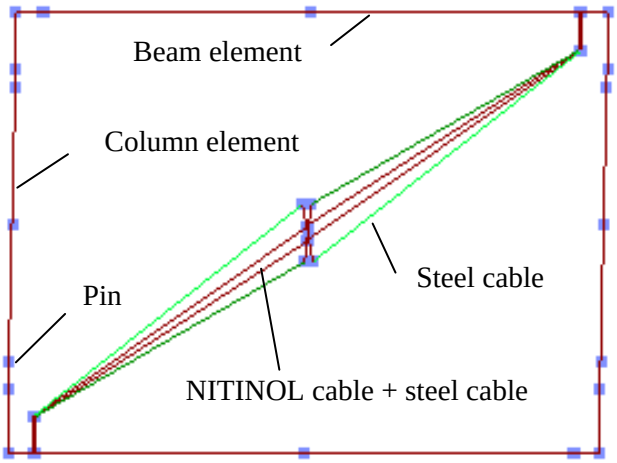

Fig 2.18(a)

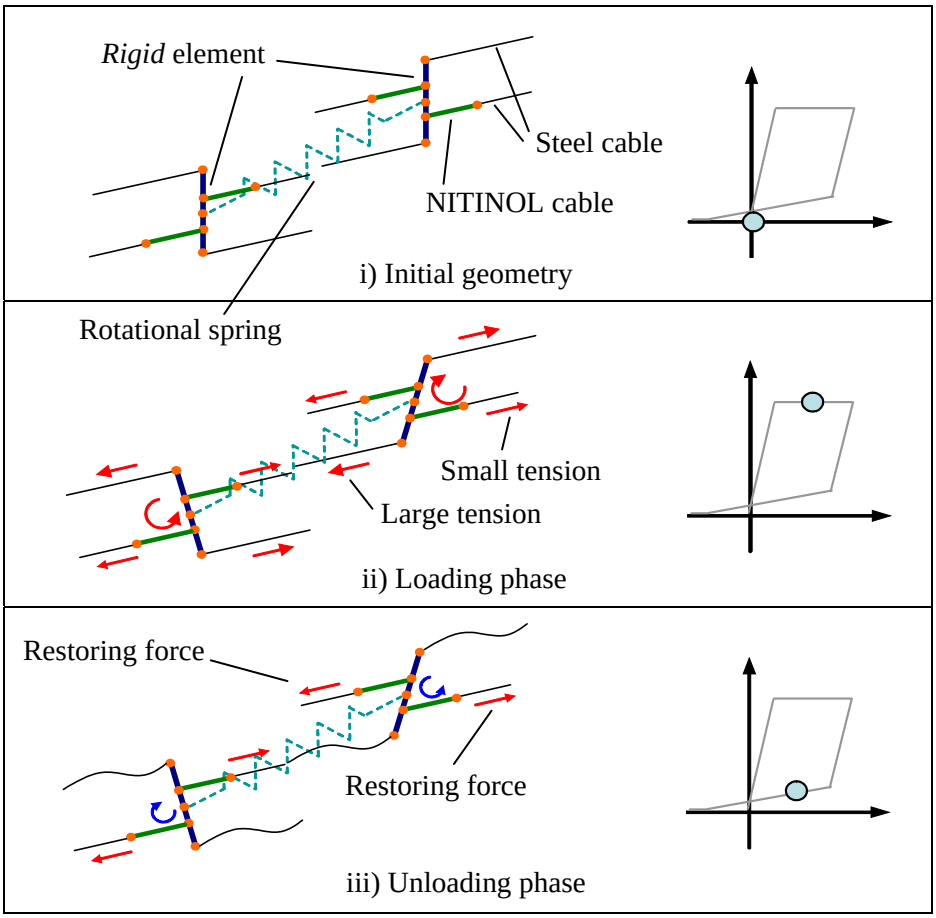

Fig 2.18(b)

Figure 2.18: Re-centering cable bracing system (a) geometry (b) conceptual behavior

Static Cyclic Analysis

An incremental quasi-static cyclic analysis was carried out using OpenSEES with amplitudes of 1, 2, and 3 % in story drift. The hysteresis of the CORE Damper obtained from the FE analyses is used for the hysteresis of the central rotational spring. The force-strain relationship obtained from a cyclic loading test of a NITINOL cable with the area of 0.5cm^2 is implemented in a SMA material model in OpenSEES [Figure 2.19]. In the analysis, the length of the NITINOL cable part is set to 167cm which is one third of the length of the steel cables. As shown in Figure 2.20, the proposed system successfully shows the expected re-centering behavior. The re-centering force of approximately 20kN is obtained by adding the four NITINOL cables with the area of 0.5cm^2. Note that the generated re-centering force is solely controlled by the area of the NITINOL cables.

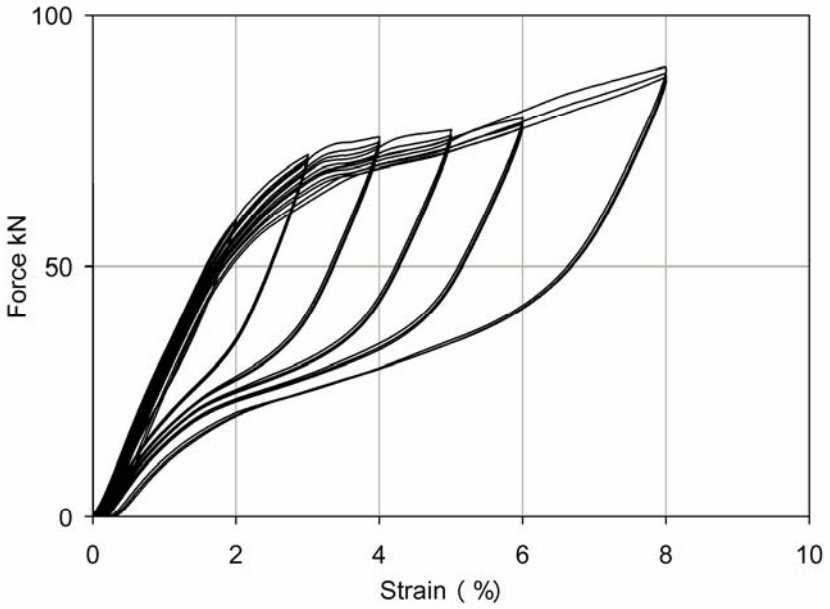

Figure 2.19: NITINOL cable test result (area of cable = 0.503 cm^2)

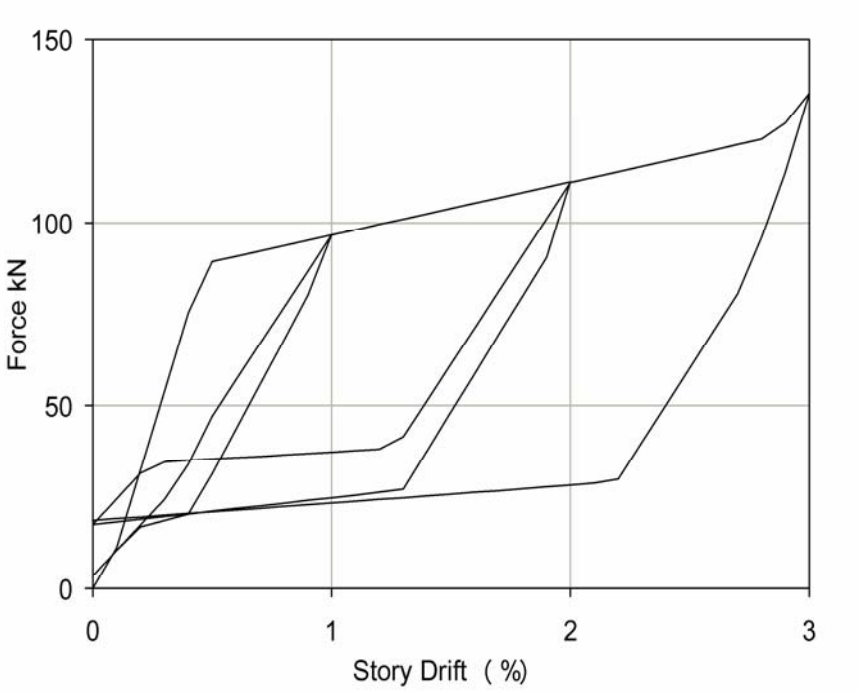

Fig 2.20(a):

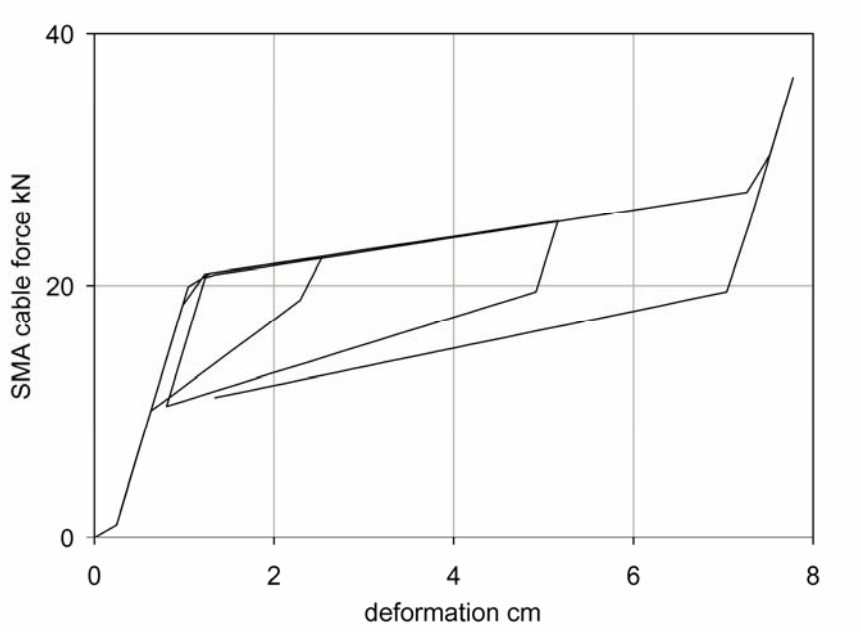

Fig 2.20(b):

Figure 2.20: Analysis results for re-centering system (a) system shear force (b) SMA cable force

2.7 Summary

In this Chapter, the concept and behavior of a cable cross bracing system with unique geometry was presented. The proposed system provides stable energy dissipation until very large deformations occur by taking advantage of permanent rotations in a central energy dissipating device. The central device, referred to as the COuples REsisting damper (CORE Damper), dissipates energy through the bending and yielding of mild steel plates and does not require periodic maintenance.

The concept of the proposed bracing system was first validated through nonlinear static cyclic analyses. The analyses provided the approximate strength demand, required deformation capacity and optimal shape for the CORE Damper. The details of the CORE Damper were designed carefully by using a general purpose finite element analysis program, ABAQUS as a design tool. The FE analyses showed that the CORE Damper could sustain a stable, bi-linear hysteresis curve until the rotation corresponding to the story drift much larger than that specified in current design guidelines.

The dynamic behavior of the proposed system with the developed CORE Damper was examined to see the effect of high-speed loading into on the performance of the system. The increments in local and global forces are limited until the frequency of 1Hz and become noticeable for higher frequencies. In general, the effects of dynamic loading were larger in the local cable forces than in the global system behavior, while the effects were limited even with very high speed loading because the effects were attenuated by the yielding of the damper device.

Utilizing the developed CORE Damper, the addition of re-centering capability to an existing bracing system is considered. The re-centering system is specifically for the

reduction of residual deformation at critical sections of existing buildings. By simply adding extra cables made of shape memory alloy (NITINOL) to the same diagonal in the base system, the system is upgraded as a re-centering system. The concept of the re-centering system is validated through non-linear static analyses in the OpenSEES platform.

CHAPTER 3

PROOF-OF-CONCEPT TESTING OF "CABLE BRACING-CORE DAMPER SYSTEM"

3.1 Introduction

The concept of the "Cable Bracing-CORE Damper system" presented in Chapter 2 was examined through a full scale experiment. The experiment had been carried out using a testing frame newly constructed in the structural laboratory at the Georgia Institute of Technology. The performance of the prototype system was examined under quasi-static cyclic loading. During the test, the displacement of an actuator which connected to the top beam of the testing frame was controlled with the loading protocol specified in the AISC guideline. The local and global behavior of the specimen was evaluated through digital measurements and visual inspections. The test was repeated for twice by replacing the steel plate energy dissipaters (SPEA) in the CORE damper. For the second test, the boundary condition at the bolt connections in the CORE Damper was slightly modified. Finally, the obtained test results were compared with the results predicted in the preliminary analyses.

3.2 Experimental Setup

A new testing frame constructed at the Georgia Institute of Technology is a portal frame with pins at its four corners and is capable of testing sub-assemblages of low-to-mid rise steel buildings under quasi-static earthquake loads [Figure 3.1(a)]. The maximum capacity of the testing frame is 2000kN. The actuator applies a quasi-static or low frequency loading rate (0.05 to 0.2Hz), through the ± 254mm displacement of the actuators. The drift capacity of the testing setup was set to 0.07 radians for positive deformation (push) and 0.04 radians for negative deformation (pull) to enable a monotonic loading of specimens after a scheduled cyclic loading. A MTS 407 stand alone controller is the primary controller of the system [MTS 2000]. The other main components of the frame are 735mm-W36x160 beams, 457mm-W14x150 columns, and specially assembled frictionless pin clevises [Figure 3.1(b)]. The bottom beam was post tensioned to the strong floor by 24 large diameter DYWIDAG bars. The top beam was braced to the strong wall to constrain out-of-plane deformation of the testing frame. The pin clevises are capable of supporting 1500kN of radial force with minimum friction force and its force sensing capability provides accurate boundary information for the test system. The detailed drawing for the main components of the testing setup can be found in Appendix A.

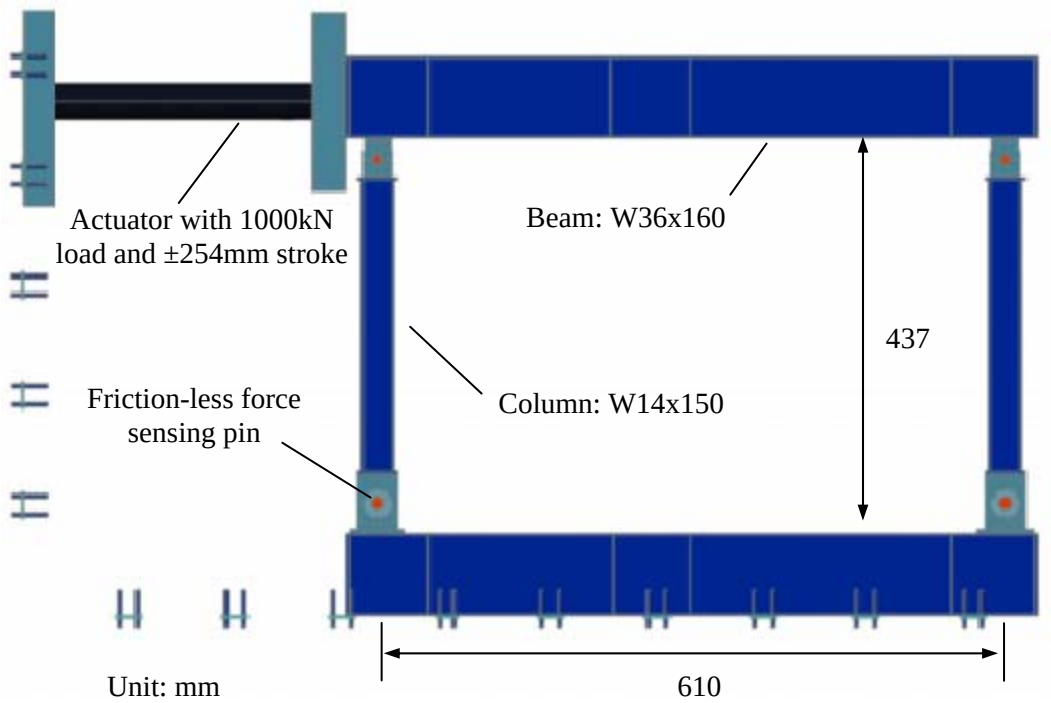

Fig 3.1(a):

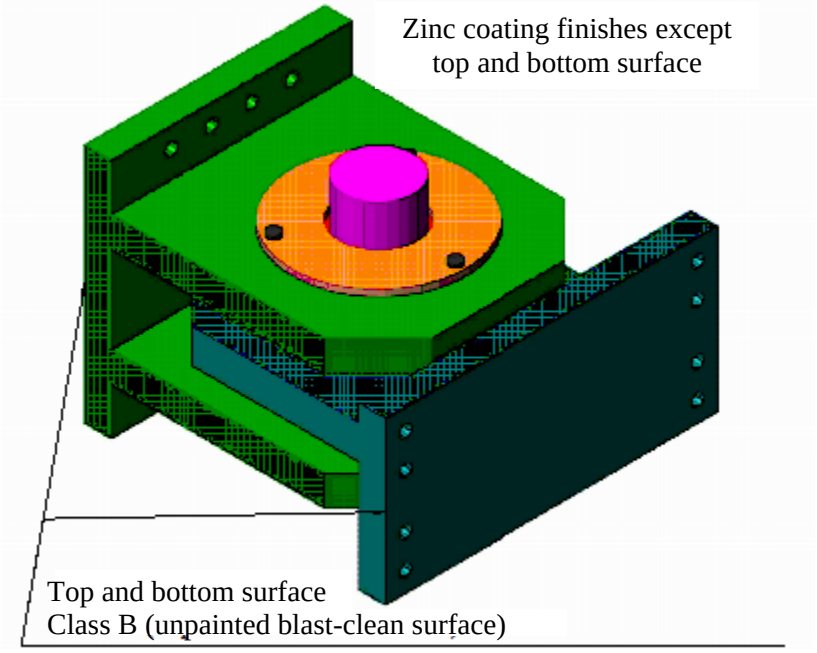

Fig 3.1(b):

Figure 3.1: Testing setup installed in Georgia Tech structural lab (a) overall configuration (b) frictionless pin clevis designed

3.3 Specimen and Instrumentation

The assembled CORE Damper was installed to the frame through 9/16" (M14) 6x19 IPS IWRC bright steel wire cables [FED RR-W-410E, 1999], 7/8"-6" (M22-150mm) jaw-jaw turnbuckle [ASTM F1145-92, 1992] and padeyes. The dimensions of the components of the prototype specimen are shown in Figure 3.3. In the cover plate, the loading part, where SPEAs were connected by high strength bolts, were welded by complete penetration welding and holed with a 7/8" (M22) UNC-9 thread tap. The spacers placed between SPEAs were two of 64mm-HSS 2"x3"x1/4"x1/4". Two 1" (M26) threaded rods were used to apply post-tensioning force on the outer surface of the SPEAs. The cables, turnbuckles and padeyes [Figure 3.4] were designed to remain elastic with the safety factors of these elements vary from 1.5 to 2.0 with respect to the core damper.

The rotations of the cover plates of the CORE Damper were evaluated from the horizontal displacements measured at the upper and lower ends of the plates [potentiometers P1-P4 shown in Figure 3.5(a)]. Two more potentiometers were installed to measure the vertical and out-of-plane deformation of the CORE Damper. Hand-made load cells were installed to the ends of lower four diagonal cables [Figure 3.5(b)]. The manufacturing of the load cells are described in Appendix A. Taking advantage of the symmetry in the system, the forces in the upper four cables were estimated from those in the lower four cables. These load cells had calibrated in advance the test as their sensitivity in the range of interest summarized in Table 3.1. LVDTs attached to padeyes checked the deformation against the testing frame. Strain gauges were attached on the surface of a SPEA to estimate the yielding point of the plate and the axial force along the

longitudinal axis. The data acquisition system consists of National Instrument LabView^{TM} software, a desktop PC platform, a PCI express DAQ, and a SCXI signal conditioning [National Instruments, 2003].

A cyclic test of the prototype system was carried out after installing pre-stressing force in the cables by tightening turnbuckles. The applied pre-stressing force was checked using the developed load cells for cables.

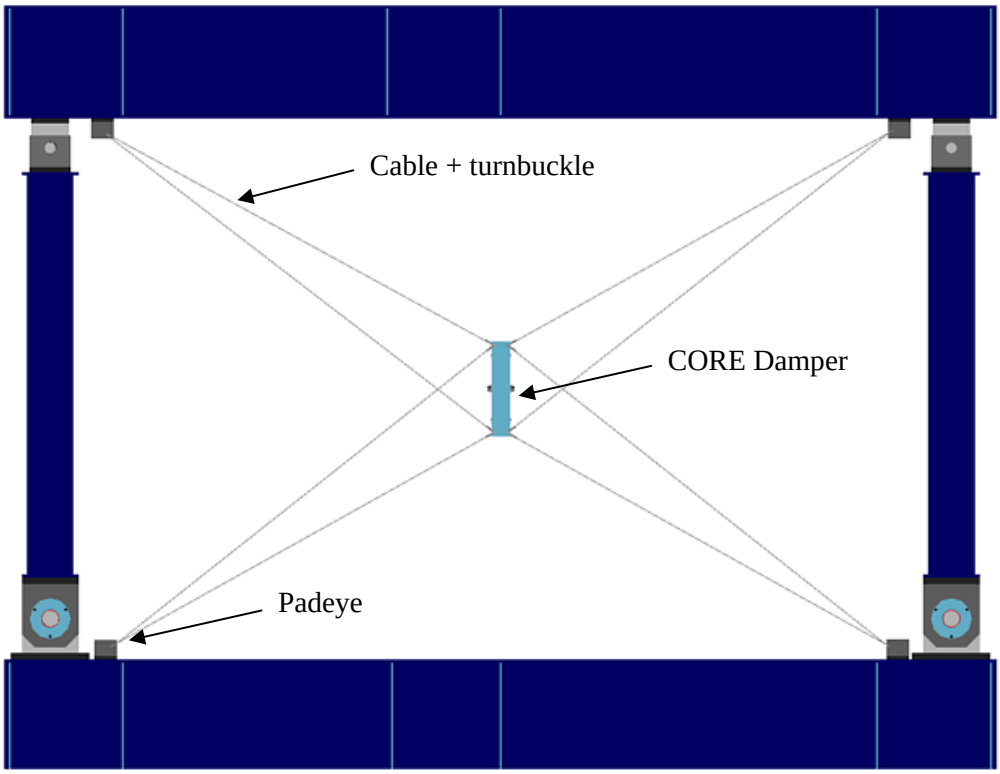

Figure 3.2: Installed specimen

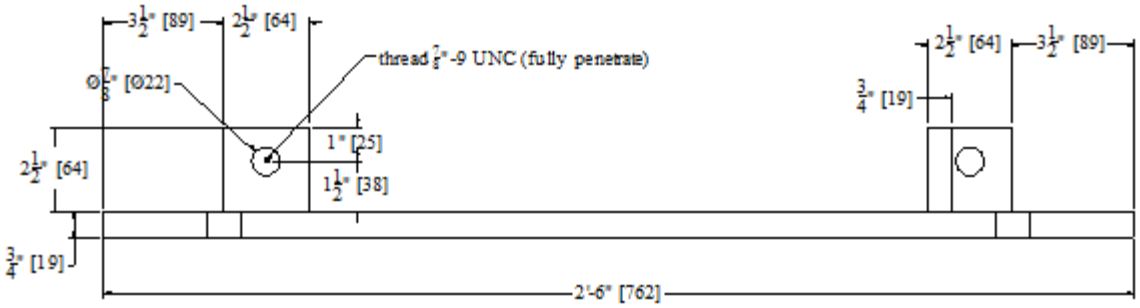

Elevation

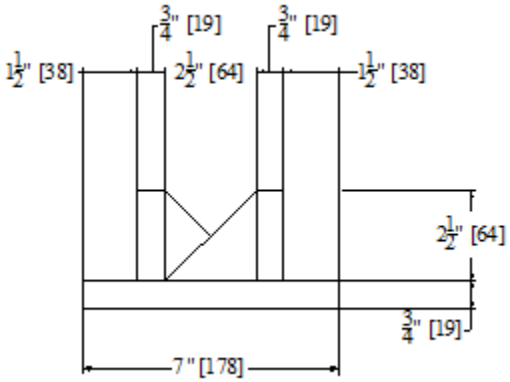

Side

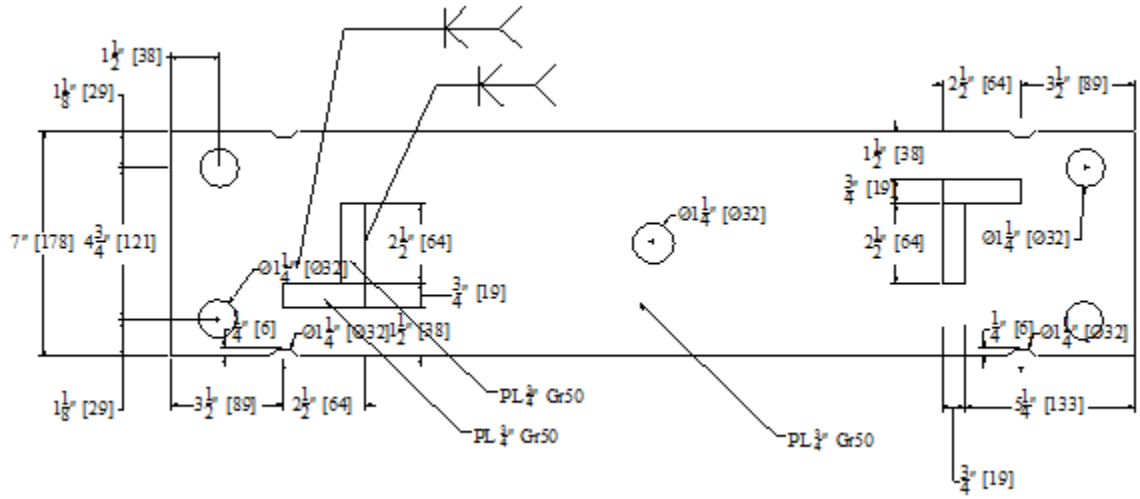

Plan

Fig 3.3 (a)

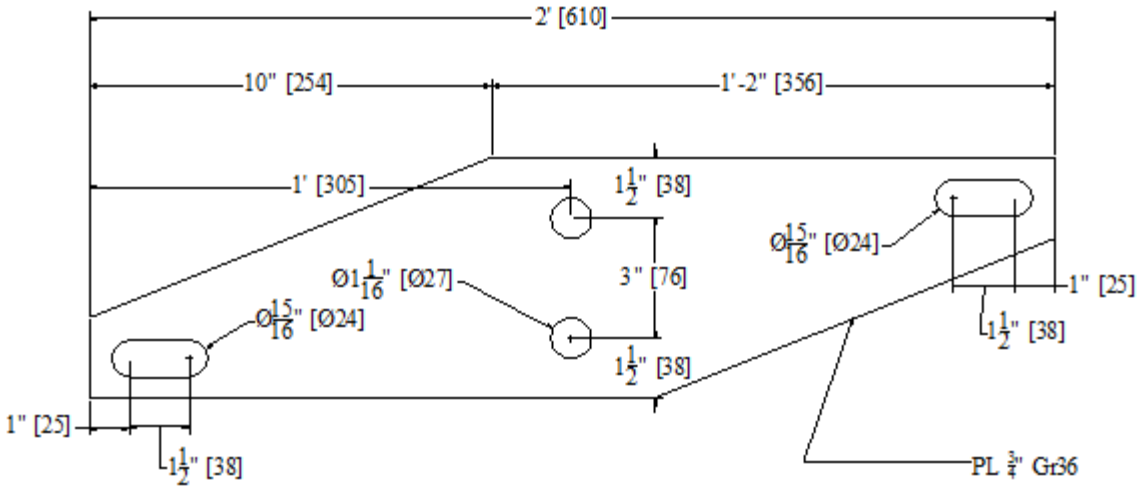

Fig 3.3 (b)

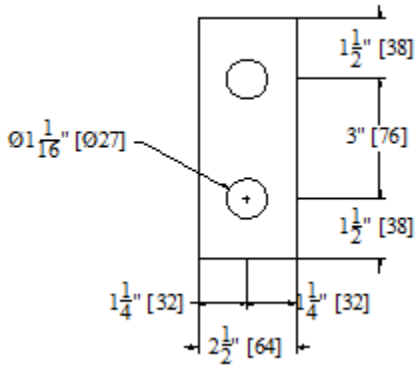

Fig 3.3 (c)

Figure 3.3: Dimension of CORE Damper (a) cover plate, Gr.50, thickness=19mm (b) SPEA, Gr.36, thickness=19mm (c) steel plate washer, Gr.36, thickness=19mm

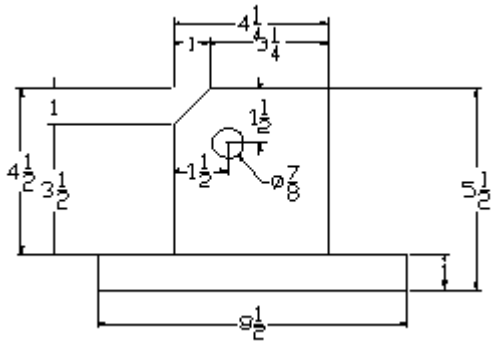

Fig 3.4(a):

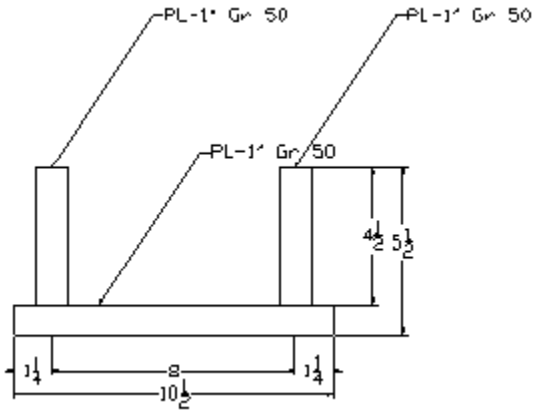

Fig 3.4(b):

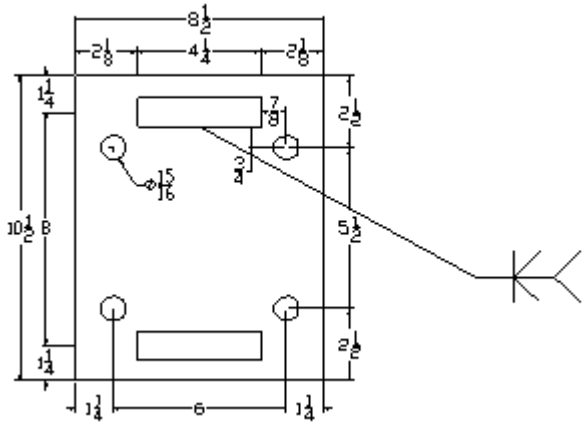

Fig 3.4(c):

Figure 3.4: Dimension of padeye, Gr. 36 (a) side (b) back (c) plan

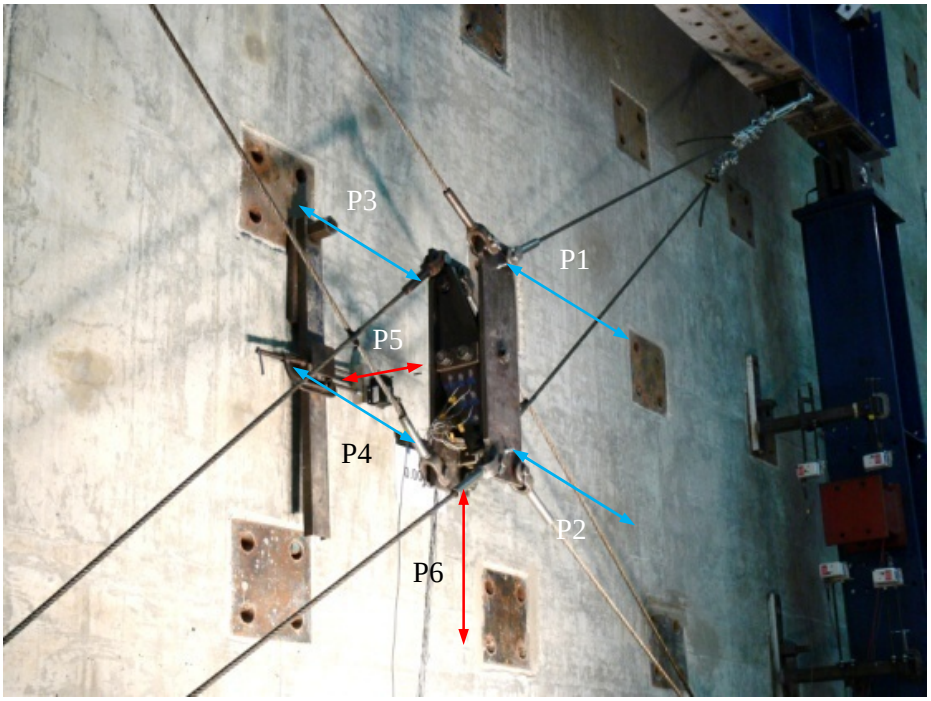

Fig 3.5 (a):

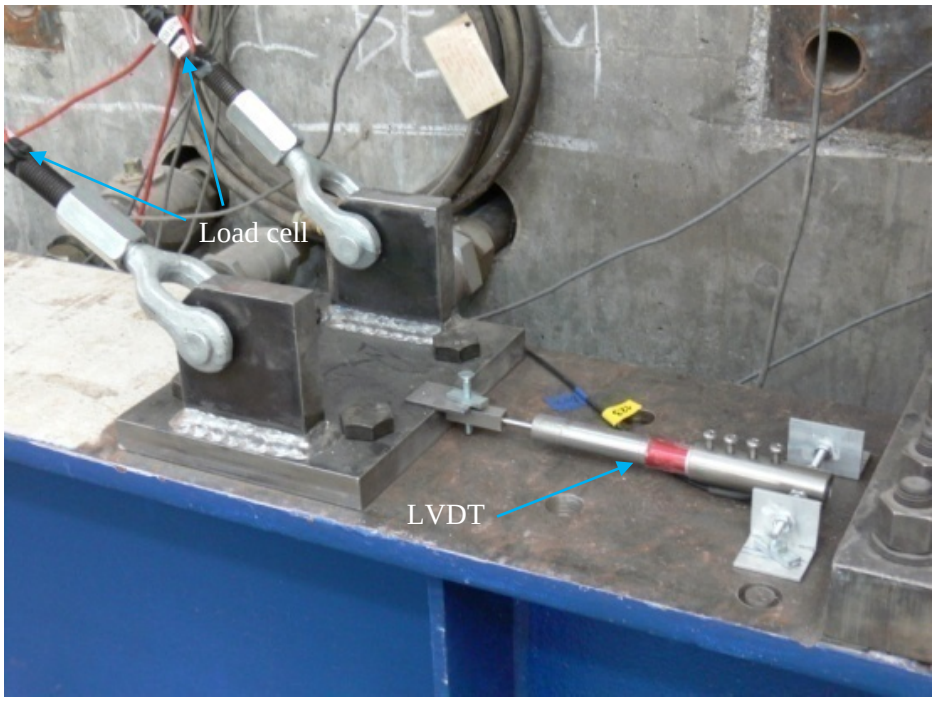

Fig 3.5 (b):

Figure 3.5: Specimen and location of measurements (a) CORE Damper with potentiometers (b) cable load cells and LVDT

Table 3.1: Cable load cell calibration

Load Cell	*Sensitivity*		
	Run1	Run2	Average
	lb/mV	lb/mV	lb/mV
LC1	826.7	822.9	824.8
LC2	862.5	870.2	866.4
LC3	829	827.9	828.5
LC4	835	832.9	834.0

Note: The sensitivities are the averaged values under 3kip to 15kip load with excitation voltage as +10V.

3.4 Material Properties

Table 3.2 shows the coupon test results for a steel plate energy absorber (SPEA) in the CORE Damper. The obtained material properties were pretty standard for A36 mild steel.

A tensile test of the cable was conducted at the Georgia Tech structural laboratory using MTS 810 universal testing system with MTS 647.25 hydraulic wedge grips; the maximum static force capacity of 333kN (75kip) and dynamic force capacity of 200kip (55kip). In the test, the end loops which made at the both ends of cable using eight of M12 clips and steel sheaves were connected to custom made grips using M26 high strength bolts. Eventually, theses grips were grabbed by the hydraulic wedge grips of the testing system. The primary purpose of the testing was to determine the prestress force needed to remove any initial slack of cables; the test was not intended to the calculation of the stiffness for the cable.

Figure 3.6 shows the relationship between the applied tensile load and the displacement of the cross head in the testing machine. The force require to remove initial slackness in the cable was around 9.1kN (2kips). For further loading the loop of the cable started to rotate involving detwisting of the cable in elastic range since the boundary conditions at grips were similar to universal joints. Eventually, the test was terminated due to the slippage observed at the end loops.

Table 3.2: Material properties of SPEA

Coupon	*Thickness*	*Yield stress*	*Tensile stress*	*Elongation*
	mm	MPa	MPa	%
S1	18.80	269.0	405.9	33.3
S2	18.80	267.7	404.7	31.9
average	18.80	268.3	405.3	32.6

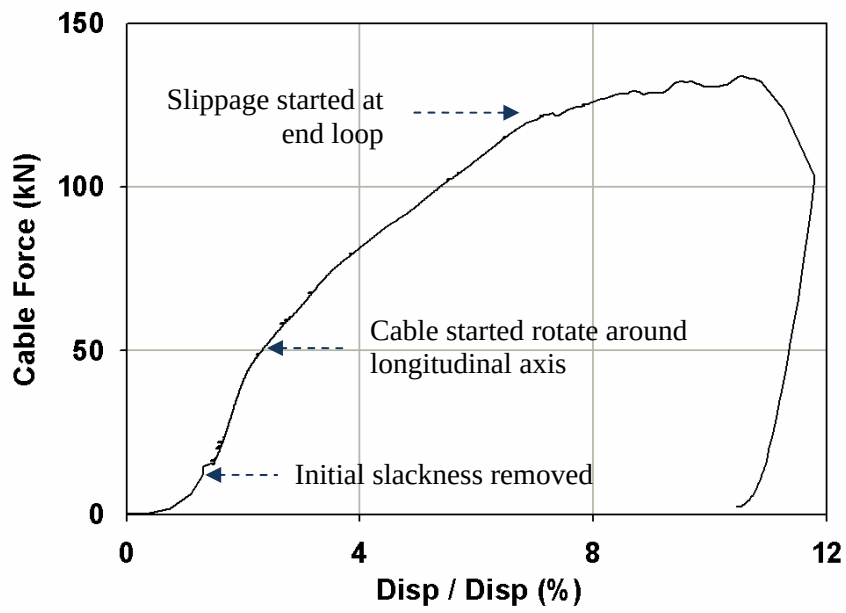

Figure 3.6: Tensile test of cable

3.5 Loading Sequence

The displacement was manually controlled using *Ramp function* in the function generator equipped in the MTS 407 controller [MTS, 2000]. The applied displacement was compared with the actual deformation monitored at the top beam. The loading sequence was the one for the testing of beam-column connections specified in the AISC provision [Table 3.3; AISC, 2007]. The loading was repeated for 6 cycles until the 0.0075rad. interstory drift, for 4 cycles with the 0.01rad. interstory drift and 2 cycles for the rest. After the scheduled loading cycles completed, the loading was continued monotonically until 0.05rad. The loading rate was 12.7mm (0.5 in) per minute for the small amplitudes, 0.00375 to 0.0075rad., and 25.4mm (1.0in) per minute for the large amplitudes, 0.01 to 0.04rad. For monotonic loading, the loading rate was increased to 50.8mm (2.0in) per minute.

Table 3.3: Loading sequence

Run number	*Interstory drift* rad.	*Number of cycles*
1	0.00375	6
2	0.005	6
3	0.0075	6
4	0.01	4
5	0.015	2
6	0.02	2
7	0.03	2
8	0.04	2

3.6 Typical Test View

The first test was used to check the overall system and its behavior; after this test minor adjustments were made to the device and the following discussion will focus on the behavior of the second specimen, unless otherwise specified.

At every target interstory drift level, the behavior of the system was investigated through a visual screening and the instrumentation data. Figure 3.7 shows the typical deformed shape of the overall system and the CORE Damper. The testing view was recorded by two video cameras; one was for deformation of the entire system and another was for the deformation of the CORE Damper. The condition of the specimen was continuously monitored by the data from measurements and the eye inspection at the end of each half loading cycle. The CORE Damper shifted horizontally with its center remained in plane of the bracing system. The padeyes did not slip through the entire loading.

Figure 3.8 shows the behavior of the CORE Damper at various loading levels. As the drift level increased, the relative rotation between the front and back cover plates increased. The rotation became notable at the 0.0075rad. cycle when the SPEAs started to yield. The cracking sound of the mill scale on the surface of the SPEAs also started at the 0.0075rad. cycle. The Lüders' bands on the surface of SPEAs became visible at the 0.01rad. cycle and continued to spread over the entire region of the plates. The slipping of bolts became noticeably audible at the 0.015 rad. cycle and became constant after 0.02 rad. loading cycles. A large amount of the mill scale flaked at large deformation cycles.

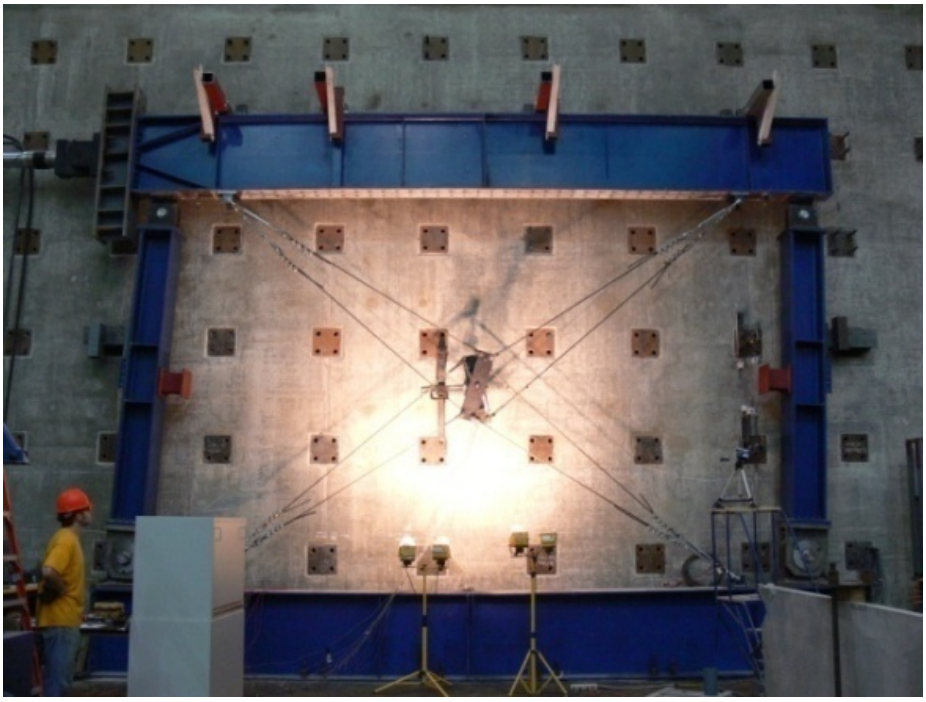

Fig 3.7(a):

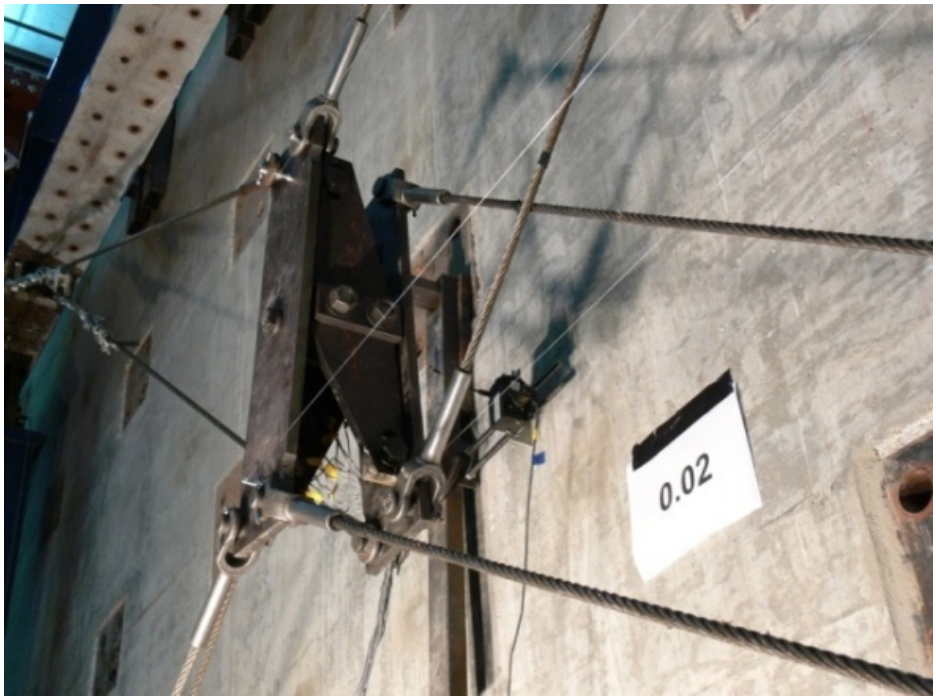

Fig 3.7(b):

Figure 3.7: Test view (a) entire view of testing setup (b) lookup view of CORE Damper

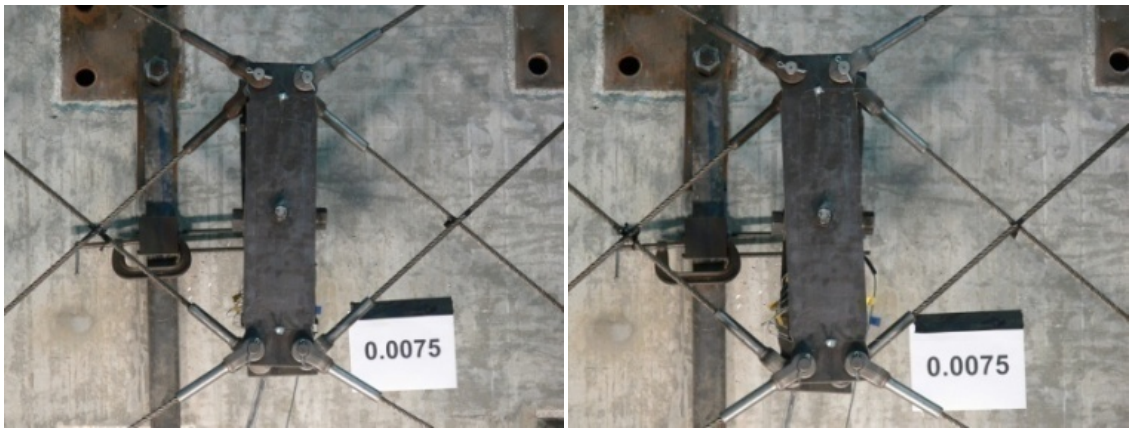

Fig 3.8(a):

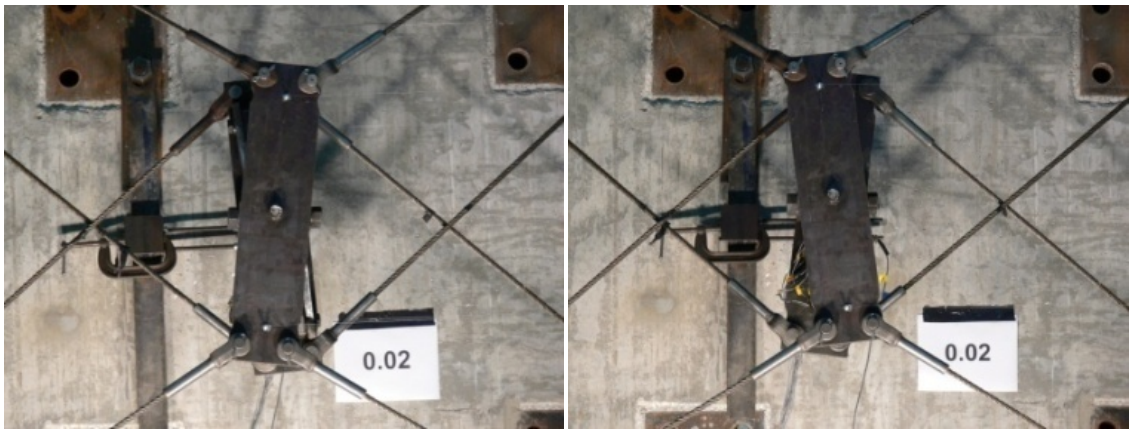

Fig 3.8(b):

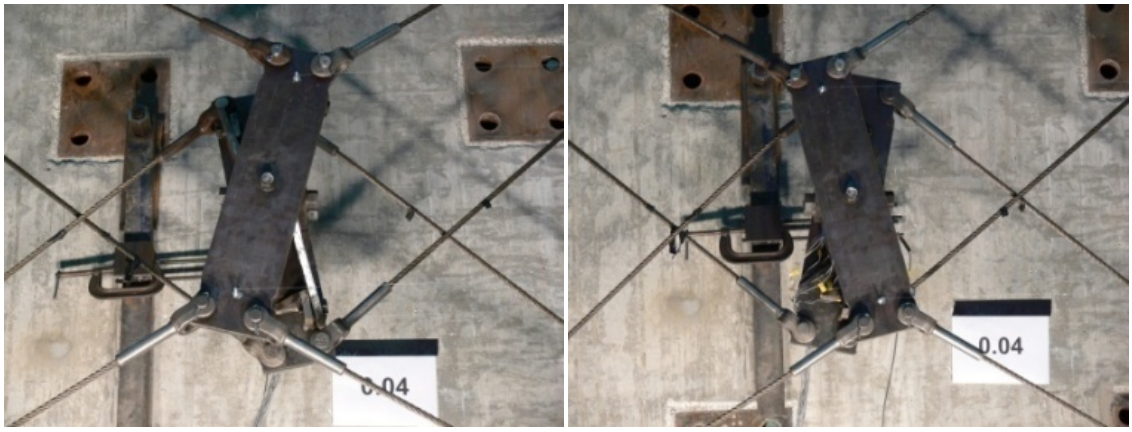

Fig 3.8(c):

Figure 3.8: CORE Damper in inward and outward deformation mode (a) 0.75% story drift (b) 2% story drift (c) 4% story drift

3.7 Test Results

The test was repeated for twice by replacing the steel plate energy dissipaters (SPEA) in the CORE damper. For the second test, the boundary condition at the bolt connections in the CORE Damper was slightly modified. The evaluation of the global hysteresis behavior and local behavior hereafter focuses on the results obtained from the second test. The results of the first test is showed later in this section along with the discussion on the effect of the boundary condition.

Hysteresis Behavior

Figure 3.9(a) shows a base shear versus story drift relationship. The system successfully showed a stable bi-linear behavior without any strength deterioration until the end of the loading. Given the same amplitude, the maximum force and minimum force at zero displacement at any one cycle were almost same, i.e. no cyclic effect exited for the same amplitude. The post yielding stiffness in the outward deformation mode became slightly higher than that in the inward deformation mode when the bolts at the connections started to slip with audible sounds at the 0.015rad. cycle. The post yielding stiffness slightly increased after 0.025rad. when the bearing force at the connections developed with slippage became significant. In the outward deformation mode, it was also notable that the post yielding stiffness in the second cycle reduced from that in the first cycle due to the some release of the bearing force at the connections.

Figure 3.9(b) is the enlarged hysteresis curve up to 2% story drift. The dotted line is the monotonic loading curve constructed from the OpenSEES blind analysis implementing the CORE Damper hysteresis curve obtained ABAQUS analysis. The analyses were executed for the outward deformation and the inward deformation

separately using the material properties of the SPEAs from the tensile coupon tests. The analysis predicted the elastic stiffness for the both deformation directions very well. The yielding strength in the experiment was slightly smaller but close to that predicted in the analyses for the both deformation directions. To obtain a post-yielding stiffness closer to that in the experiment, the finite element model should be further improved.

Deformation in Local Elements

The rotation history of front and back cover plates is shown in Figure 3.10(a). The rotation of the front cover plate was approximately 25% larger than that of the back cover plate due to the nature of the geometry as the cables connected to the front plate were shorter than those connected to the back plate. The difference in stiffness of the cables resulted in the difference in cable forces and thus resulted in the overall rotation of the CORE Damper [see Figure 2.5(a)].

The relative rotation between two cover plates was approximately 0.4rad. at the 3% story drift. This result was consistent with the prediction in the preliminary analyses. The maximum cable force observed during the specified cyclic loading was 60kN and was a half of the capacity defined as the slip critical force at their end loops.

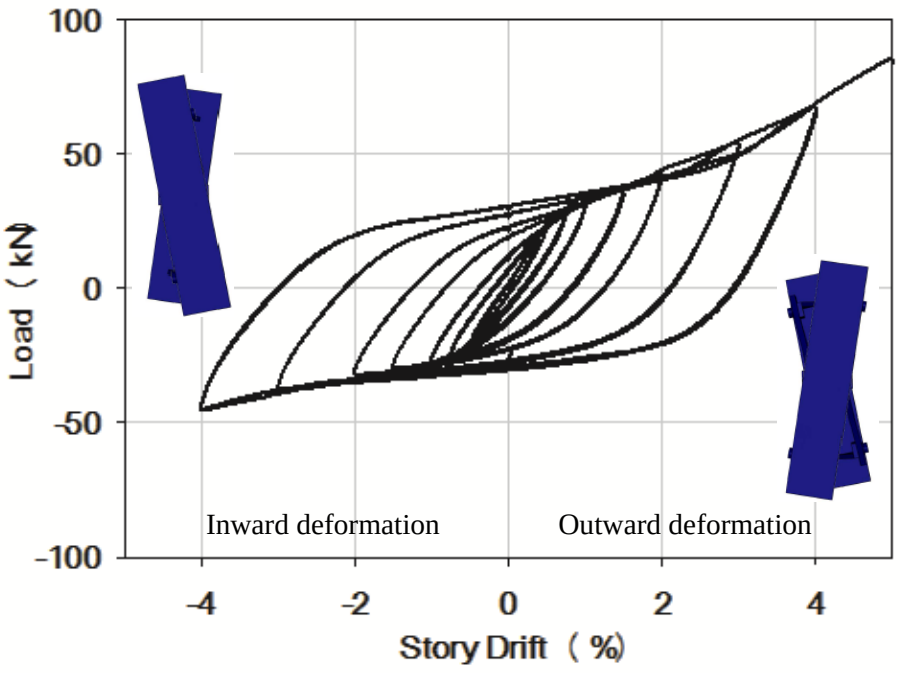

Fig 3.9(a):

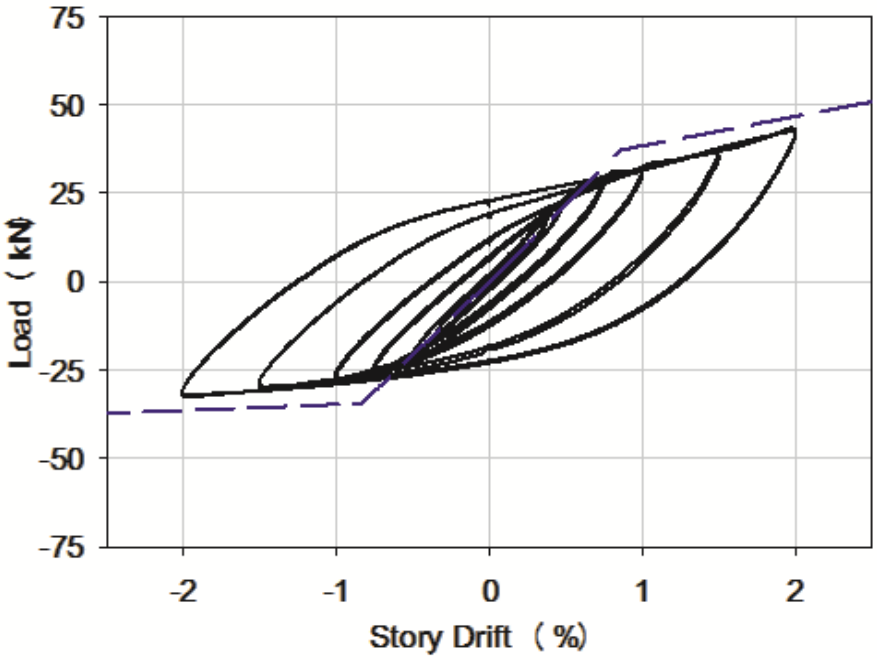

Fig 3.9(b):

Figure 3.9: Hysteresis behavior (a) overall behavior (b) system behavior up to 2% story drift compared with monotonic curve predicted from blind analysis

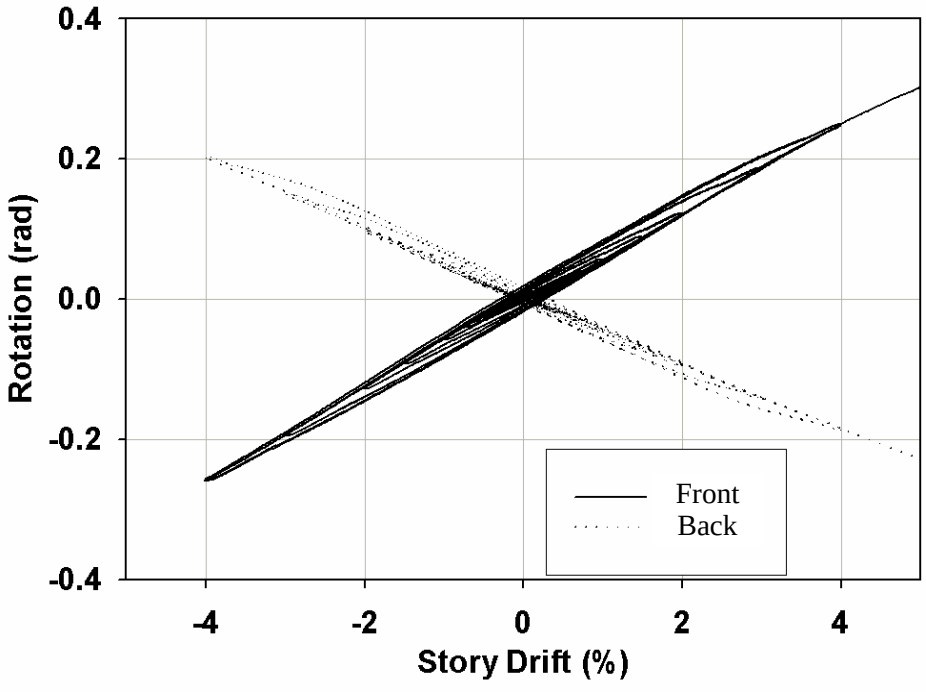

Fig 3.10(a):

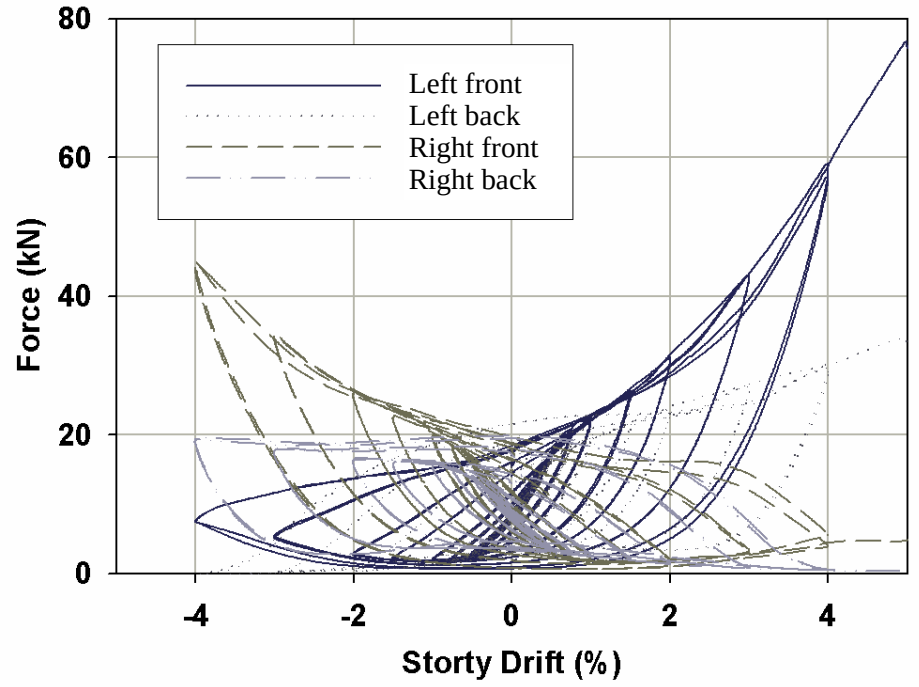

Fig 3.10(b):

Figure 3.10: Local behavior (a) rotation history of cover plates (b) cable force history

Effect of Condition at Connection

Figure 3.11 shows the comparison between the first and second specimens up to 2% story drift. In the second specimen, extra circular washers were placed between the inner surface of the SPEA and the loading surface of the cover plate to obtain closer boundary conditions in the outward and inward deformation modes. For the first specimen washers were only installed between the outer surface of the SPEA and bolt heads. A larger post-tensioning force was applied at the middle part of SPEAs to restrict the in-plane rotation of the SPEAs. The difference between the strength in outward and inward deformation modes decreased in the second specimen compared to those in the first specimen. The second specimen showed fatter hysteresis loops in the outward deformation mode.

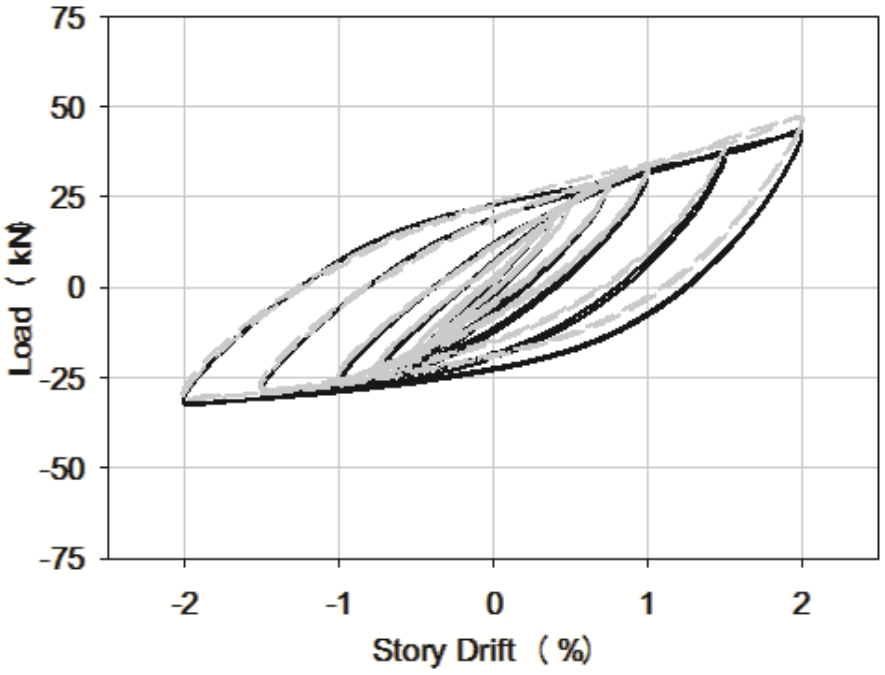

Figure 3.11: Effect of boundary condition at loading point

Surface Strain and Axial Load in SPEA

The surface strain history of the SPEA is shown in Figure 3.12 until the strain exceed the value corresponds to the yielding strain of steel, 2000με. The strain values are plotted separately depends on the location of measurements [see Figure A.6]. The gauges S1-S7 and S11-S17 were placed on the inner and outer surface of SPEA, respectively. The gauge S5 was damaged during the assembly of the CORE Damper and did not work properly. The yielding strain was reached first at the part close to the center washer during the 0.0075rad. cycle. The strain at the intermediate and loading part also reached to the yielding value during the 0.015rad. and 0.04rad. cycles, respectively. The strain remained in elastic range at the loading part. When the values in the two deformation mode were compared, the values at the center part were higher in the outward deformation mode than in the inward deformation mode [Figure 3.12(a)]. This was opposite for the values at the loading part [Figure 3.12(c)].

The sign of the strain values on the same surface, i.e.; S1-S7 or S11-S17, were consistent in one deformation mode. This indicated that the SPEA deformed in single curvature rather than in double curvature. At the loading and intermediate part, the absolute strain values were pretty similar on the inner and outer surface, for example, S4 and S14. These values differed at the center part due to the existence of slight twisting moment. The axial strain in the SPEA was evaluated at the loading point where no twisting moment exists [Figure 3.13]. The strain started to increase after 2% story drift mainly due to the bearing force induced at the loading point but successfully remained small under large deformation. It was also notable that the axial strains were only developed in tensile (positive) direction.

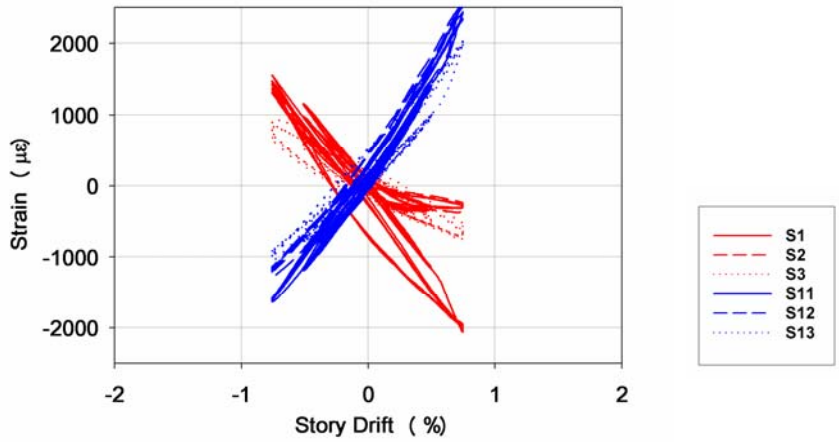

Fig 3.12(a):

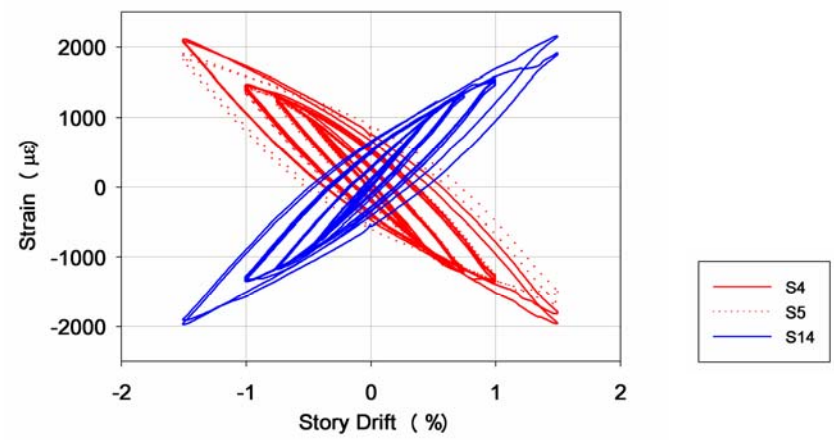

Fig 3.12(b):

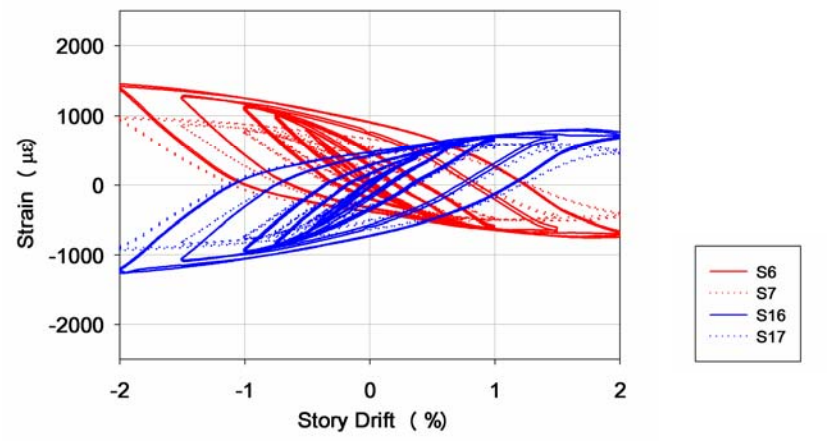

Fig 3.12(c):

Figure 3.12: Strain at SPEA surface (a) center part (b) intermediate part (c) loading part

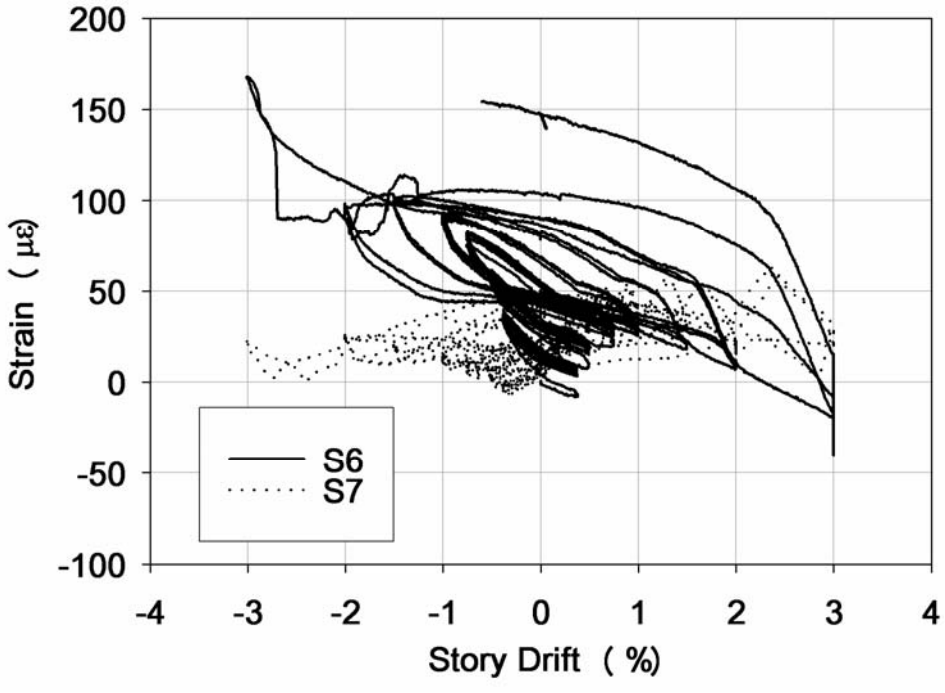

Figure 3.13: Axial strain in loading part of SPEA

Limit State and After Test Observations

The system exhibited stable behavior under large deformation, while the CORE Damper remained below the limit state condition, which was defined as contact between the two SPEAs in the inward deformation mode [Figure 3.14(a)]. The in-plane rotation of the SPEAs started after 0.04rad. in conjunction with the rotation of the post-tensioned high strength bolts [Figure 3.14(b)].

After the test had been completed, the CORE Damper was taken out from the system by loosening turnbuckles and disassembled in each piece [Figure 3.14(c)]. The investigation of the components confirmed that damage was concentrated only in the SPEAs. The damaged SPEAs in the first test were replaced and the system was easily reassembled for the second test. The whole reassembling process should not take more than an hour when performed by two construction workers. This demonstrated the ease of replacement of the system after a significant seismic event.

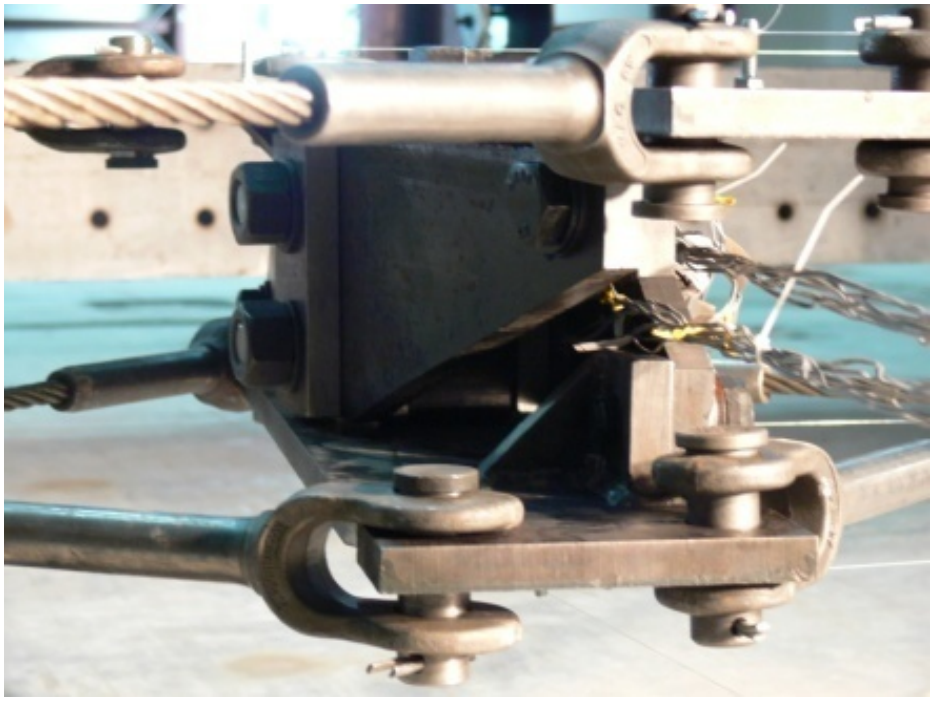

Fig 3.14 (a):

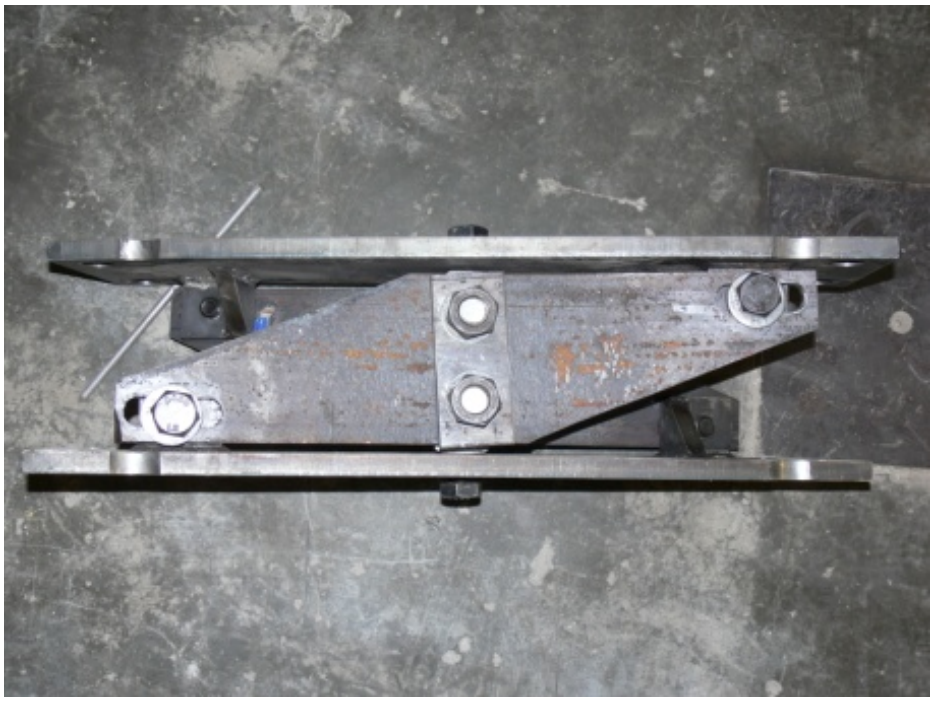

Fig 3.14(b):

Fig 3.14(c):

Figure 3.14: Ultimate behavior at 0.04rad. cycle and after test observation (a) inward deformation mode (b) side view (c) disassembled specimen

3.8 Summary

The proof of concept testing for the cable bracing system with a Couples Resisting Damper (CORE Damper) was undertaken through the use of the full scale testing frame constructed in the structural laboratory at the Georgia Institute of Technology. The system was designed to withstand for the deformation under a maximum credible earthquake.

The post-tensing force required for the removal of initial slackness in the cables was defined using the hysteresis curve obtained from tensile test of a cable beforehand. The material properties of the steel used for the SPEAs were pretty standard for A36 steel according to preliminary tensile coupon tests.

The performance of the system was evaluated at various drift levels under quasi-static cyclic loading. The local behavior of the system was carefully monitored using digital instrumentations including hand-made load cells made for the cables. The surface strains of the SPEAs were acquired by numbers of uniaxial strain gauges.

The proposed system successfully showed stable bi-linear hysteresis, even through very large deformations. As the drift level increased, the relative rotation between the front and back cover plates increased. The rotation became notable at the 0.0075rad. cycle when the SPEAs started to yield. The cracking sound of the mill scale on the surface of the SPEAs also started at the 0.0075rad. cycle and the most part of the surface of the SPEAs were flaked at the end of the loading. The slipping of bolts became noticeably audible at the 0.015 rad. cycle and became constant after 0.02 rad. loading cycles. The post-yielding stiffness of the system increased after the 0.02rad. cycle when the bolts at the connections between the SPEAs and the cover plates started to slip along

long slotted holes. The base shear of the system was slightly higher when the Couples Resisting Damper (CORE Damper) deformed outward than when it deformed inward. This was due to the change of the boundary condition in outward and inward deformation modes.

The hysteresis curve was compared to that predicted by the preliminary analyses in ABAQUS and OpenSEES. The analyses predicted pretty well the elastic stiffness and yielding strength of the system.

At the 0.04rad. cycle, the CORE Damper remained below the limit state condition, defined as a physical contact between two SPEAs under the inward deformation mode. The out-of-plane deformation of the cover plates was observed after the 0.04rad. cycle due to the in-plane rotation of the SPEAs. The investigation of the components after the test confirmed that damage was concentrated only in the SPEAs. The process of reassembling the system by replacing the damaged SPEAs was simple and rapid. This demonstrated the ease of replacement after a significant seismic event.

CHAPTER 4

ANALYTICAL STUDY OF SESMIC UPGRADING WITH "CABLE BRACING-CORE DAMPER SYSTEM"

4.1 Introduction

The analytical study presented in this chapter demonstrates the upgrading of seismically deficient steel frames using the "Cable Bracing-CORE Damper System" proposed and validated in Chapters 2 and 3. The model building considered for the upgrading is a multi-story steel frame originally designed for gravity and wind loads in the 1960's, which now needs to be evaluated for seismic loads due to the update of the seismic hazard map. The main lateral-load-resisting system in the original building is a diagonal cross bracing system located at the end bents. Each element (i.e. girder, column and brace member) is designed for the force under gravity load only and under the combined gravity and wind loads including $P\Delta$ effects. Only limited plastic deformation capacity is available for these elements due to the lack of proper seismic detailing. In the design, the cross bracing is considered to resist only in tension and, as a result, the building is not qualified as a concentrically braced frame which requires balanced tension and compression brace components [AISC, 2007; Tremblay, 1996]. The bracing members are very slender and are susceptible to brittle fracture at midspan where global buckling creates a hinge. An accumulation of inelastic deformation in one direction, "racheting" sideways under repetitive cyclic loading is also typical for such brace members designed only in tension. Consequently, the development of a "soft story",

where deformation concentrates at a certain story, becomes a concern under a cyclic seismic load.

To improve the performance of the building under seismic loads, the replacement of the existing diagonal cross bracing with the “Cable Bracing-CORE Damper System” is proposed. This rehabilitation action impacts the performance by: (1) a minimizing the possibility for the development of “soft story” by providing stable bi-linear hysteretic performance, (2) reducing story drift by enhancing the energy dissipation capacity of the building, and (3) eliminating the concern for brittle failure in brace elements. The performance of the original and upgraded frames under a seismic load is evaluated through nonlinear dynamic analyses using recorded and synthetic ground motions.

4.2 Model Building Design

Building Plan and Design Load

The model building is a five-story steel frame with 5 bays and 2 spans in plan [Figure 4.1]. The floor plan of the building resembles a design example of a multistory braced frame in a structural engineering textbook written in 1970's [Disque, 1971]. The vertical and lateral load resisting systems in the building are designed for a gravity load only and for the combined gravity and wind loads, respectively. In the north-south direction, a diagonal cross bracing is permitted only in column lines 1 and 5 between bents A and B, while the structure is assumed to be braced in the east-west direction. Hereinafter, the discussion of the seismic performance of the building focuses only in the north-south direction.

The lateral load design is controlled by a drift index defined as the deflections at the center of mass at the roof divided by the building height. The drift index shall be 0.0025 at working load and 0.004 at the factored loads, i.e., 0.0025 multiplied by a factor of 1.3 plus an allowance for additional drift due to $P\Delta$ effect. The total working load on the girders is taken to 43.6kN/m (3kips per ft) resulting from the dead load of 2.3kPa (48psf) and the live load of 3.45kPa (72psf) on each floor. The wind load is simply assumed to be 0.96kPa (20psf) along the entire height of the building. The sizes of original members meet design guidelines in the 1960's [AISC, 1963].

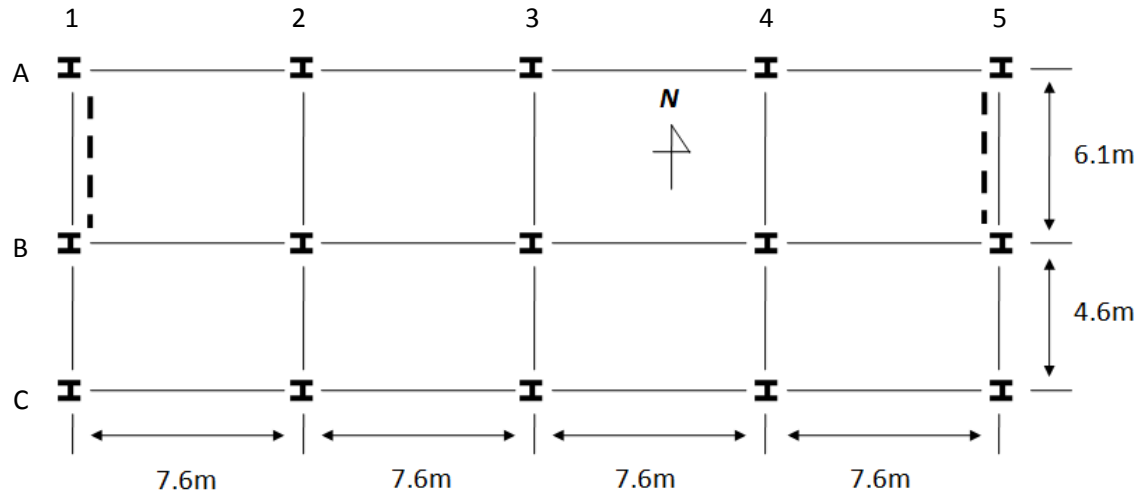

4.1(a):

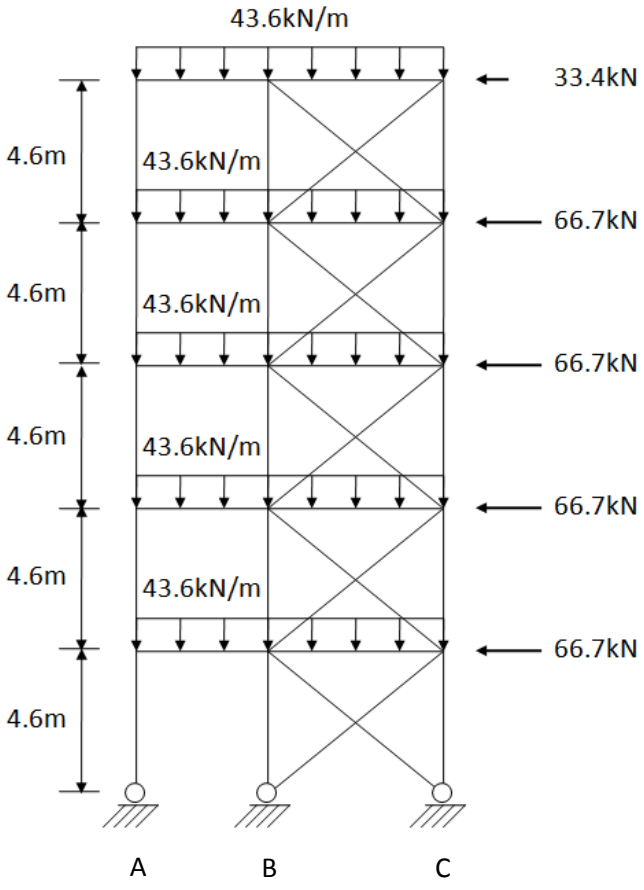

4.1(b):

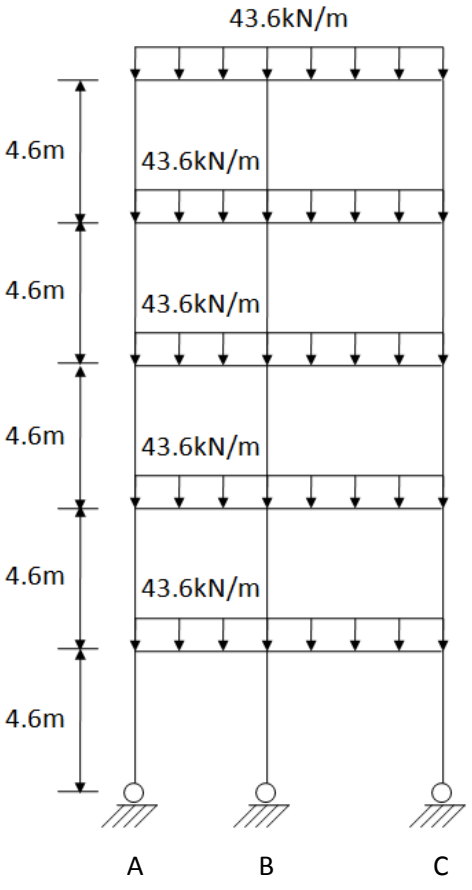

4.1(c):

Figure 4.1: Building geometry (a) building plan (b) bents 1 and 5 (c) bents 2-4

Original Building with Diagonal Cross Bracing

The members in the original building are designed using a plastic design procedure. For gravity loads a global factor of 1.7 was used for both dead and live loads; for wind a 1.3 factor was used. Therefore, the gravity and lateral load resisting systems in the building have some reserved strength compared to the systems designed following current design guidelines. The design procedure of the multistory braced frame in plastic design can be subdivided into two main parts. One is the preliminary design of girders, columns and brace members under gravity loads (Step 1-3). This follows the secondary design of these members under the combined load of wind and gravity loads (Step 4-6). Finally, the drift at the top floor is checked for the requirement of the appropriate drift limit of 0.004.

1. The required plastic moment, $M_{p,}$ of the girders under a uniform gravity load is computed with a safety factor, F=1.7 [Table 4.1]:

$$M_P = \frac{1}{16}(1.7w)L^2 \qquad 4.1$$

, where

w = working load on the girder

L = clear distance between column flanges

2. The column members under a gravity load are selected so that the plastic moment capacity of the columns under axial load M_{pc} is larger than the required end moment M with a safety factor F=1.7.

$$M_{pc} = 1.18\left(1 - \frac{P}{P_y}\right)M_p \qquad 4.2(a)$$

$$M = M_p + V\frac{d}{2} \qquad 4.2(b)$$

, where

P = factored axial load on the column section

P_y = yielding axial strength of column sections

V = factored shear load at the column surface

d = column depth

After the member size of columns are selected, the allowable moment considering the lateral tensional buckling (LTB) M_{LTB} is checked in Table 4.3 using the column design chart in AISC specification [AISC 1969]. The end moment ratio q is taken as 0 and 1.0 for the first story column and upper story columns, respectively. In-plane bending (IPB) does not govern the moment capacity in this case.

3. The third step is to determine the area of brace members to stabilize the columns under a gravity load with a safety factor F=1.7 [Table 4.3]. The stability of a braced frame under a gravity load depends on the stiffness and angle of the brace members. The required area for the brace members A_b are calculated by equating the restraining moment provided by the brace members and the overturning moment induced by a $P\Delta$ effect as follows. It is assumed that the diagonal bracing only works in tension.

$$\frac{E\Delta A_b h \cos\theta^2}{L_b} = \sum P\Delta$$

$$A_b = \frac{L_b \sum P}{Eh \cos\theta^2} \qquad 4.3$$

, where

ΣP = factored axial load on braced frame at each floor level

L_b = length of braced member

E = Young's modulus

h = story height

θ = inclined angle of brace member

Table 4.1: Girder design for gravity load

Girder	L_{span}	D_{column}	L	M_p	$Z_{required}$	R_p	Member	Z
	m	m	M	kN-m	cm^3	kN		cm^3
A-B	4.6	0.30	4.27	84.4	340	169.4	W10x19	354
B-C	6.1	0.30	5.79	155.4	626	225.9	W12x27	623

Table 4.2: Column design for gravity load

Column	P	M	Mem	P_y	M_p	r_y	P/P_y	h/r_y	M_{pc}	M/M_{pc}	M_{LTB}
	kN	kN-m		kN	ft-kips			in	ft-kips	LTB	
A1-A2	847	54.2	W8x40	1890	161	2.04	0.45	26.9	105	0.66	69.1
q = 0											OK
A2-A4	678	54.2	W8x35	1650	141	2.03	0.41	27.0	98	1	97.8
q = 1.0											OK
A4-A6	339	54.2	W8x24	1130	94	1.61	0.30	34.1	77	0.98	75.9
q = 1.0											OK
B1-B2	1977	39.8	W8x67	3154	286	2.12	0.63	25.9	125	0.27	33.8
q = 0											OK
B2-B4	1581	39.8	W8x58	2740	243	2.1	0.58	26.1	120	0.57	68.6
q = 1.0											OK
B4-B6	791	39.8	W8x35	1650	141	2.03	0.48	27.0	86	0.87	75.1
q = 1.0											OK
C1-C2	1130	94.0	W8x58	2740	243	2.1	0.41	26.1	168	0.78	130.9
q = 0											OK
C2-C4	904	94.0	W8x40	1890	161	2.04	0.48	26.9	99	0.89	88.1
q = 1.0											OK
C4-C6	452	94.0	W8x35	1650	141	2.03	0.27	27.0	121	1	120.6
q = 1.0											OK

Table 4.3: Brace design for stability under gravity load

P kN	L_B m	E Mpa	$cos\phi$	Member	SPL_B kN-m	A_b cm^2
1160	7.62	200000	0.8	Level 1-2	44300	0.757
				Level 2-3	35400	0.606
				Level 3-4	26600	0.454
				Level 4-5	17700	0.303
				Level 5-6	8860	0.151

4. The preliminary members of the vertical truss are selected based on a hypothetical lateral force which represents the $P\Delta$ effects. The drift index is assumed to be 0.004 and a safety factor F=1.3 is used for the factored combined load of gravity and wind loads.

$$H_{P\Delta} = 1.3P(drift\ index) \qquad 4.4$$

, where

P = gravity load at each floor level

The axial force in the brace members under the combined wind load, gravity load and the hypothetical lateral force are tabulated in Table 4.4. For the analysis, the brace members are treated as pin-ended truss members that resist load only in tension.

5. The girders in the bracing system are redesigned under the combined loads with a safety factor F=1.3 (Table 4.4). The following interaction formula for concurrent axial loads and bending moments under the combined factored load is used for the design.

$$M = \frac{1}{16}(1.3w)L^2 \qquad 4.5(a)$$

$$\frac{P}{P_{cr}} + \frac{C_m M}{\left(1-{}^{P}/_{P_e}\right)M_m} \leq 1.0 \qquad 4.5(b)$$

, where

P = applied factored axial load

P_{cr} = 1.7 AF_a where F_a is the factored allowable stress for compression members

M = concurrent permissible moment from factored loads

P_e = 1.92 AF_e' where F_e' is the allowable Euler stress

M_m = maximum moment that can be resisted by the member in absence of axial loads

C_m = 1.0 since rotation is not restrained

6. The columns in the bracing system are redesigned under the combined lateral and gravity loads (Table 4.6). As with the girders, the axial loads resulted from the previous step and the end moment resulted from a gravity load are substituted into the interaction formula used in the second step.

7. The brace members in Table 4.7 are selected for the required area under the factored combined gravity and axial loads with a safety factor F=1.3.

$$A_b = \frac{P_b}{(.85)F_y} \qquad 4.6$$

, where P_b= brace axial force under the factored combined gravity and wind loads from Table 4.4

Table 4.4: Brace design for combined wind and gravity loads

w	L_{total}	*F*	*span*	*drift index*	$H_{P\Delta}$
kN/m	m				kN
43.6	10.7	1.3	2.5	0.004	6.05

Member	*1kN load applied at 6th level*	$H_{P\Delta}$=6.05kN	*Wind load from right*	*Total Wind + $H_{P\Delta}$ from right*	*Total Wind + $H_{P\Delta}$ from left*
	kN	kN	kN	kN	kN
R_B	3.75	68	813	881	-881
R_C	-3.75	-68	-813	-881	881
B1-B2	-3.75	-68	-813	-881	566
B2-B3	-3	-46	-520	-566	320
B3-B4	-2.25	-27	-293	-320	144
B4-B5	-1.5	-14	-130	-144	37
B5-B6	-0.75	-5	-33	-37	4
C1-C2	3	46	520	566	-881
C2-C3	2.25	27	293	320	-566
C3-C4	1.5	14	130	144	-320
C4-C5	0.75	5	33	37	-144
C5-C6	0	0	4	4	-37
C1-B2	1.25	38	488	526	526
B2-C2	-1	-30	-390	-421	-421
C2-B3	1.25	30	379	410	410
B3-C3	-1	-24	-304	-328	-328
C3-B4	1.25	23	271	294	294
B4-C4	-1	-18	-128	-146	-146
C4-B5	1.25	15	163	178	178
B5-C5	-1	-12	-130	-142	-142
C5-B6	1.25	8	54	62	62
B6-C6	-1	-6	-43	-49	-49

Table 4.5: Brace design for combined gravity and wind loads

Girder	L_{span}	D_{column}	L	M	Mem.	P_y	M_p	r_x	A	
	m	m	m	kN-m		kN	kN-m		cm^2	
B2-C2	6.1	0.026	6.07	130.5	W12x35	1648	208	13.3	66.5	
	l	l/r_x	F_a	F'_e	P_{cr}	P_e		Unity	d/t	P/P_y
	cm		Mpa	Mpa	kN	kN				
	610	45.7	128	466	1450	5947		0.930	42.8	0.26
								OK	>40.1	<0.27

Table 4.6: Column design for combined gravity and wind loads

Col	*Gravity*	*Wind* + $H_{P\Delta}$	*Tot.*	M	Mem.	P_y	M_p	r_y	$\frac{P}{P_y}$	$\frac{h}{r_y}$	M_{pc}	$\frac{M}{M_{pc}}$	M
	kN	kN	kN	kN-m		kN	kN-m			cm	kN-m	LTB	kN-m
B1-B2	1512	881	2393	30	W14x74	3492	513	2.5	0.69	56	190	0.3	57
q = 0													OK
B2-B4	1209	566	1775	30	W12x58	2740	353	2.5	0.65	56	146	0.75	110
q = 1.0													OK
B4-B6	605	144	748	30	W12x35	1648	208	1.5	0.45	90	134	0.73	98
q = 1.0													OK
C1-C2	864	881	1745	72	W12x58	2740	353	2.5	0.64	56	151	0.5	76
q = 0													OK
C2-C4	691	566	1257	72	W12x50	2353	296	2.0	0.53	71	162	0.55	89
q = 1.0													OK
C4-C6	346	144	489	72	W12x35	1648	208	1.5	0.30	90	173	0.85	147
q = 1.0												OK	

Table 4.7: Brace design for combined gravity and wind loads

Brace	P	A_b	Member
	kN	cm^2	
C1-B2	526	24.9	2Ls-5x3x1/4
C2-B3	410	19.4	2Ls-5x3x1/4
C3-B4	294	13.9	2Ls-3x2.5x1/4
C4-B5	178	8.4	2Ls-3x2.5x1/4
C5-B6	62	2.9	2Ls-3x2.5x1/4

8. The drift of the top floor is estimated by computing the elastic deflection of the braced frame treated as a pin-ended cantilever truss structure. The applied loads are the wind and the hypothetical $P\Delta$ forces. The deflection of the top floor is determined by the virtual work method where dummy unit load is applied to the top of the braced frame. As shown in Table 4.8, the drift coming from each member is calculated separately to see the relative contribution of the various members. The total drift is sufficiently smaller than the target drift index of 0.004.

Table 4.8: Drift calculation

Column	Member	*Vert* kN	*Wind+PΔ* kN	*Total* kN	*m* *1k at 6th level*	*L* M	*A* cm^2	*PL(m)/AE* cm
B1-B2	W14x74	-1512	-881	-2393	-3.75	4.6	141	1.46
B2-B3	W12x58	-1209	-566	-1775	-3	4.6	110	1.10
B3-B4	W12x58	-907	-320	-1227	-2.25	4.6	110	0.57
B4-B5	W12x35	-605	-144	-748	-1.5	4.6	66	0.39
B5-B6	W12x35	-302	-37	-339	-0.75	4.6	66	0.09
C1-C2	W12x58	-864	566	-298	3	4.6	110	-0.19
C2-C3	W12x50	-691	320	-371	2.25	4.6	95	-0.20
C3-C4	W12x50	-518	144	-375	1.5	4.6	95	-0.14
C4-C5	W12x35	-346	37	-308	0.75	4.6	66	-0.08
C5-C6	W12x35	-173	4	-168	0	4.6	66	0.00
						Drift due to columns =		3.01
Brace	Member		*P* kN	*L* m	A cm^2	*M*	*PL(m)/AE* cm	
C1-B2	2Ls-5x3x1/4		526	7.6	25	1.25	1.00	
C2-B3	2Ls-5x3x1/4		410	7.6	25	1.25	0.78	
C3-B4	2Ls-3x2.5x1/4		294	7.6	17	1.25	0.82	
C4-B5	2Ls-3x2.5x1/4		178	7.6	17	1.25	0.50	
C5-B6	2Ls-3x2.5x1/4		62	7.6	17	1.25	0.17	
						Drift due to braces =		3.28
Girder	Member		*P* kN	*L* m	A cm^2	*M*	*PL(m)/AE* cm	
B2-C2	W12x35		421	6.1	66	1.0	0.193	
B3-C3	W12x35		328	6.1	66	1.0	0.150	
B4-C4	W12x35		146	6.1	66	1.0	0.067	
B5-C5	W12x35		142	6.1	66	1.0	0.065	
B6-C6	W12x35		49	6.1	66	1.0	0.023	
						Drift due to girders =		0.498
						Total =	6.782	cm
				Working load drift index		Δ_{top}/HF	0.0023	

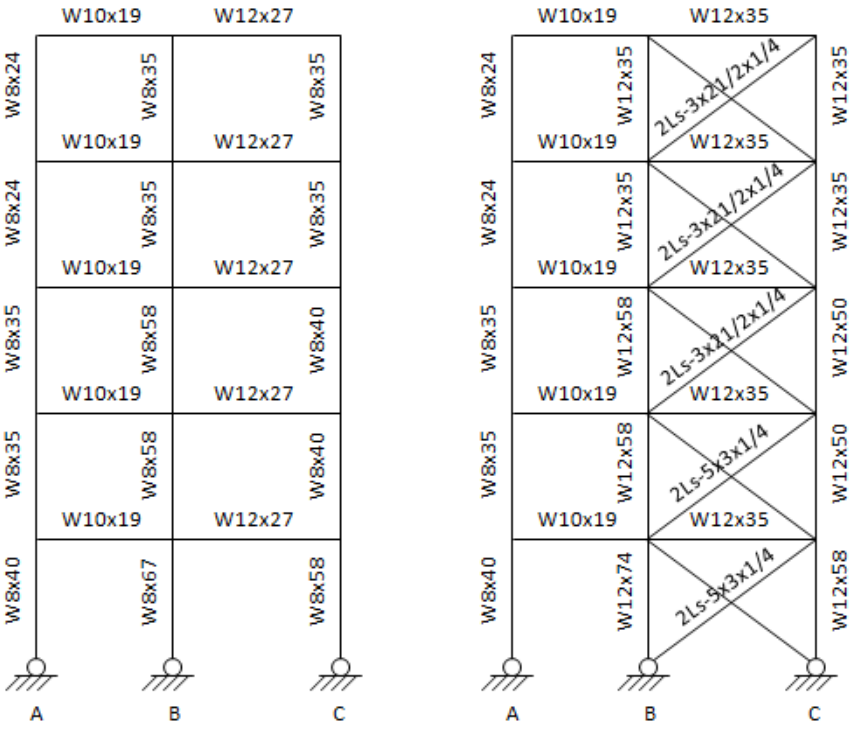

4.2(a): **4.2(b):**

Figure 4.2: Elevation of original building with diagonal cross bracing (a) bents 1 and 5 (b) bents 2-4

Figure 4.2 shows the final design of the braced and support bents in the original building with the diagonal cross bracing.

Upgraded Building with "Cable Bracing-CORE Damper System"

The seismically upgraded building with the "Cable Bracing-CORE Damper System" is designed so that the yield strength of the damper bracing system at each floor is equivalent to that of the diagonal cross bracing system in the original building. As is the case of the original building, the bracing system in the first and second stories and the third through fifth stories are identical. The stiffness of the bracing system is set to provide a similar fundamental period for the upgraded building as that of the original

building to highlight the effect of the hysteresis characteristics of dampers in building responses.

4.3 Analysis Model

In order to examine the seismic performance of the original and the upgraded buildings, nonlinear dynamic analyses were performed in the OpenSEES analysis platform [Mazzoni *et al.,* 2009]. Beam and column members are modeled using the *nonlinearBeamColumn* element with the number of integration points set to 5. The integration along the element is based on the Gauss-Lobatto quadrature rule. The beam and column elements have fiber sections formed by the sub-regions of quadrilateral shapes which are discretized into fibers. The individual fibers are associated with *uniaxialMaterial* objects, which enforce the Bernoulli beam assumption. The modeling of brace elements are explained later, as it was different for the two buildings.

All members are A36 mild steel with an expected strength factor R_y = 1.2 ($R_y F_y$=294MPa). These values were used considering the fact that the 1960's was a transition period from ASTM A7 mild steel (F_y=225MPa) to ASTM A36 steel (F_y=245MPa) [Newman, 2001]. The material model for the steel is a bi-liner hysteresis curve with the strain hardening ratio of 0.28%.

The dead load and the weight of beams are divided by the gravitational acceleration and are applied to beams as a distributed mass. The weight of the columns is applied at column nodes as nodal mass. The $P\Delta$ effect is accounted for by applying a co-rotational transformation to the column and brace elements. Numerical damping is considered by specifying 5% Rayleigh damping in the first and third modes of vibration. The natural frequencies of the original building with diagonal cross bracing and the

upgraded building with the CORE Damper bracing were computed as 0.83 sec. and 0.82 sec., respectively, indicating a relatively flexible structure.

The transient earthquake analyses are executed after the application of a gravity force to the building models. In the transient analysis, constraints are handled by a transformation method which performs a condensation of constrained degrees-of-freedom. The system of equations are stored and solved using a *BandGeneral* solver which is suitable for banded unsymmetric matrices. The solution algorithm used for solving nonlinear equations is a Modified Newton-Raphson iteration procedure where a tangent stiffness matrix is held constant, an assumption suitable for mildly non-linear problems. The two parameter time-stepping method developed by Newmark is used as an integrator to determine the next time step in the analysis including inertial effects.

Original Building with Diagonal Cross Bracing

Brace members are modeled using a *nonlinearBeamColumn* element command with the 7 integration points. The brace elements also utilized a fiber section command. The brace members in the analysis model are able to carry compression and tension, although the compressive strength of the brace members is not accounted for at design stage because of their very large slenderness ratios [Figure 4.3]. A brace member buckles when the applied axial load exceeds the specified maximum compressive strength and continues to lose its compressive strength for a further deformation. The brace model does not include a ductility limit but includes a simplified model for strength deterioration of the brace members. The nominal compressive and yielding strength of the brace members are computed as Table 4.9 by following the AISC steel construction manual [AISC, 2005]. Here, the lengths of the brace members are taken as the diagonal

length of the adjacent frame times 0.9 considering the physical size of a beam-column connection and end connections of a brace member.

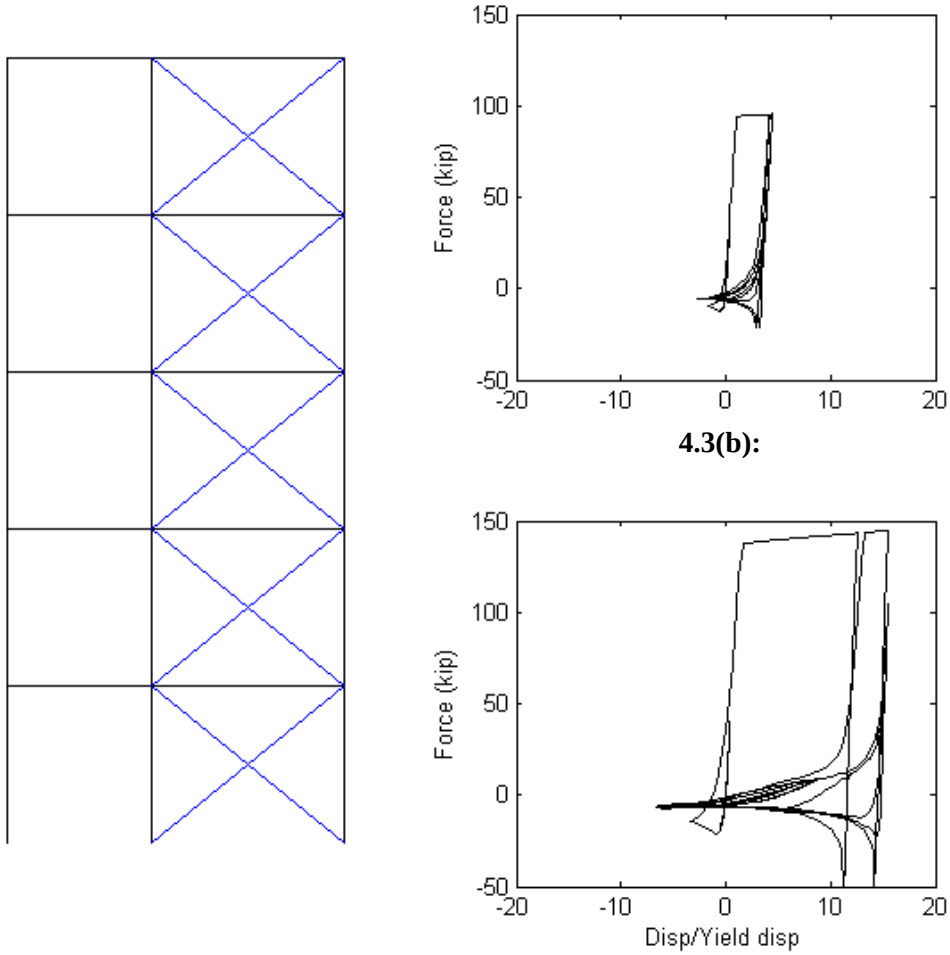

4.3(a): **4.3(b):** **4.3(c):**

Figure 4.3: Diagonal cross bracing model (a) model elevation (b) brace hysteresis on third floor (c) brace hysteresis on first floor

Table 4.9: Mechanical properties of diagonal cross braces

Member	A	K	L	K_xL/r_x	K_yL/r_y	F_e	F_{cr}	P_n	P_y
	cm^2		m			Mpa	Mpa	kN	kN
2Ls-5x3x1/4	25.0	1	6.9	83	227	42.2	37.0	93	621
2Ls-3x2.5x1/4	17.0	1	6.9	144	241	37.4	32.8	56	423

The brace model shown in Figure 4.4 utilizes a fiber-based *nonlinearbeamcolumn* element to simulate the buckling behavior of a brace member. This model, originally developed for a chevron brace configuration, has an additional node at the midspan of a brace member to introduce an initial geometrical imperfection [Uriz, 2008; Yang, 2006, 2008]. The maximum compression strength of the brace member (P_n) is controlled by the amount of the initial imperfection. Two rotational springs at the end of the brace member help control the post-buckling strength of the brace member. An adequate initial stiffness of the rotational spring is set to obtain $0.3P_n$ at 10-20 times the yielding displacement of the brace member [AISC, 2007]. These parameters, initial imperfection ratio R_{im}= (imperfection) / (brace length), and stiffness of rotational spring K_{sp}, are determined based on an iterative procedure in the Pushover analysis of the entire building model [Table 4.10]. A large initial imperfection is required to provide relatively small compression strength to the brace member due to its large slenderness ratio. In this specific case, the small stiffness of the rotational spring indicated that it could be replaced with a simple moment release connection.

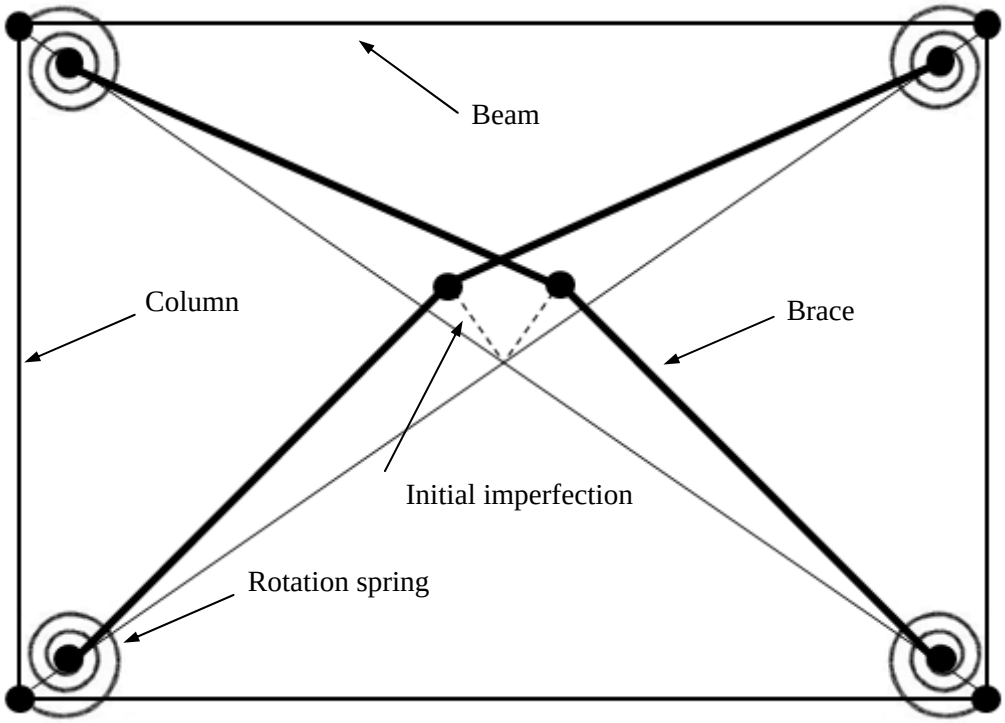

Figure 4.4: Schematic configuration of a diagonal cross brace model

Table 4.10: Parameters summary for buckling behavior

Location	Member	*Initial imperfection ratio* R_{Im}	*Stiffness of rotational spring* K_{sp}
1-2 story	2Ls-5x3x1/4	1/95	0.1
3-5 story	2Ls-3x2.5x1/4	1/250	0.1

Upgraded Building with "Cable Bracing-CORE Damper System"

The analysis model used in Chapter 2 is implemented at each floor of the building [Figure 4.5]. The weight of the CORE Damper is applied at damper nodes as a nodal mass. The yield strength and the elastic stiffness of the CORE Damper system are tuned to match with those of the diagonal cross bracing system in a preliminary static pushover analysis. The post-buckling stiffness of the CORE Damper is set to 1/13 based on the hysteresis curve from the experiment of the prototype reported in Chapter 3.

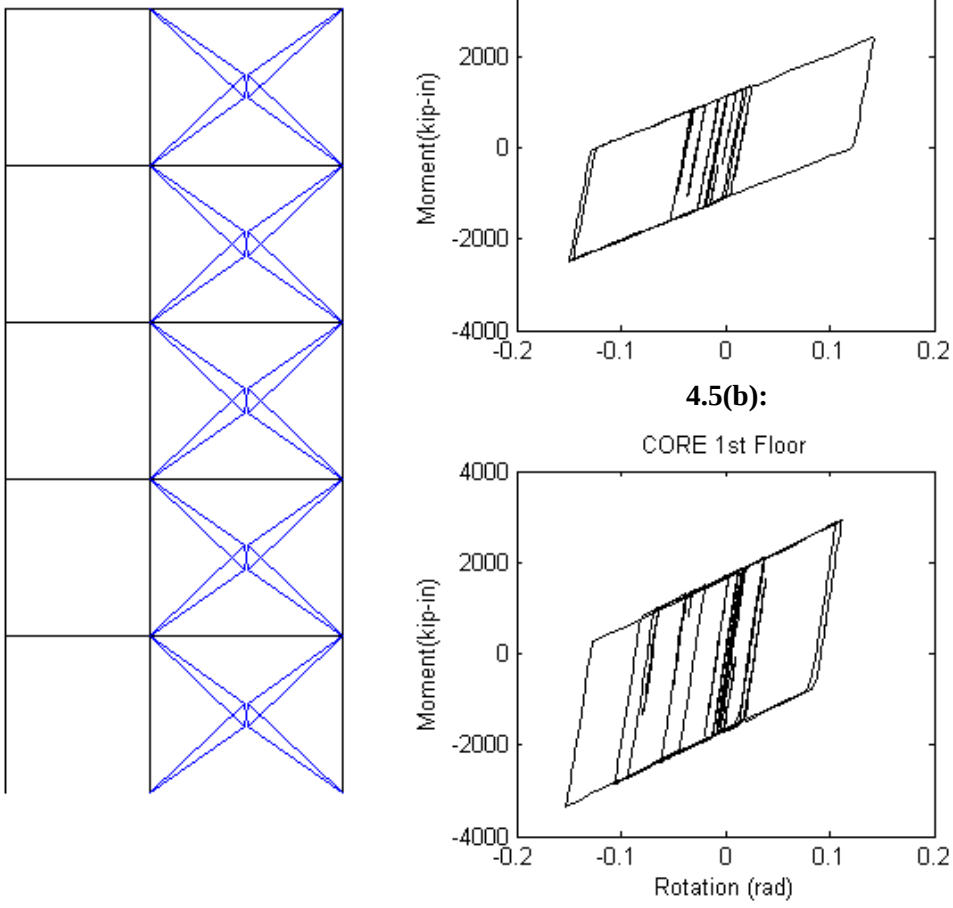

4.5(a): **4.5(b):** **4.5(c):**

Figure 4.5: CORE Damper bracing model (a) overall model (b) damper hysteresis on third floor (c) damper hysteresis on first floor

4.4 Analysis Results

The analyses consisted of a pair of ground motions in an attempt to bracket the behavior of the two structural systems. One ground motion is a large, near-fault ground motion (LA22 record) and another is a long, far field ground motion (1985 Chile record). The LA22 record is one representative ground motion generated for Los Angeles having a probability of exceedance of 2% in 50 years [Somerville *et al.*, 1997]. This acceleration time history, with a peak ground acceleration of 0.92g and an effective duration of 60 seconds, corresponds to the fault-normal component of the 1995 Takatori Kobe record. It has been altered so that the mean response spectrum matches the 1997 NEHRP design spectrum [SAC, 1997]. The Chile ground motion, with a peak ground acceleration of 0.71g and an effective duration of 116 seconds, was recorded in the 1985 Chile earthquake at the Llolleo station located approximately 60 km from the epicenter.

Near fault earthquake: LA22 ground motion

The LA22 ground motion has large peak ground acceleration with short duration. Figure 4.6 shows the response history of each floor under the LA22 ground motion for the two building cases. For the case of the diagonal cross bracing system (dotted lines), the first story suffered from a very large deformation (4.4% drift) under the first large motion at 7 sec. The accumulation of inelastic deformation in one direction resulted in a permanent residual deformation after the earthquake event (0.8% drift). The ground motion resulted in inelastic excursions for the second through fourth stories, but the maximum and residual deformations at these levels were not significant compared to those of the 1st story. The deformation time history indicated that the period of the building significantly elongated after the first story was significantly damaged and lost its

initial stiffness after the large motion at 7-10 sec. For the case of the CROSS Damper bracing system (solid lines), damage did not concentrate in a particular story and rather distributed itself along the entire height of the building. The maximum story drifts were similar for the first through fourth stories with the largest maximum story drift observed at the third story. The building did not exhibit a significant residual deformation after the earthquake event at any stories. The building also retained its initial stiffness as indicated by the high frequency responses after large shaking at 7-10sec.

The lateral seismic loads resisted by the two bracing systems at the first story are shown in Figure 4.7. In the diagonal cross bracing system, the seismic energy was dissipated mainly in the first large hysteresis loop and inelastic deformation was accumulated in one direction. In the CORE Damper system, the energy was dissipated in a stable hysteretic manner under cyclic loading. After the CORE Damper system experienced relatively large deformations, the system showed a slight slip-type behavior when the unloading curve crossed the zero threshold. This behavior comes from the slack of cables under the high speed loading when the frame is subjected to a large near fault earthquake. This deformation will probably disappear if the analysis model considers some post-tensioning forces which are necessary during the installation of the damper system, as described in the report of the experimental tests in Chapter 3.

The main response indices of the two bracing systems are summarized in Figure 4.8. As discussed above, the building with the diagonal cross bracing system exhibited severe damage with a soft story developing at the first story. The ductility demand for the brace members in the first story was very large and fractures were likely to occur at the hinges developed in repetitive global buckling before the ground motion terminated.

The CORE Dampers in the building were evenly subjected to a large deformation and dissipated a seismic energy. The deformation capacity of the damper had been confirmed in the proof-of-concept testing [Chapter 3]. The residual deformation at each story remained under the operational limit of 0.5% story drift.

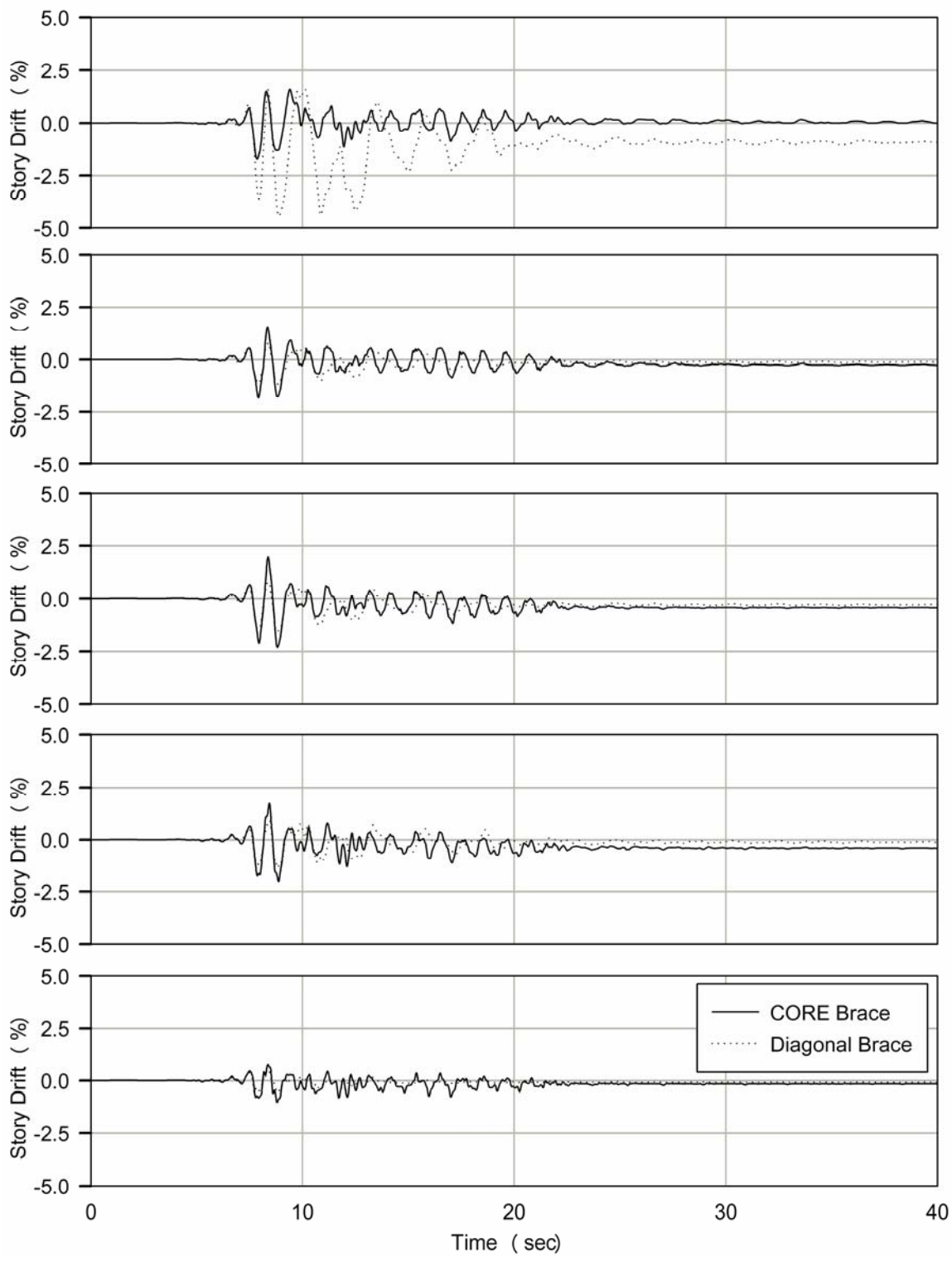

Figure 4.6: Displacement history under near fault earthquake

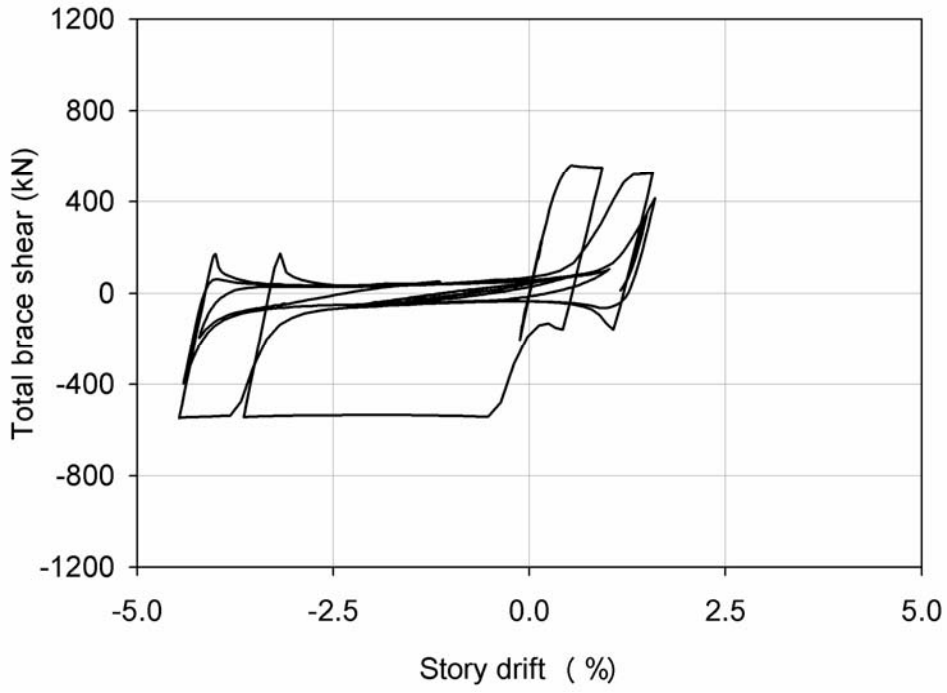

4.7(a):

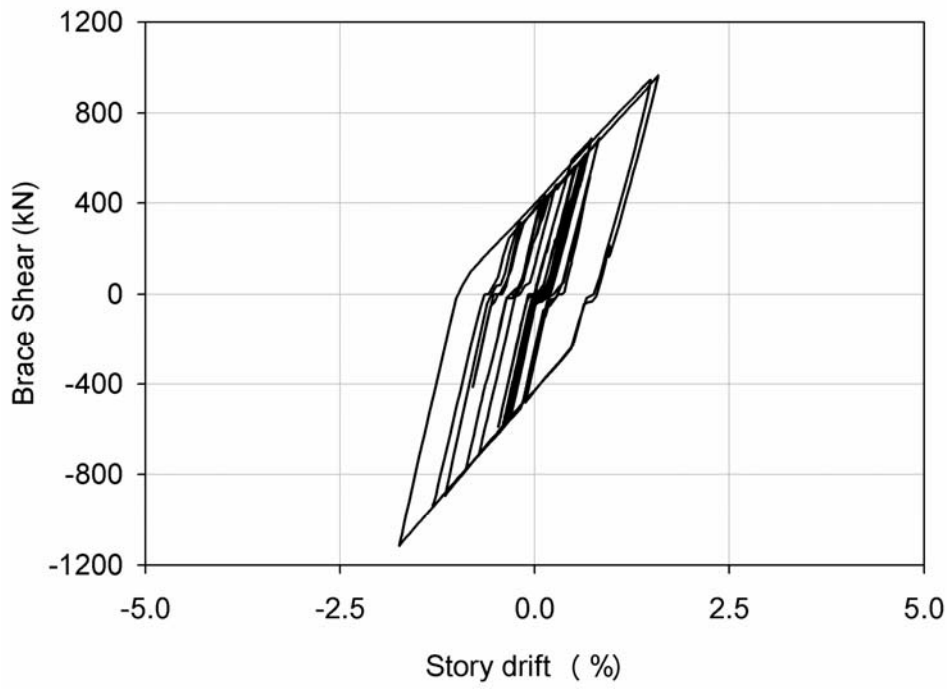

4.7(b):

Figure 4.7: Response of first story brace system under near fault earthquake (a) diagonal cross bracing (b) CORE Damper bracing

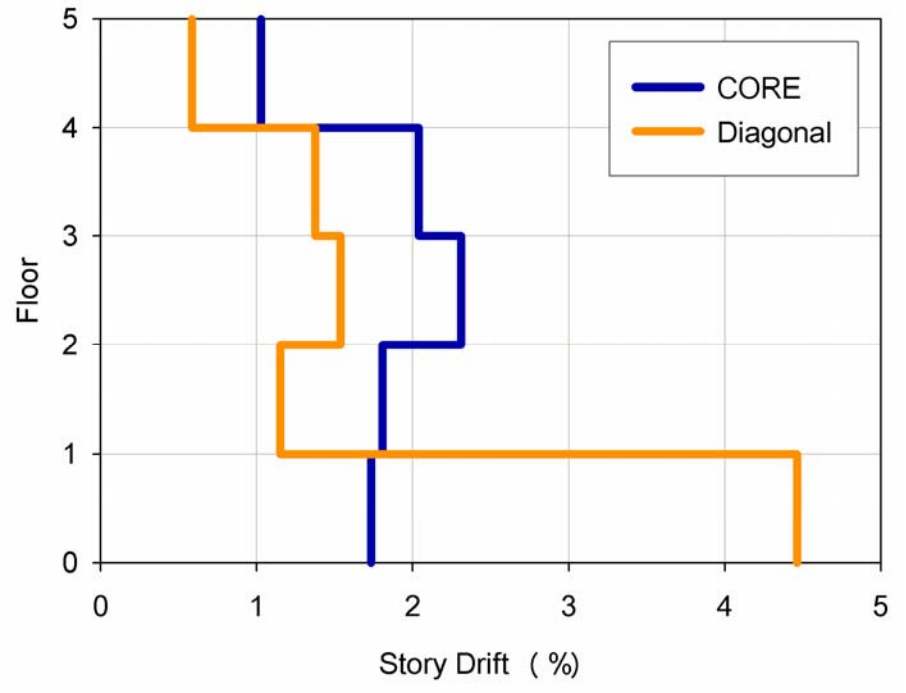
CORE
Diagonal
Floor
Story Drift (%)
0
1
2
3
4
5

4.8(a):

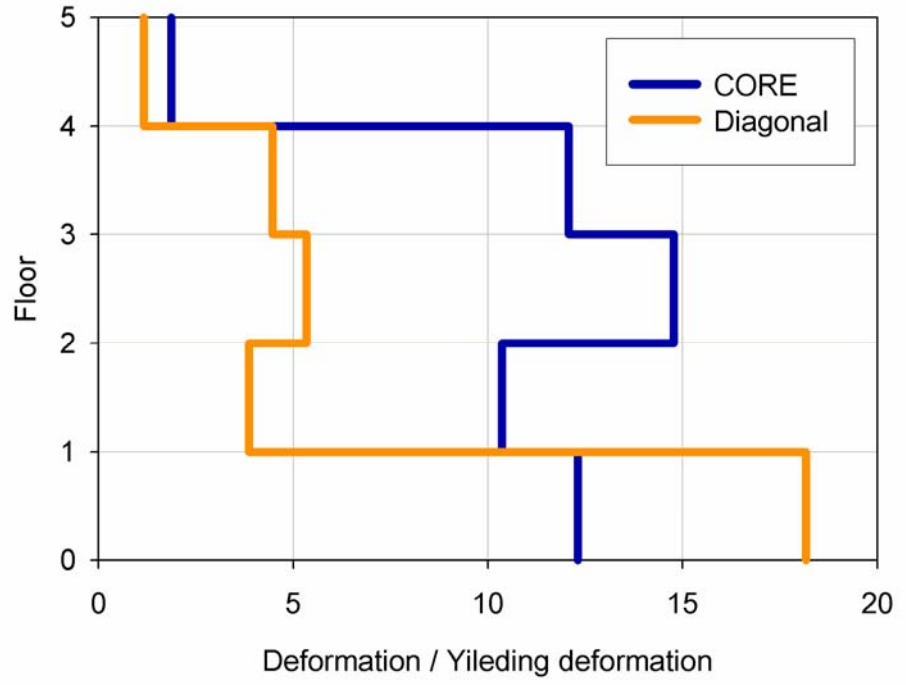
CORE
Diagonal
Floor
Deformation / Yileding deformation
0
5
10
15
20

4.8(b):

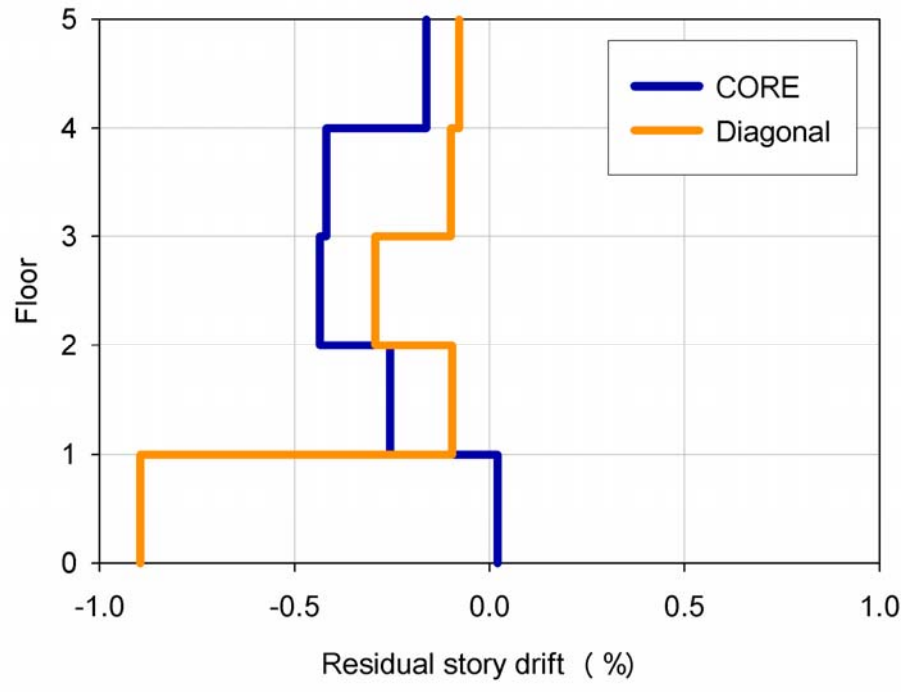

4.8(c):

Figure 4.8: Response summary under near fault earthquake (a) maximum story drift (b) maximum brace deformation demand (c) residual story drift

Far Fault Earthquake: Chile Ground Motion

The Chile ground motion consists of a large number of small to midsized cycles and has a long effective duration. Figure 4.9 shows the response history for each floor for the two building cases. For the building with the diagonal cross brace system, the largest deformation was observed at the first story and is at least 30% larger than other stories. The first large wave at 35sec severely deformed the building and was followed by a number of cycles with similar amplitude. Therefore, the brace system at the first story experienced a large number of inelastic deformation cycles as seen in its hysteresis plot in terms of total brace shear vs. story drift [Figure 4.10(a)]. The large number of inelastic loading cycles into a slender brace member will cause severe strength deterioration and likely lead to a low cycle fracture at local buckling where global buckling creates a plastic hinge. The indication of the slight elongation of the building natural period was observed when the frequency of story response at 0-20sec was compared to that at 80-100sec.

The building with the CORE Damper system had less variation in story drifts along its height, ranging from 0.6% to 0.9%. No period elongation was observed for the building over the entire duration of the ground motion. The CORE Damper at the first story also experienced a large number of inelastic deformation cycles and dissipated a seismic energy through its stable plate bending energy dissipation mechanism [Chapter 2]. The seismic energy was dissipated mainly at the first, third and fourth stories.

Figure 4.11 compares the responses in the two systems. Although the average of the maximum story drift along the building height was similar for both systems, the observed damage was rather concentrated at the first story for the diagonal bracing

system. For both cases, the deformation in brace members was below their ductility limit and the residual deformation was smaller than the operational story drift limit of 0.5%.

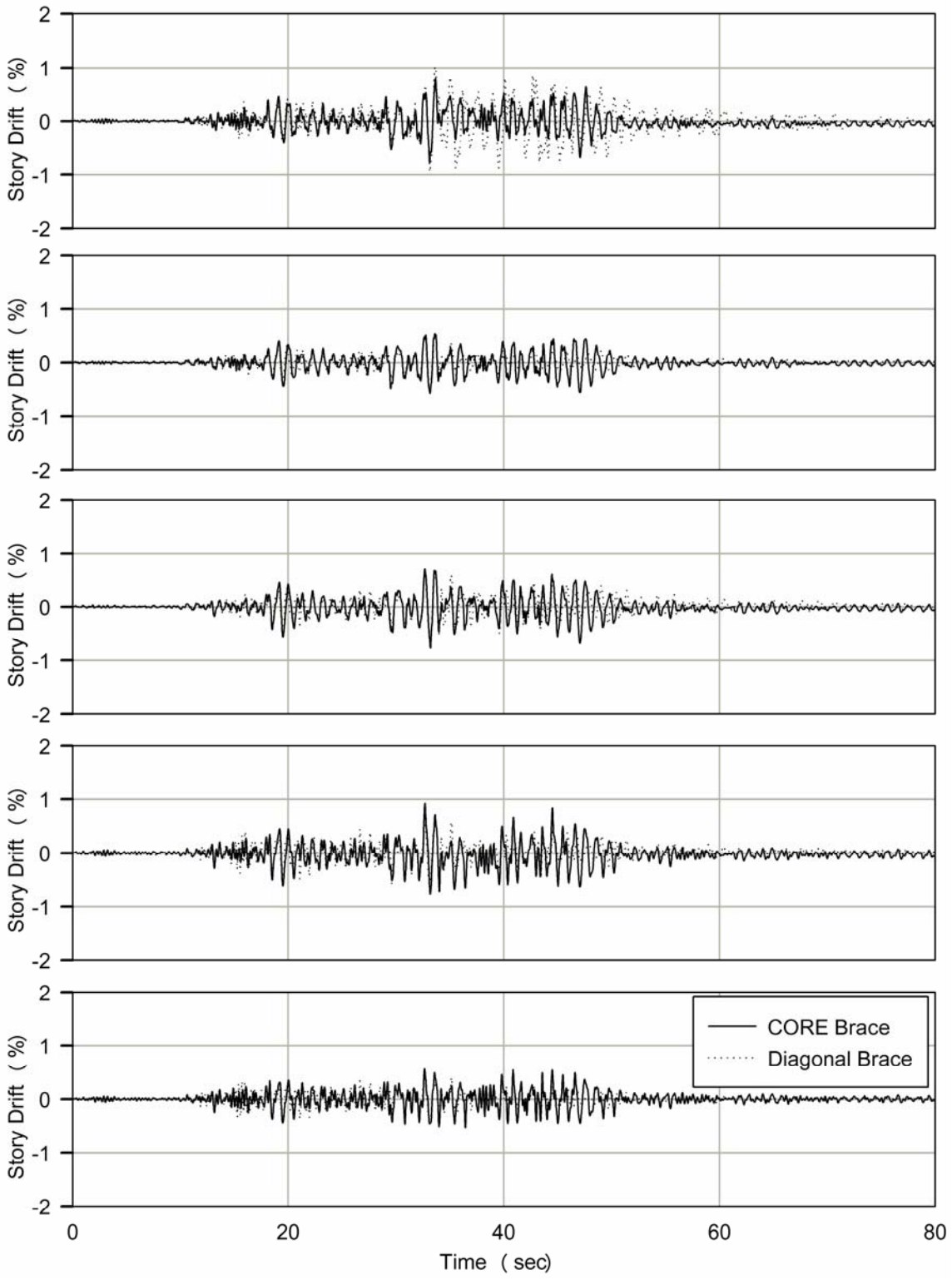

Figure 4.9: Displacement history for far fault earthquake

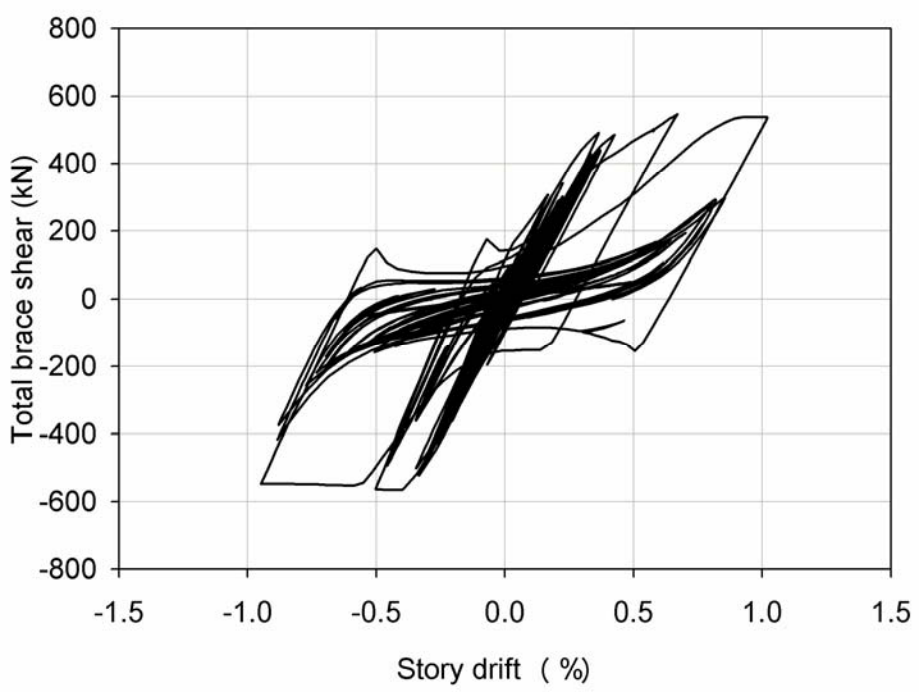

4.10(a):

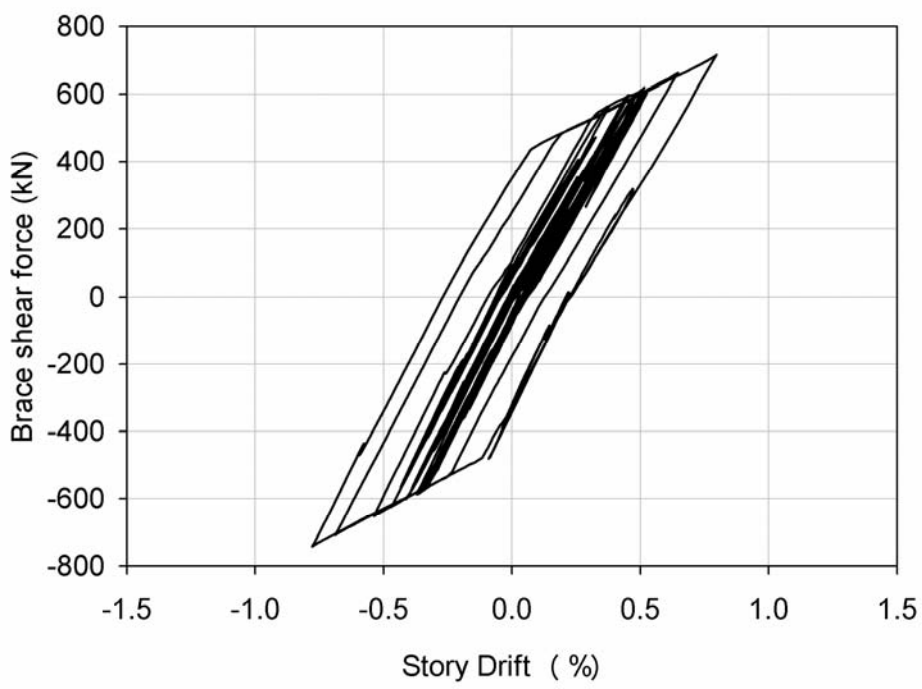

4.10(b):

Figure 4.10: Response of first story brace system under far fault earthquake (a) diagonal cross bracing (b) CORE Damper bracing

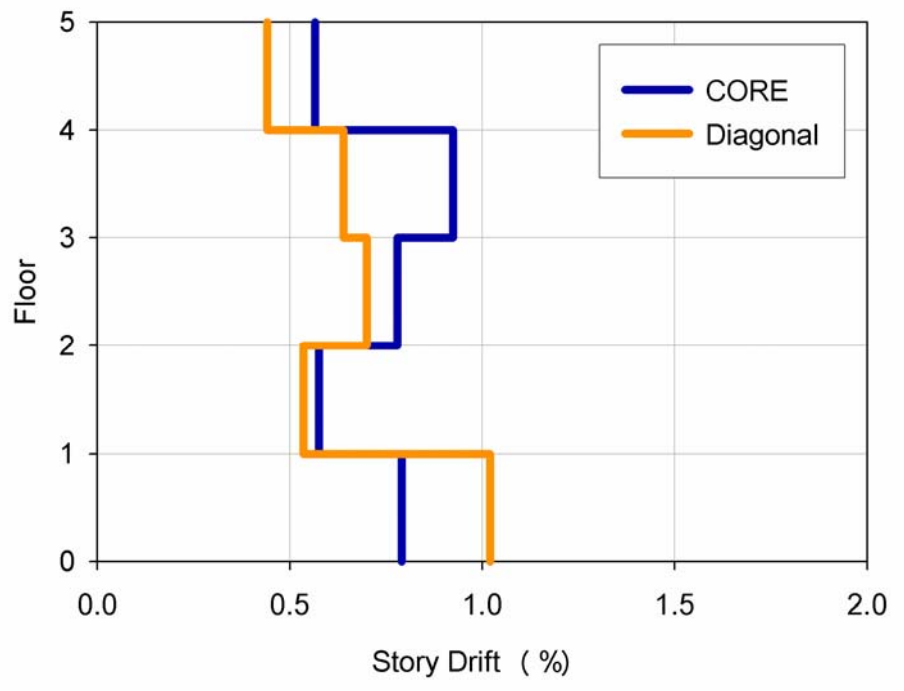
CORE
Diagonal
Floor
0
1
2
3
4
5
0.0
0.5
1.0
1.5
2.0
Story Drift (%)

4.11(a):

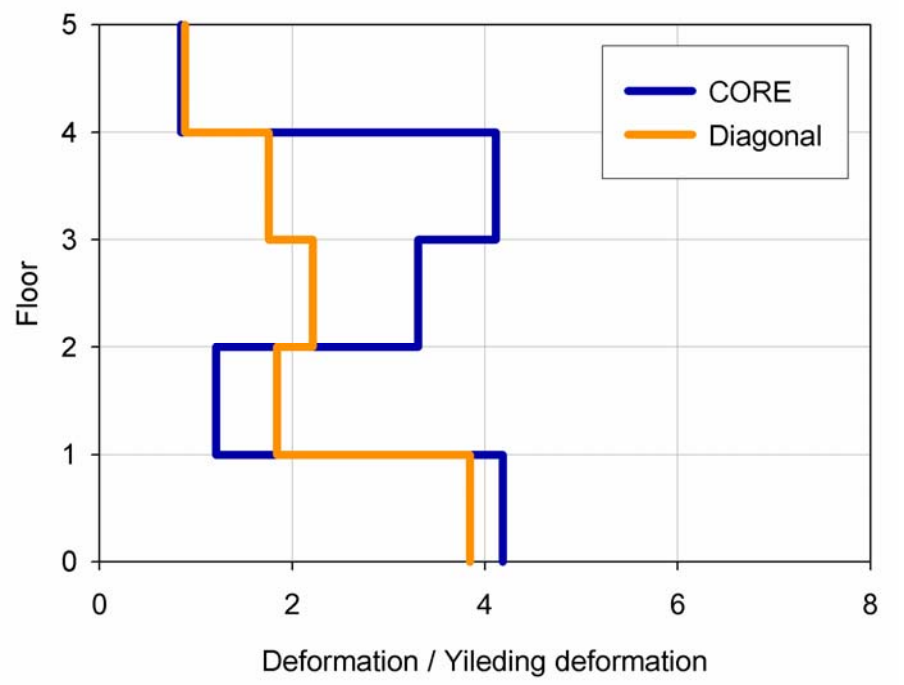
CORE
Diagonal
Floor
0
1
2
3
4
5
0
2
4
6
8
Deformation / Yileding deformation

4.11(b):

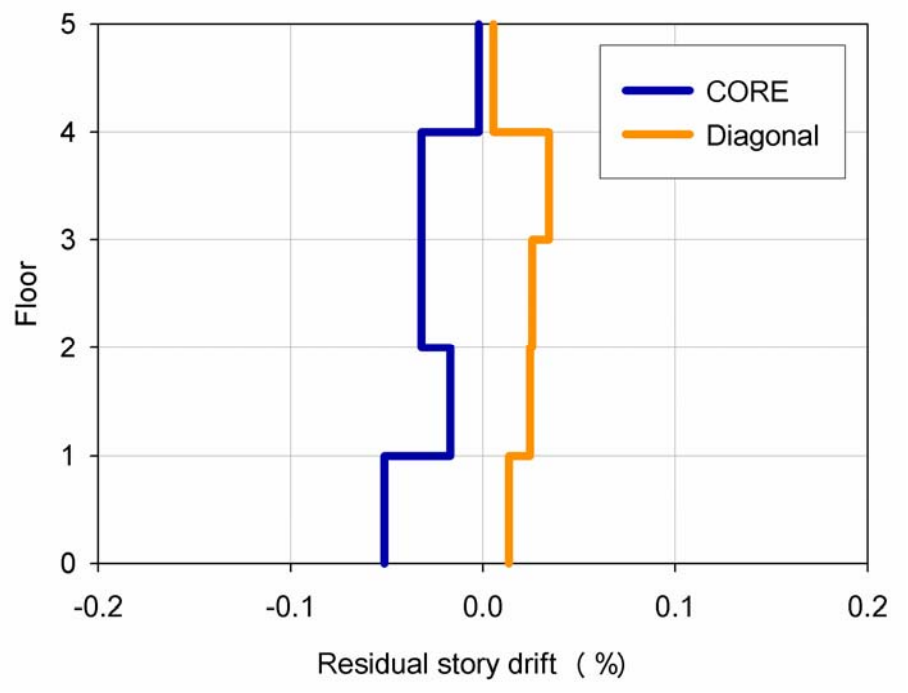

4.11(c):

Figure 4.11: Response summary under far fault earthquake (a) maximum story drift (b) maximum brace deformation demand (c) residual story drift

4.5 Summary

An example application of the newly developed "Cable Bracing-CORE Damper system" to the upgrading of a seismically deficient steel frame was presented in this Chapter. In the study, the original building was assumed to be built in late 1960's and was designed for the combined load of the gravity and wind force using the plastic design procedure. In this example, it is assumed that the seismic response of the original building became a concern due to the change of seismic category in the region where the building is located. The seismic performance of the building was enhanced by replacing the original diagonal cross bracing with the CORE Damper bracing system. The main difference between the two systems arises from their post yielding behavior. Once the diagonal cross bracing system experiences severe inelastic deformation, it loses its elastic stiffness until its deformation exceeds the maximum previous deformation. When subjected to several inelastic cycles of deformation, the diagonal brace member becomes highly susceptible to fracture at a plastic hinge created by global buckling. In contrast, the CORE Damper bracing system retains its initial stiffness with stable bi-linear hysteresis behavior. It is also notable that the post yielding stiffness of the CORE Damper system is significantly higher than the diagonal cross bracing system. In the analysis, the yielding strength of the brace systems at each floor and the natural period of the buildings were set equivalent to highlight the performance enhancement provided by the difference of the hysteresis shape between the two systems. This also limited the influence on the adjoining framing resulting from the replacement of the bracing system.

The seismic performance of two building systems under the near and far fault earthquakes were evaluated through the nonlinear dynamic analyses in the OpenSEES

platform. The original building with the diagonal cross bracing system suffered from concentrated damage in the first story with the development of a “soft story” by the several large amplitude waves in the near fault earthquake. The bracing system at the first story was severely damaged, experienced very large deformations (beyond its ductility limit), and probably failed by low-cycle fatigue of its first story braces (note that this phenomenon was not directly modeled and thus collapse can only be inferred indirectly). The original building also had a large residual story drift in the first story due to the development of a “soft story”. The deformation of the building with the CORE Damper system was well distributed along its height and a seismic energy was dissipated through the stable inelastic cyclic deformation of the CORE Dampers in several stories.

In the far fault earthquake, the maximum and residual story drifts were similar for two building cases. However, the diagonal bracing system experienced a large number of repetitive inelastic cyclic deformations in tension and compression and subsequently became highly susceptible to critical damage with brittle fractures initiating at hinges created by global buckling.

The example analytical study successfully demonstrated the effectiveness of the seismic upgrading with the application of the CORE Damper bracing system. The performance improvement was achieved thorough the different shape of the hysteresis behavior without the increase of strength or stiffness of the building system. A series of model buildings with various shapes should be examined for the further understanding of the effectiveness of the proposed system in a general building configuration. A statistical evaluation of the seismic response of these frames under the ground motions with a

various spectral characteristic and at various intensity levels are also desirable for providing the probabilistic information for the performance of the proposed system.

CHAPTER 5

NARROW STEEL PLATE SHEAR WALL WITH TENSION-ONLY BRACING: DESIGN AND ANALYSIS

5.1 Introduction

Addition of a properly designed and detailed unstiffened thin steel plate to a steel moment frame can give the system a substantial increase in stiffness, load-carrying capacity, and energy adsorption [Figure 5.1; Sabelli, 2006]. The advantage of such system, named Special Plate Shear Walls (SPSW), are the significant increase of stiffness and strength provided to buildings compared to other lateral load resisting systems. This system is also lighter and more ductile compared to reinforced concrete shear wall and applicable for new design or retrofit project [Astaneh-Asl, 2001]. Moreover, the SPSW system is more economically attractive compared to reinforce concrete shear walls [Timler *et al*., 1998]. The first application of such system was the Nippon Steel Building in Japan, 20-story office building completed in 1970 and since then the system were applied to a wide variety of structure [see for summary, Thorburn *et al*., 1983]. Design philosophy of SPSW prior to 1980s prevented global shear buckling and ensured shear yielding of the infill panel by utilizing thick plate and/or adding heavily stiffeners [: Similar philosophy can been seen today in the design of Composite steel Plate Shear Wall (C-PSW) [AISC, 2007]. Since Thorburn *et al*. (1983) introduced the design philosophy for the use of unstiffened thin plates and considered the post-buckling strength of the infill plate for the calculation of shear strength of system, this new design philosophy has

been widely adopted among researchers and in the current design codes [e.g., Trompoch and Kulak, 1987; Ghomi 1992, 2005; Caccese *et al*., 1993; Driver *et al*., 1997; Elgaaly 1993, 1997, 1998; Driver 1998a, 1998b; Behbahanifard *et al.*, 2004; Shinshkin, 2005 ; AISC, 2007; CSA, 2006; etc].

Since the SPSW system possess significantly large strength, in some applications, the available steel for infill plate material results in thicker or stronger than require by design. According to capacity design principle, which is widely accepted in seismic community, the overstength of the infill panel is not desirable and misleads to unexpected failure mode of structure. Several solutions proposed to remove this concern include the system utilizing light-gauge cold-rolled and Low Yield Strength (LYS) steel [Berman, 2003a, 2005; Vian, 2005]. Roberts (1992), Vian (2005) and Purba (2007) also investigated the behavior of unstiffened thin steel pate shear walls having opening on the infill plate analytically and experimentally. Hitaka (2003) thoroughly studied a steel plate shear wall with vertical slits where the steel plate segments between the slits behave as a series of flexural links, which provide a fairly ductile response without the need for heavy stiffening of the wall.

As seen in the free body diagrams, VBEs are subjected to the axial and shear force induced by the overturning moment as well as the inward flexural force induced by tension field action in the infill panel. When a slender, thin plate is used, inelastic behavior commences by yielding of the plate and the system strength is governed by plastic hinge formation in the VBEs. When relatively thick plates are used the failure mode is governed by the VBE instability. Once the failure mode is governed by the VBEs, only a negligible increase in system strength is achieved when the plate is

thickened, and the additional plate material used is essentially wasted. Therefore, effective use of thin steel plate shear walls to resist seismic forces is possible only when the boundary elements, especially VBEs are designed to yield after the yielding of the infill plate take place.

Figure 5.2(a) shows results of experiments where improper inward flexure of the boundary elements resulted in an hourglass effect with only a limited area of tension field action developing in the infill panel [Lubell *et al*., 2000]. Qu and Bruneau (2008) concluded that the failure of the Lubell *et al.* specimen [Figure 5.2(b)] was actually caused by the insufficient out-of-plane buckling strength of VBEs rather than excessive column flexibilities. Figure 5.2 (c) shows severe damage in VBE with local flange buckling [Behbahanifard *et al*., 2003].

Qu and Bruneau (2008) recently reported on flexibility limits for VBEs design. They reviewed the derivation of a flexibility factor in plate girder theory and how that factor was incorporated into current codes. Based on this review, they developed analytical models for preventing shear yielding and estimation out-of-plane buckling strength of VBEs of SPSWs.

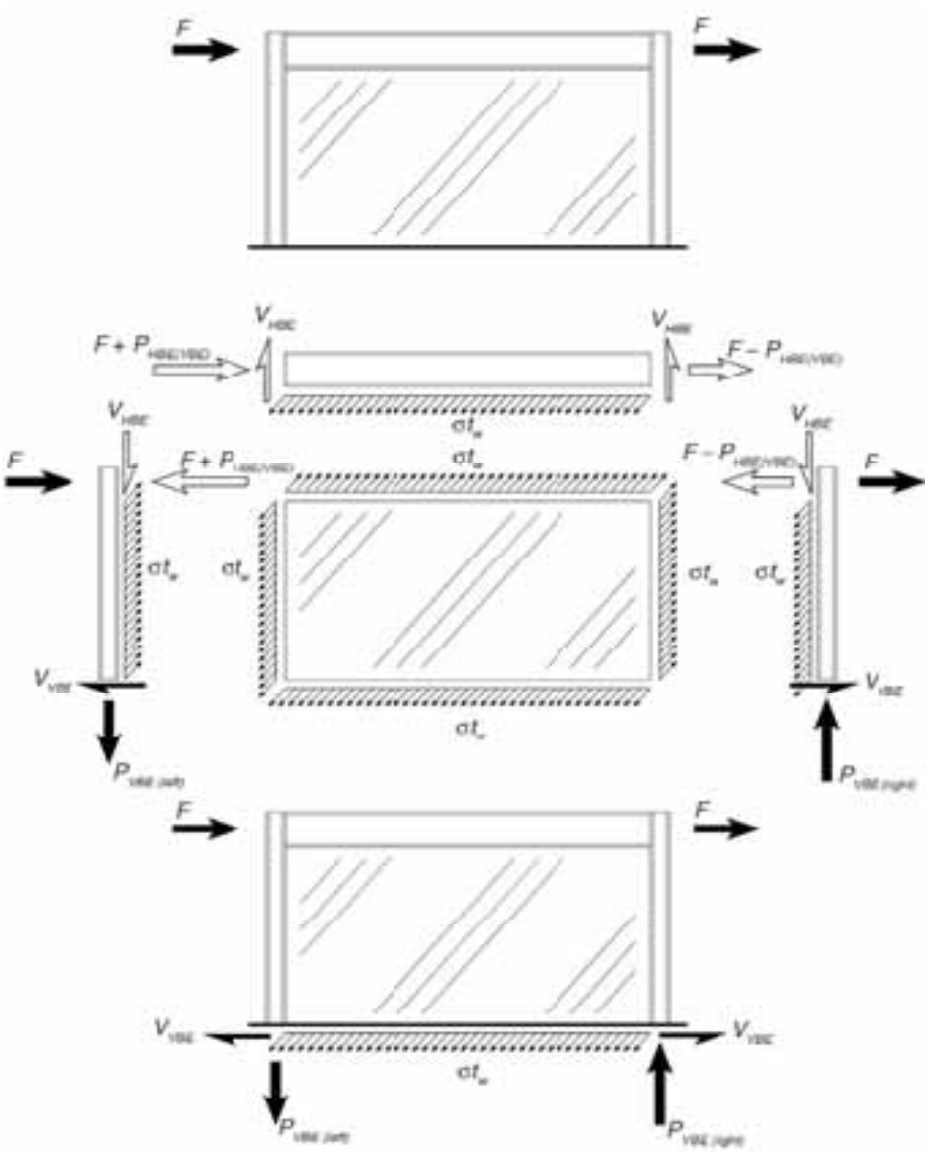

Figure 5.1: Steel plate shear wall system with free body diagram [Sabelli and Bruneau, 2006]

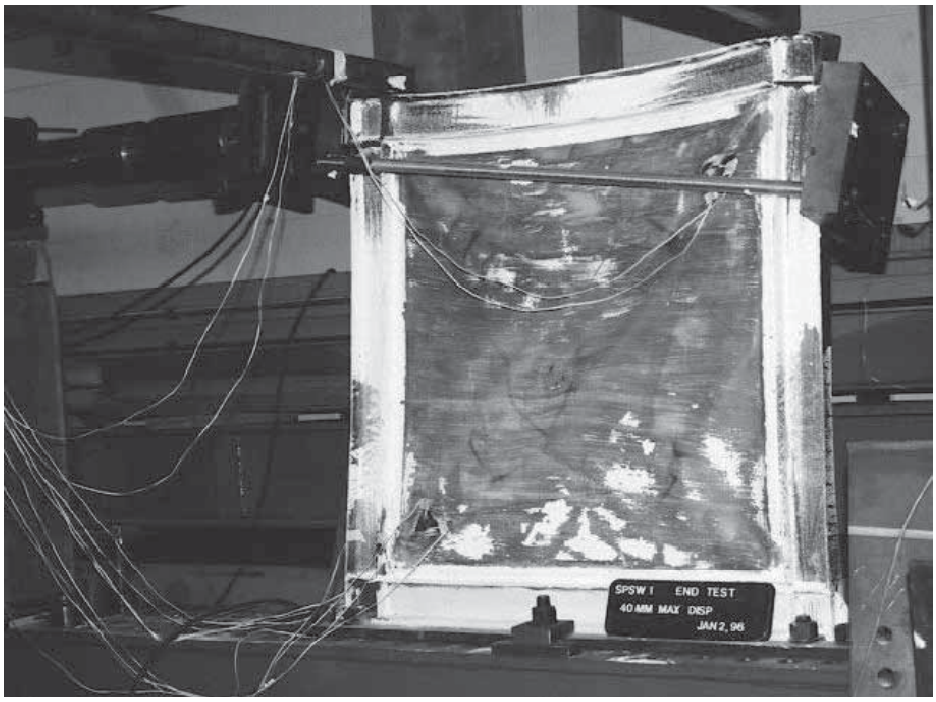

Fig 5.2(a):

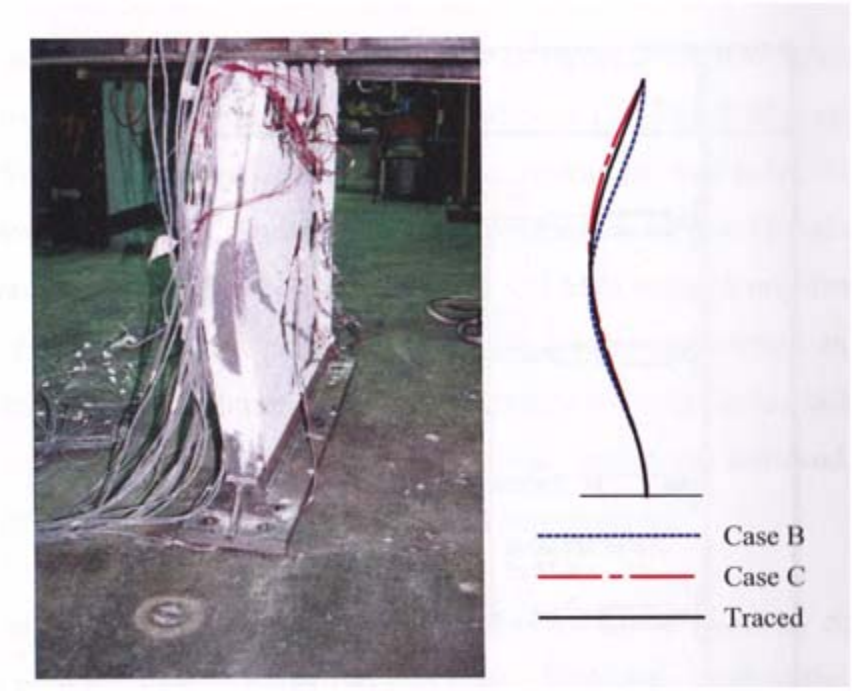

Fig 5.2(b):

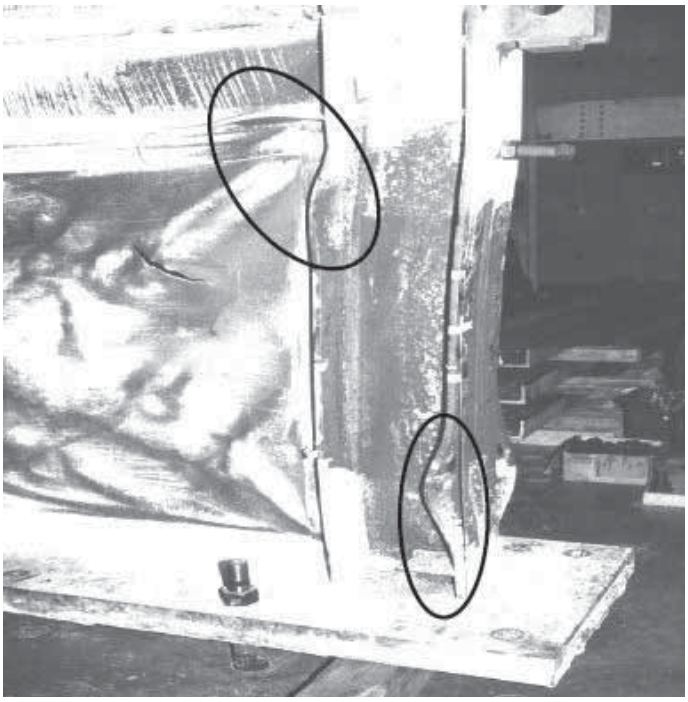

Fig 5.2(c):

Figure 5.2: Behavior of boundary elements (a) improper boundary element flexibility [Lubell *et al*., 2000] (b) out of plane buckling of bottom VBE [Courtesy of Ventura, adopted from Qu and Beubeau, 2008] (c) Local buckling of VBE [Behbahanifard *et al.*, 2003]

In order to utilize a thin steel plate as a supplemental lateral load resisting system for relatively small seismic rehabilitation projects, a geometry where a plate with surrounding boundary elements is installed at the middle span separately from existing columns is proposed herein. The proposed geometry intends to minimize impact and to reduce the need to strengthen the existing columns. These columns would have typically been designed for the combined forces of gravity and wind. The Vertical Boundary Elements (VBE) in the proposed system need to have enough strength and stiffness relative to the infill steel plate, otherwise the thin plate will not resist seismic effectively.

This objective is achieved by the use of a relatively weak beam supported by tension-only bracing elements. Installation of a strong beam as a VBE will require much effort and result in large force demands on the existing beams where the VBE is attached.

Figure 5.3 shows a free-body diagram of the infill steel plate, boundary elements, and tension-only elements for the proposed "Narrow Steel Plate Shear Wall with Tension-Only Bracing (NPSW-TB)". In the figure, the connections between the Horizontal Boundary Elements (HBE) and Vertical Boundary Elements (VBE) are treated as pinned. In this system, the bracing rods attract a large amount of the inward force in the VBE and transfer them to beam elements. A proper design of tension-element strength and stiffness enables the VBE to remain in the elastic range until the infill panel reaches its shear yielding strength.

In this chapter, a design approach and design procedure, including a design flowchart, were developed for the proposed NPSW-TB system. The geometry of the prototype was selected following the design flowchart developed based on the proposed design approach. For this work, a simplified analysis model was constructed in the OpenSEES platform as a design support tool. The performance of the prototype was evaluated by a displacement-controlled static pushover analyses. A scaled system was also designed for proof-of-concept testing; the details of the experimental work are discussed in Chapter 6. The performance of the scaled system was predicted with both simplified analyses using OpenSEES and advanced finite element analyses using ABAQUS.

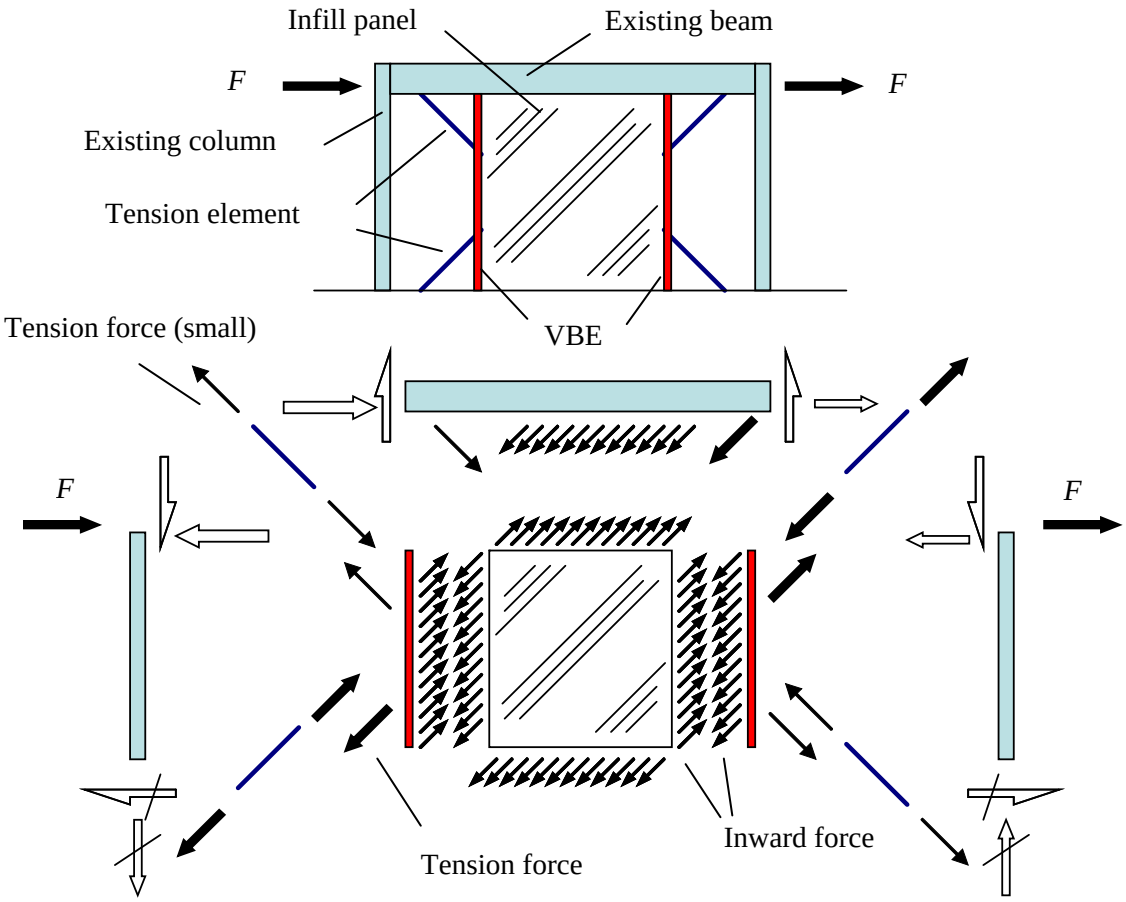

Figure 5.3: Concept and free-body diagram of "Narrow Steel Plate Shear Wall with Tension-only Bracing (NSPW-TB)"

5.2 Prototype Design

A prototype of the proposed shear wall system was designed based on preliminary parametric analyses. The performance goal of the system was to achieve a total system shear strength of 707kN (236kips), which is compatible approximately to the shear force carried by three columns with standard section in low-to-mid size steel moment resisting frames when columns were assumed to have fixed-fixed end conditions; one column with Japanese standard section, H-300x300x10x15 (section modulus, Z_x =1350cm^3, roughly equivalent to an American W12x58 section), can sustain approximately 236kN (53kips) shear force with its plastic moment capacity, M_p, when story height, h, is 4m (157in) and the expected yield strength as 305MPa (45ksi, or 1.3 times its nominal value of 36ksi).

Design Approach

A main design constraint for the prototype system is the requirement that yielding of the infill panel should occur prior to yielding of the boundary elements. The Vertical Boundary Elements (VBE) is subjected to inelastic deformation later due to the inward flexural force induced by the tension field developed in the infill panel. The design of the VBE requires an iterative procedure since its behavior interacts with the behavior of the tension-only rod and the local geometry of the arm. The strength and stiffness of the VBEs greatly affect the global behavior of the system while the behavior of the Horizontal Boundary Elements (HBE) does not influence to the global behavior as long as they are designed to be stronger than the infill panel. The proper design of the HBEs is relatively easy task since they are directly attached to the top and bottom beams of a frame. The tension-only elements are designed to remain elastic until very large deformation.

Prototype Geometry

The story height of a frame to be rehabilitated is assumed to be 4m (157in) with its clear height as 3.5m (137in). The aspect ratio of the infill panel is arbitrarily taken as 4:3 (height to width). Figure 5.4 shows the geometry of the prototype determined based on parametric analyses in OpenSEES using a strip model for the wall (see next section for details). The thickness of the infill panel was 3.2mm and the required section for Vertical Boundary Elements (VBE) were defined as CT-200x200x8x13 (I_x = 1390cm^4, Z_x = 88.6cm^3, roughly equivalent to an American WT6x22.5 section in terms of section modulus). The expected yield strength of the infill panel made of hot-rolled thin steel plate was assumed to be 207MPa (30ksi). The expected yield strength of the VBEs was assumed as 305MPa (45ksi, or 1.3 times its nominal value of 36ksi). The tension-rods were M30 (ϕ=1 5/32") with at yield strength of 222kN (50kips). Two tension rods were placed at each diagonal, sandwiching the VBEs with the inclination of 45 degrees: eight tension-rods were used in total. The other ends of the tension rods are anchored to beams at the position outside of protected zones (one half of beam depth away from column surfaces). The arms (brackets) shown in the figure were designed with the intention for limiting force demand in the tension rods by their rotational movement involving inelastic deformation at their connection to the VBEs.

Hysteresis of Prototype from Preliminary OpenSEES Analysis

The performance of the prototype was analyzed in OpenSEES platform using the simplified analysis model described later in this section. The global hysteresis of the system in terms of shear strength versus story drift is shown in Figure 5.5(a). The system yielded approximately at 0.5% story drift with a yield shear strength of 710kN (160kips).

The yield shear strength was estimated from the bi-linearization of the hysteresis curve as indicated in the figure. The hysteresis of the tension-rods located in the extended and shortened diagonals in the frame are shown in Figure 5.5(b). The rods connecting in the extended diagonal carried a large tension force as expected. The rods connecting in the shortened diagonal also carried a slight tension force in the pushover analysis. All rods remained elastic until 2.5% story drift as envisioned in the design approach.

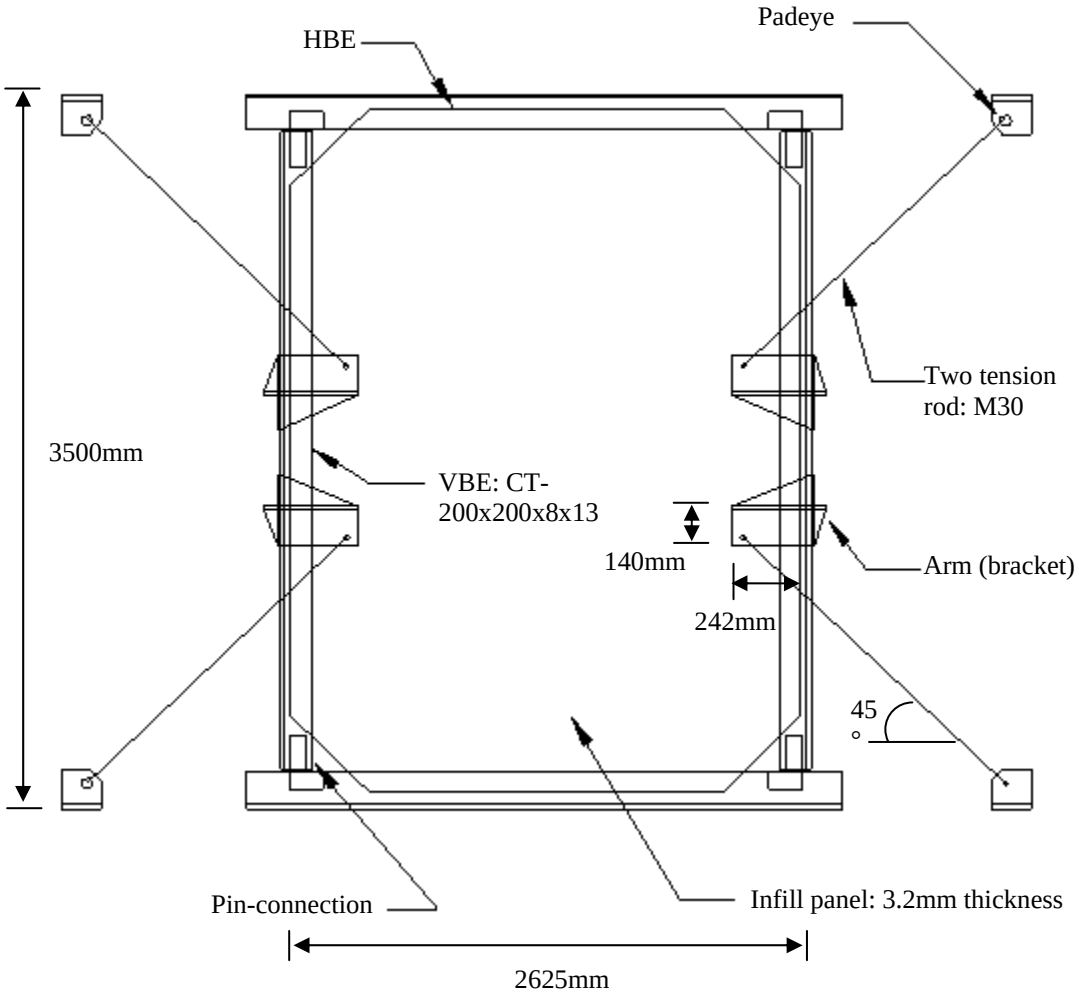

Figure 5.4: Geometry and components of prototype

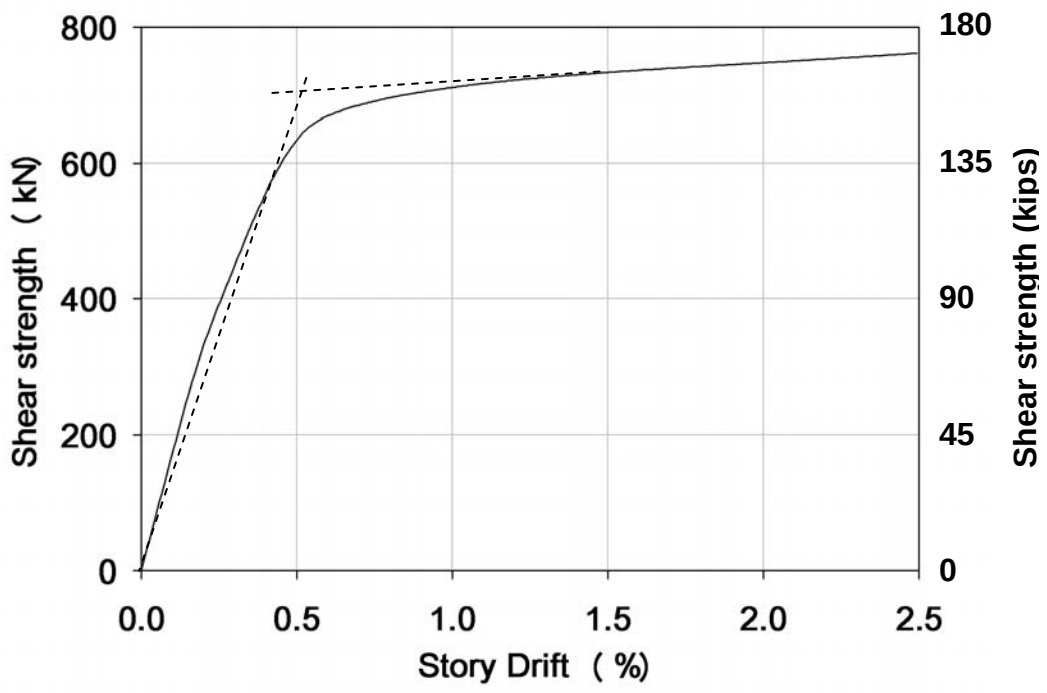

Fig 5.5(a):

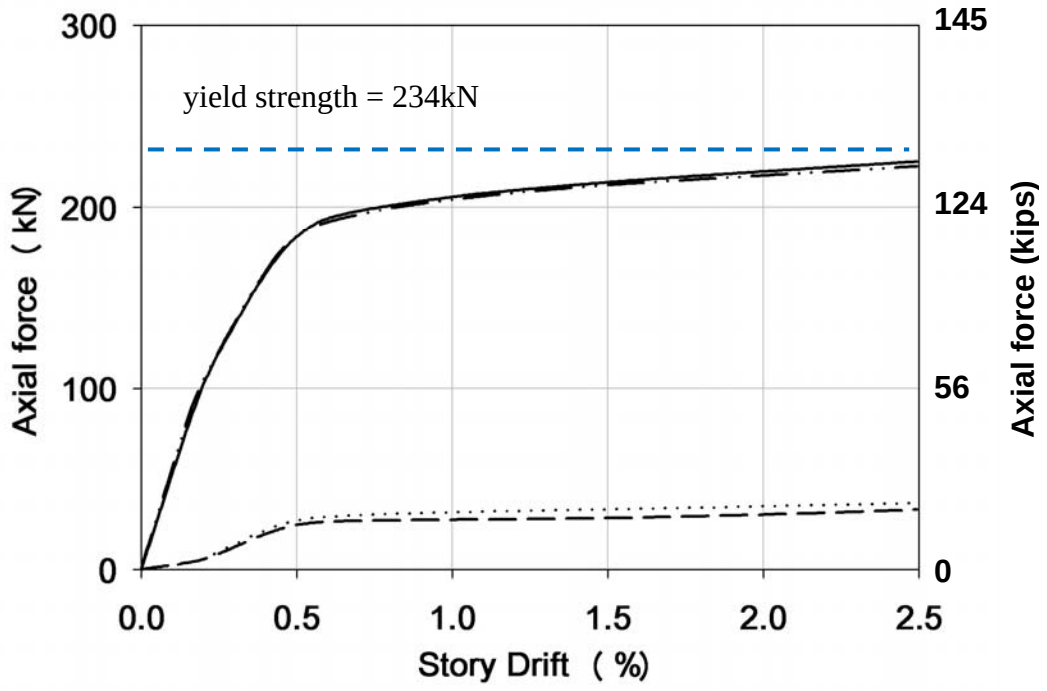

Fig 5.5(b):

Figure 5.5: Hysteresis of prototype in pushover analysis (a) global hysteresis (b) force histories of tension-rods

5.3 Design Procedure

Design Flowchart

The flowchart shown in Figure 5.6 schematically describes the design procedure. Given the geometry of a frame and a target shear force, the approximate thickness of a infill panel is estimated using the formula specified in the U.S. and Canadian seismic codes for the calculation of the nominal shear strength of infill panel for Special Plate Shear Wall system (SPSW) [CSA, 2006; AISC, 2005]. This formula includes including overstrength factor of 1.2. ;

$$\boldsymbol{V_n = 0.42 F_y t_w L \sin 2\alpha} \qquad 5.1$$

where, F_y = yielding stress of the infill panel, t_w = thickness of the infill panel, L = distance between the centerlines of VBEs and α = the inclination of the tension field.

It should be noted here that this equation is valid when the aspect ratio of the infill panel is larger than 0.8 and the boundary elements satisfy the specified stiffness limitation [Rezai, 1999; Qu and Bruneau, 2008]. The shear strength of the infill panel is used as a rough estimate of the total shear strength of the system as a simplification since the pin connected boundary elements do not carry shear force. In reality, the shear strength of the boundary frame should be added to the panel shear strength to obtain the total shear strength of SPSW systems. The inclination of the tension field is assumed to be 45 degree.

Once the thickness of the infill panel has been selected, a trial section is picked for the VBEs. In the first nonlinear static pushover analysis, the behavior of tension-rods is assumed to be elastic. Reasonable dimensions are assigned to tension-rods and arms. Using the analysis result, the requirement that the infill panel yields prior to the VBEs is

checked. This judgment is rather arbitrary since not all areas of the infill panel yields even with very stiff and strong VBEs. For the design of the prototype, the criterion was whether most of the middle part of the infill panel yielded or not.

When the criterion is satisfied, the diameter of the tension-rods is selected based on the force at 1% story drift. A second analysis is then executed to see if the total shear strength of the system is acceptable. If the error is within a reasonable tolerance, the dimension of the arm is determined in an iterative manner to ensure that the tension-rod remains elastic to at least a 2.5% story drift; otherwise the thickness of the infill panel need to be updated.

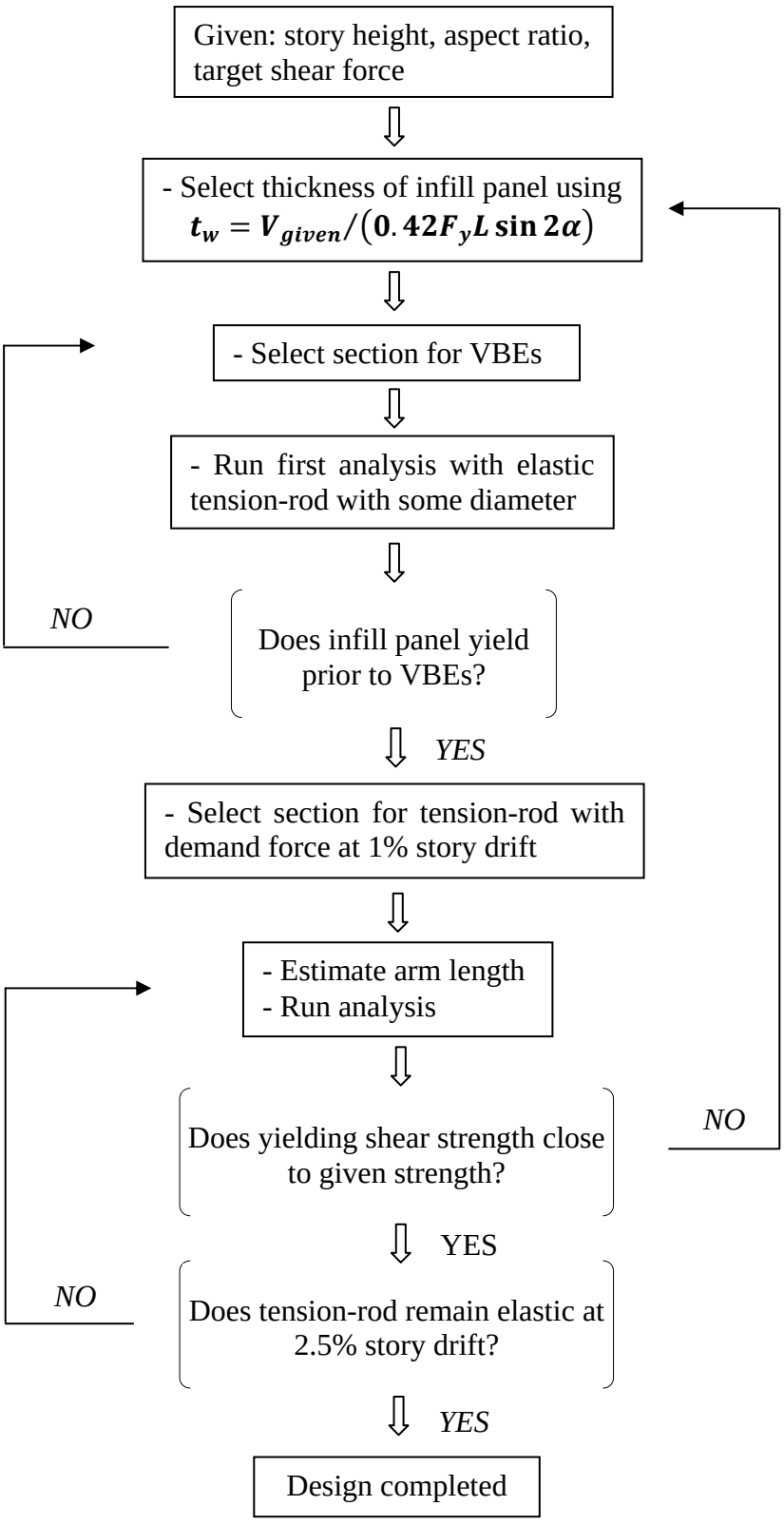

Figure 5.6: Design flowchart

Analysis Model in OpenSEES

Figure 5.7 shows the simplified analysis model in OpenSEES. The infill panel is modeled using strip model in which an infill panel is represented by a series of inclined pin-ended tension-only members [Thorburn *et al.*, 1983; Driver *et al.*, 1997; AISC, 2005]. The cross-sectional area of each strip is equal to the strip spacing times the panel thickness;

$$\boldsymbol{A_s = t_w(L\cos\alpha + H\sin\alpha)/n} \qquad 5.2$$

where, t_w = thickness of panel, L = width of panel, H = height of panel, α = angle of inclination and n = number of strips per panel.

The tension-only strips are modeled by *truss* element with *ElasticPPGap* material which is used to construct an elastic perfectly-plastic gap uniaxial material object [Mazzoni *et al.*, 2009]. The angle of inclination is assumed as 45 degree since there are no experimental data yet for the proposed geometry. Arms are connected to the VBEs at with the inclination of 30 degree [Figure 5.7]. The location and inclination of the arms are determined from preliminary analyses and by reasonable engineering judgment. In the analysis, the arms are treated as rigid members using *elasticBeamColumn* elements with large stiffness. Beams and columns are modeled by *nonlinearBeamColumn* elements with *Steel02* material which is used to construct a uniaxial Giuffre-Menegotto-Pinto steel material object.

The translational degree-of-freedoms of all nodes in the bottom beam are fixed and a static displacement is incrementally applied to left and right ends of the top beam until a target displacement is reached.

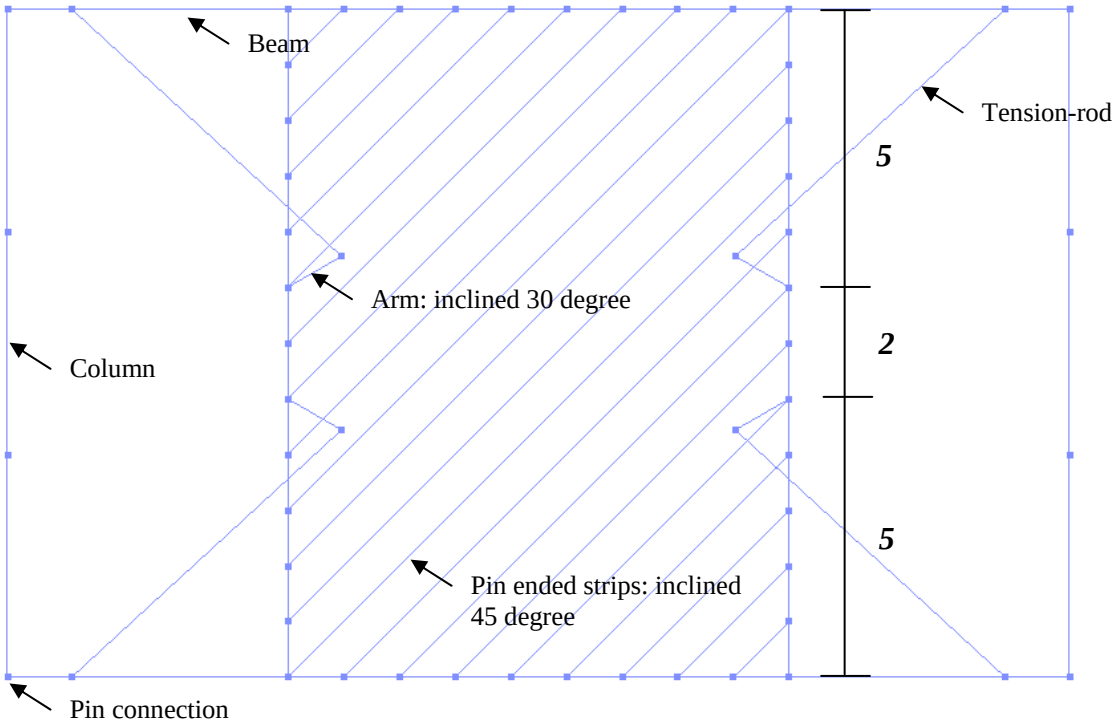

Figure 5.7: Analysis model in OpenSEES

Example Design: Prototype Design Review

1. The target shear strength of the prototype was 525kN (118kips). The clear story height of a frame was 3.5m and the aspect ratio of the infill panel was 4:3 (height-to-width).
2. The nominal shear strength of panel was with F_y = 200MPa (30ksi) with the selected thickness of the infill panel of 2.3mm (0.091in):

$$\boldsymbol{V_n = (0.42)(207)(3.2)(3500 \times 0.75)\sin 90°/1000 = 730kN} \qquad 5.1$$

The area of the strips was calculated as:

$$\boldsymbol{A_s = (3.2)(2625\cos 45° + 3500\sin 45°)/20 = 693mm^2} \qquad 5.2$$

3. Figure 5.8 shows the shear strength of the system and the hysteresis of the strips at in middle part of the infill panel with three different sections of the VBEs, CT-150x150x6.5x9 (CT-150, Z_x=33.8cm^3, roughly equivalent to an American WT4x12 section in terms of section modulus), CT-175x175x7x11 (CT-175, Z_x=59.3cm^3, roughly equivalent to WT5x16.5), CT-200x200x8x13 (CT-200, Z_x=88.6cm^3, roughly equivalent to WT6x22.5), and CT-225x200x9x14 (CT-225, Z_x=124cm^3, roughly equivalent to WT6x32.5). The yielding strength doubled when the section was changed from CT-150 section to CT-200 section. The yield shear force with CT-200 section was approximately 725kN (163kips) which was slightly larger to the target shear strength. The behaviors of 10 strips in the middle part of the infill panel are shown in Figure 5.9. With the CT-175 section, only 1 strips yielded prior to the yielding of VBEs, which is indicated in the non-linear force hysteresis of some strips before the force reached the yielding force of strips, 143kN (32kips) [Figure 5.9(a)]. The numbers of the yielded strips prior to the yielding of the VBEs were 6 both with

CT-200 section and CT-225 section, respectively [Figure 5.9(b) and (c)]. Table 5.1 summarizes the estimated yield shear from bi-linearization of hysteresis curves with various sections. The increase of section modulus affected significantly to the shear strength when section was upsized from CT-150 to CT-200. Once the shear strength of system was governed by the shear strength of the infill panel, the increase of section size did not lead to significant increase of the system shear strength. CT-200 section was selected for the section of VBEs in the prototype. Here, the tension rods were treated as elastic elements and the length of the arm was arbitrarily set to 280mm (11in).

4. The size of the tension-rod was defined based on the elastic force demand at 1% story drift, which was around 230kN (52kip) [Figure 5.10]. In the figure, the rods carrying larger forces were located in the extended diagonal of the frame and the others were located in the shortened diagonal of the frame. The size of the rods selected was M30 (ϕ = 1 5/32") with the yield strength of 234kN (53kip).
5. The yield shear strength of the system was 710kN (160kip) and was close enough to the target shear strength. It was also notable that the yield strength was pretty close to the nominal yield strength of the infill panel computed by the formula specified in the seismic codes.
6. The last step of the design was to define the length of arm. Figure 5.11 shows the force histories of tension-rods with the arm length of 254mm (10in), 280mm (11in) and 305mm (12in). The length was defined as 280mm (11in).

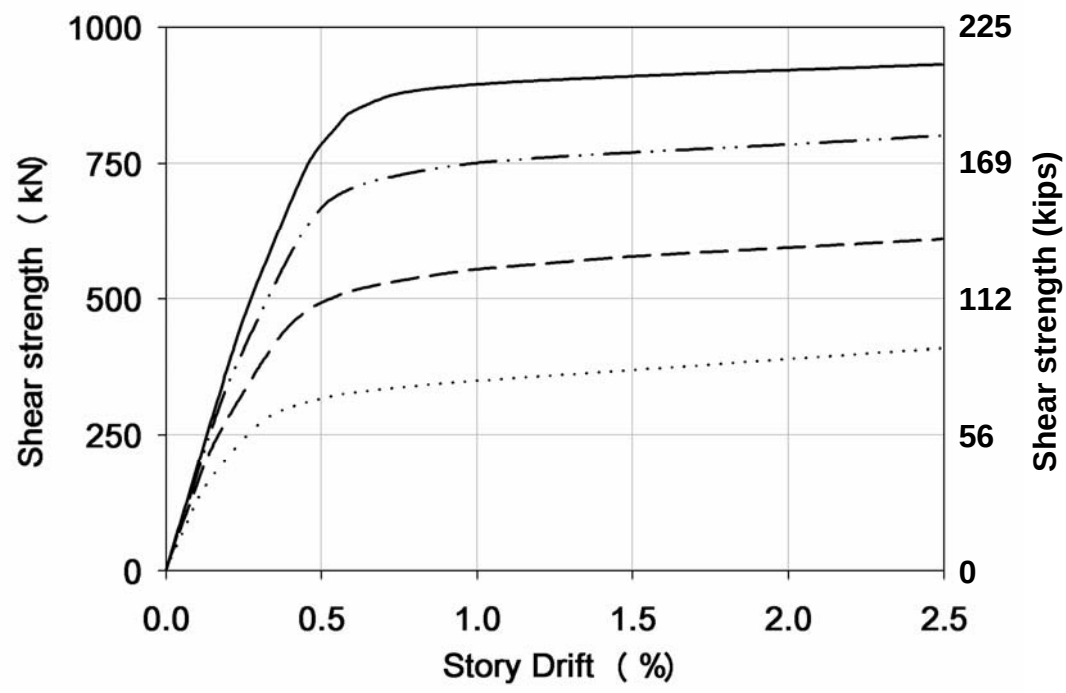

Figure 5.8: Shear strength with different VBEs

Table 5.1: Yield shear strength for various sections

Section	Z_x	*Increase from Z_x of CT-150*	*Yield strength*	*Increase from yield strength of CT-150*
	cm^3	%	kN	%
CT-150	33.8	0	300	0
CT-175	59.3	75	510	70
CT-200	88.6	162	725	142
CT-225	124	267	860	187

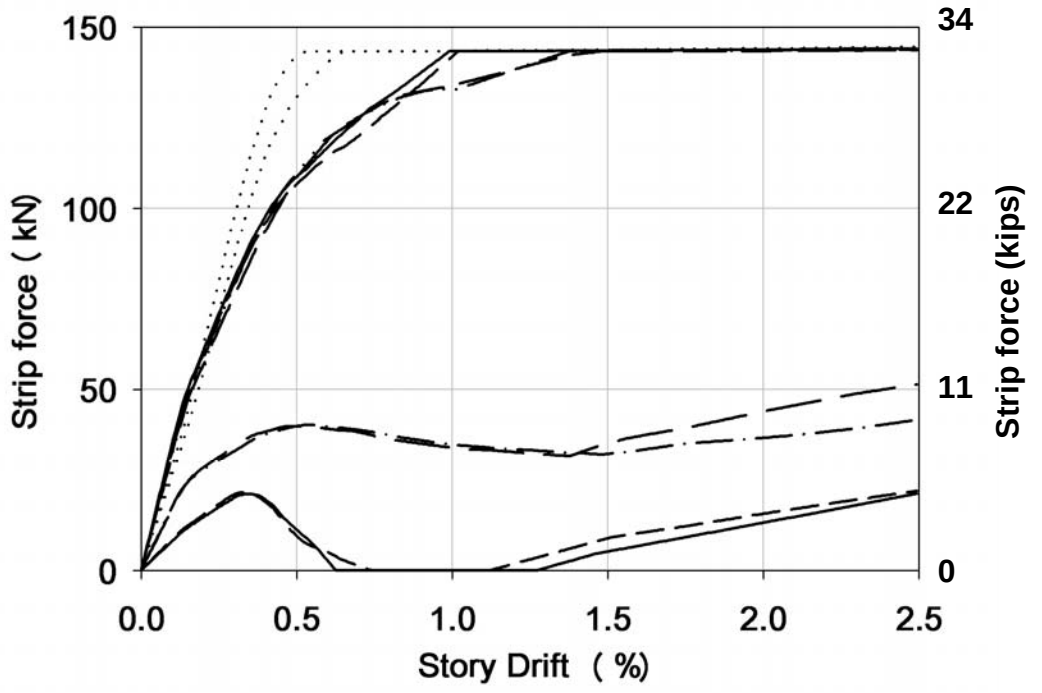

Fig 5.9 (a):

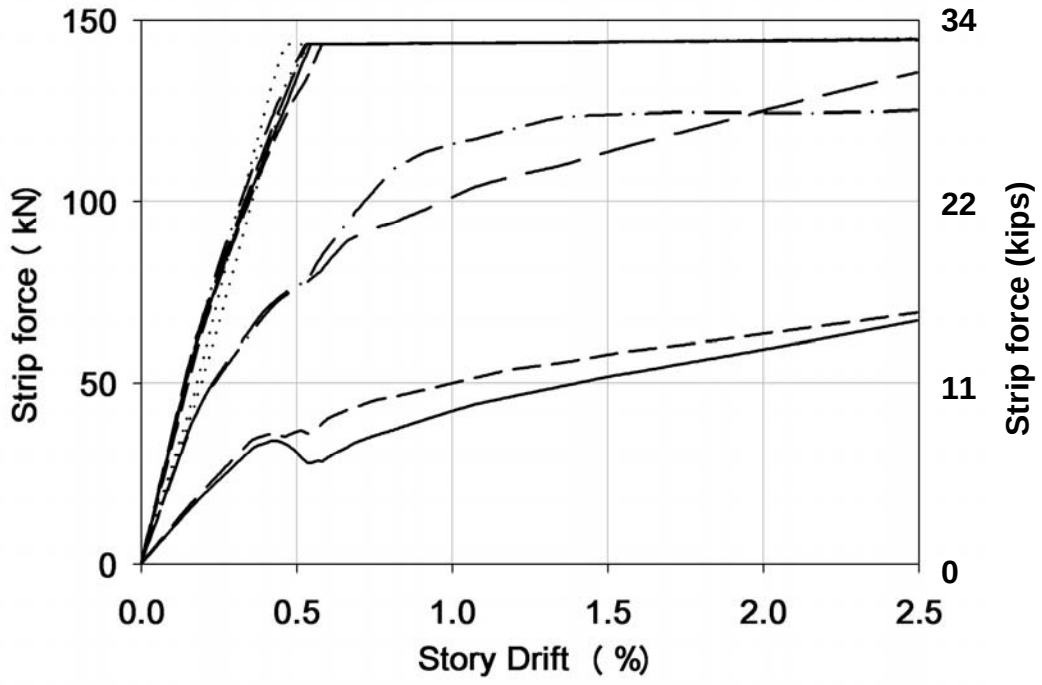

Fig 5.9 (b):

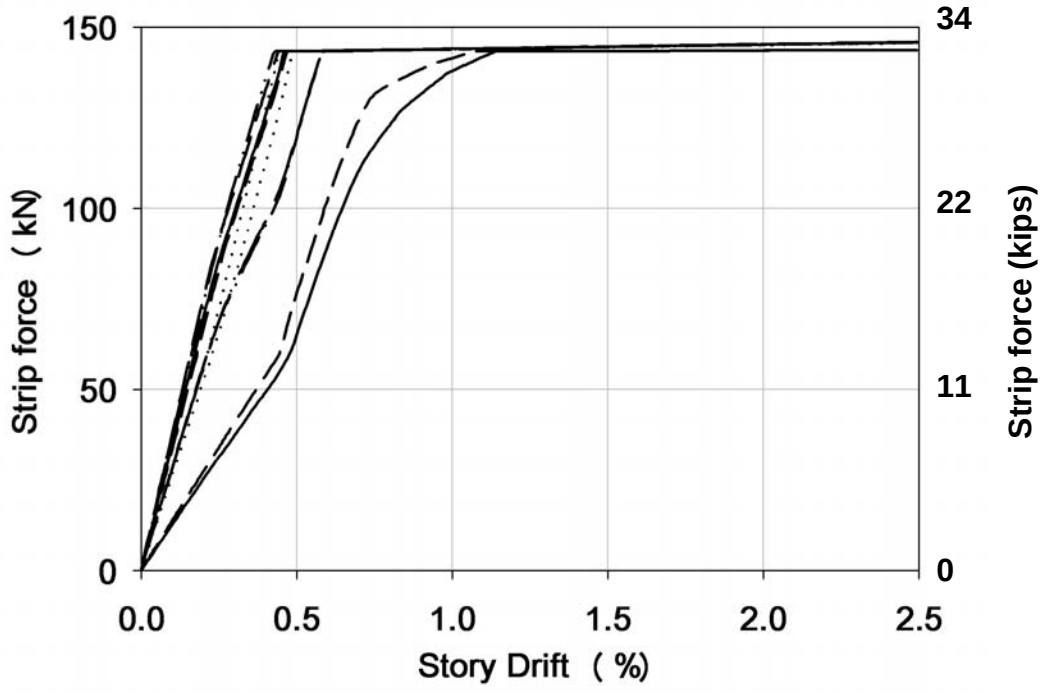

Fig 5.9 (c):

Figure 5.9: Hysteresis of 10 strips in middle part of infill panel (a) CT-175x175x7x11 (b) CT-200x200x8x13 (c) CT-225x200x9x14

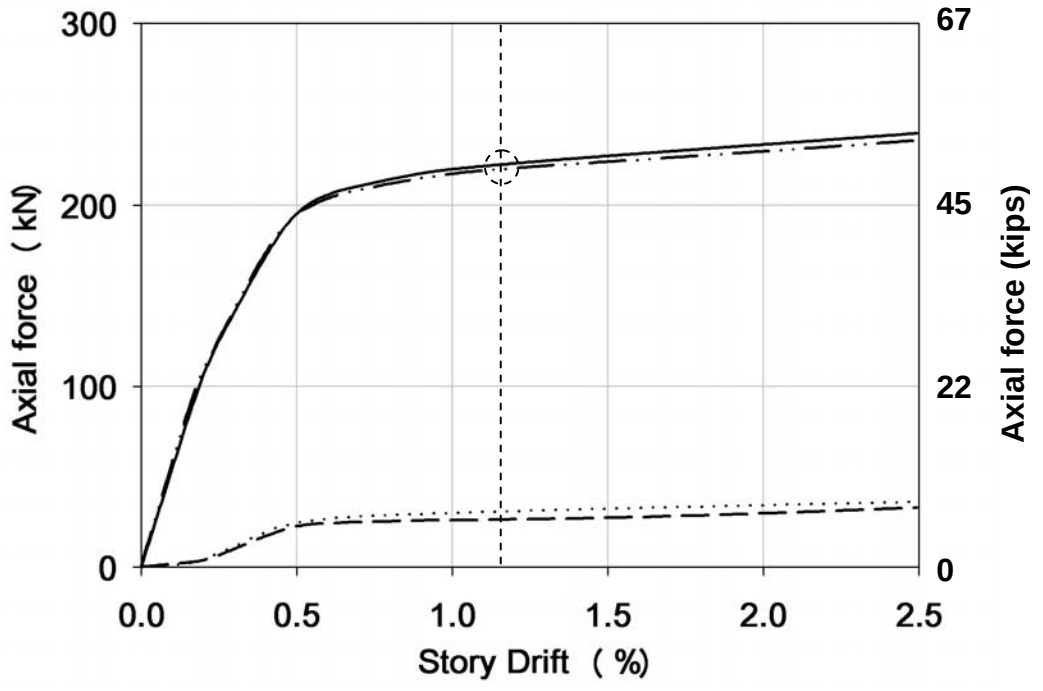

Figure 5.10: Force histories in elastic tension-rods

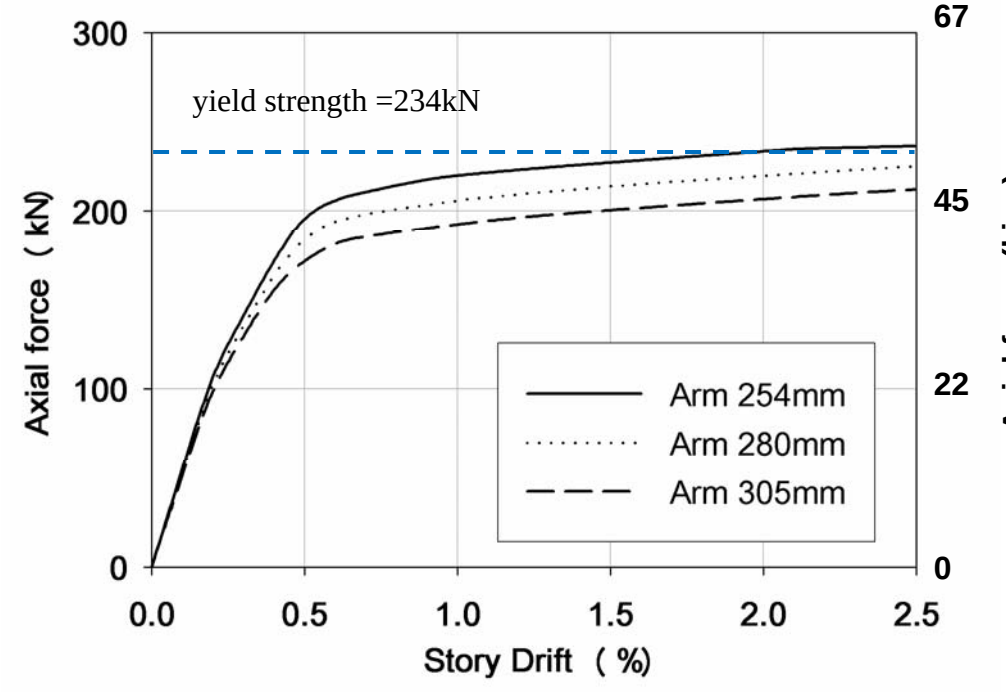

Figure 5.11: Force histories in tension-rods with various arm length

5.4 Analysis of Scaled System

The prototype system was scaled for the proof-of-concept testing whose details are described in Chapter 6. The scaled system was designed using the proposed design procedure with the clear story height of 1750mm (69in) and the story height of 2000mm (79in): the system was scaled to 50% with respect to width and height. The thickness of the infill panel was 1.6mm (0.063in) so that the prototype is scaled to 50% in all dimensions. The target shear strength of the system was scaled down to 25% of the prototype strength, 177kN (40kip).

The geometry of the scaled system is described with more details in Chapter 6. Using the proposed design procedure, the section of VBEs, the size of tension-rods and the length of arms were selected as CT-75x100x6x9, M16 (ϕ=5/8") and 100mm (3.9in), respectively.

OpenSEES Analysis Results

The predicted behavior of the scaled system is shown in Figure 5.12. The shear strength of the system was around 180kN (40kips) at 0.45% story drift which was close enough to the target shear strength and the nominal shear strength of the infill panel computed by the code equation. All tension-rods remained elastic until 2.5% story drift. The more than half of middle strips yielded prior to the infill panel.

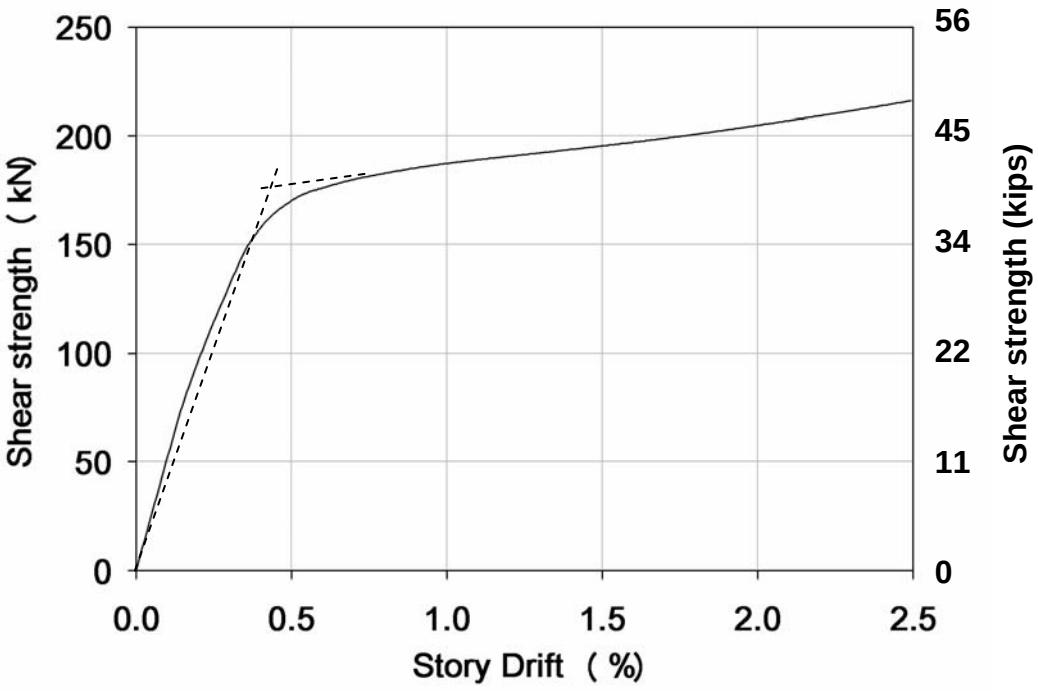

Fig 5.12(a):

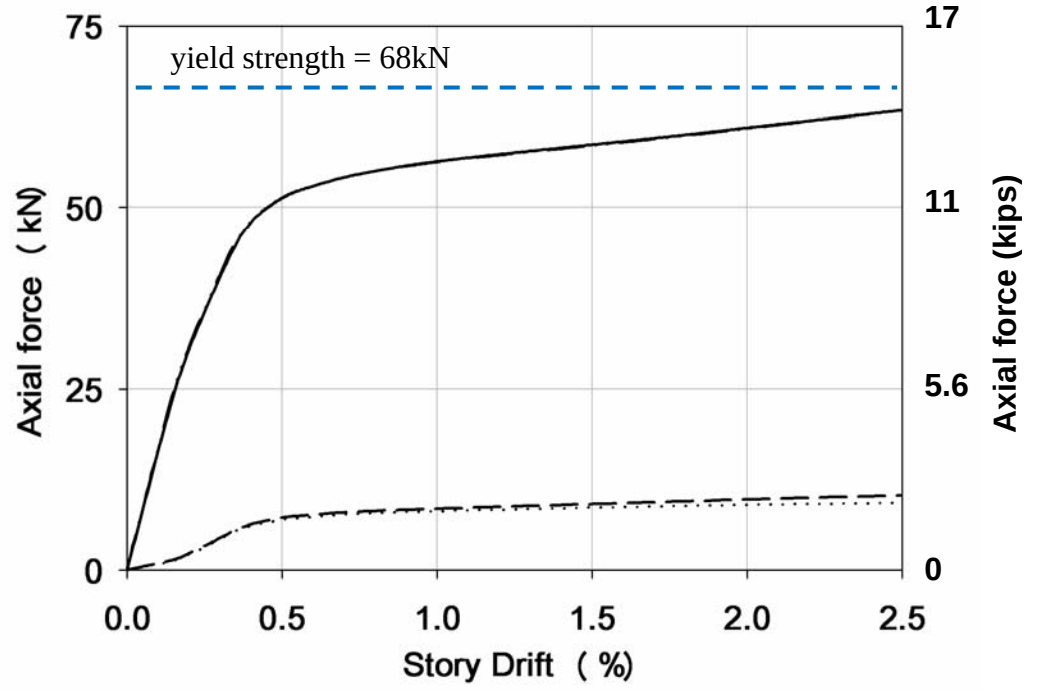

Fig 5.12(b):

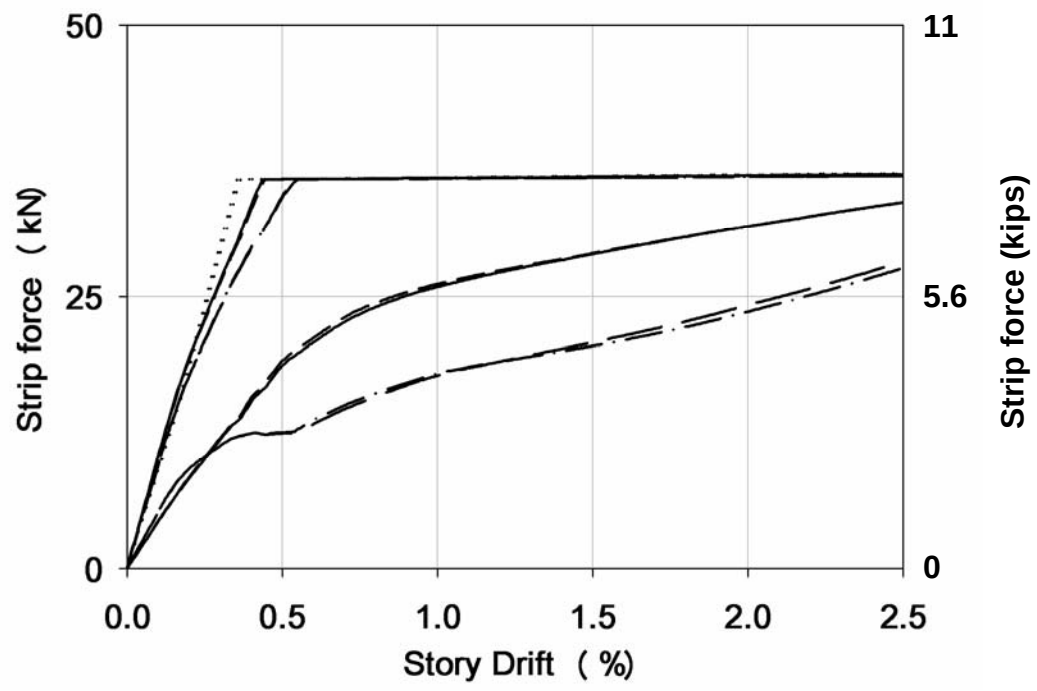

Fig 5.12(c):

Figure 5.12: Hysteresis of scaled system in OpenSEES analysis (a) global hysteresis (b) force histories of tension-rods (c) hysteresis of strips

FE Analysis of Scaled System

The detailed behavior of the scaled system was examined using a general-purpose finite element program, ABAQUS. The purpose of the FE analyses was to provide an accurate prediction of both global and local behavior for the experimental study and to validate the OpenSEES analyses system. The scaled system was analyzed together with the test setup used in the proof-of concept test at the Disaster Prevention Research Institute (DPRI) in Kyoto University [see details in Chapter 6 and Appendix B].

Figure 5.13 shows the analysis model constructed in ABAQUS. The bottom beam was ignored in the system. The bottom boundaries such as bottom pins and the flanges of the bottom HBE were fixed instead. All components except tension-only rods and arms were modeled using a general-purpose four-node, doubly curved, finite membrane strain shell element (S4R) with reduced integration and linear geometric order. A two-node linear truss element (T3D2) was used for the modeling of the tension-rods. The arms were modeled by connecting the ends of the tension-rods and the flanges of the VBEs where arms were attached with a *rigid constraint* feature. The HBE-VBE connections as well as beam-column connections were modeled by the combined use of *beam* and *link* connectors. The infill panel was rigidly connected to the boundary elements using the *tie constraint* feature. The top HBE was connected to the bottom flange of the top beam again using the *tie constraint* feature.

For comparison, nonlinear finite element analyses were conducted for the scaled system as well as the scaled system without tension-only elements. The displacement-controlled analyses were executed up to 2.5% story drift. Prior to the pushover analyses,

an out-of-plane imperfection of 0.05% was applied to the top beam to initiate global buckling in the infill panel.

FE Analysis Results

The hysteresis curves of two systems in terms of shear strength versus story drift relationship are shown in Figure 5.14(a). The predicted yield shear strength for the system with tension-rods was slightly higher than that from OpenSEES analysis and was around 185kN at 0.3% story drift. The FE analysis predicted 50% larger initial stiffness and very small post-yielding stiffness compared to those from a strip model. The shear strength increased by approximately 65% with the presence of the tension-only elements.

The deformed shape of the scaled models are shown in Figure 5.14(b) and (c) with the von Mises stress contours. Most of the middle part of infill panel yielded for both cases, but the yielded area, indicated by green color, was larger with tension-only elements. More notably, most of the VBEs yielded with tension-only elements while, without tension-only elements, damage was highly concentrated to the area of HBE-VBE connections involving plastic hinge formation. The HBE-VBE connections located in the extended diagonal suffered from large closing deformation for the system without tension-only elements. The closing deformation was much moderate with the presence of tension-only elements.

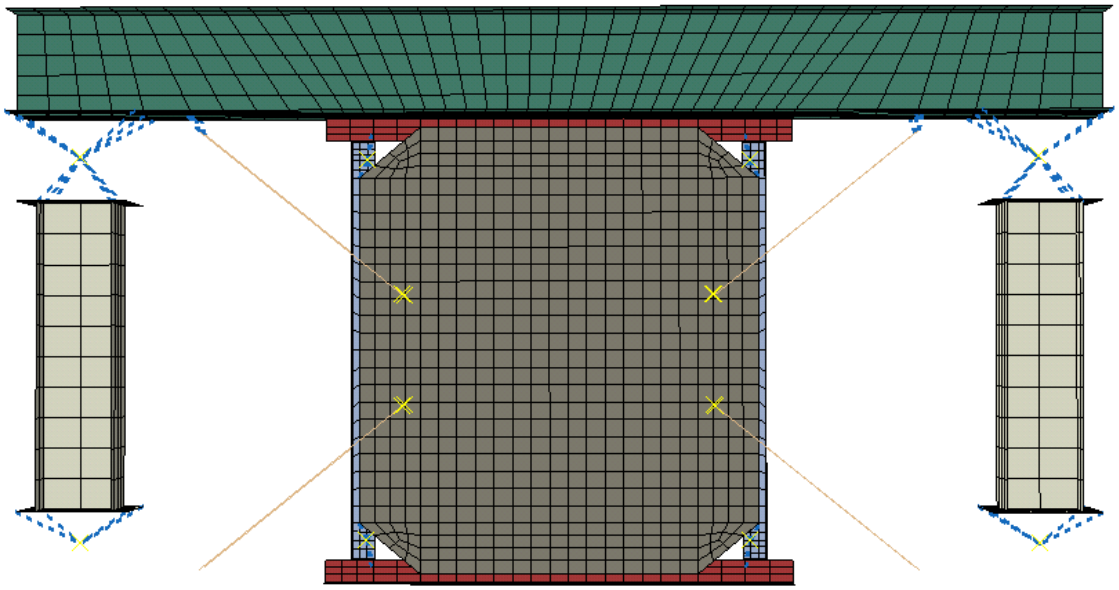

Figure 5.13: FE analysis model

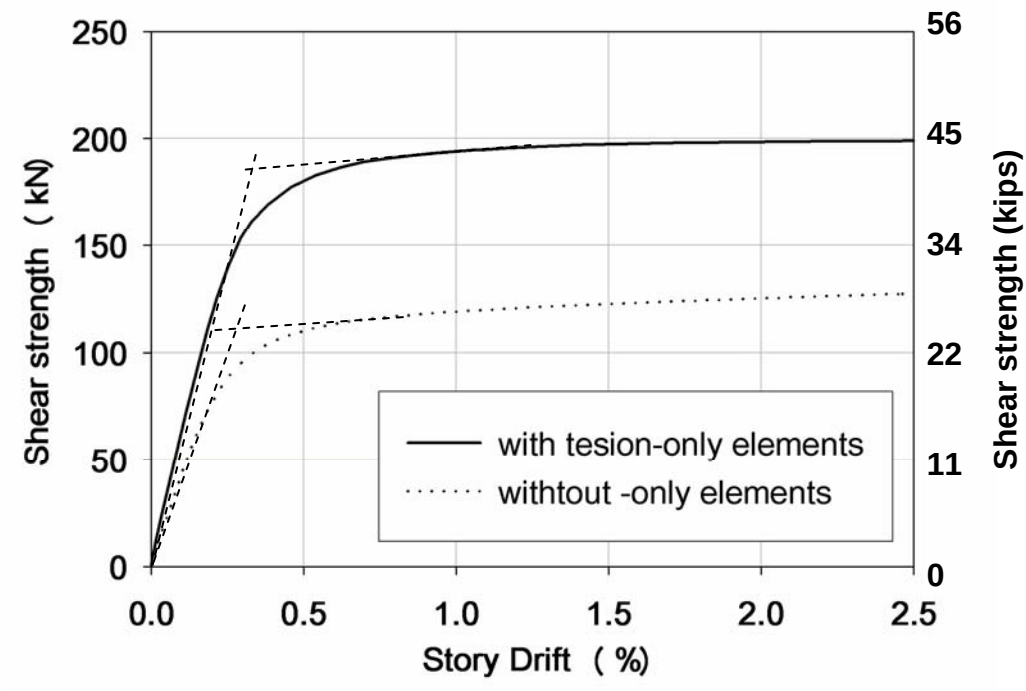

Fig 5.14(a):

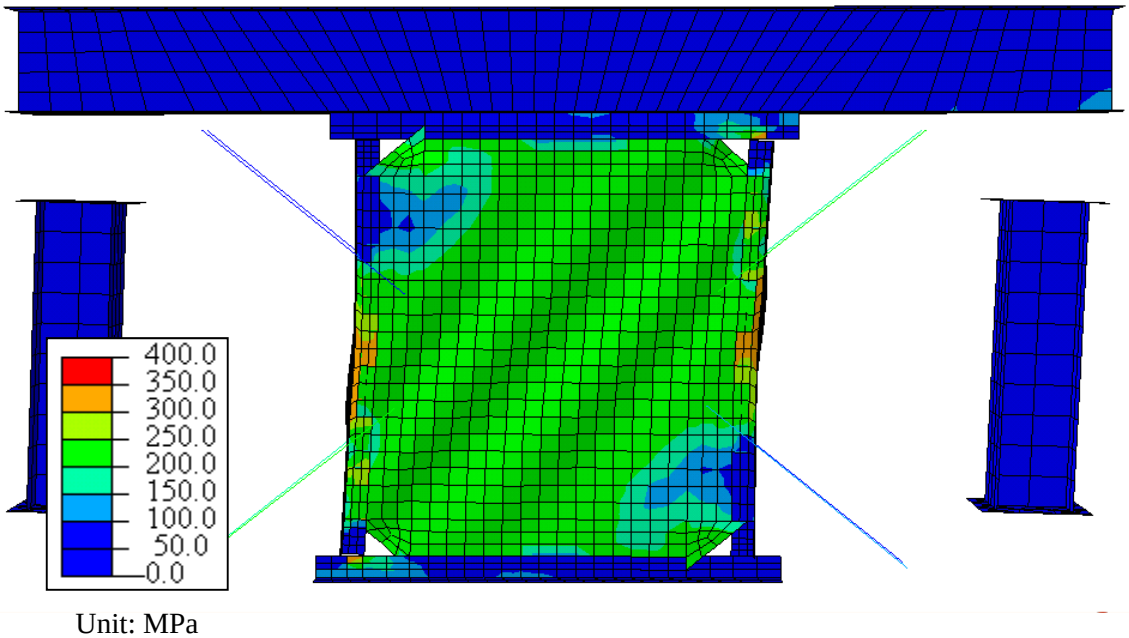

Unit: MPa

Fig 5.14(b):

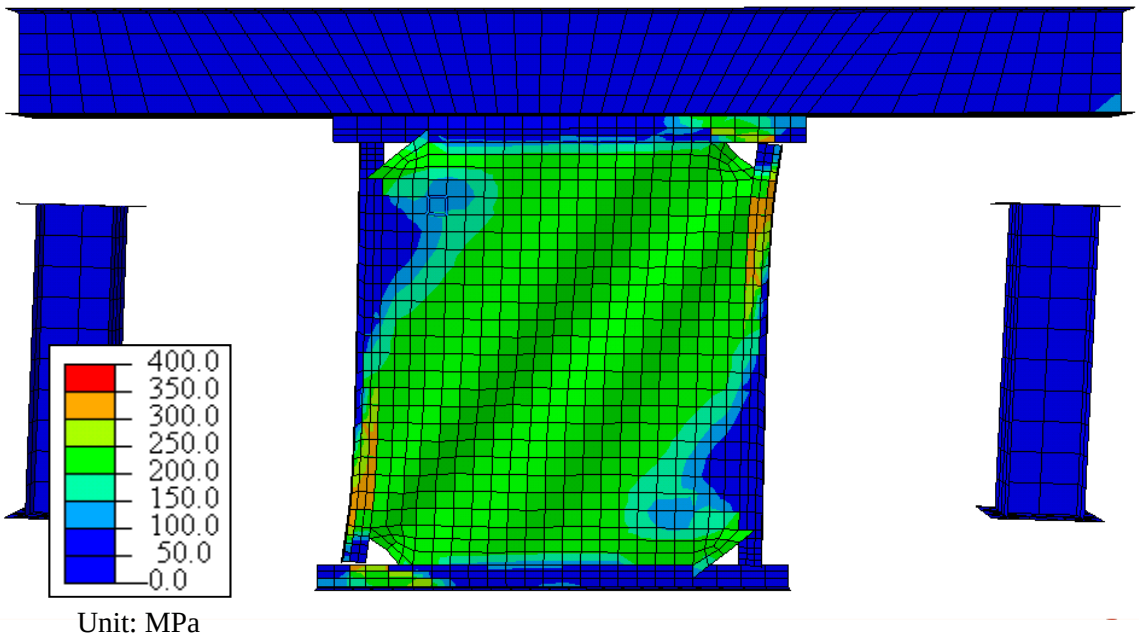

Unit: MPa

Fig 5.14(c):

Figure 5.14: FE analyses results (a) hysteresis curve (b) stress contour for scaled model (c) stress contour for scaled model without tension-only element

5.5 Summary

In order to utilize a thin steel plate as a supplemental lateral load resisting system for relatively small seismic rehabilitation projects, a geometry where a thin steel plate with boundary elements was installed in the middle of the span, separately from exiting columns, was examined. The proposed geometry intends to minimize impact and to reduce the need to strengthen the existing columns. These columns would have typically been designed for the combined forces of gravity and wind. The Vertical Boundary Elements (VBE) in the proposed system need to have enough strength and stiffness relative to the infill steel plate, otherwise the thin plate will not resist seismic effectively.

The prototype of the proposed system "Narrow Steel Plate Shear Wall with Tension-Only Bracing (NPSW-TB)" was presented. The performance goal of the system was to achieve a total system shear strength of 707kN (160kips), which is compatible approximately to the shear force carried by three columns with standard section in low-to-mid size steel moment resisting frames when columns were assumed to have fixed-fixed end conditions. The geometry of the prototype was selected following the design flowchart developed based on the proposed design approach. A main design constraint for the prototype system is the requirement that yielding of the infill panel should occur prior to yielding of the boundary elements. The vertical boundary elements (VBE) was also subjected to inelastic deformation later due to the inward flexural force induce by the tension field developed in the infill panel. The design of the VBE requires an iterative procedure since its behavior interacts with the behavior of the tension-only rod and the local geometry of the arm. The tension-only elements are designed to remain elastic until very large deformation.

The performance of the prototype was evaluated by a displacement-controlled static pushover analyses. The performance goal of the prototype system was to achieve a total system shear strength which is compatible approximately to the shear force carried by three columns with standard section in low-to-mid size steel moment resisting frames when columns were assumed to have fixed-fixed end conditions. The shear strength of the prototype system obtained from a simplified analysis model was close to the shear strength of the infill panel computed by the formula specified in the current seismic codes in U.S. and Canada.

A scaled system was also designed for proof-of-concept testing using the proposed design procedure for a frame 50% scaled with respect to width and height. For comparison, nonlinear finite element analyses were conducted for the scaled system as well as the scaled system without tension-only elements. The detailed behaviors of the scaled systems were examined using a general-purpose finite element program, ABAQUS and were compared with the prediction from the preliminary simplified analyses in OpenSEES. Most of the middle part of infill panel yielded for both cases, but the yielded area was larger with tension-only elements. More notably, most of the VBEs yielded with tension-only elements while, without tension-only elements, damage was highly concentrated to the area of HBE-VBE connections involving plastic hinge formation. The HBE-VBE connections located in the extended diagonal suffered from large closing deformation for the system without tension-only elements. The closing deformation was much moderate with the presence of tension-only elements. The predicted yield shear strength in both analyses was very close to the design shear strength. The initial stiffness of the system predicted in the FE analysis was 50% higher

than that in the OpenSEES analysis. The shear strength increased by approximately 65% with the presence of the tension-only elements.

CHAPTER 6

EXPERIMENTAL STUDY OF NARROW STEEL PLATE SHEAR WALL WITH TENSION-ONLY BRACING

6.1 Introduction

The performance of the scaled prototype of the narrow steel plate shear wall system [Chapter 5] was evaluated through an experimental program conducted at Kyoto University, Japan. This program was embedded into a series of experiments for shear wall type structures planned at the Disaster Prevention Research Institute (DPRI) of Kyoto University, in cooperating with Dr. M. Nakashima. For these experiments a test setup was designed by the author and installed into an existing, large load reaction frame at the structural laboratory of DPRI.

In the experimental program, two shear wall specimens were tested. One was the prototype specimen with tension only bracing and another was a specimen without tension-only bracing to evaluate the effects of the bracing on the global and local behavior of the prototype. The test specimens had a dimension scaled to approximately 50% of the prototype size due to size limitations of the existing load reaction frame. The test setup and specimens were fabricated by a local fabricator in Kyoto using members and materials specified in Japanese standard [JIS, 2005]. As a part of the experimental program, a pre-qualification tests for the unique welding method specifically intended for shear walls with light gauge steel plate were also conducted.

The first coordination meeting was held at Georgia Institute of Technology in May, 2008 for planning the overall scope and schedule of the experimental program. This was followed by a second planning meeting at the DPRI in July, 2009 for the draft design of a test setup and a budgetary plan. The third planning meeting to finalize the specimen design was held in conjunction with the pre-qualification test of the welding method, and took place at DPRI in November, 2008. The tests were carried out over a two week period in March 2009. Each test encompassed two days for the assemblage of the test setup, three days for the installation of each specimen and instrumentation, one day for the tensile coupon tests, two days for testing and one day for cleanup. The program was successfully completed without any time delay thanks to an invaluable support from the local specimen manufacturer and the graduate students of Dr. M. Nakashima's research group. The timeline of the experimental program is summarized in Table B.1 [see Appendix B].

6.2 Test Setup

For this work, a new testing setup was installed into an existing load reaction frame at the structural laboratory in the DPRI. The testing setup is a portal frame with four pins at each corner and has an inter-story height of 1748mm and a column centerline spacing of 3000mm [Figure 6.1]. The main components of the testing bed were as follows: (a) top and bottom H-400x400x13x21 beams (b) two H-250x250x9x16 columns (c) four pin-clevis subassemblies with load carrying capacity of 900kN each (d) a fixed support for the actuator loading. The beam and column designations indicate the overall height and width of the section and the thickness of the webs and flanges, respectively; there are no corresponding US rolled section sizes for these members. The dimension of the components are shown in Appendix B.

The assembly is capable of applying a horizontal force more than 750kN which is determined by slip critical force at bolted connections. The assembly was installed into the reaction frame by fixing its bottom beam to a foundation beam using 12-F10TM22 (A325 7/8 in. approximately) high strength bolts and by connecting the top beam to the horizontal actuator via fixity.

The deformation of the test setup was restrained to in-plane deformations using out-of-plane restrainers and guiding beams [Appendix B]. Two restrainers, each of which consists of a short wide flange beam and two frictionless rollers, were attached to the top beam of the test setup. The top beam was guided to deform in-plane by the physical contacts between the frictionless rollers and the guiding beams attached to the loading frame.

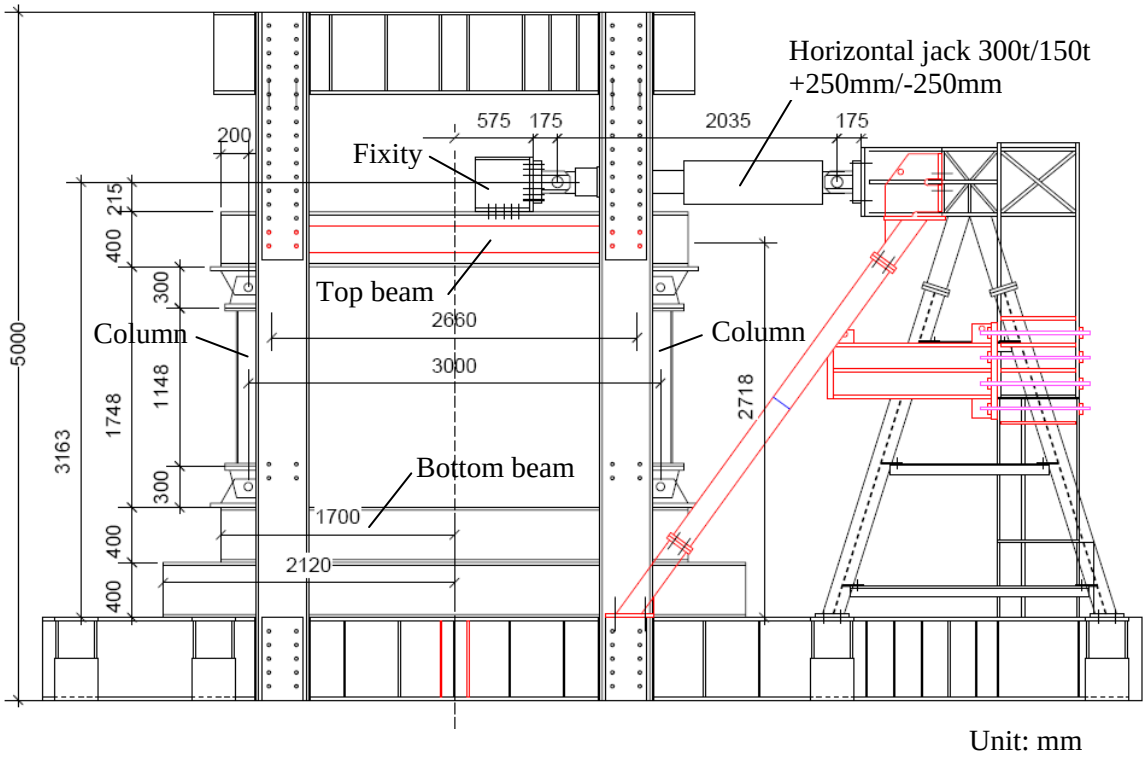

Figure 6.1: Loading frame and test setup

6.3 Loading System

The loading system at the DPRI was a fully automated system. Primary hardware devices included: (1) a quasi-static horizontal loading actuator, (2) a hydraulic pump system activated by an inverter motor, (3) a load cell which measures the reaction force of the actuator (4), a digital displacement transducer which measures the displacement of the actuator (5) a pump controller that control the frequency of the inverter motor to adjust the actuator's ram speed (6) a switch box and data logger that collects strain gauges, LVTDs, and other date (7) a PC that controls the controllers (8) another PC that stores the data collected by the data logger.

The horizontal actuator had a stroke capacity of ±250mm and a force capacity of ±1500kN. In order to measure the movement of the cylinder, a digital transducer was attached. The controllers selected the direction of actuator motion ("push" or "pull"), the frequency of the inverter motor during loading, the frequency of the valve during unloading, and change between the loading and unloading modes.

6.4 Specimen Details

The geometrical properties of the two specimens are shown in Figure 6.2. The two specimens, S1 and S2, were identical except for the tension-only bracing attached to Vertical Boundary Elements (VBE) in S2. The typical assembly of a specimen was as follows: (1) Horizontal Boundary Elements (HBE) were attached to top and bottom beams of the test setup with high strength bolts, (2) VBEs were pin-connected to HBEs with L-shape plates and M16 high strength bolts, and (3) an infill thin steel panel was welded to HBEs and VBEs. For the specimen with tension-only bracing (S2), the assembly continued as follows: (4) four steel brackets were installed to VBEs using M14 high strength bolts after the welding of the infill panel (5) four pad-eyes were installed to top and bottom beams (6) eight tension-only braces, composed of a 5/8" steel threaded rod and a 5/8" steel turnbuckle, were connected the steel brackets and the pad-eyes.

The dimensions of each component are shown in Appendix B. The HBEs and VBEs were CT-100x175x8.5x11 and CT-75x100x6x9, respectively. The connection between the HBE and the VBE was assumed as a pinned connection. The L-shape connector was allowed to slip at oversized holes under in-plane bending moment but not under axial or shear force. The infill steel panel was a 1.6mm thin steel plate with its dimension of 1250mmx1673mm. The material of the panel was a low carbon mild steel, SHPC whose the chemical composition shown in Table 6.1. The corners of the infill panel were cut to avoid interference with the connectors. A series of small holes (ϕ=10mm) along the edge of the infill panel were for welding inside of holes to attach the infill panel and boundary members. The steel bracket consisted of mild steel plates (SS400) with thickness of 6 mm and 9 mm. The wall of the bracket was enforced by

cheek plates and stiffener plates. The material properties of the infill panel, the web of the HBE, the flange and web of the VBE were obtained from tensile coupon tests and summarized in Table 6.2. The shape of the coupons followed the Japanese Industry Standard [JIS, 2005].

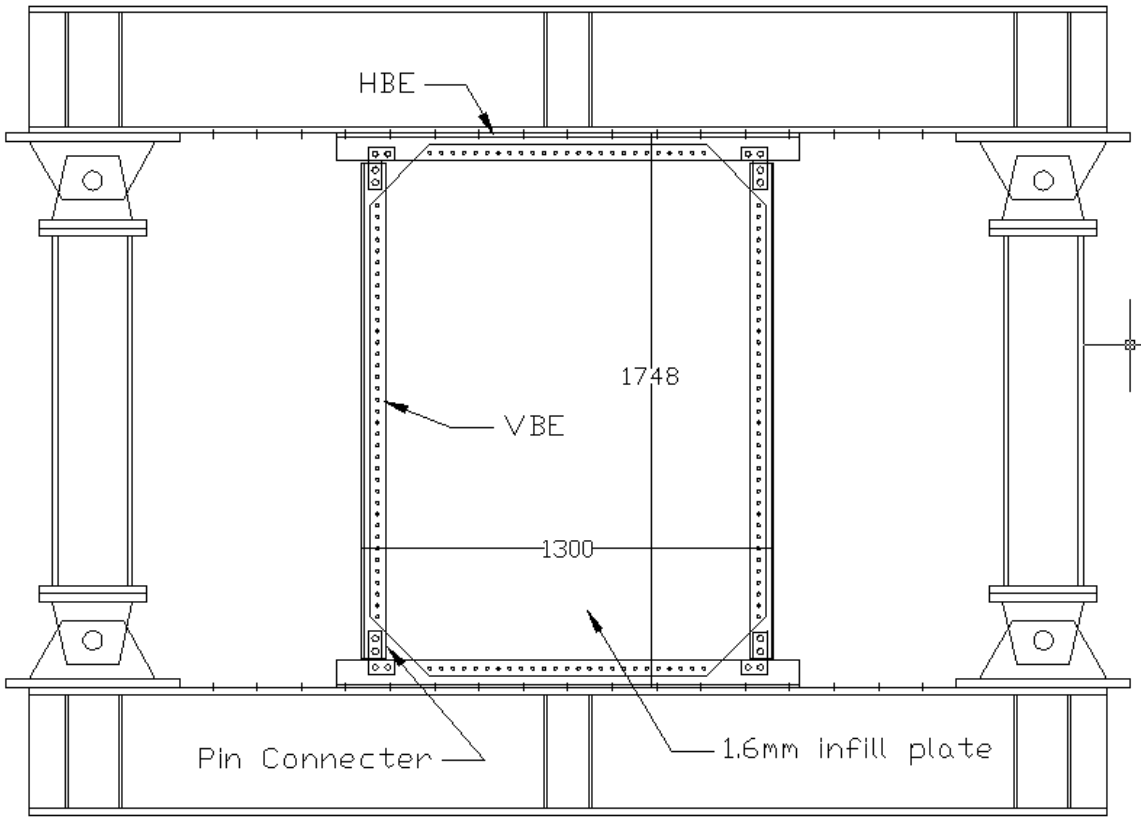

Specimen

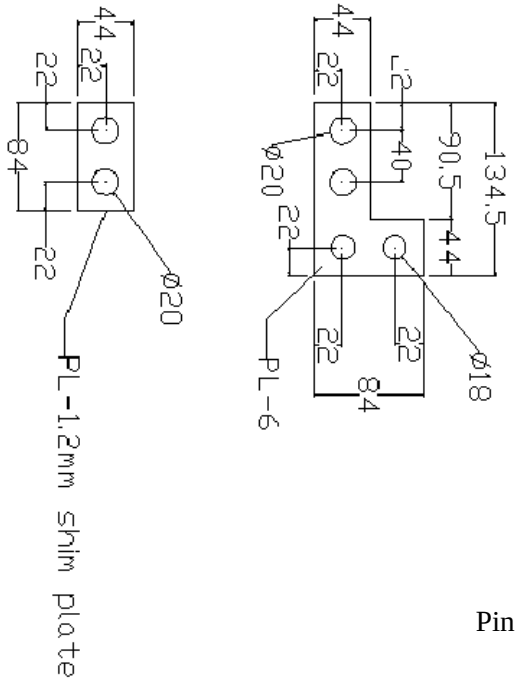

Pin connector close up view

Fig 6.2(a):

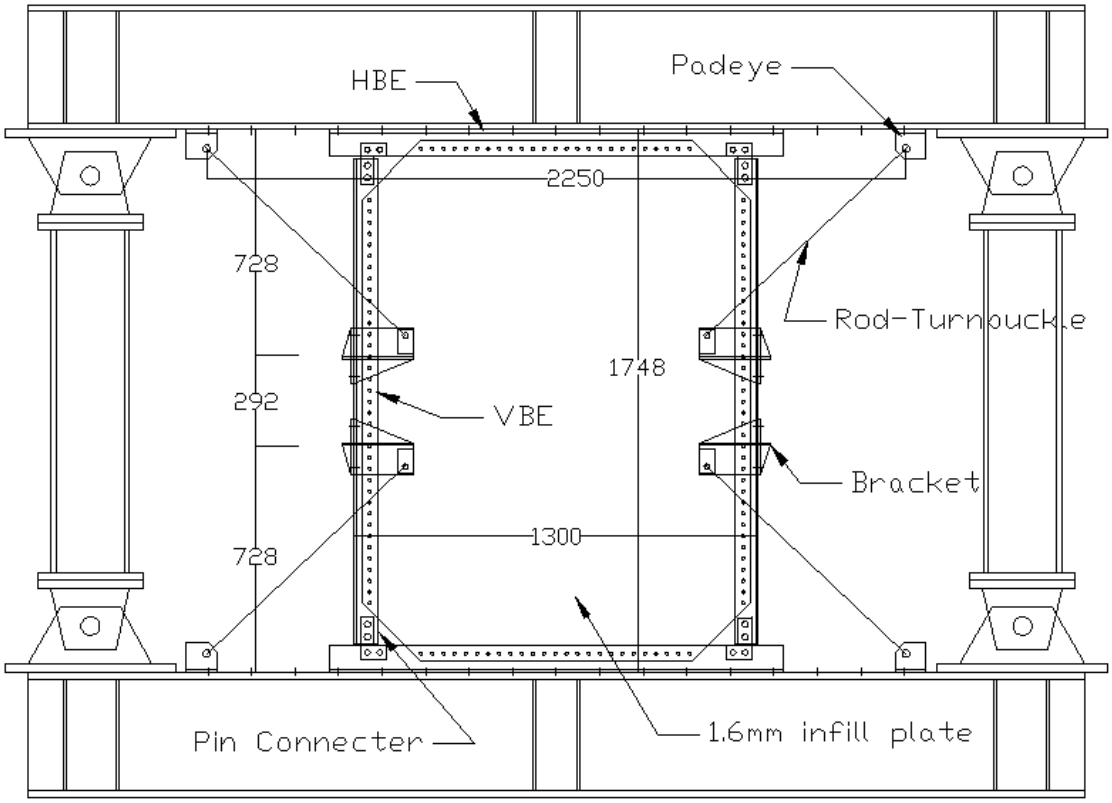

Specimen

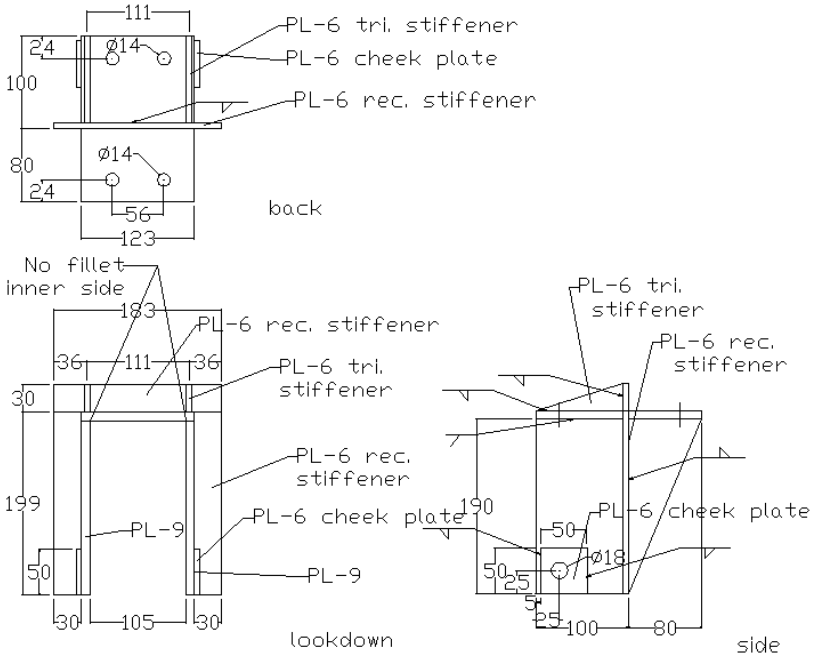

Bracket close up view

Fig 6.2(b):

Figure 6.2: Specimen dimensions (a) specimen 1 - no bracing (b) specimen 2 - with bracing

Table 6.1: Chemical composition

Element	Material	*C* (%)	*Si* (%)	*Mn* (%)	*P* (%)	*S* (%)
Infill panel	SPHC-P*	0.07	0.021	0.070	0.020	0.011

* Steel Plate Hot Commercial Pickling (JIS G3131, JSA 2005)

Table 6.2: Mechanical properties

Name	Element	Coupon Shape*	*Thickness* t (mm)	*Yield strength* σ_y (MPa)	*Tensile strength* σ_u (MPa)	*Elongation* *EL* (%)
C-A	Infill panel	JIS 1B	1.60	201.9	329.6	34.4
C-B	VBE web	JIS 1A	5.61	328.9	438.1	28.0
C-C	HBE web	JIS 1B	6.88	343.4	482.1	19.9
C-D	VBE flange	JIS 1A	8.63	299.7	430.1	28.7

* Coupon shape refers to the Japanese Standard Association (JIS Z2201, JSA 1980)

6.5 Method for Connecting Infill Panel to Boundary Elements

For structural efficiency, the infill steel panel need to be continuously connected on all edges to the boundary elements with welds and/or slip-critical high strength bolts. This will allow the wall to develop the nominal shear strength of the panel [AISC, 2007]. Per capacity design principles, the connections to the surrounding HBE and VBE are required to develop the expected tensile strength of the infill steel panel. Net sections must also provide this strength for the case of bolted connections. Designs of connections between the infill panel and the boundary elements should also anticipate the buckling of the infill panel as the connections are subjected to tension and compression force during cyclic loading. Previous results indicate that thin steel plates, which are adequately supported along all edges and subjected to cyclic shear loading, have stable hysteretic behavior in the post-buckling region [Elgaaly, 1998; Berman and Bruneau, 2003]

Background

In the majority of past experiments, the infill wall was attached to the boundary elements via a continuous fillet welding method [ex. Sabelli and Bruneau, 2006]. Elgaaly reported that the bolted plate shear walls had smaller elastic stiffness and lower initial yielding load than welded shear walls [Elgaaly, 1998]. For a bolted plate, loss of initial stiffness can occur when the bolted connection starts slipping or when the plate yields locally near the boundaries. The load to cause slippage is controlled by the friction coefficient between the connected surfaces and the normal force applied by the bolts.

A thin steel plate available in commercial market changes as its thickness gets thinner. A steel plate commonly used as a structural steel (SS400 in Japanese standard or

A36 in US standard) is available in thicknesses of 4.5mm or thicker. Steel plates thinner than 4.5mm are available with the material as SPHC (Steel Plate Hot Commercial) or as SPHC (Steel Plate Cold Commercial) in the Japanese market. These materials are commonly used for mechanical engineering applications and contain more carbon and have surfaces smoother than typical structural steel. Bacuse of the lower friction coefficients for this type of plate, the design of a bolted connection with these materials requires more bolts than that with a common structural steel.

When welding is selected as the method for attachment, distortion and residual stresses in the thin steel panel becomes a concern. The distortions and residual stresses are primarily caused by an angular bending of the plate itself due to the shrinkage of weld metal in unsymmetrical welds [Bruneau *et al*., 1998]. For the case of Special Plate Shear Wall (SPSW) Caccese *et al*. reported a loss and nonlinearity in initial stiffness attributed to the slenderness of the infill plate; the imperfections in the plate due to fabrication cause out-of-plane deformations that commence almost immediately and the plate can sustain virtually no in-plane force without transverse movement [Caccese *et al*. 1993]. In modern design guidelines, the effect of residual stress due to welding are considered indirectly through strength reduction factors for the design column buckling strength [AISC, 2007; Galambos, 2008].

The magnitude of the distortions depends on several design-related and process-related variables. Examples of design-related variables include weld joint details, plate thickness, transition thickness, and assembly sequence, while important process-related variables include welding process, number of welding pathes, heat input, travel speed,

and welding sequence. The analytical studies of the distortion mechanism and the effect of welding sequence on panel distortion can be found in [Tsai *et al*., 1999].

The common strategy for welding a thin steel panel is a single path continuous fillet welding, as the angular distortion increses almost proportionally with the number of welding path increases [Wakabayashi, 1985]. As a plate become thinner, the welding around all edges should be completed in shorter time since the distortion increase as the speed of welding decreases. However, the single path, continuous, and rapid welding technique demands high skilled and experienced welders and results in sacrifying the reliability on the welding strength.

Pre-Holed Fillet Welding

The infill panel used in the scaled specimen was 1.6mm. After a discussion with the local manufactures in Japan, it was decided that a discrete welding method would work better than a continuous fillet one for this specimen in order to minimize initial out-of-plane imperfections and residual stresses. These two phenomena result in the loss of initial stiffness and yield strength as discussed earlier. One of the commonly used discrete welding methods in construction sites is a deep arc spot welding (puddle welding), used for the attachment of deck plates to steel beams. The installation of deck plate in a construction site and sections of a deep spot arc weld are shown in Figure 6.3. The welding procedure specified in a Japanese manual is as follow [BCJ, 2009]: (1) hold deck plate to the surface of a beam (clearance less than 2mm) and establish arc electrode with the position of a welding rod perpendicular to the deck plate; (2) slightly pull up the welding rod and spark arc and burnout the deck plate for a circle shape with a diameter of 10mm; (3) push the welding rod to reach the surface of the steel beam and move the

welding rod along the inner boundary of the circle for two-three times; (4) shape the weld metal and gently pull up the welding rod at the center of the circle; and (5) remove slag and check the finishing. Normally, welding at each spot takes around 10sec and generates an excessive weld metal in a circle. For the welding, a welding machine with AW250A or more with a non-covered hydrogen arc welding rod with a diameter of 4mm are specified in the manual. For design calculations, a minimum, long-term tensile strength of one spot weld is specified as 4.9kN.

The deep arc spot welding is widely use for the installation of deck plates but not for critical welding such as the installation of steel plate shear wall. The main reasons include the larger uncertainty of weld strength compared to that in fillet welding and the location of the weld. This welding method is not suitable for the installation in an upright position because an excessive amount of melted weld metal drops from the circle [Figure 6.3(c)].

To reduce the uncertainty in welding strength and to reduce the amount of excessive melted weld metal, the author and a local manufacture in Kyoto developed a "pre-holed fillet welding method". In this method, small diameter circles are prefabricated at the location of welding along the edges of a steel panel. The infill panel is attached to the surrounding boundary elements by fillet welding along the inner boundary of the holes.

Fig 6.3(a):

Fig 6.3(a):

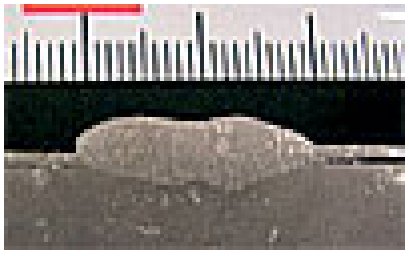

Fig 6.3(c)

Figure 6.3: Photos of deep spot arc welding photos (courtesy of JFE steel) (a) installation of deck plate (b) in-plane section of a spot welding (c) out-of-plane section of a spot welding

Preliminary Welding Test

To investigate the performance of this newly developed welding method, preliminary welding tests were conducted using the same thin steel plate as the infill panel in the scaled specimens. For comparison, the performance of the deep arc spot welding method was investigated as well. The main parameters in the preliminary welding tests were the method of welding, the posture of the welder, the welding size in diameter and a welding pitch [Table 6.3]. The dimension of specimen for the tensile test was 180 x 300mm [Figure 6.4]. The shape of a loading grip made of 9mm A36 steel plate was designed specifically for the universal loading machine in the structural laboratory at the DPRI. The pitch of the location for welding was calculated using a minimum, long-term tensile strength of one spot weld specified in the manual [BCJ 2005].

The stress and strain relationship of a specimen was monitored and recorded using Visual Log Light, a software developed by Tokyo Sokki and utlizing a TDS-530 data logger from Tokyo Sokki.

Table 6.3: Welding test parameter summery (Unit: mm)

Specimen	*Welding method*	*Welder's posture*	*Size (diameter)*	*Pitch*
7W1	Deep Arc Spot	Look down	7	36
7W2	Deep Arc Spot	Upright	7	36
7W3	Pre-holed fillet	Look down	7	36
7W4	Pre-holed fillet	Upright	7	36
10W1	Pre-holed fillet	Upright	10	36
10W2	Pre-holed fillet	Upright	10	30

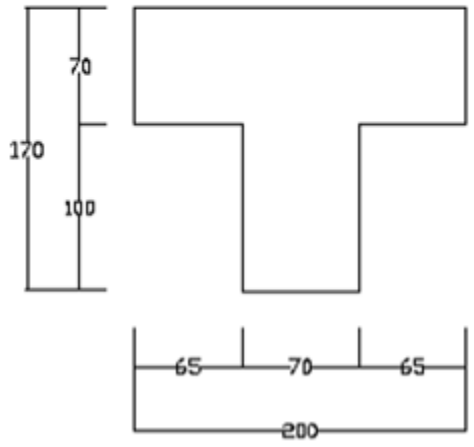

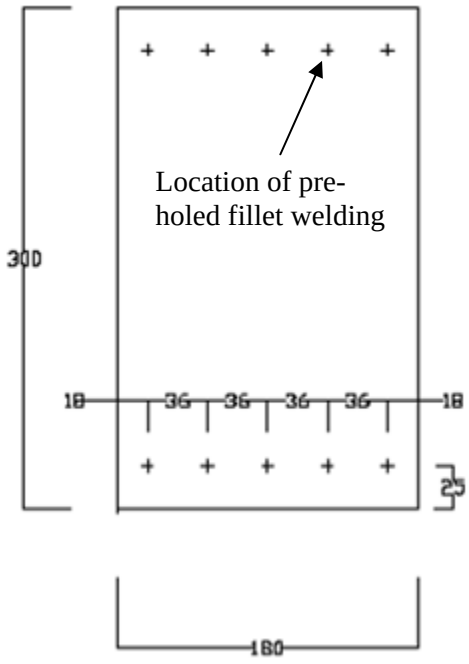

Fig 6.4(a): **Fig 6.4(b)**

Figure 6.4: Dimension of connection test specimen (a) testing grip (b) steel plate

Preliminary Test Results for Welding

All specimens except the specimen 10W2, pre-holed welding with 10mm diameter at upright position, failed in the weld metal. Specimen 10W2 successfully failed by fracture of the thin plate [Figure 6.5].

The shear strength per one welding spot obtained for different combinations of welding methods and welder's posture are summarized in Table 6.4. The specimen with a pre-hold fillet welding was 50% stronger than that with the deep arc spot welding for the same diameter. It was also notable that pre-holed fillet welding in an upright posture was only 10% weaker than that at a look down posture.

Figure 6.6 shows the test results for pre-hole welding specimens in terms of the force and displacement relationship. When failure occurred in the weld metal (7W4), the specimen failed in brittle manner without the indication of any post yielding deformation. The specimen showed large ductility if the failure occurred at the thin steel plate (10W2). Specimen 10W1 showed the combined behavior of two failure modes. The elastic stiffness of the specimen with the plate failure mode (10W2) was higher than that of the specimen with the weld failure mode (7W4 and 10W1). The elastic stiffness of the specimens 7W4 and 10W1 was similar although these specimens had different yielding strengths.

Figure 6.5: Failure modes; weld metal fracture (up) plate fracture (bottom)

Table 6.4: Welding test results

Specimen	*Failure mode*	*Shear Strength per spot*	
		(kN)	(kip)
7W1	weld metal fracture	8.2	1.80
7W2	weld metal fracture	8.1	1.78
7W3	weld metal fracture	12.5	2.75
7W4	weld metal fracture	11.0	2.41
10W1	weld metal fracture	15.5	3.41
10W2	plate fracture		

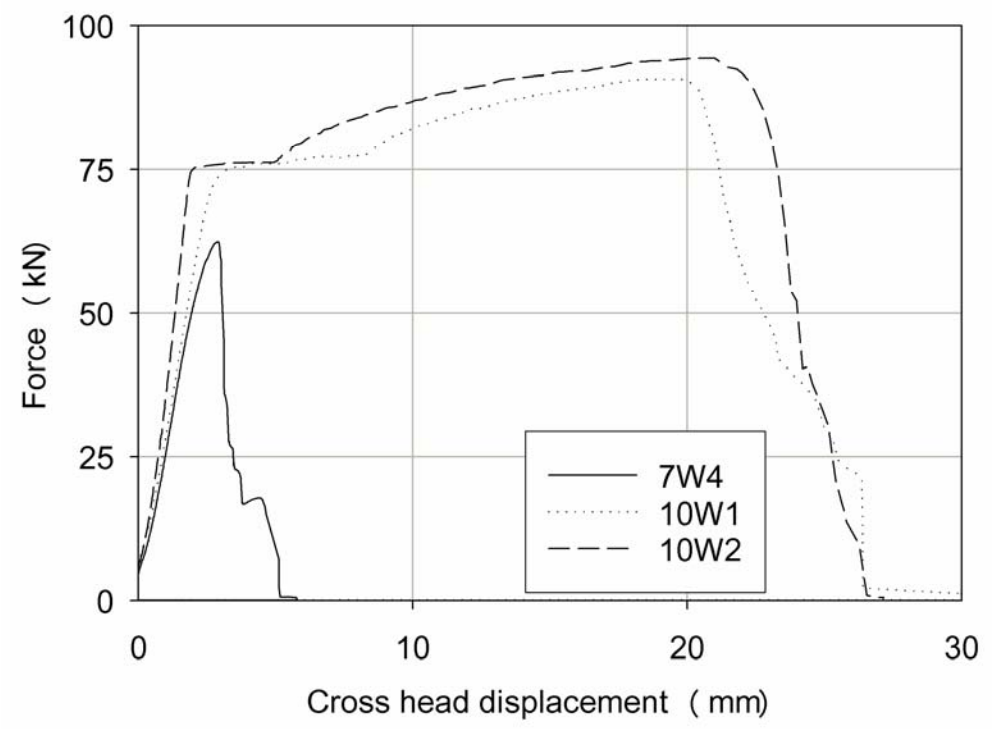

Figure 6.6: Force displacement relationship for pre-holed welded specimens

6.6 Loading Protocol

The loading protocol used in the test is shown in Table 6.5. The displacement controlled cyclic loading was repeated three times for rotations up to 0.0075 rad. drift angle and repeated two times for larger amplitudes. The applied loading protocol was determined after a review of the loading protocols used in previous tests and the design guidelines [Vian and Bruneau, 2005; AISC, 2007; ATC-24, 1992].

Table 6.5: Loading Protocol

Drift angle rad.	*Cycle*	*Displacement* mm
0.00375	3	6.56
0.005	3	8.74
0.0075	3	13.11
0.01	2	17.48
0.015	2	26.22
0.02	2	34.96
0.03	2	52.44
0.04	2	69.92

6.7 Measurement Plan

The load and displacement of the hydraulic jack were measured using a load cell with the maximum loading capacity of 2000kN and a digital Linear Variable Differential Transformer (LVDT) with the maximum deformation capacity of ±20in. To measure the local deformation of the specimens, twelve high resolution potentiometers were installed. The slippage between the specimen and the test setup was monitored using digital LVDTs. The strain histories for the infill panel and the Vertical Boundary Elements (VBE) were measured using rosette strain gauges and uniaxial strain gauges. The location of the measurements and the strain gauges is shown in Figures 6.7 and 6.8, respectively. The capacity and the resolution of the measurements and the strain gauges are listed on Table B.1 with the corresponding input channels in a data logger [Appendix B].

For the specimen with tension-only bracing (S2), forces in the tension-only bracing elements were monitored using uniaxial strain gauges attached on the sides of the turnbuckles. The relationship between the strain and the axial load in the turnbuckles were calibrated from preliminary tension tests so that the turnbuckles could be used as load cells [Table 6.6]. The yielding strength of turnbuckles T2 and T5 were obtained by tensile loading tests after all the test were completed. The rest of turnbuckles were stored as load cells for the future experimental programs at the DPRI.

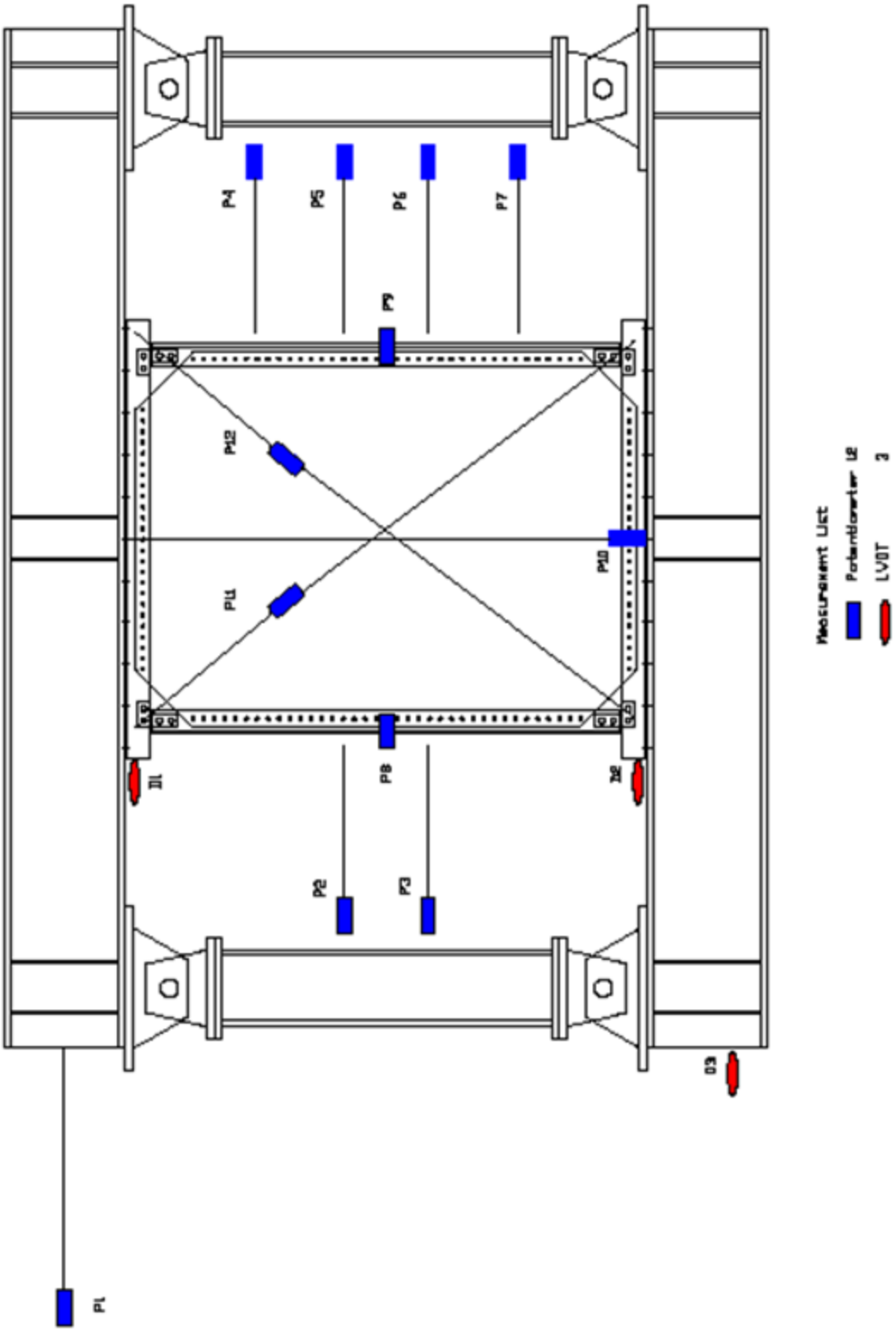
P1
P2
P3
P4
P5
P6
P7
P8
P9
P10
P11
P12
D1
D2
D3
Measurement List
Potentiometer
LVDT

Fig 6.7(a):

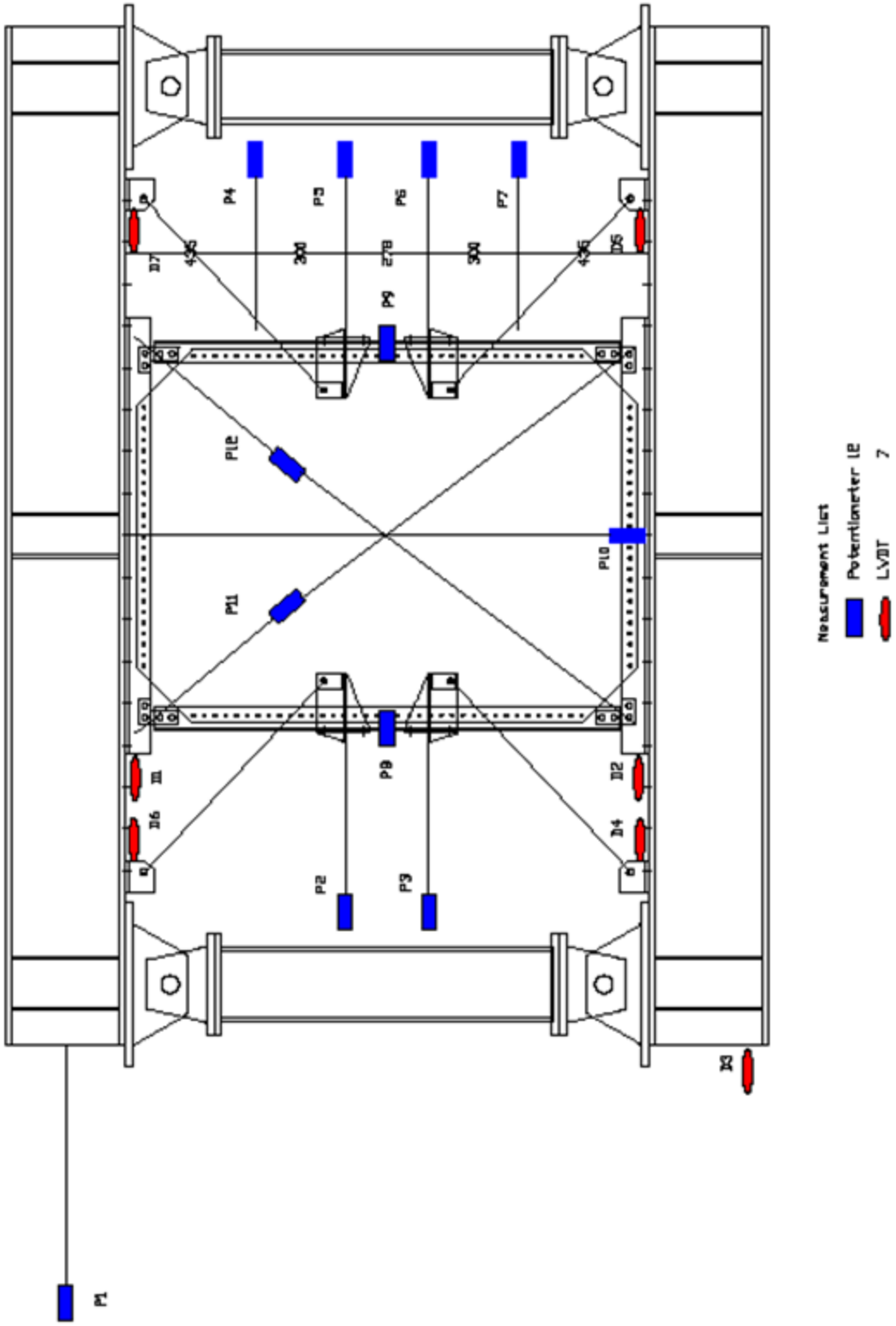

Fig 6.7(b):

Figure 6.7: Location of measurements (a) specimen 1 (b) specimen 2

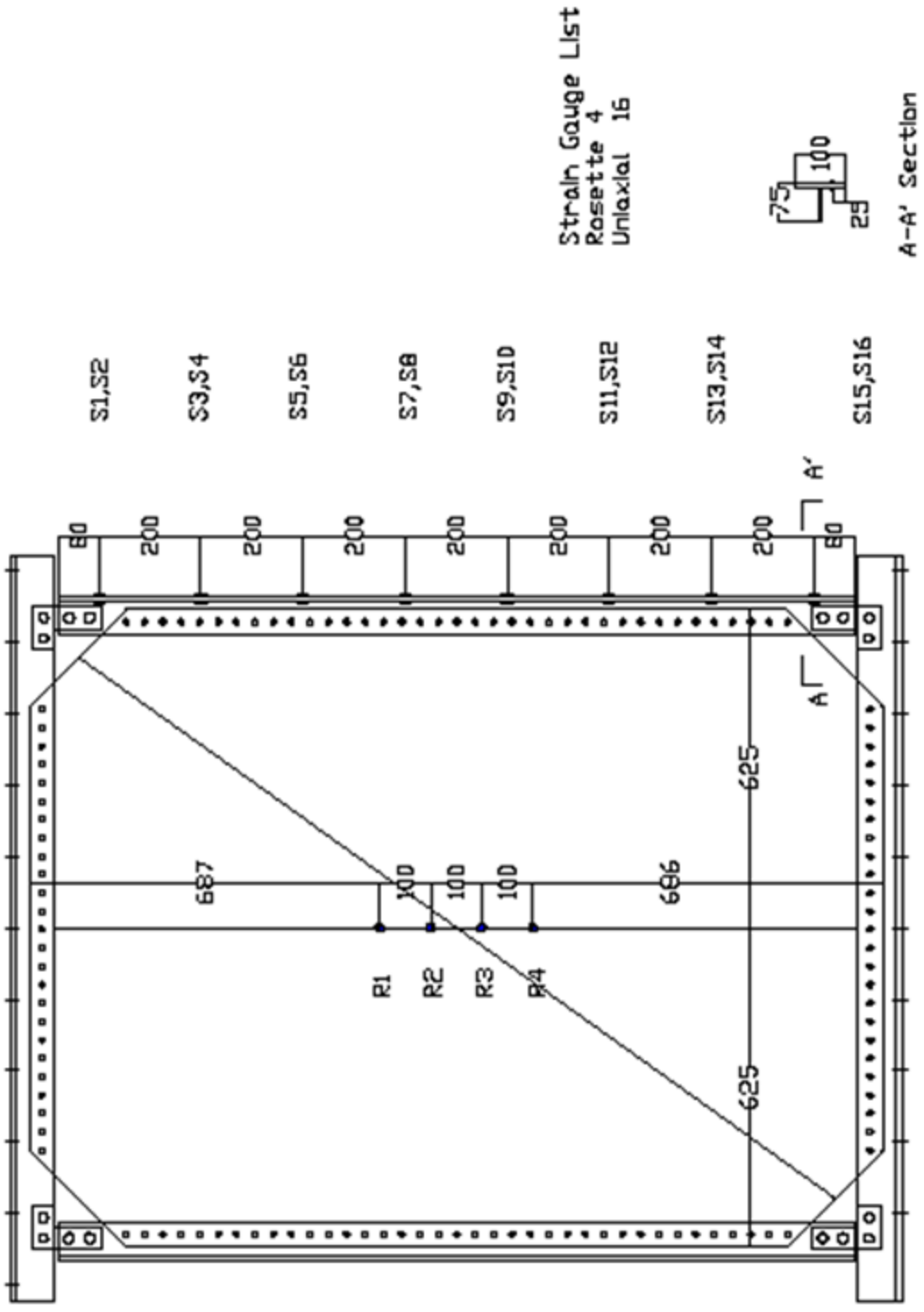
Strain Gauge List
Rosette 4
Uniaxial 16
A-A' Section
75
100
25
S1,S2
S3,S4
S5,S6
S7,S8
S9,S10
S11,S12
S13,S14
S15,S16
A
A'
80
200
625
687
100
686
R1
R2
R3
R4

Fig 6.8(a):

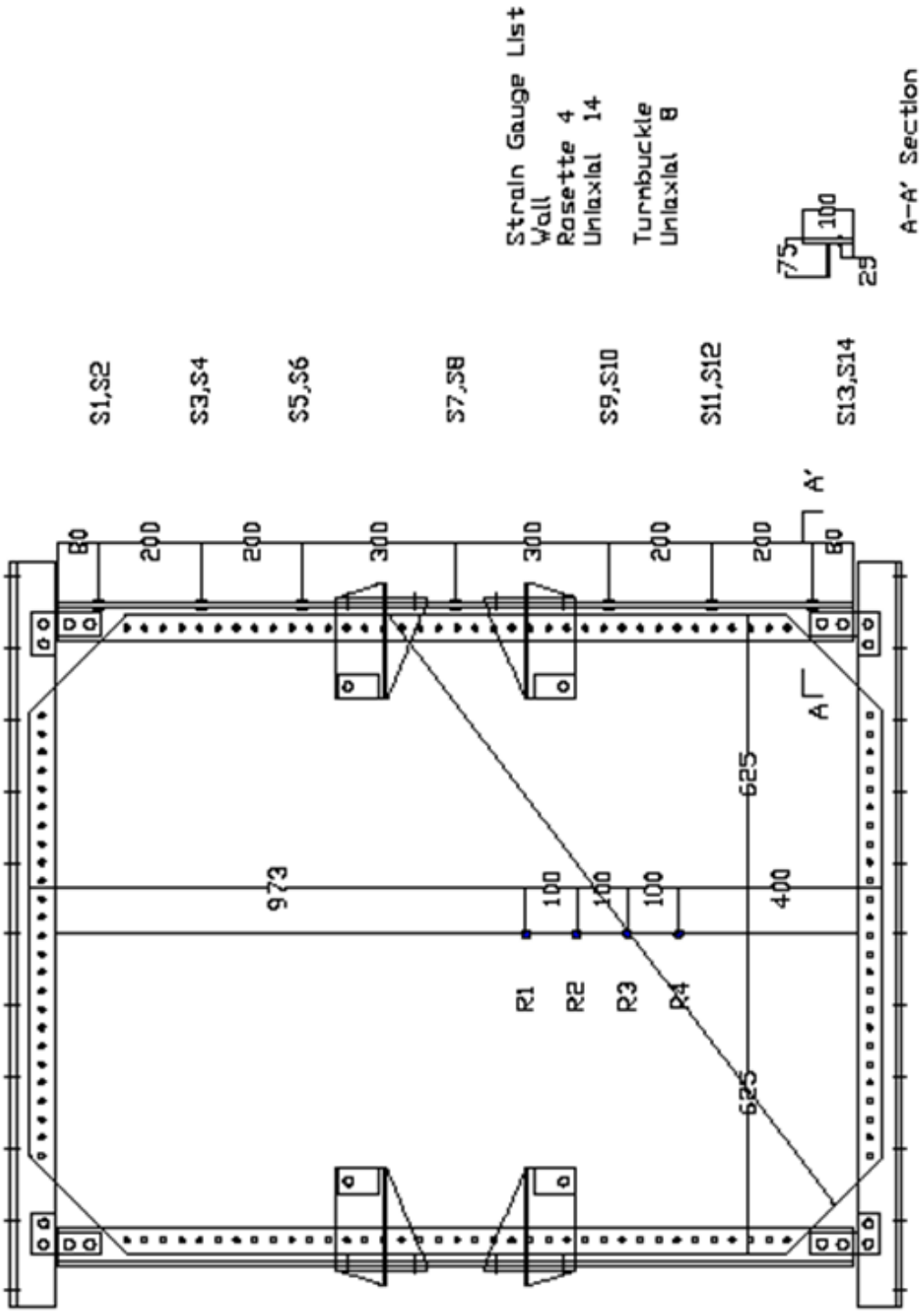

Fig 6.8(b):

Figure 6.8: Location of strain gauges (a) specimen 1 (b) specimen 2

Table 6.6: Turnbuckle calibration results

Name	Location	*Sensitivity* kN/με	*Yield strength* kN	*Tensile strength* kN
T1	left bottom	0.0777	60	81
T2	left bottom	0.0809		
T3	left top	0.0919		
T4	left top	0.0877	61	82
T5	right bottom	0.0759		
T6	right bottom	0.0951		
T7	right top	0.0918		
T8	right top	0.0900		

6.8 Test Views

The overall view of the entire testing system icluding a loading frame, testing setup and specimen is shown in Figure 6.9. Grid lines were drawn on the surface of the infill panel with white markers to help tyrack the local deformed shape under loading. Figure 6.10 shows the details of the specimens. The HBE and the VBE were connected with the L-shape steel plates with the clearance of 9mm to allow the rotation of the VBEs at the connection. The tension-only braces were hand-tightened after installation.

The installation of the infill panel was completed with three major steps [Figure 6.11]. First, the infill plate was fixed at the correct location with several cramps. Second, the plate was tack-welded to the boundary elements at all welding spots. Third, the installation was completed with the fillet welding of all holes. The two steps of welding were selected to minimize the initial imperfection and the residual stresses in the infill panel. The strain in the infill panel during the welding was monitored during the entire duration of the welding procedure [Figure 6.12]. The maximum principal strain values during the welding were around 230$\mu\varepsilon$ and 175 $\mu\varepsilon$, for the specimen 1 and the specimen 2, respectively. These values are 10% of the yield strain, and much smaller than the values of the residual stress accounted for the column buckling strength (30% of the yield stress) in the modern steel design guidelines [AISC, 2007].

Figure 6.13 shows the data acquisition system and the load control system used in the tests.

Figure 6.9: Load reaction frame and test setup

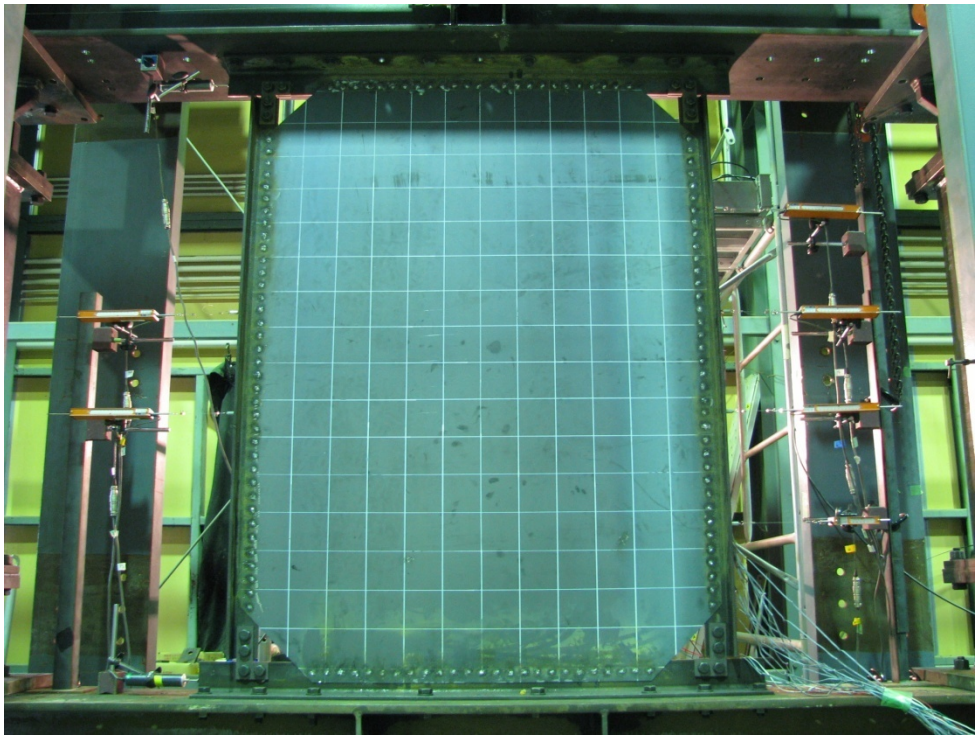

Fig 6.10(a):

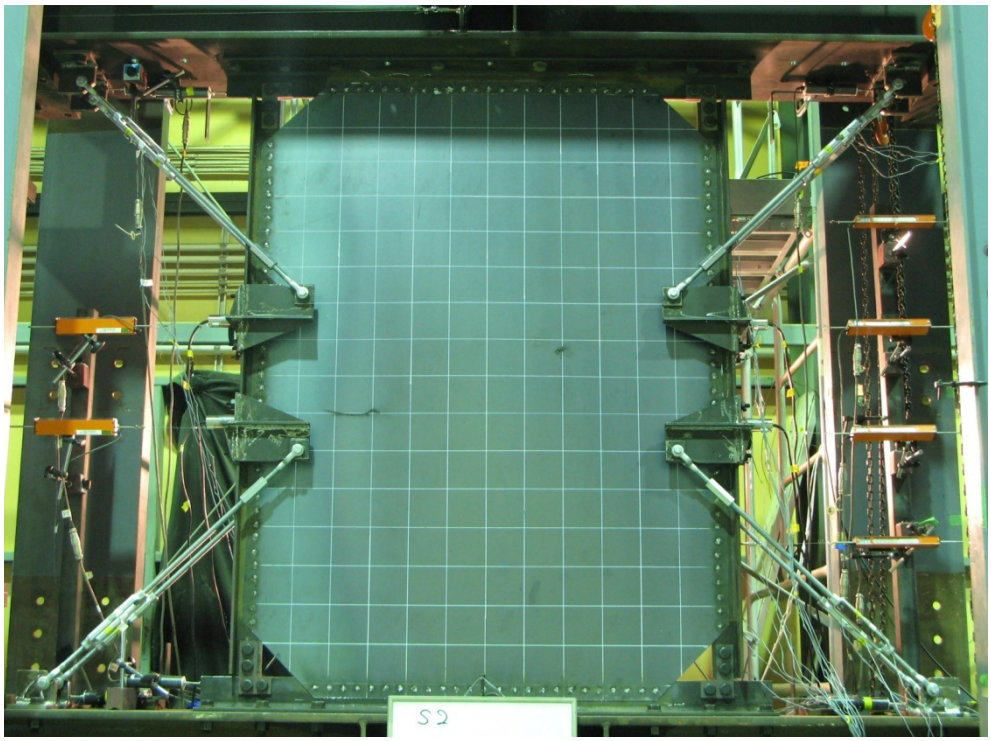

Fig 6.10(b):

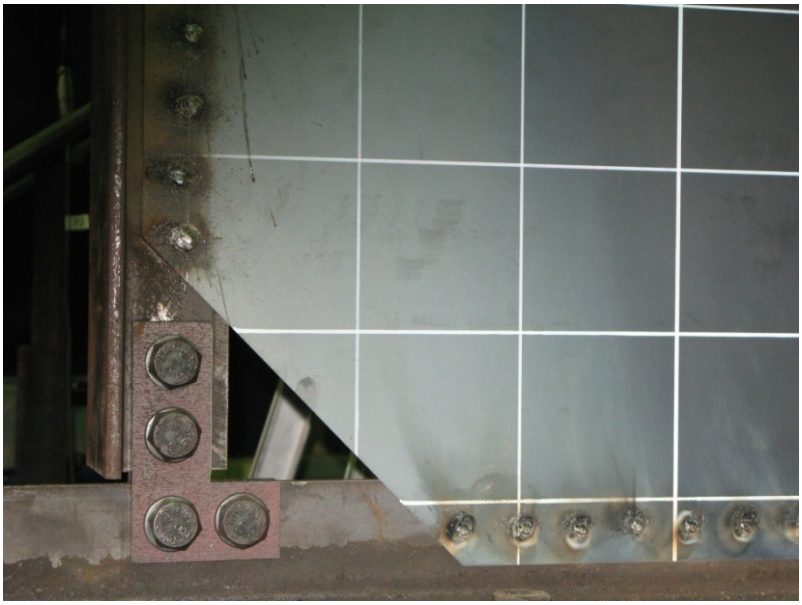

Fig 6.10(c):

Fig 6.10(d):

Figure 6.10: Specimen views (a) specimen 1 (b) specimen 2 (c) HBE-VBE connection (b) steel bracket and tension-only bracing

Fig 6.11(a):

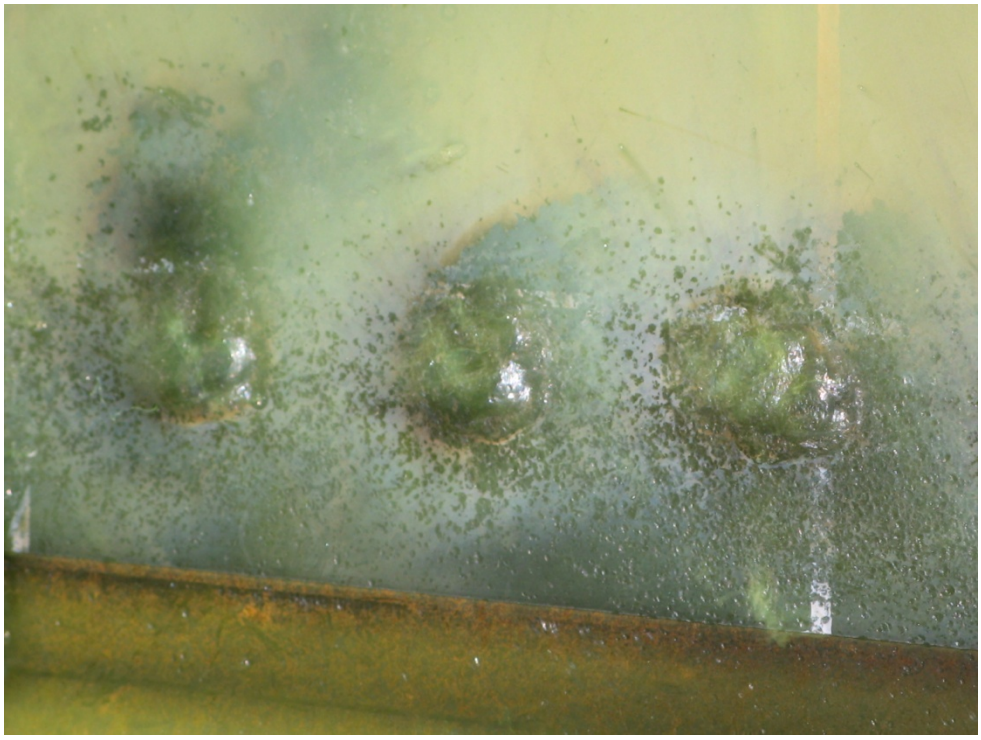

Fig 6.11(b):

Figure 6.11: Welding condition (a) preliminary tack welding (b) welding final condition

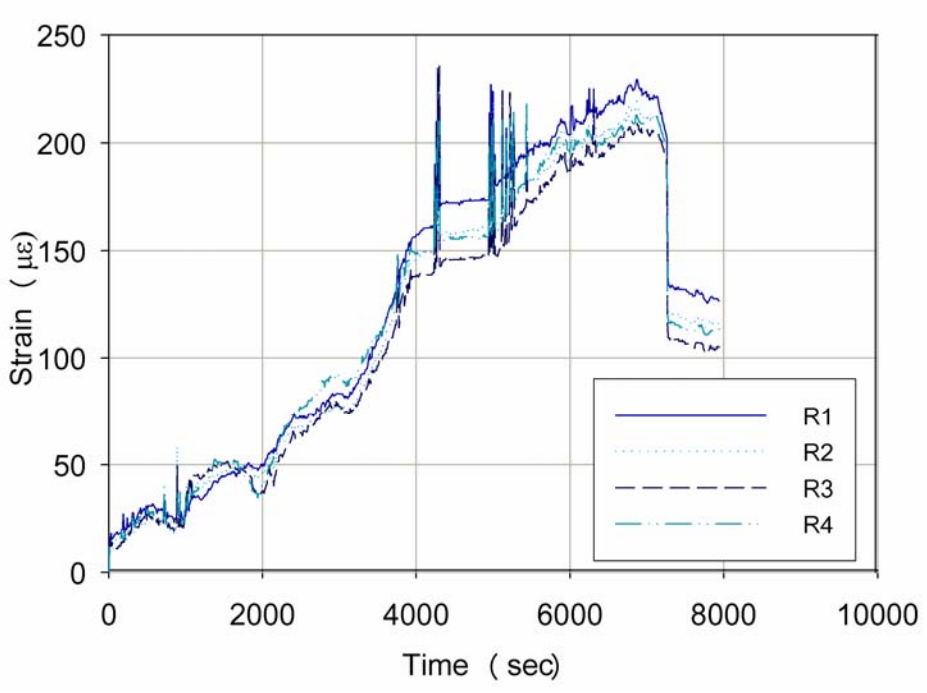

Fig 6.12 (a):

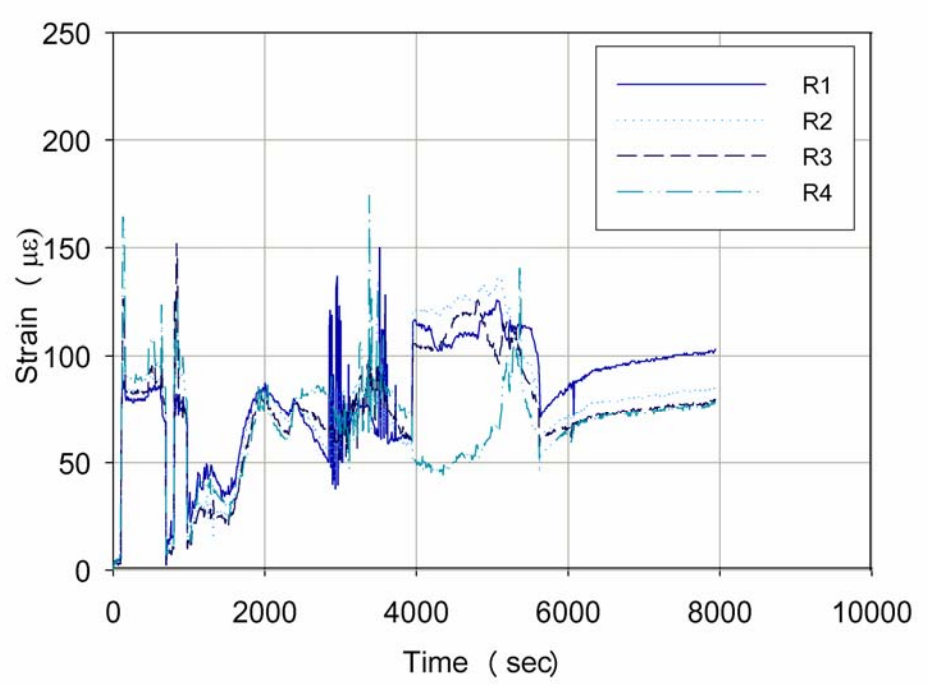

Fig 6.12 (b):

Figure 6.12: Maximum principle strain history during welding (a) specimen 1 (b) specimen 2

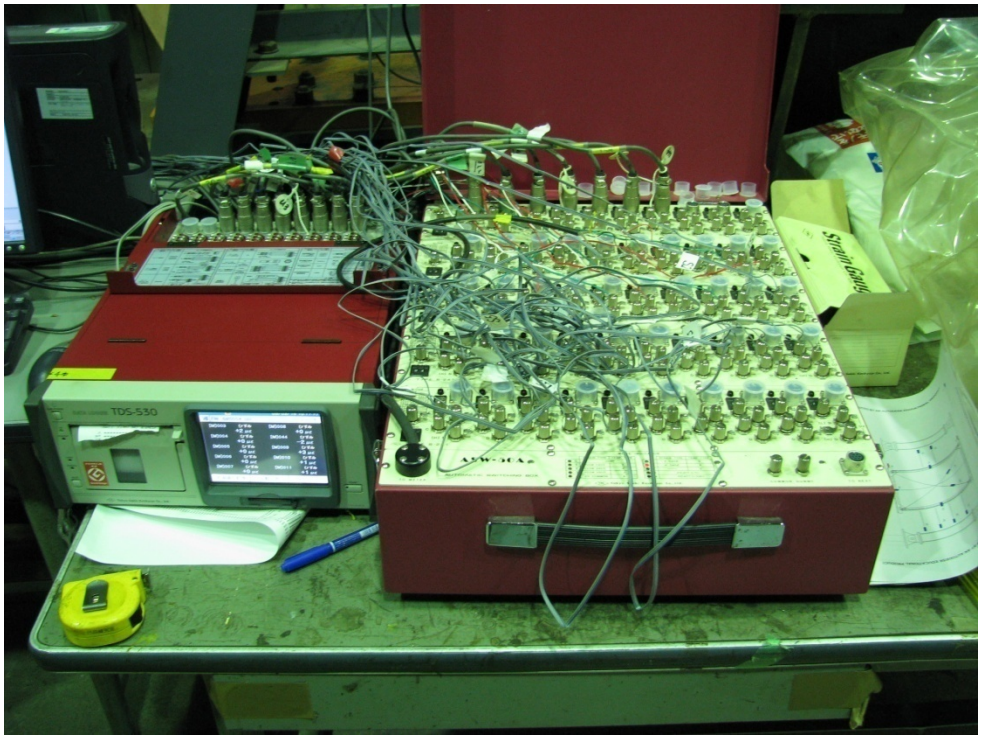

Fig 6.13(a):

Fig 6.13(b):

Figure 6.13: Loading and data acquisition system (a) data logger (b) control box and PCs

6.9 Test Results

Test Observation

Specimen 1

Global buckling of the infill plate took place immediately in the first load cycle with the amplitude of 0.00375rad. with the development of tension-field action in the infill plate [Figure 6.14(a)]. The buckling of the plate involved a single low tone sound following a series of high tone sounds accompanied by vibration of the infill plate. The main wave line in the global buckling ran exactly diagonally across the corners in the infill panel. At every each half cycle, the shape of global buckling reversed making a loud, low tone, impact-like sound. There was no residual deformation observed at the end of the three cycles of 0.00375rad. loading. One of the four rosette strain gauges at the centerline of the infill panel indicated the yielding of steel (2000$\mu\varepsilon$) at the first cycle of 0.005rad. loading [Figure 6.14(b) and (c)]. At this stage, the maximum out-of-plane deformation of the Vertical Boundary Elements (VBE) was a negligeble 2mm. Figure 6.14(d) shows the in-plane rotation of VBE induced by the tension-field action and the deformation of the infill panel at the connection between the HBE and VBE. The infill plate at the corner was subjected to compressive stress and was deformed out-of-plane. This out-of-plane deformation caused the weld metal at the boundary to be loaded under a combined tension and shear stress. The residual deformation observed visually at the end of the 0.005rad. loading cycle was very limited.

Under further loading, a slight residual deformation was observed mainly in the corner area of the infill panel as indicated by several folded lines [Figure 6.15(a) and (b)]. During the 0.0075rad. loading cycle, three of the four rosette strain gauges at the

centerline of the infill panel showed values above the yielding strain (2000$\mu\varepsilon$). The two welds at the left bottom and the right top of the boundaries fractured during the second half cycle of the 0.01rad. loading while all four rosette gauges showed values above the yielding strain (2000$\mu\varepsilon$) [Figure 6.15(c)]. The HBE-VBE connection successfully worked as pin-connection rotating under bending moment in VBEs without any translation deformations [Figure 6.15(d)].

Figure 6.16 (a)-(c) shows the transition of deformed shapes in one cycle of the 0.015rad. loading. The tension-field action reversed as the direction of loading changed without generating any fracture in the infill panel while a significant amount of deformation remained at zero story drift [Figure 6.16(b)].

At the 0.02rad. loading cycle, the VBEs deformed inelastically due to the inward forced generated by the tension-field action of the infill panel [Figure 6.17(a) and (b)]. At the left bottom corners of the infill panel, most of fractures occurred in the welds while some of them occurred in the infill plate.

Under further loading, fractures at the boundary connection propagated rapidly, with the bottom boundary of the infill panel almost disconnected at the end of the 0.04rad. loading [Figure 6.18]. After the scheduled loading cycles completed, a monotonic loading was applied to the specimen until the bottom boundary of the infill panel completed disconnected at the amplitude of 0.053rad.

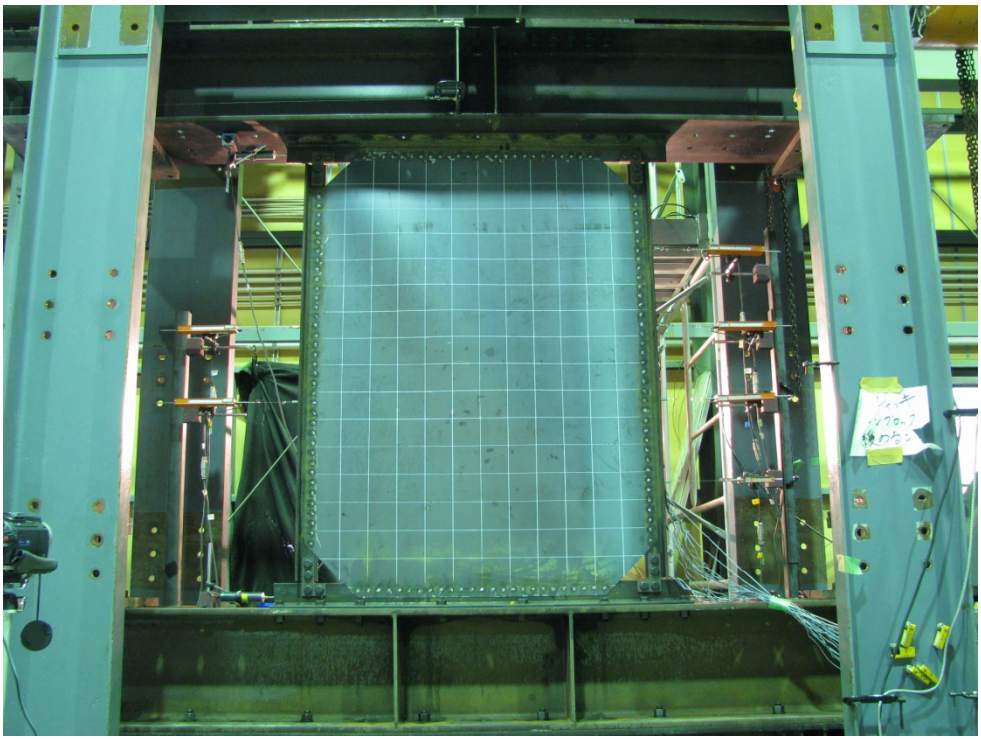

Fig 6.14(a):

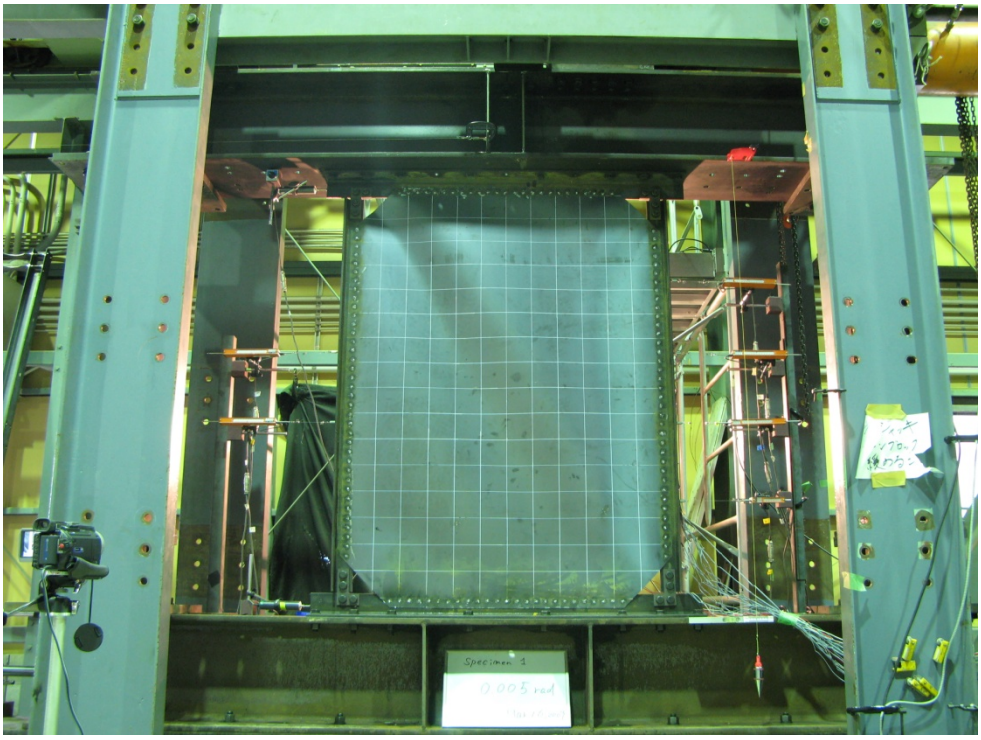

Fig 6.14(b):

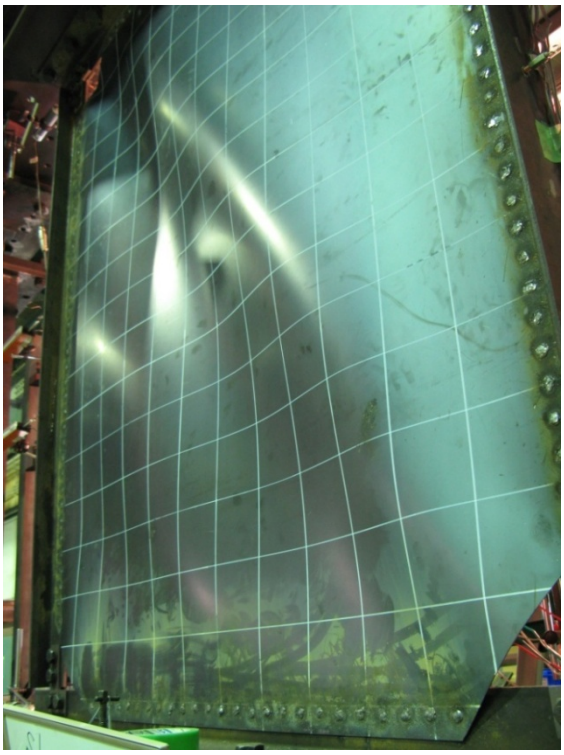

Fig 6.14(c):

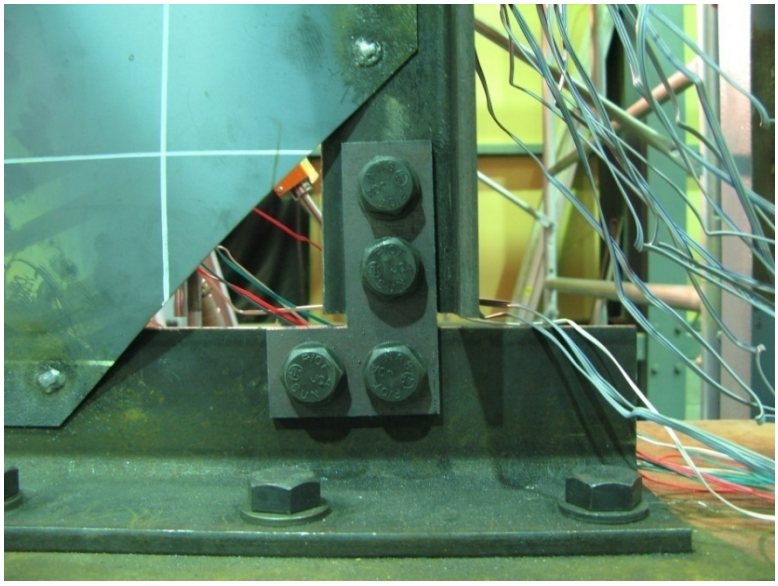

Fig 6.14(d):

Figure 6.14: Behavior at small amplitudes (a) global buckling at 0.00375rad. (b) global buckling at 0.005rad. (c) shape of bucking at 0.005rad. (d) rotation at HBE-VBE connection

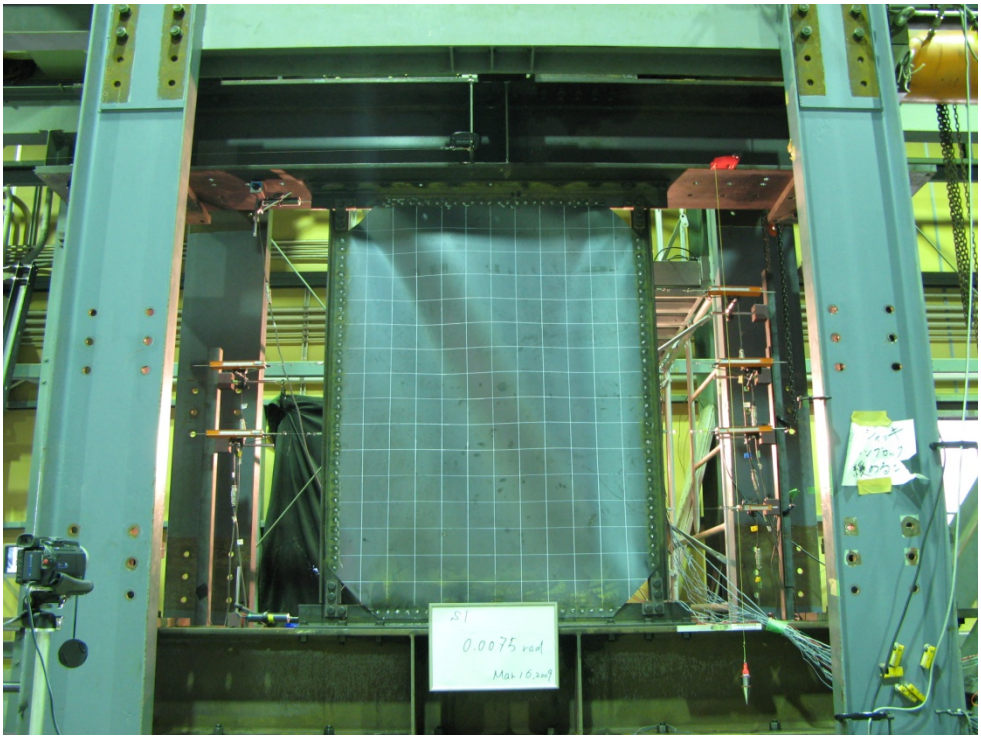

Fig 6.15(a):

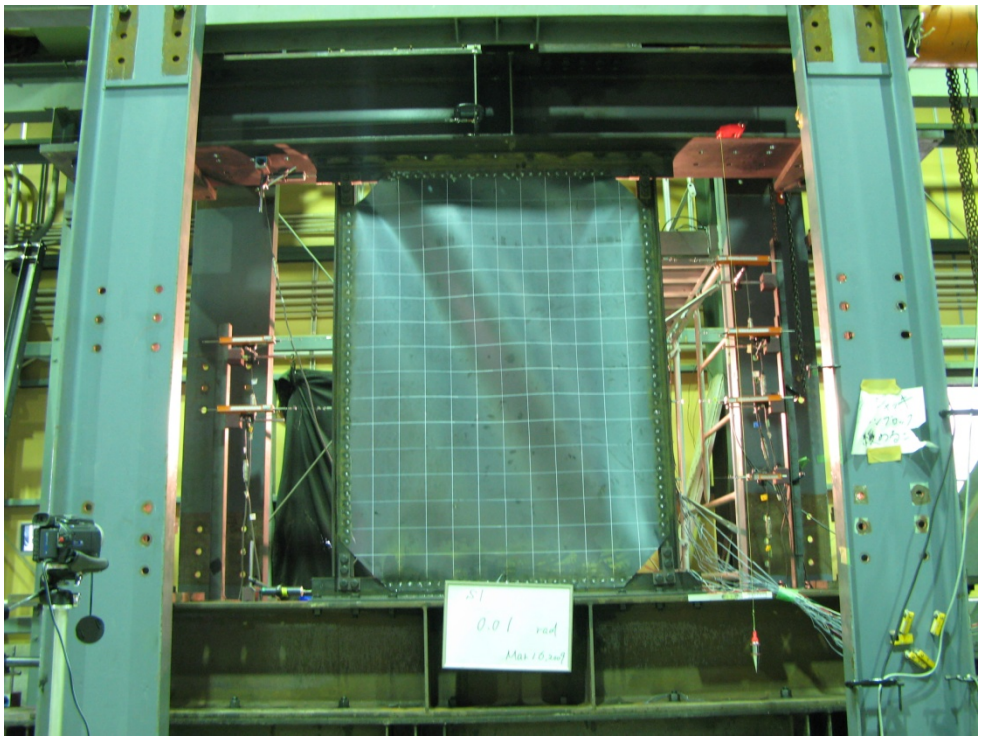

Fig 6.15(b):

Fig 6.15(c):

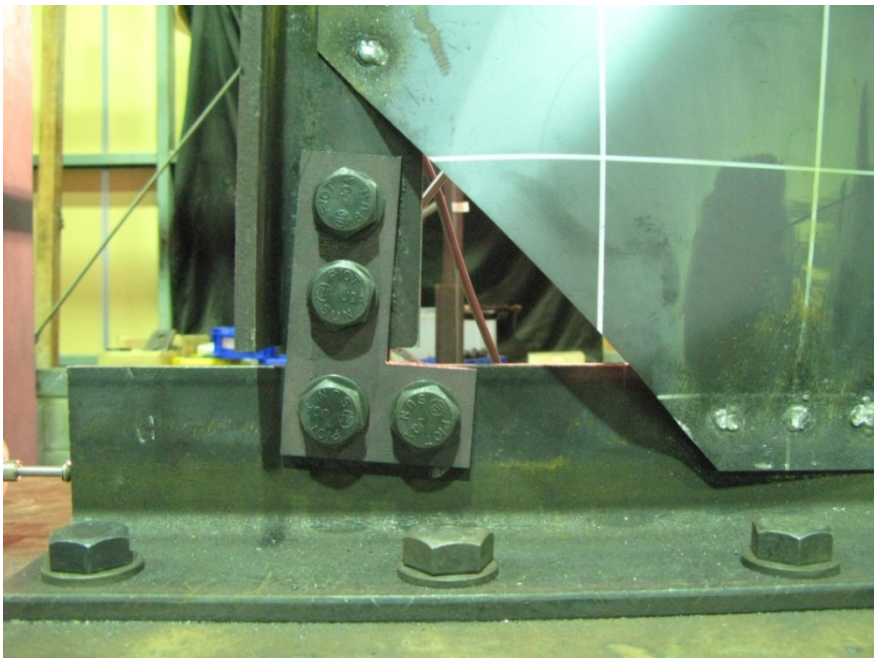

Fig 6.15(d):

Figure 6.15: Deformation at middle amplitudes (a) deformed shape at 0.0075rad. (b) deformed shape at 0.01rad. (c) fractured welds at left bottom corner (d) behavior of pin-connection

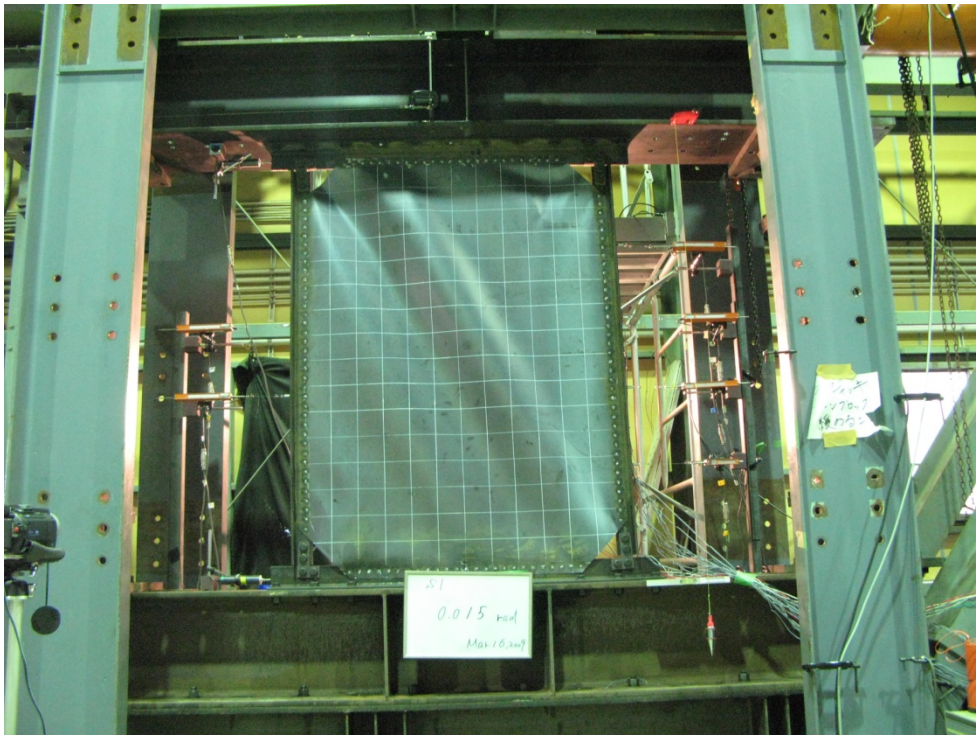

Fig 6.16(a):

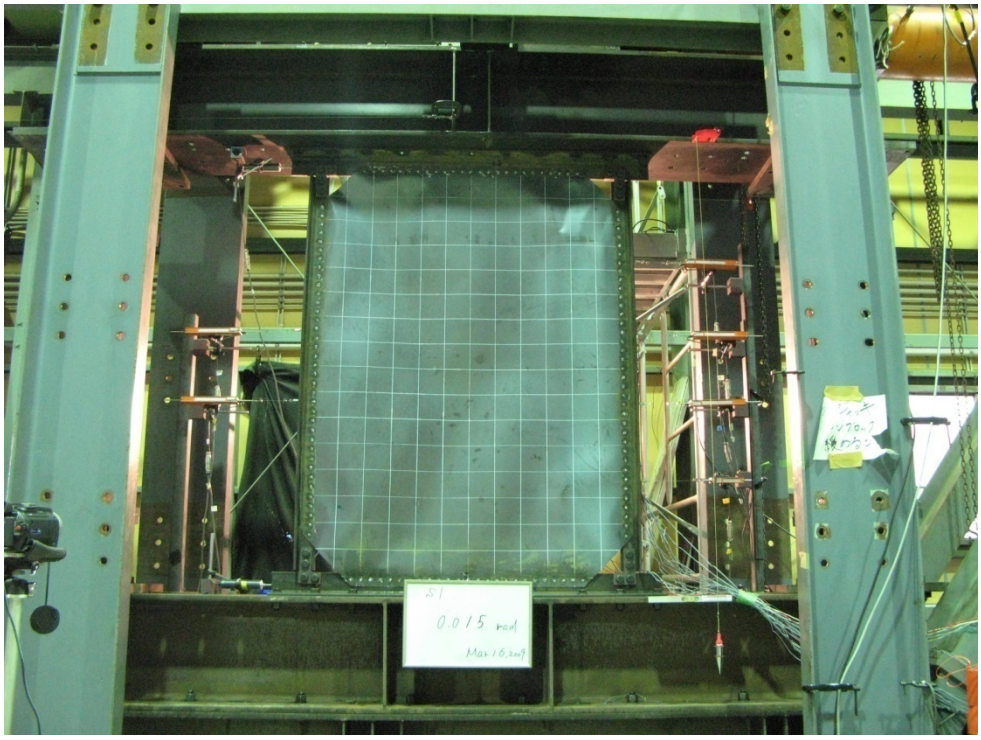

Fig 6.16(b):

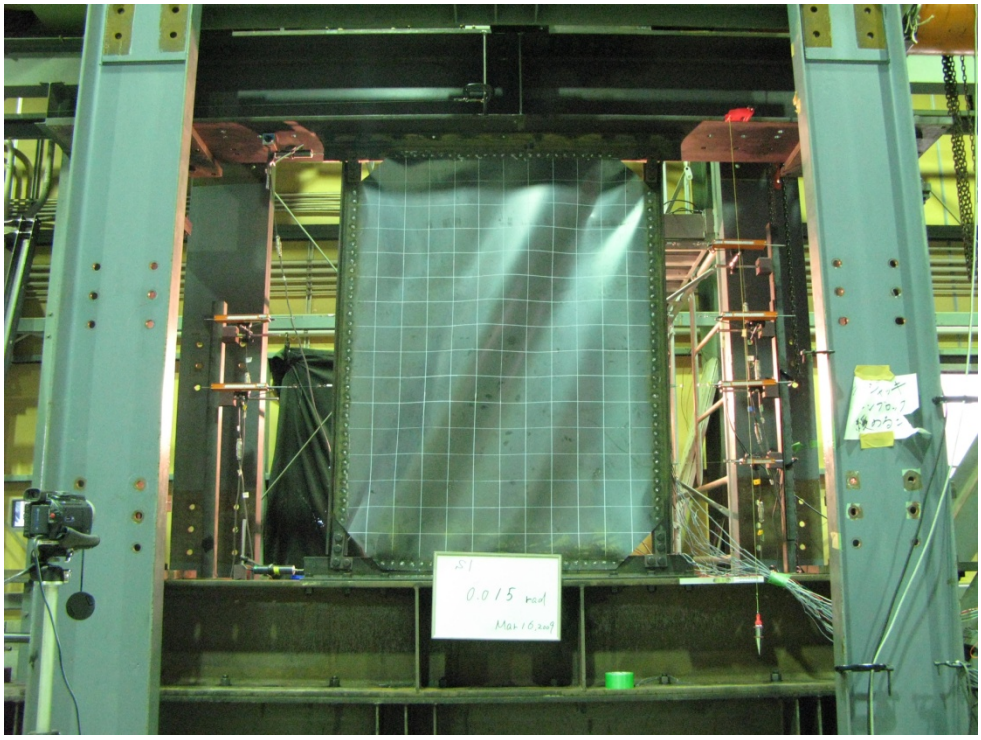

Fig 6.16(c):

Figure 6.16: Transition of deformed shape during 0.015rad. loading cycle (a) deformation at positive loading (b) residual deformation at zero displacement (c) deformation at negative loading

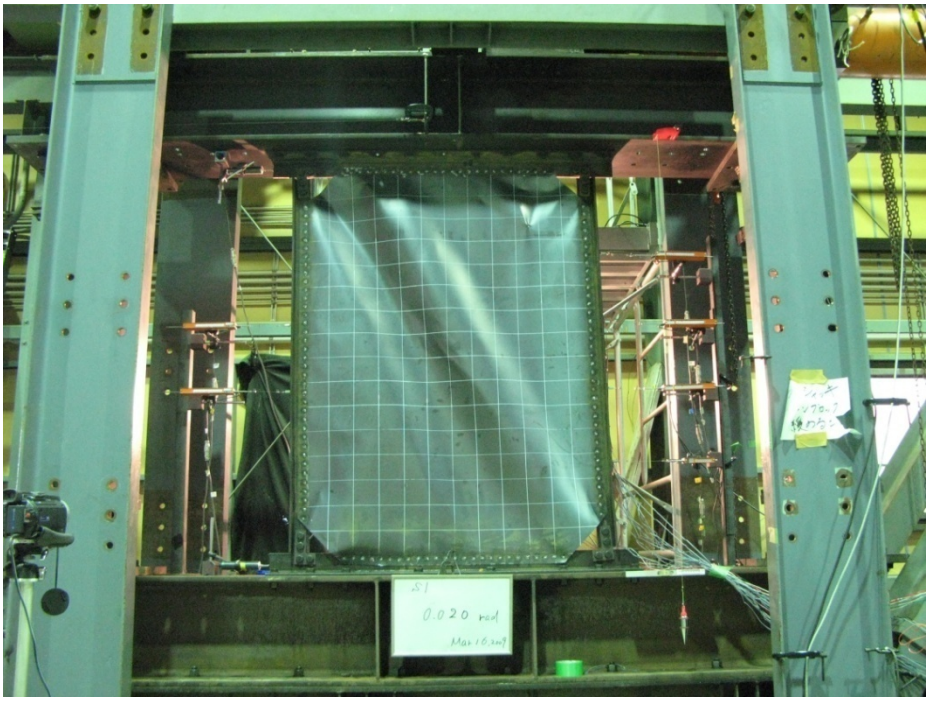

Fig 6.17(a):

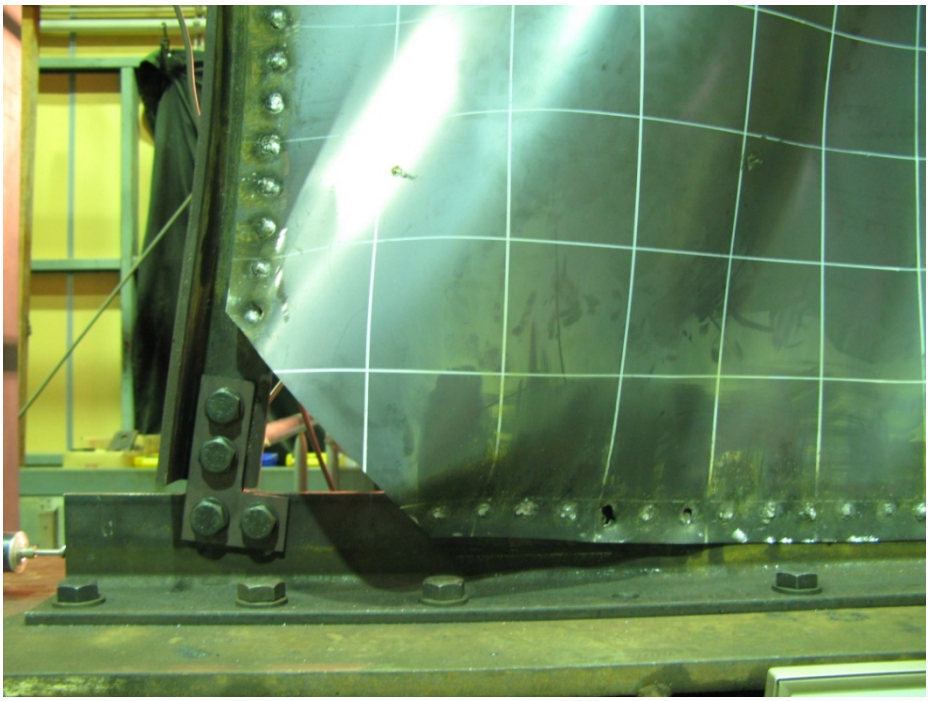

Fig 6.17(b):

Figure 6.17: Behavior at 0.020rad. loading (a) inelastic deformation of VBE (b) condition of left bottom corner

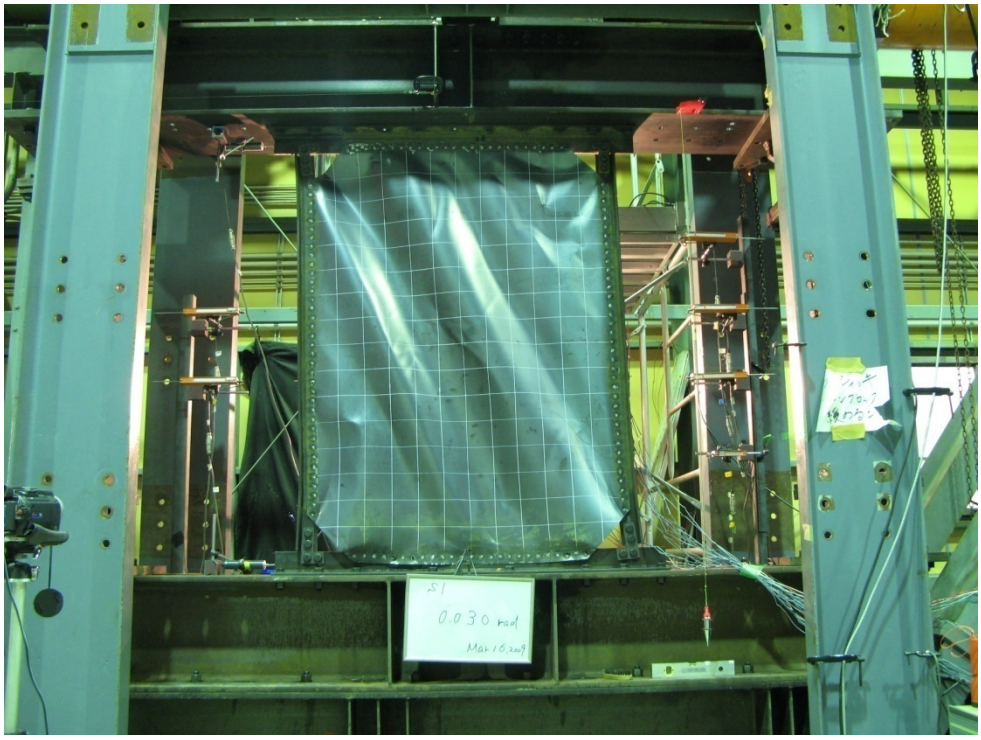

Fig 6.18(a):

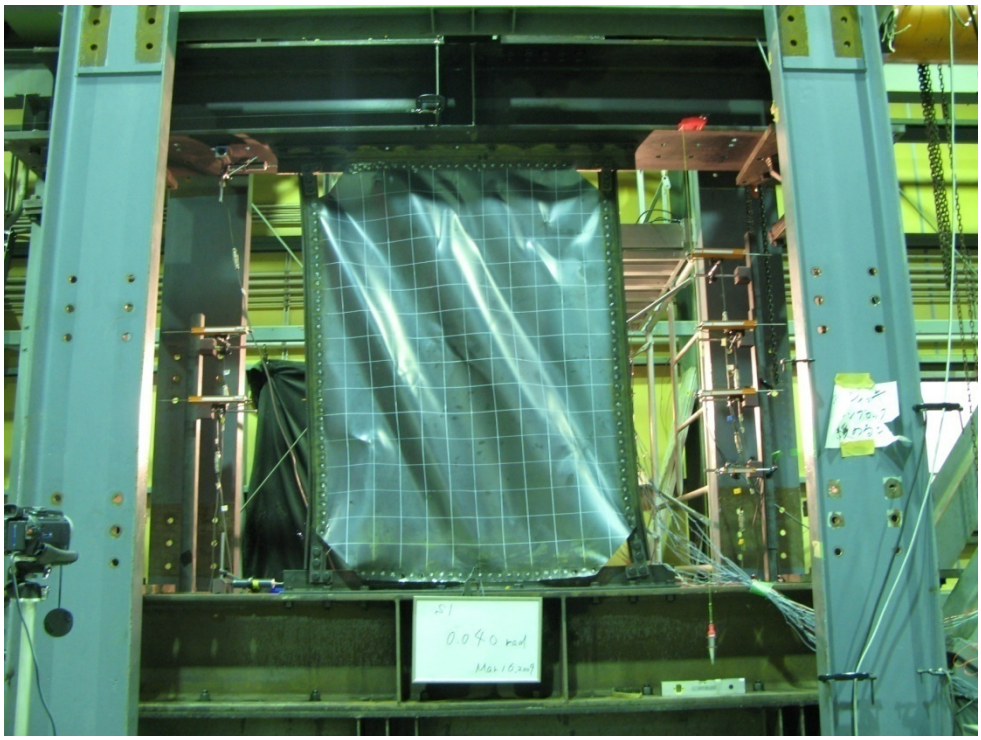

Fig 6.18(b)

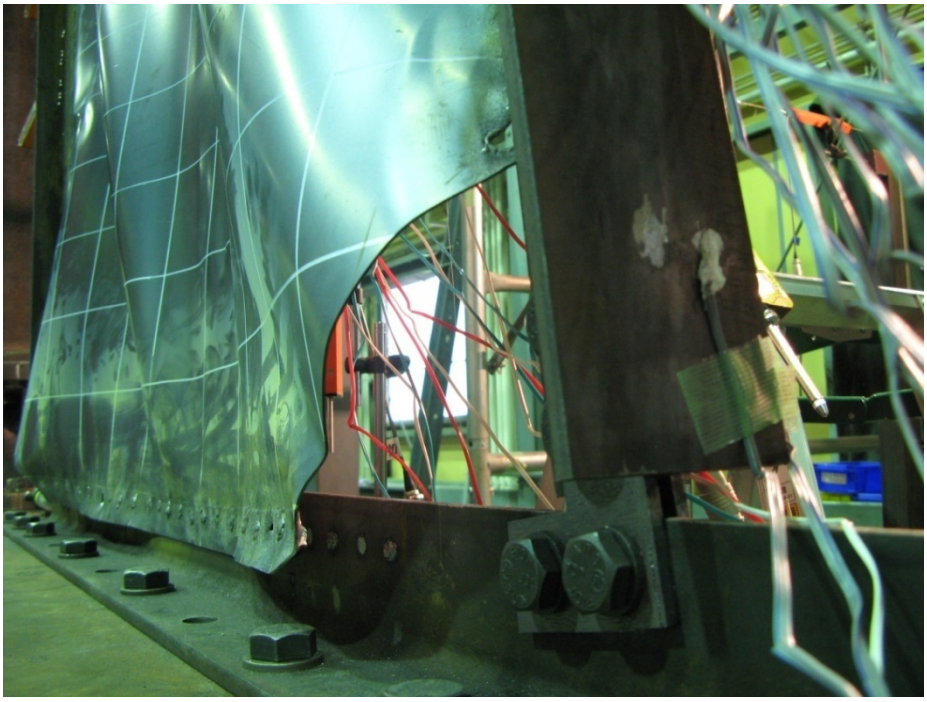

Fig 6.18(c)

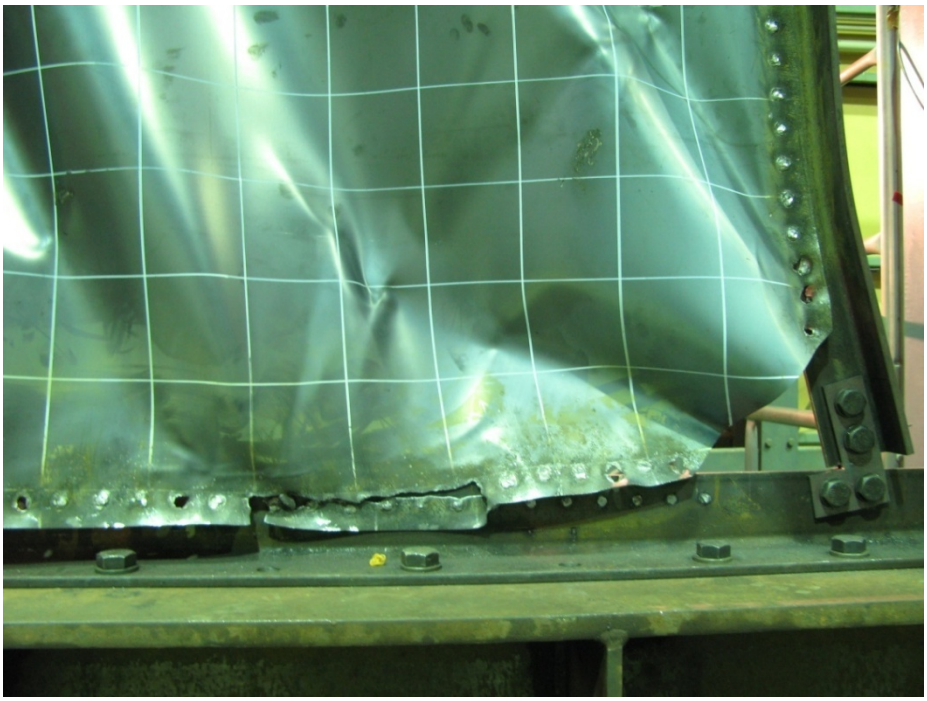

Fig 6.18(d)

Figure 6.18: Strength deterioration and final condition (a) deformation at 0.03rad. (b) deformation at 0.04rad. (c) damage at 0.04rad. (d) final condition at 0.054rad.

Specimen 2

As for Specimen 1, global buckling of the infill plate took place immediately in the first load cycle with the development of tension-field action in the infill plate [Figure 6.19(a)]. However, the deformed shape exhibited more short wave lines for specimen 2 than for specimen 1, which indicated that the buckling mode was higher for the specimen 2 than for the specimen 1. The main wave line in the global buckling ran diagonally across the corners in the infill panel while two other wave lines initiated from the location of the steel brackets [Figure 6.19(b)]. Again, the buckling of the plate was accompanied by a single low tone sound following series of high tone sounds with vibration of the infill plate. At every each half cycle, the shape of global buckling reversed making a loud, low tone, impact-like sound. No residual deformation was observed at the end of the three cycles of 0.005rad. loading. The rotation at the HBE-VBE connection was smaller than that in the specimen 1 and the deformation at the corners of the infill panel was not large [Figure 6.19(c) and (d)].

Three of the four rosette strain gauges at the centerline of the infill panel indicated the yielding of steel panel (2000$\mu\varepsilon$) during the second cycle of 0.0075rad. loading [Figure 6.20(a)]. As deformations became larger, the number of wave lines increased and thus the buckling mode became higher [Figure 6.20(a)-(c)]. This is because the tension-only bracing started to resist against the inward deformation of the VBEs and the tension load paths in the infill panel changed. The deformations at the corners of the infill panel were still limited as a benefit of the tension-only braces. No damage was observed at the boundary connections at end of the 0.01rad. loading cycle. At the 0.01rad. loading cycle, large deformation were observed in the steel brackets [Figure 6.20(d)]

Figure 6.21(a)-(c) shows the transition of deformed shapes in the 0.015rad. loading cycle. A large number of folded lines and out-of-place deformation of the infill panel were observed. Several weld fractures were observed at the right bottom of the infill panel. Yielding of the still brackets and the VBE occurred due to the large local force input from the tension-only braces [Figure 6.21(d) and (e)]. The yielding of the steel brackets at top left and bottom right of the plate were confirmed. Some permanent rotation remained at zero displacement with a series of Lueder's lines on the bracket surface. These two brackets were tension-only braces and worked primarily under loading in the positive story drift direction.

The steel bracket located at left bottom fractured during the 0.03rad. loading cycles [Figure 6.22]. This undesirable fracture resulted in the slight buckling of the tension-only element located at the bottom left. The yielding of all steel brackets affected the mode of the inelastic buckling and the deformed shape of the infill panel [Figure 6.22(b)]. This increased the force input in the corner of the infill panel and resulted in fractures at the bottom boundary connection. Under further loading, fractures at the bottom boundary increased excessively. After the scheduled loading cycles completed, the specimen was monotonically loaded until 0.055rad. [Figure 6.23].

After the test was completed, the tension-only bracing elements and steel brackets were removed from the VBEs [Figure 6.24]. The severe damage including the development of yield lines in the flanges was observed in the VBEs with residual plastic deformations. The infill panel was also torn at the location of the steel brackets. The damage in the steel brackets was inspected carefully [Figure 6.25]. The steel brackets

suffered from very severe damage involving large deformations around holes where high strength bolts pulled and the fractures at fillet welded lines.

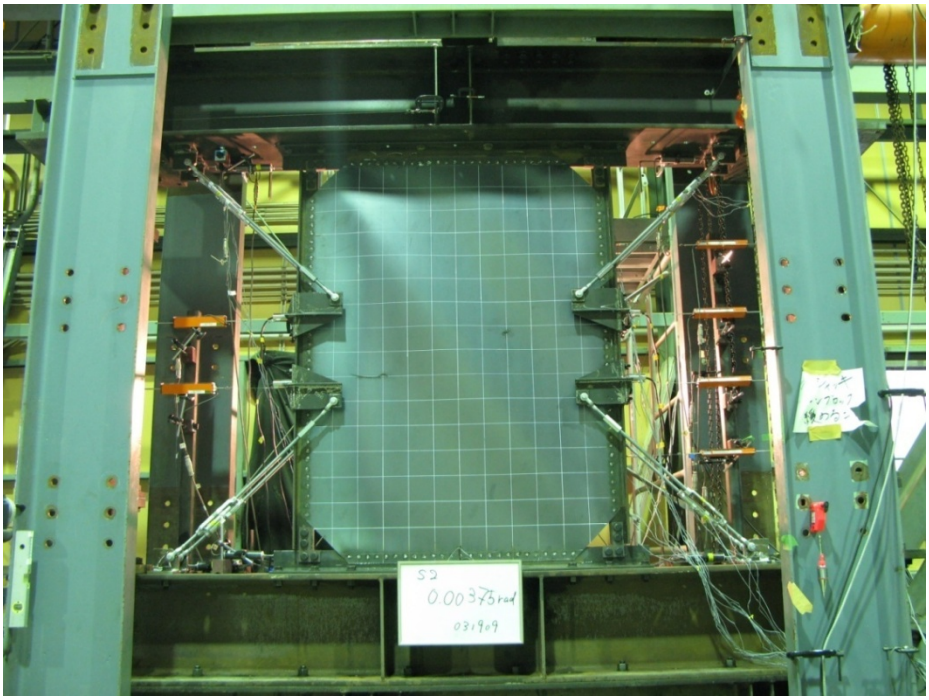

Fig 6.19(a):

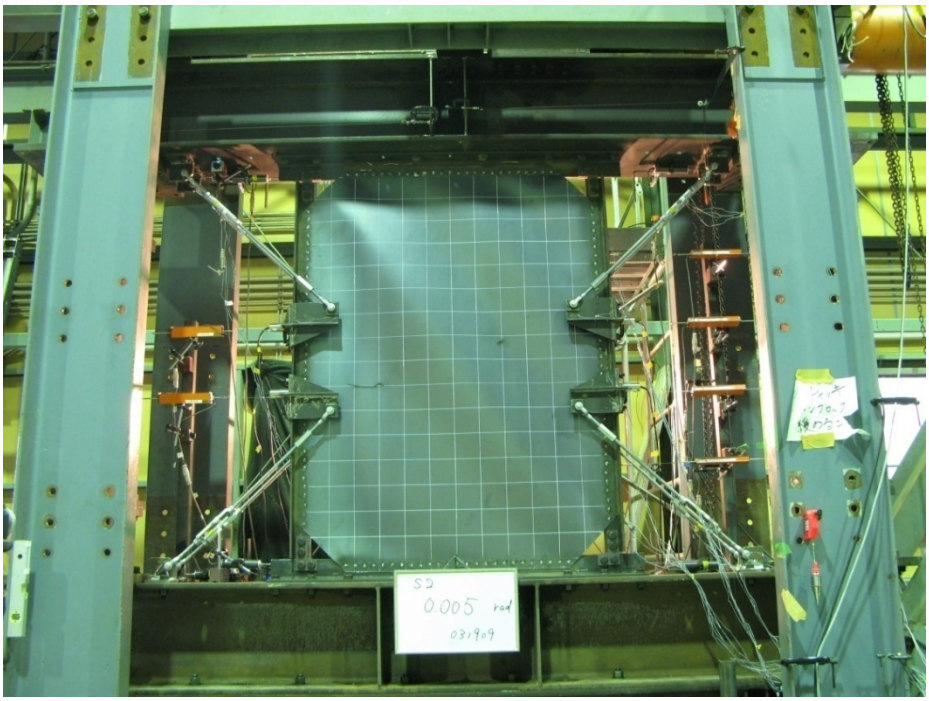

Fig 6.19(b):

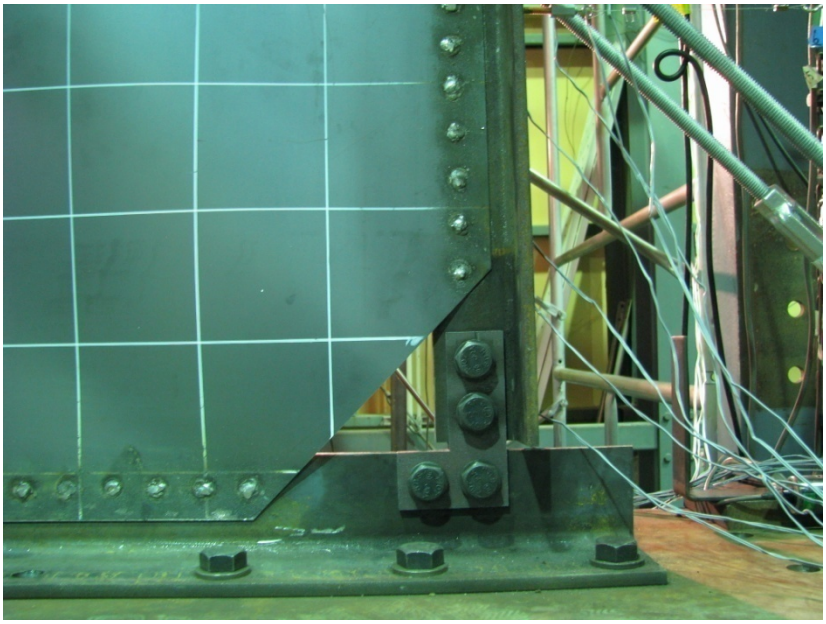

Fig 6.19(c):

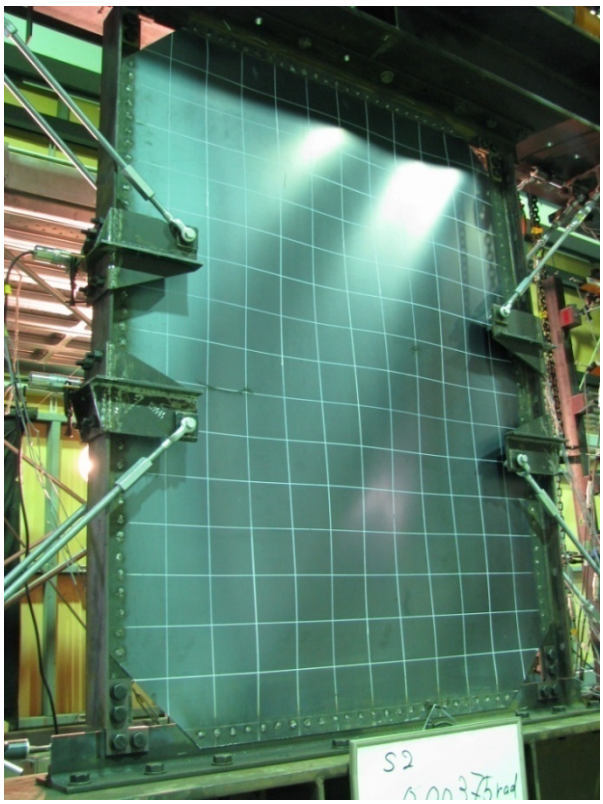

Fig 6.19(d):

Figure 6.19: Deformed shape at small deformation (a) global buckling at 0.00375rad. (b) global buckling at 0.005rad. (c) rotation of HBE-VBE connection (d) buckling wave lines

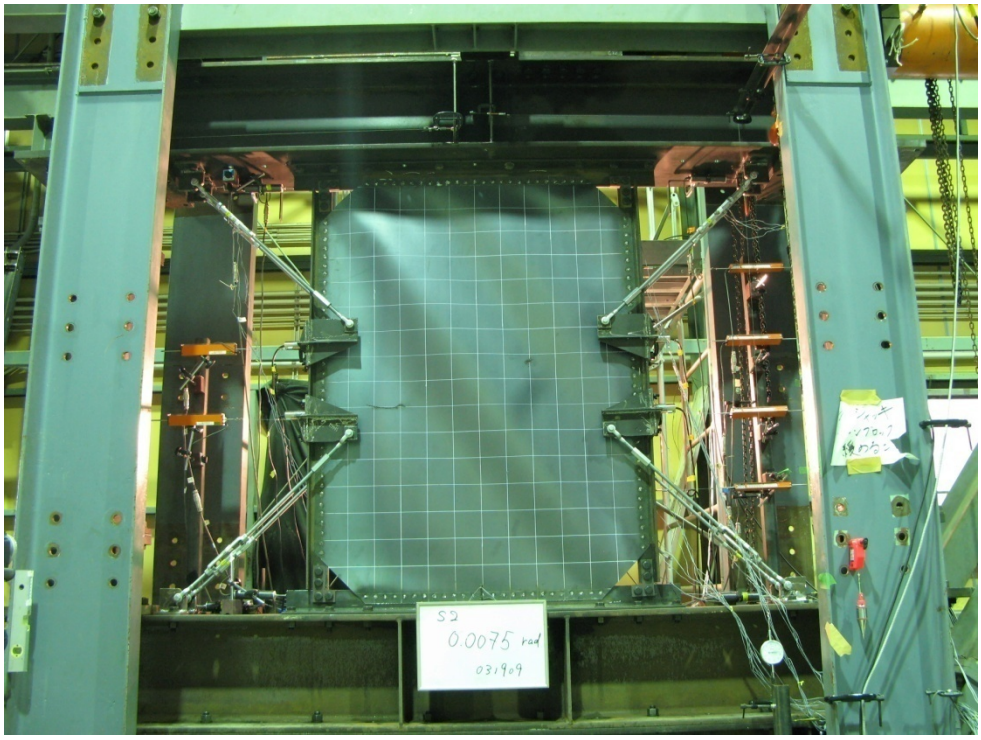

Fig 6.20(a):

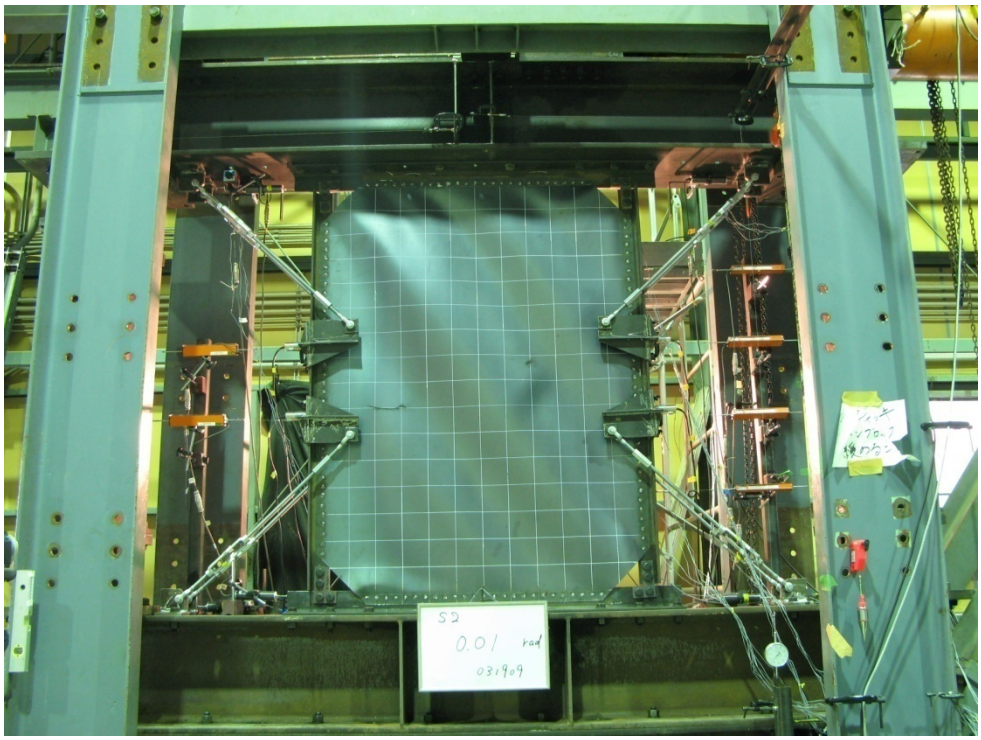

Fig 6.20(b):

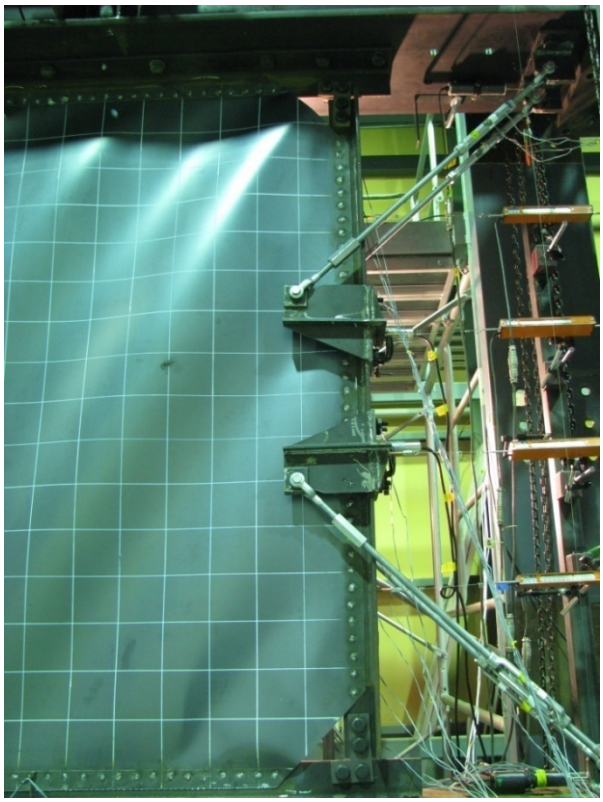

Fig 6.20(c):

Fig 6.20(d):

Figure 6.20: Behavior in mid amplitude loading (a) inelastic buckling at 0.0075rad. (b) higher mode buckling at 0.01rad. (c) wave line at corners (d) deformation of steel bracket

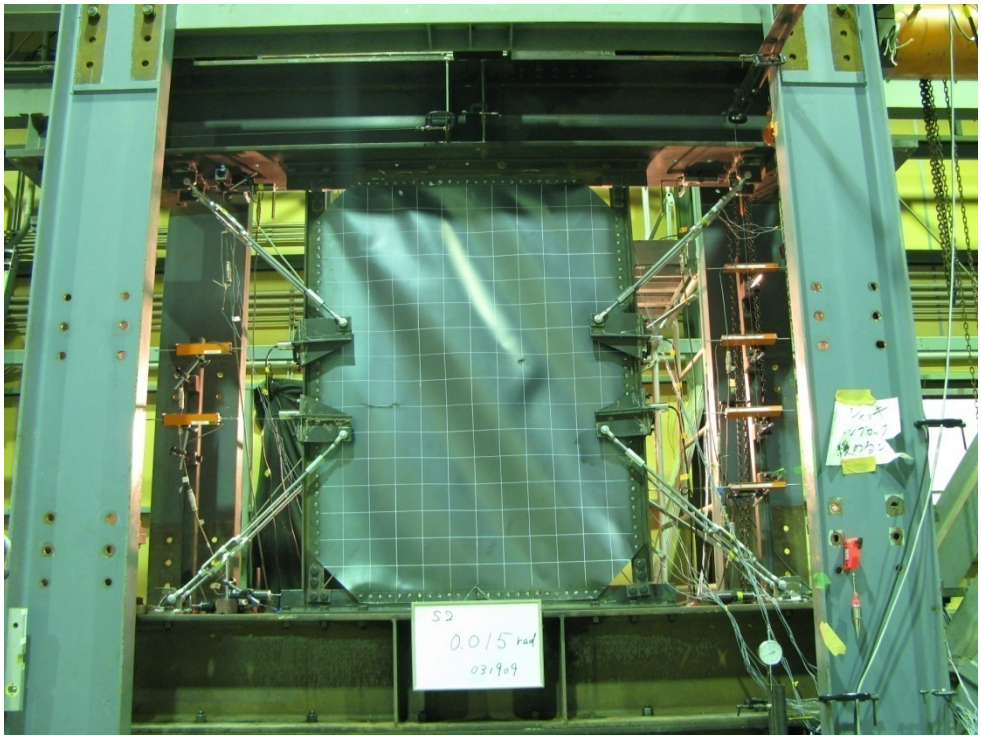

Fig 6.21(a):

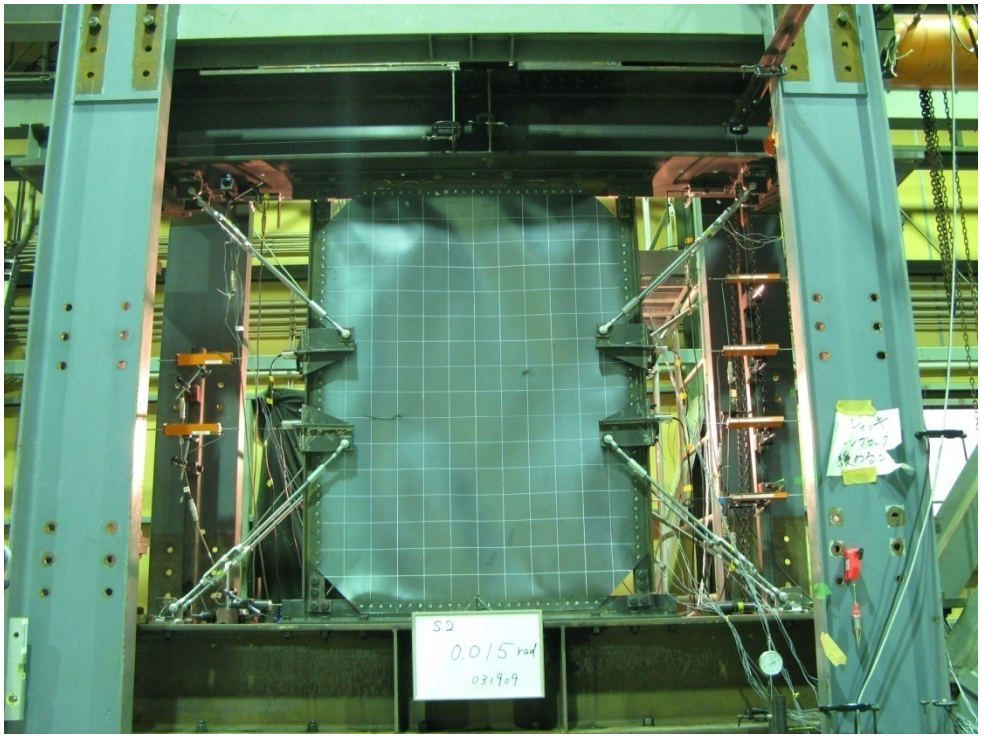

Fig 6.21(b):

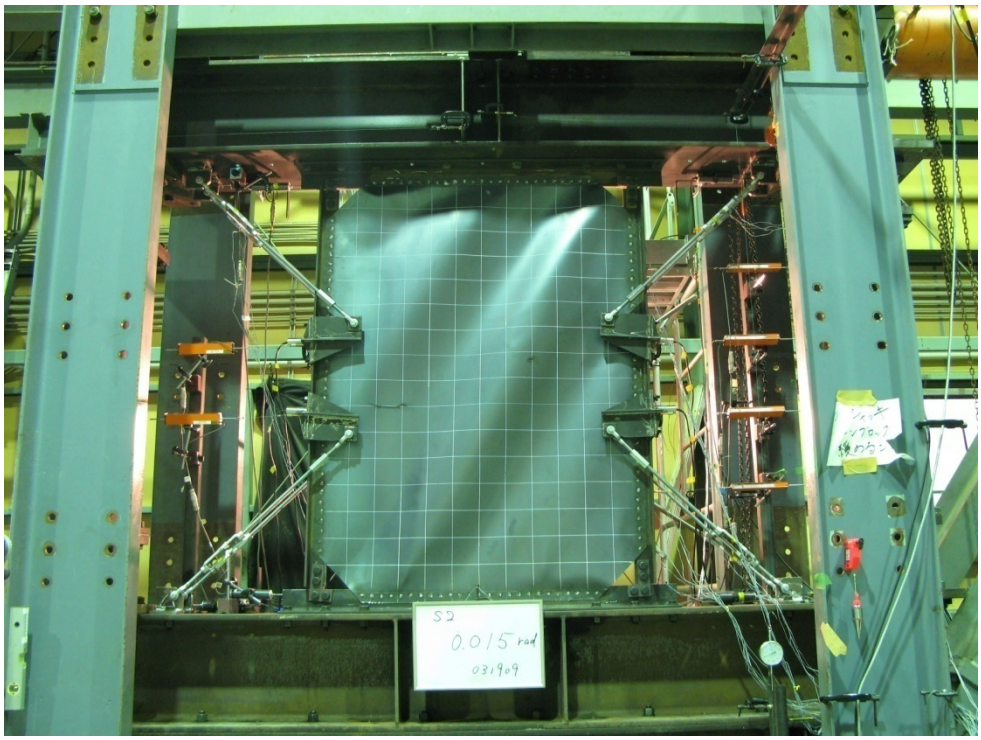

Fig 6.21(c):

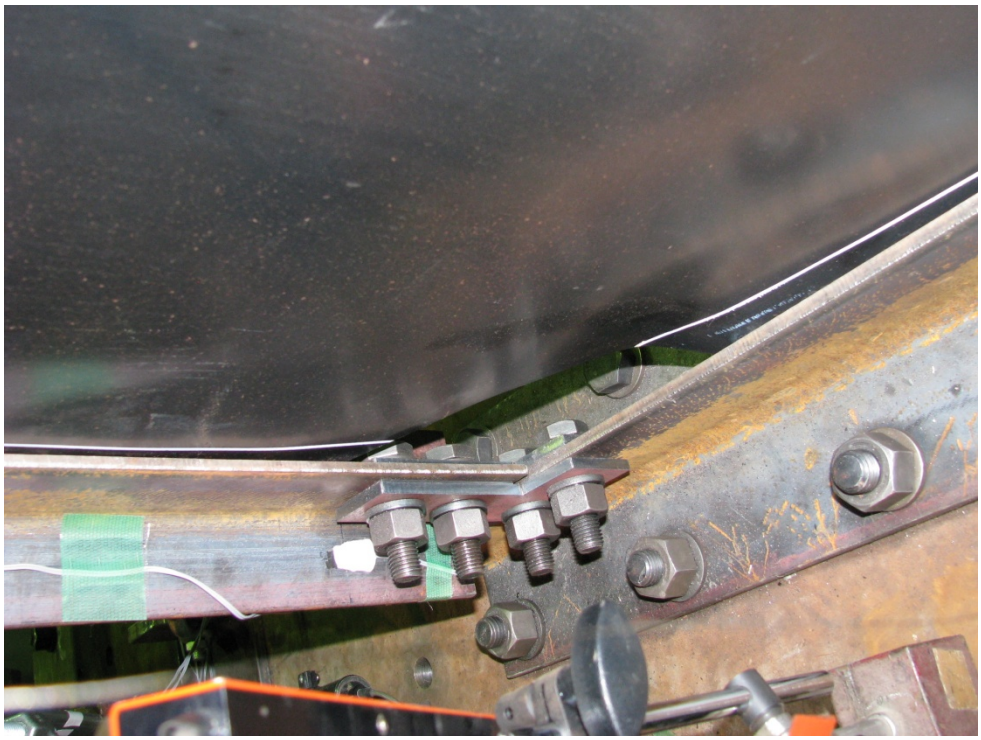

Fig 6.21(d):

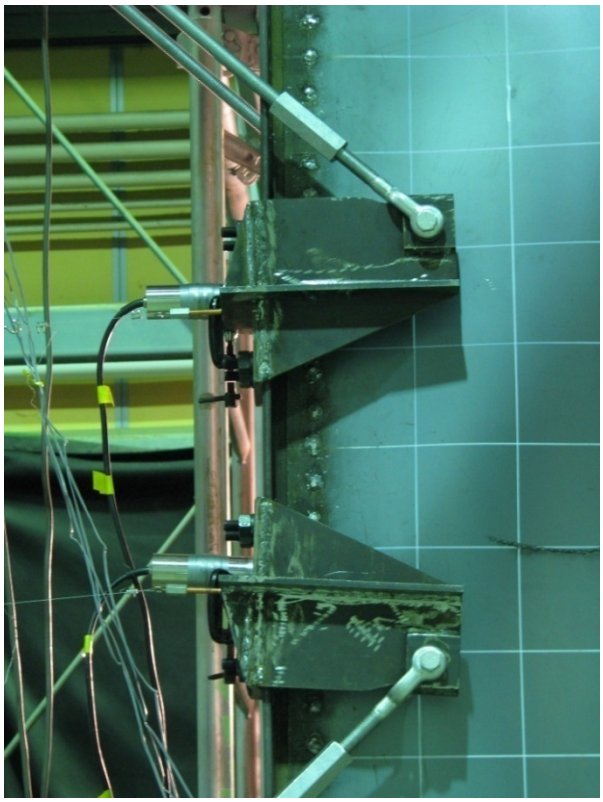

Fig 6.21(e):

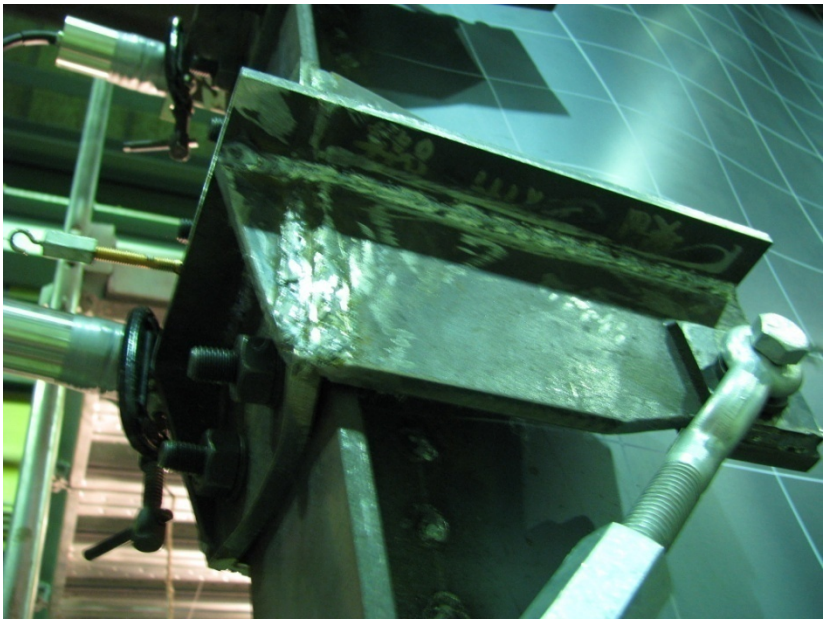

Fig 6.21(f):

Figure 6.21: Condition at 0.015rad. loading (a)-(c) transition of buckled shape (d) fracture at right bottom corner (e) permanent rotation of brackets (e) yielding of brackets

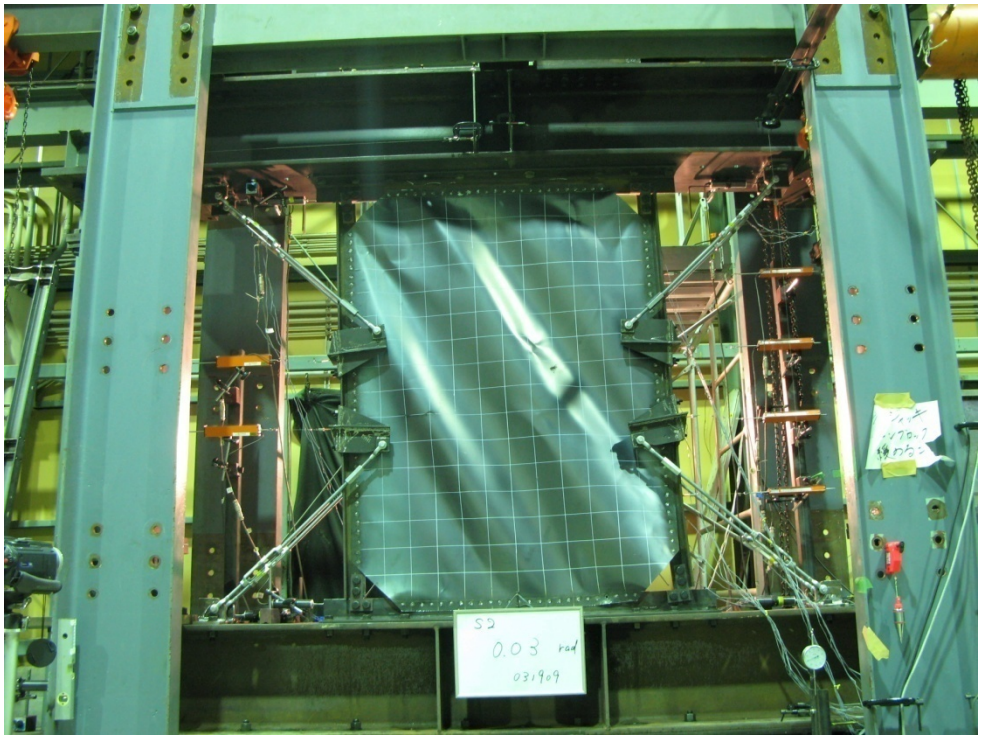

Fig 6.22(a):

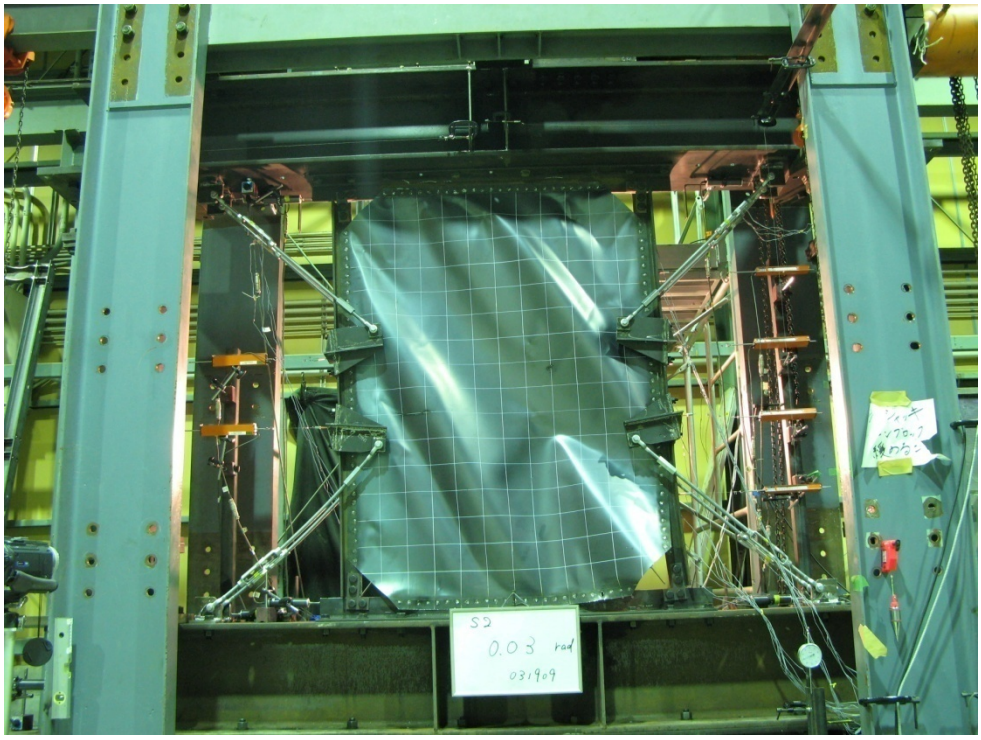

Fig 6.22(b):

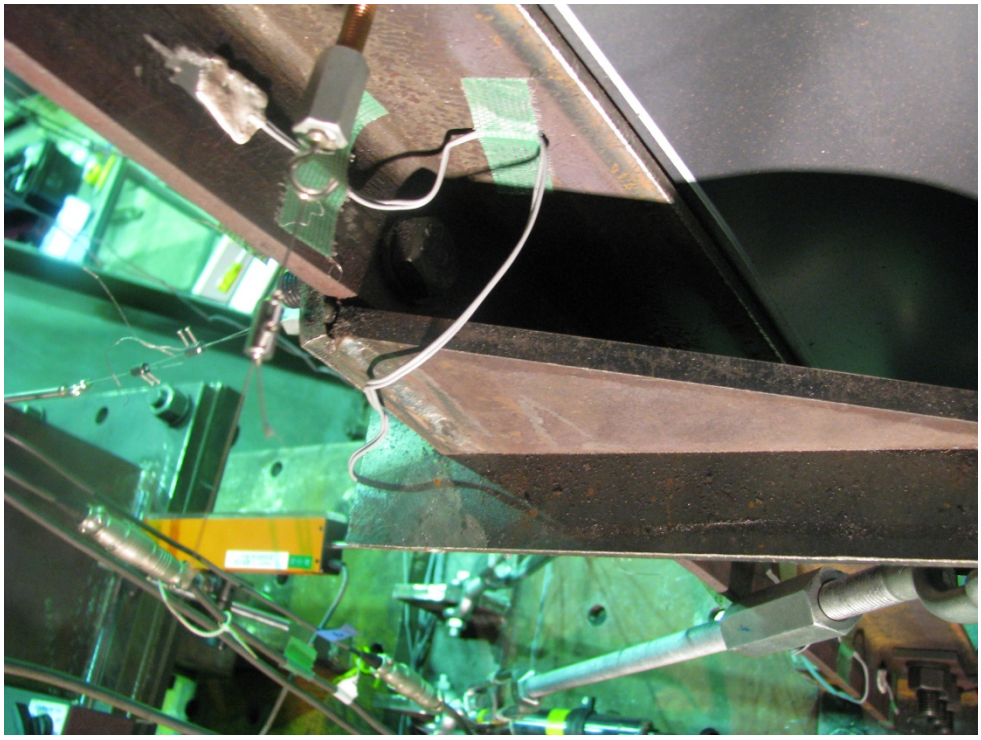

Fig 6.22(c):

Figure 6.22: Damage at 0.03rad. loading (a) deformation mode before bracket fracture (b) deformation mode after bracket fracture (c) bracket fracture

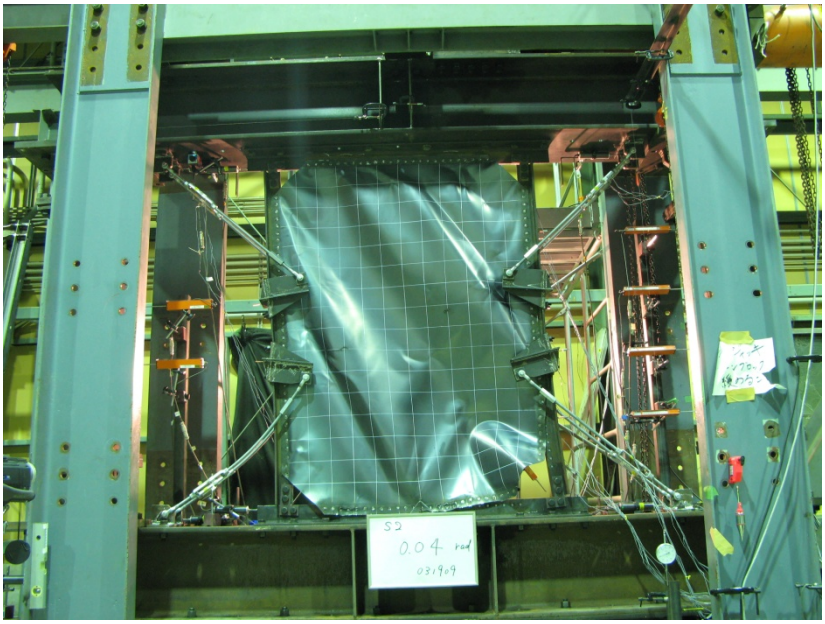

Fig 6.23(a):

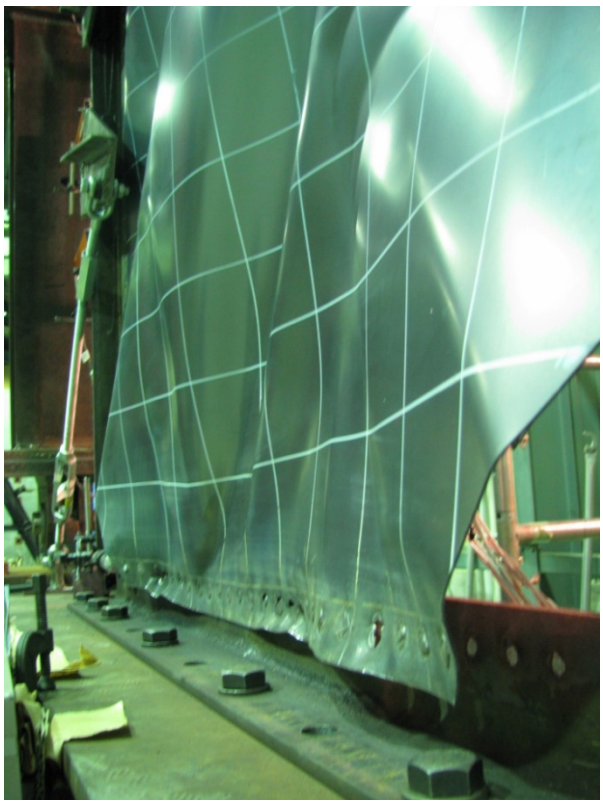

Fig 6.23(b):

Figure 6.23: Condition at end of loading (a) buckling of tension-only element (b) fractures at bottom boundary

Fig 6.24(a):

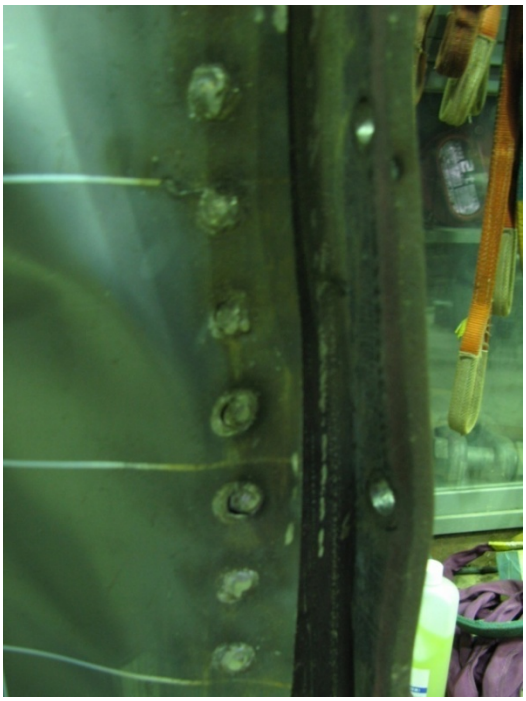

Fig 6.24(b):

Figure 6.24: VBE after removal of brackets (a) residual inelastic deformation (b) infill panel tearing

Fig 6.25(a):

Fig 6.25(b):

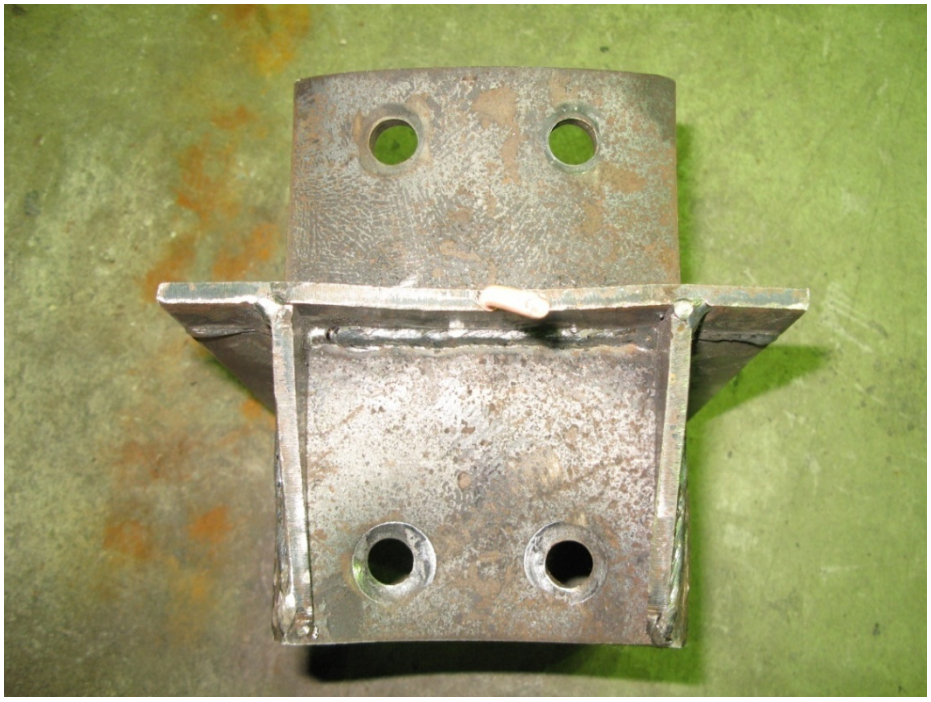

Fig 6.25(c):

Fig 6.25(d):

Figure 6.25: Inspection of steel bracket (a) from top (b) from side (c) from back (d) fracture

Hysteresis Behavior

Initial behavior

The performance of the two specimens can be compared in terms of actuator force versus interstory drift. Figure 6.26(a) shows the hysteresis behavior of the two specimens during the first loading cycle with at 0.375% story drift. Both specimens showed nonlinearly in their hysteresis curves immediately after the loading started. This was mainly caused by the global buckling of the infill plate. The large stiffness changes in both specimens in the 0.25-0.3% story drift range indicates initial yielding of the infill plates. The nominal yield strengths were estimated as 80kN for specimen 1 and 115kN for specimen 2. The yield strength and initial secant stiffness were increased by approximately 45% by the addition of the tension-only braces.

The hysteretic behavior until the end of the 1% story drift cycles is shown in Figure 6.26 (b). Both specimens showed pinched behavior after the second loading cycle at the 0.375% story drift. The pinching was more severe for the second and/or third cycles at each amplitude. For both specimens, it was notable that unloading curves crossed a zero displacement line with the approximately same amount of residual forces even for loading with different amplitudes. The sources of residual forces are estimated to be the force required to change the deformed shape during the transition of global buckling modes.

The post yielding stiffness of the specimen 2 was larger than that of the specimen 1 [Figure 6.26(b)]. As a result, the strength of the specimen 2 became 67% larger than that of the specimen 1 at the 1% story drift.

Global behavior

The global behavior before the specimens degraded are shown in Figure 6.27. The maximum strength of the specimens differed slightly for the positive and negative story drifts. The strength of the specimen 1 reached its maximum value, 108kN, during the first loading cycle at 2.0% story drift. The strength started to deteriorate slightly earlier (1.5% story drift) for the negative loading direction due to the fractures that propagated at the left bottom of the boundary connections. The strength of the specimen 2 reached its maximum value, 175kN, during the first loading cycle at 3.0% story drift. The strength stopped increasing earlier in the positive loading direction due to early, undesirable yielding of the steel brackets at their left top and right bottom locations. The design of the steel brackets should be reexamined to prevent this early termination of the strength increase. At 3% story drift, the strength deterioration in the positive loading direction became significant due to the fracture of the steel brackets and the development of the yielding line in the flange of the VBEs. In the negative loading direction, the deterioration was milder where the steel brackets deformed rather in a ductile manner withouth fracture at welding.

When two specimens were compared, the maximum strength was 62% larger in specimen 2. The ductility of the specimens, defined as the deformation where strength deteriorated to 80% of the maximum strength divided by the deformation at yield, were roughly estimated as 10 (2.5%/0.25%) for the specimen 1 and 14 (3.5%/0.25%) for the specimen 2. The energy dissipated by the two specimens did not differ much until 1% story drift [Figure 6.28]. This fact indicates that the tension-only bracing elements contributed to stiffness and strength of the specimen 2 without adding much energy

dissiapting capacity to the system. The difference of the amount of dissipated energy between two specimens increased notably after 1% story drift and reached approximately 30% of the energy dissipated by specimen 1 at a 4% story drift. The difference was mainly achieved by the energy dissipated by the steel brackets and VBEs and by the more ductile behavior of the infill panel in the specimen 2 given the smaller damage at the boundary connection.

Boundary behavior

The numbers of fractured weld points are listed in Table 6.7. The fractures mostly occurred at the bottom boundary connection. One possible reason for this phenomenon might be because the welder was forced to weld in an uncomfortable posture for the low height location. The numbers of fractured weld points were significantly smaller for specimen 2 until 3% story drift due to the small closing at the corners of the infill panel.

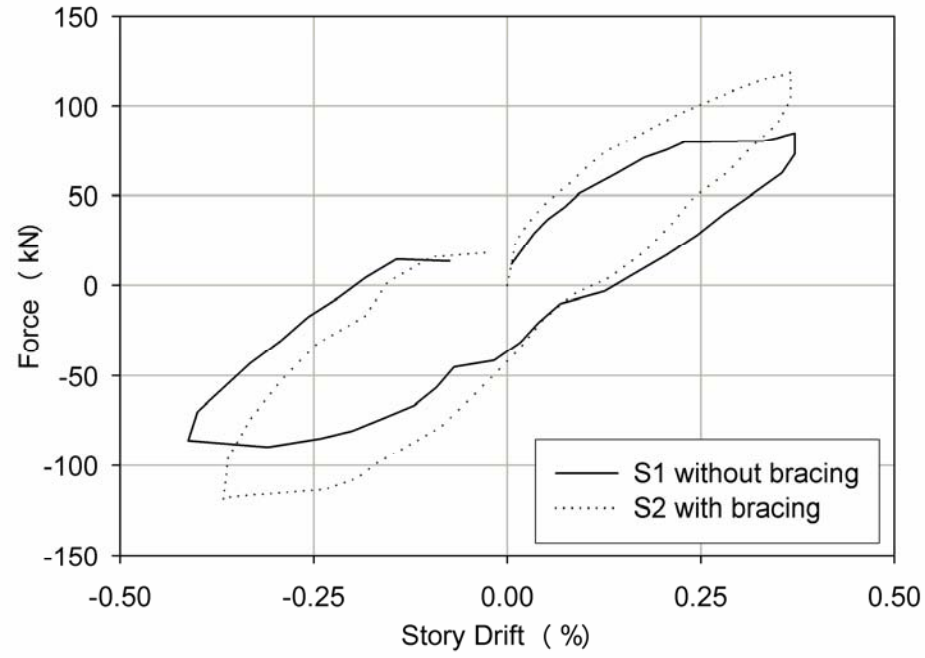

Fig 6.26(a):

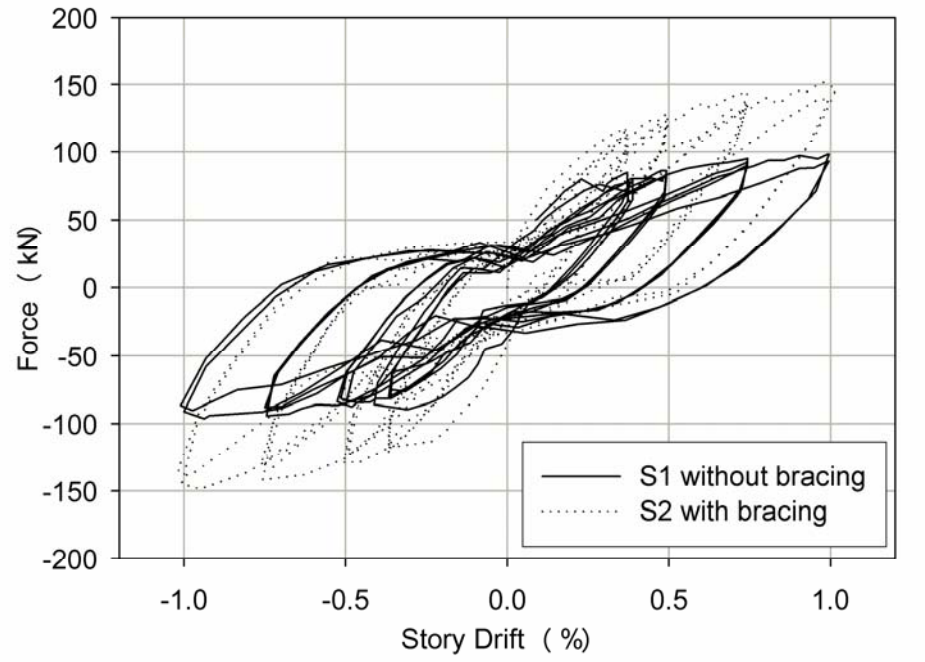

Fig 6.26(b):

Figure 6.26: Hysteresis until large deformation (a) first cycle (b) until 1% story drift

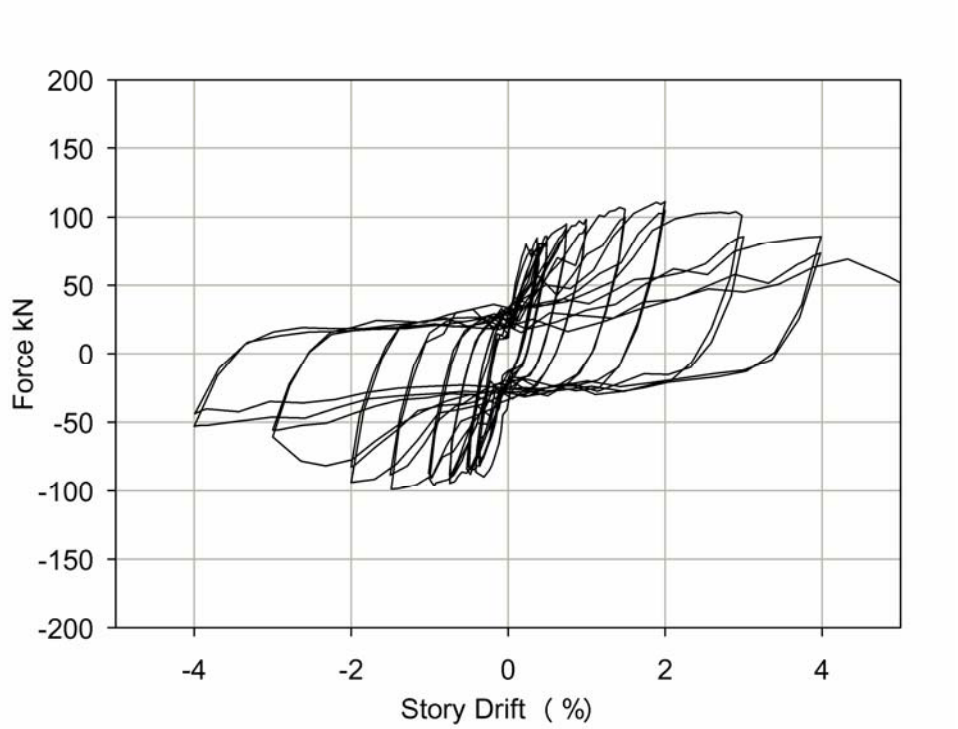

Fig 6.27 (a):

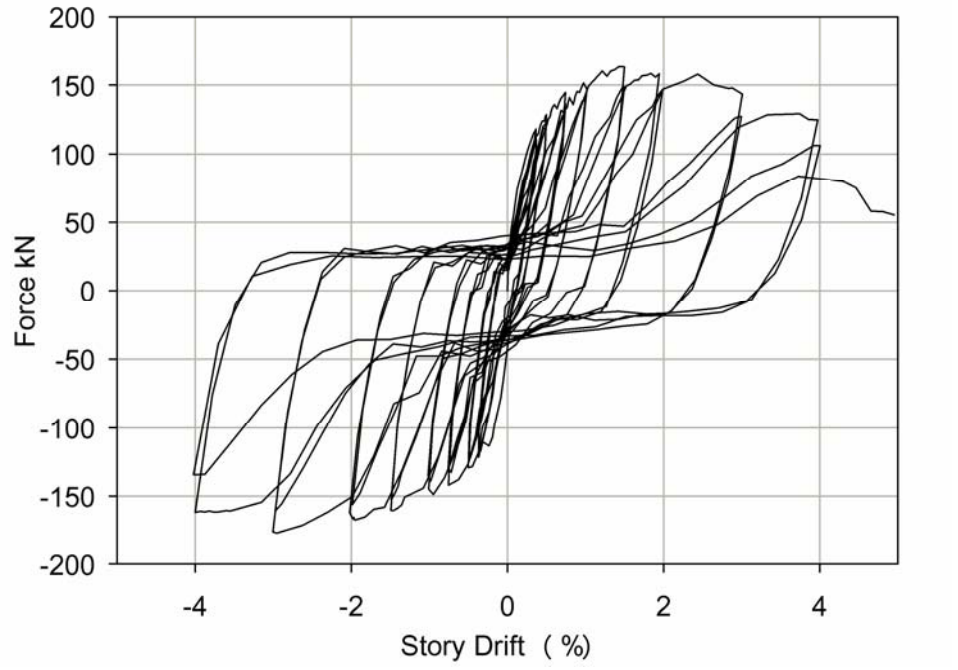

Fig 6.27 (b):

Figure 6.27: Behavior until end of loading (a) specimen 1 (b) specimen 2

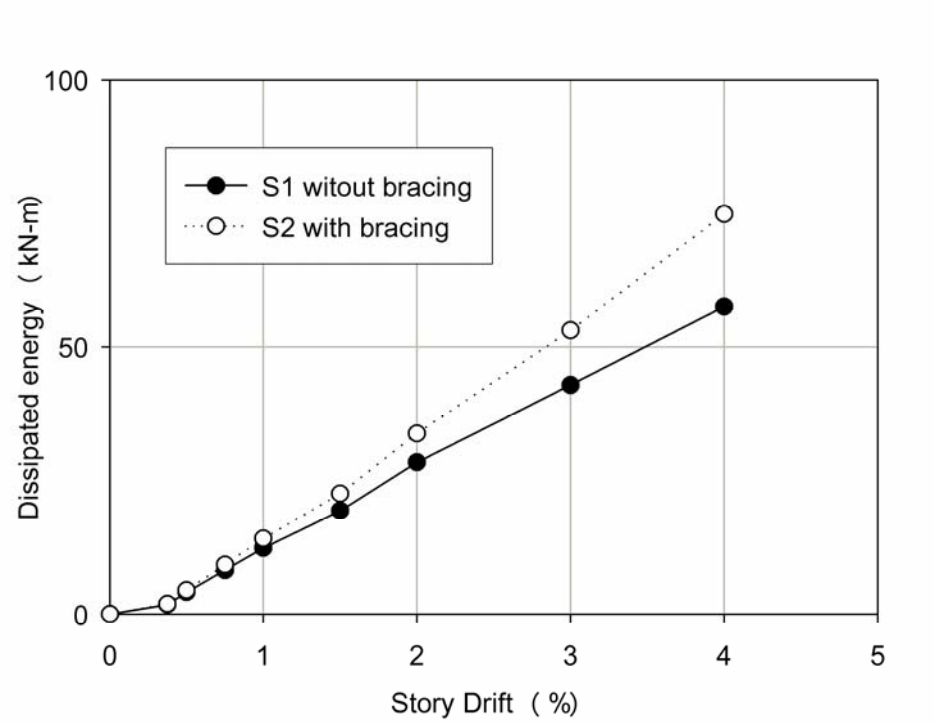

Figure 6.28: Cumulative dissipated energy at end of each amplitude cycle

Table 6.7: Number of fractured welds for two specimens

	Specimen 1					Specimen 2				
Cycle	*Number of fractured welds*					*Number of fractured welds*				
	bottom		top		total	bottom		top		total
rad.	left	right	left	right		left	right	left	right	
0.00375	0	0	0	0	0	0	0	0	0	0
0.005	0	0	0	0	0	0	0	0	0	0
0.0075	0	0	0	0	0	0	0	0	0	0
0.01	2	0	0	1	2	0	0	0	0	0
0.015	3	1	0	1	5	1	4	0	0	5
0.02	12	3	3	1	19	2	6	0	0	8
0.03	17	7	3	1	28	3	15	0	0	18
0.04	22	9	4	1	36	7	24	0	0	31

Strain history

The direction of the principal axes of strain at the centerline of the infill panels were computed from the data of the rosette gauges [Figure 6.29]. The angles are measured off the vertical center line of the infill panel. The location of the rosette gauges can be found in Figure 6.11. In the specimen 1, the gauges showed similar peak values for the positive and the negative loading direction. The peak value started at around 30 degrees and decreased gently to 23 degrees probably due to the fracture of welds at the corners of the infill plate. In specimen 2, the gauges showed different peak values for the positive and the negative loading direction, which indicates that the data was highly influenced by the local behavior at the location of measurement. The rosette gauge R1 had the peak values for the positive loading direction that were almost constant and around 38 degree through the entire loading. This indicates that the angle of the tension field action in specimen 2 was larger than that in the specimen 1.

The force histories in the tension-only braces are plotted in Figure 6.30. The forces in all tension-only elements were successfully smaller than their yielding strength (around 60kN), as intended in the capacity design approach used. The hysteresis indicates that the yielding of the steel brackets and/or the VBEs started approximately at a 1% story drift. For large deformation after the 3% story drift loading, the tension-only braces at left bottom ended up carrying a slight compressive force and globally buckled as confirmed in the Figure 6.23(a).

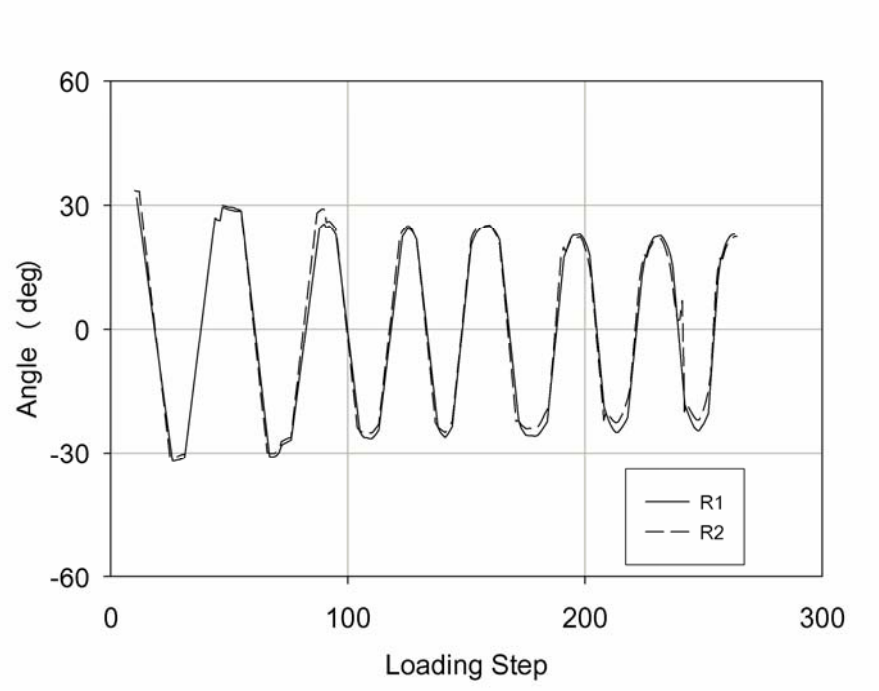

Fig 6.29 (a):

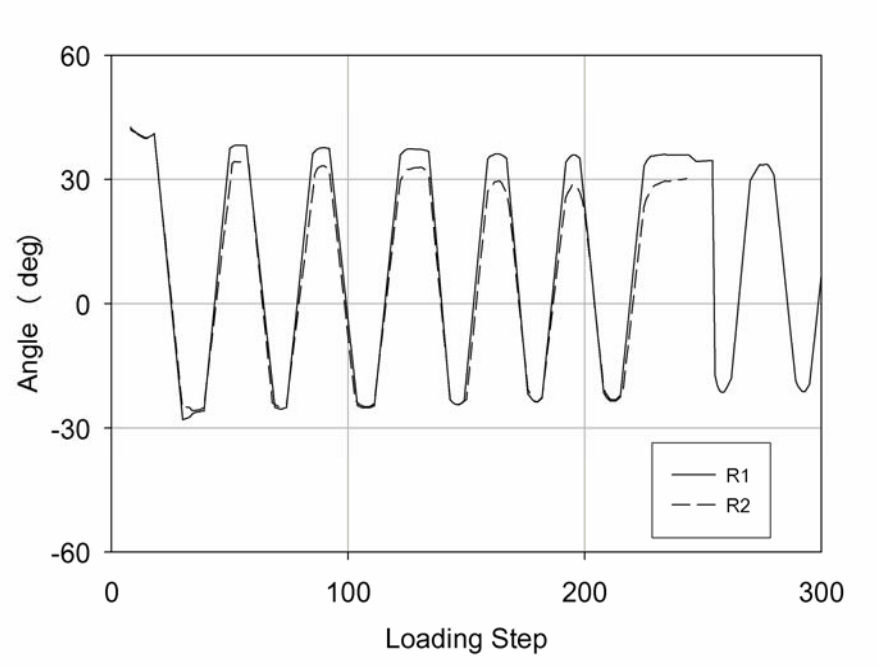

Fig 6.29 (b):

Figure 6.29: Direction of principal strain axes from R1 and R2 (a) speciemen 1 (b) specimen 2

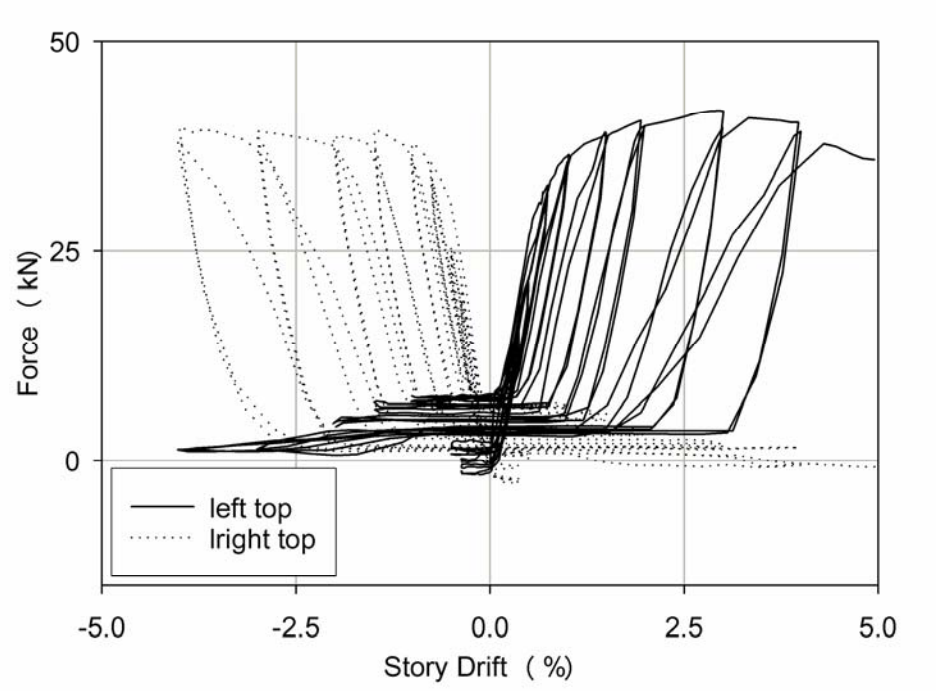

Fig 6.30 (a):

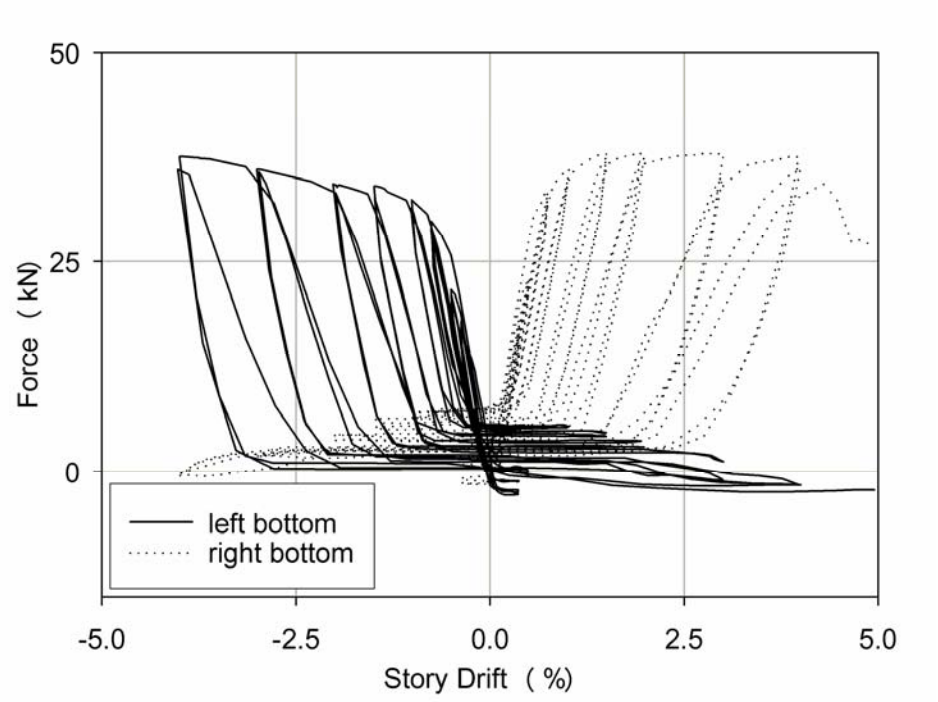

Fig 6.30 (b):

Figure 6.30: Average force hysteresis of tension-only rods (a) left top and right top (b) left bottom and right bottom

VBE behavior

The in-plan deformation of the right VBE in specimens are tracked using four potentionmeters [Figure 6.31, see Figure 6.7 for location of potentionmeters]. The measurement of the deformation terminated at 2% story drift due to the capcities of LVDTs. For both spesimens, the shape of the VBE was close to linear until 0.5% story drift. Nonlinearity in the deformed shape became significant after 0.75% story drift. The VBE shape of specimen 1 in large story drifts showed kinks at the location of 1300mm and 400mm in positive and negative loading direction, repectively [Figure 6.31(a)]. The kinks indicate the formation of plastic hinges. The VBE shape of specimen 2 was rather smoooth without severe kinks which indicate the speread inelasticity in the VBE. Therefore, the closing rotational deformation at HBE-VBE connections in specimen 1 were larger than those in specimen 2.

Figure 6.32 shows the out-of-deformation of the left and right VBEs measured at the middle section of the members. In specimen 1, the out-of-deformation was accumulated under cyclic loading and reached 0.55% and 0.75% in left and right VBEs, respectively. These defomation were not significant given the flexibility of the member with CT section in weak axis. The out-of-deformation in specimen 2 did not accumulate and returned to origin during unloading cycles. The tension-only elements also behaved similar to stability bracings for out-of-deformation.

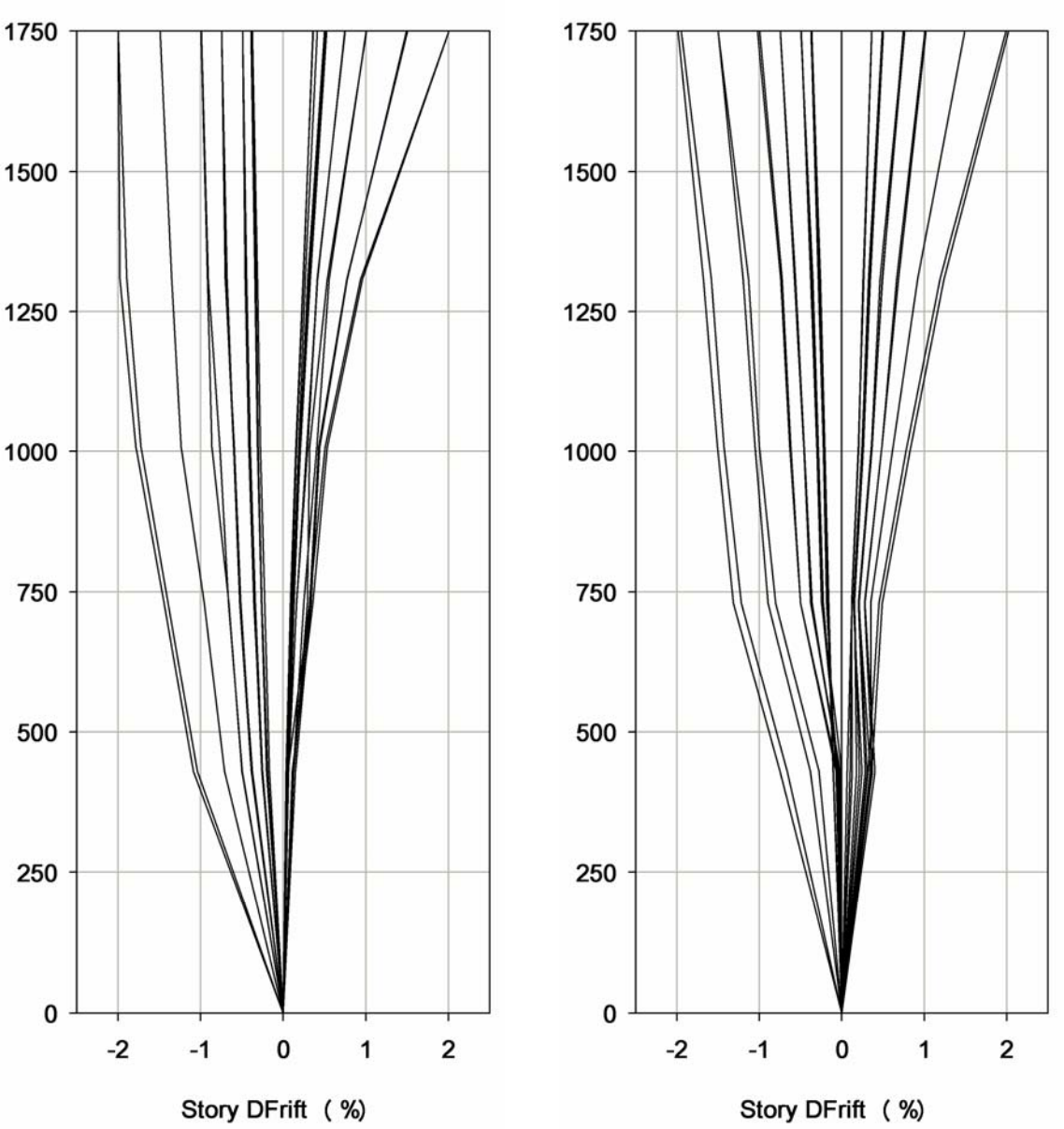

Fig 6.31(a): **Fig 6.31(b):**

Figure 6.31: In plane deformation of right VBE (a) specimen 1 (b) speceimen 2

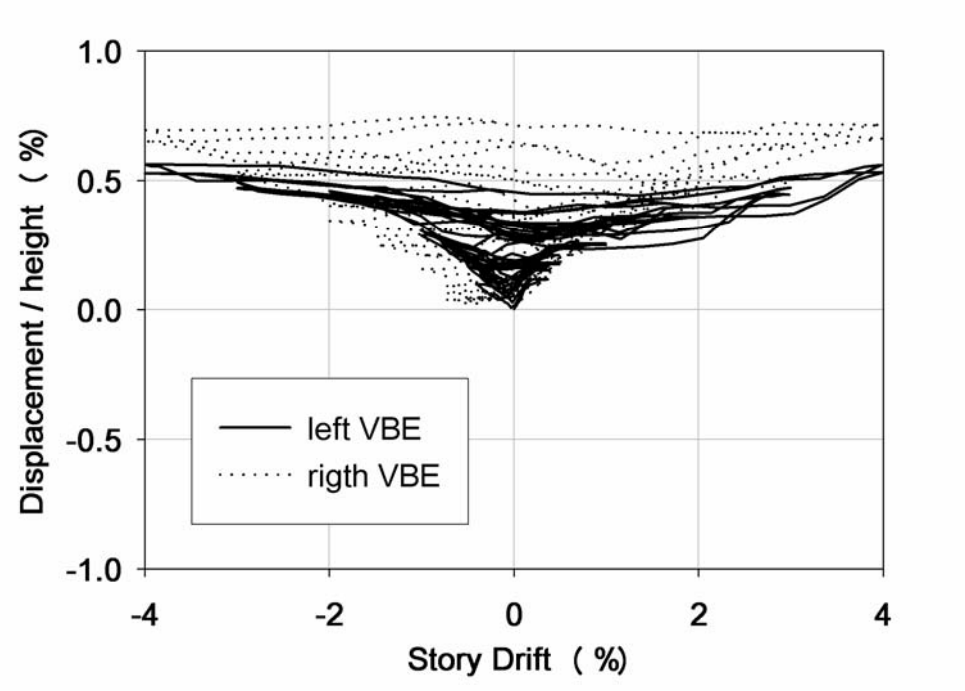

Fig 6.32(a):

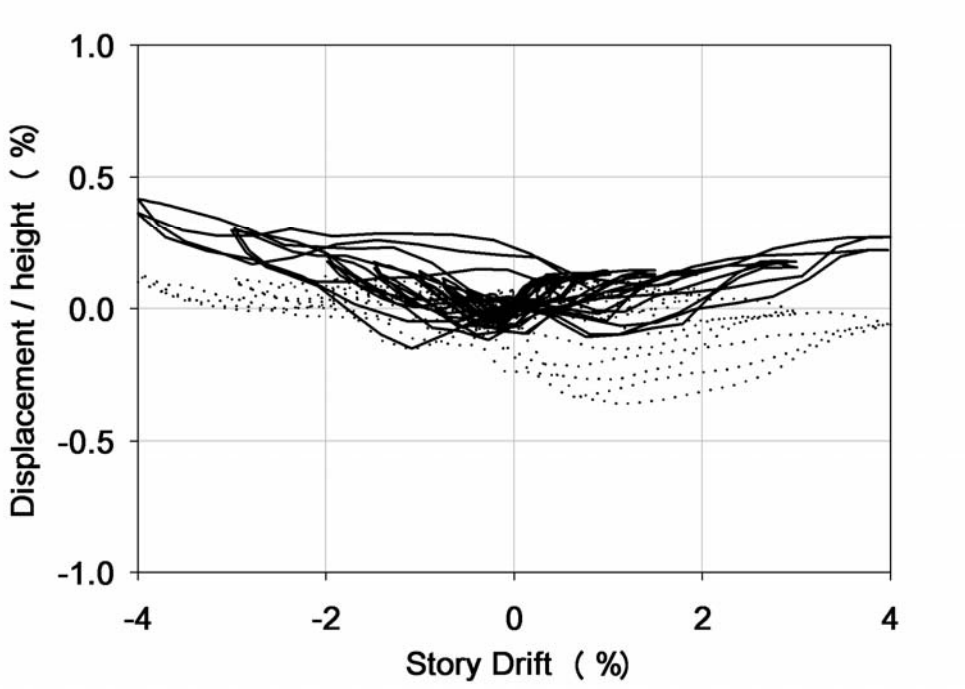

Fig 6.32(b):

Figure 6.32: Out-of-deformation of VBEs (a) specimen 1 (b) specimen 2

6.10 Summary

The proof of concept testing of the narrow steel plate shear wall system was conducted at the structural laboratory of the DPRI of Kyoto University, Japan. The experimental program was completed successfully with the scheduled timeline.

In the experimental program, two shear wall systems were tested. One was a specimen with tension-only bracing and another was the specimen without tension-only bracing. The two specimens were prepared to investigate the benefits of the bracing on the global and local behavior of the prototype. The specimens had a dimension scaled to approximately 50% of the original. The specimens were fabricated using members and materials specified in Japanese standard [JIS, 2005]. As the part of the experimental program, a pre-holed fillet welding method intended for shear walls with light gauge steel plates was proposed collaboratively by the author and a local manufacture. The performance of the welding method was evaluated through the preliminary tensile testing of the welded thin steel plates. Using the test results, the pitch and the size of holes were determined for the welding of the boundary connection in the shear wall specimens.

The performance of the two specimens was evaluated through the incremental cyclic loading using displacement controlled hydraulic actuators. Both specimens showed nonlinear hysteresis curves immediately after the loading started. This was mainly caused by the global buckling of the infill plate. Initial yielding of the specimens took place at 0.25-0.3% story drift. The yield strength and initial secant stiffness was increased by approximately 45% by the addition of tension-only braces. Both specimens showed pinched behavior after the second loading cycle with the 0.375% story drift. The pinching was severer for the second and/or third cycles of each amplitude. The strength

of specimen 2 became 67% larger than that of the specimen 1 at the 1% story drift because of the larger post-yielding stiffness of specimen 2 as compared to specimen 1.

In specimen 1, the strength started to deteriorate slightly at the 1.5% story drift due to the fractures that propagated at the left bottom of the boundary connections. In specimen 2, the strength stopped increasing earlier in the positive loading direction due to early, undesirable yielding of the steel brackets at left top and right bottom. At the 3% story drift, the strength deterioration in the positive loading direction became significant due to the fracture of steel brackets and the development of the yield lines in the flange of the VBEs. The maximum strength was 62% larger for specimen 2 than for specimen 1. The ductility of the specimens, defined as the deformation where strength deteriorated to 80% of the maximum strength divided by the deformation at yielding, were roughly estimated as 10 for specimen 1 and 14 for specimen 2. The energy dissipated by the two specimens did not differ much until 1% story drift was exceeeded. The difference of the amount of dissipated energy between two specimens increased notably after 1% story drift and reached approximately 30% of the energy dissipated by the specimen 1 at 4% story drift. The difference was mainly achieved by the energy dissipated by both the steel brackets and VBEs, and by the more ductile behavior of the infill panel in the specimen 2 given the smaller damage at the boundary connection.

The in-plan deformation of the right VBE in specimens are tracked using four potentionmeters. For both spesimens, the shape of the VBE was close to linear until 0.5% story drift. Nonlinearity in the deformed shape became significant after 0.75% story drift. The VBE shape of specimen 1 showed kinks under large story. The kinks

indicate the formation of plastic hinges in the VBE. The VBE shape of specimen 2 was rather smoooth without severe kinks which indicate the speread inelasticity in the VBE.

The out-of-deformation of the VBEs in specimen 1 accumulated under cyclic loading but the maximum defomation was not significant given the flexibility of the member with CT section in weak axis. The out-of-deformation in specimen 2 did not accumulate and returned to origin during unloading cycles. The tension-only elements also behaved similar to stability bracings for out-of-deformation.

CHAPTER 7

SUMMARY, CONCLUSION AND IMPACT

7.1 Summary and Conclusions

Two innovative strategies were proposed for rapid seismic rehabilitation in the context of sustainability, where environmental impact and social consequence were minimized by the limited usage of heavy construction equipment and disruption to occupants. These strategies are primarily intended for relatively small rehabilitation projects and are suitable for a multi-stage rehabilitation methodology. This thesis presented the work completed for the development of the two proposed systems including: verification through analyses, prototype design, development of design procedure, and proof-of-concept testing. Both systems have the common trait of stable hysteretic performance under seismic load, while benefitting from reduced installation effort and minimal environmental impact.

"Cable Bracing System-CORE Damper"

The cable cross bracing system developed by the author has a unique geometry to maintain key elements always in tension under cyclic lateral loading, and provides stable energy dissipation until very large deformations are reached by taking advantage of permanent rotations in a central energy dissipating device. The central device, referred to as the COuples REsisting Damper (CORE Damper), dissipates energy through the bending and yielding of mild steel plates and does not require periodic maintenance. In order to achieve stable hysteretic behavior and allow for easy replacement after a major seismic event, the connections in regions of anticipated maximum ductility are designed

using high strength bolted connections to avoid potential brittle weld failures. The main objectives of this study were to provide the first prototype design and analytical model validated through a proof-of-concept testing for the system. An example application of the proposed system for the seismic upgrading of steel frame buildings was also presented.

The first task undertaken was to verify the concept and behavior of the proposed cable bracing system with unique geometry. This task was accomplished through preliminary simplified analyses in the OpenSEES platform, the prototype design of the CORE Damper using FE analysis models and the identification of the dynamic behavior of the prototype system under high-speed loading. In the preliminary analyses, a bi-linear hysteresis behavior was implemented for the rotational spring and one cycle of 3% story drift amplitude was statically applied to the model frame. The approximate strength demand, required deformation capacity, and optimal shape for the CORE Damper were determined through parametric analyses using this simplified analysis model. The details of the CORE Damper were designed carefully by using a general purpose finite element analysis program, ABAQUS, as a design tool. The dynamic behavior of the prototype system was identified through the nonlinear dynamic analyses using the simplified analysis model with the hysteresis of the prototype CORE Damper obtained from FE analyses.

Utilizing the developed CORE Damper, an option to add re-centering capability to an existing bracing system was also considered. The re-centering system was specifically for the reduction of residual deformation at critical sections of existing buildings. By simply adding extra cables made of shape memory alloy (NITINOL) to the

same diagonal in the base system, the system was upgraded as a re-centering system. The concept of the re-centering system was validated through nonlinear static analyses in the OpenSEES platform.

The second task undertaken was to proof the proposed concept for the cable bracing system through physical testing. The testing for the prototype system was carried out through the use of a full-scale testing frame constructed in the structural laboratory at the Georgia Institute of Technology. The performance of the system was evaluated at various drift levels under quasi-static cyclic loading. The local behavior of the system was carefully monitored using digital instrumentations including hand-made load cells made for the cables. The surface strains of the SPEAs were acquired by strain gauges.

The third task undertaken was to demonstrate an example application of the newly developed "Cable Bracing-CORE Damper system" to the upgrading of a seismically deficient steel frame. In the study, the original building was assumed to be built in late 1960's and was designed for the combined load of the gravity and wind forces using the plastic design procedure. It was assumed that the seismic response of the original building became a concern due to the change of seismic category in the region where the building is located. The seismic performance of the building was enhanced by replacing the original diagonal cross bracing with the CORE Damper bracing system. The main difference between the two systems arises from their post yielding behavior. Once the diagonal cross bracing system experiences severe inelastic deformation, it loses its elastic stiffness until its deformation exceeds the maximum previous deformation. When subjected to several inelastic cycles of deformation, the diagonal brace member becomes highly susceptible to fracture at a plastic hinge created by global buckling. In contrast,

the CORE Damper bracing system retains its initial stiffness with stable bi-linear hysteresis behavior. It is also notable that the post yielding stiffness of the CORE Damper system is significantly higher than the diagonal cross bracing system. The seismic performance of two building systems under both a near and far fault earthquakes was evaluated through nonlinear dynamic analyses in the OpenSEES platform.

The key findings and conclusions for the study of "Cable Bracing-CORE Damper System" are summarized below:

- In the proposed cable bracing geometry, if the rotational spring could deliver a stable bi-linear curve, then the behavior of the entire subassemblage, as characterized by its force vs. story drift curve, is also stable and bi-linear.
- The CORE Damper is carefully designed using a finite element analyses as a design tool and can sustain a stable, bi-linear hysteresis curve until the rotation corresponding to a story drift much larger than that specified in current design guidelines.
- The analytical study of cable bracing system under high speed loading showed that the increments in local and global forces are limited until a frequency of 1Hz and become noticeable for higher frequencies. In general, the effects of dynamic loading were larger in the local cable forces than in the global system behavior, while the effects were limited for the CORE device even with very high speed loading because the effects were attenuated by the yielding of the damper device.
- A re-centering system can be realized by simply adding extra cables made of shape memory alloy (NITINOL) to the same diagonal in the base system.

- The prototype of the proposed system successfully showed stable bi-linear hysteresis, even through very large deformations. As the drift level increased, the relative rotation between the front and back cover plates increased. The rotation became noticeable at the 0.0075rad. cycle when the SPEAs started to yield.
- The SPEAs successfully exhibited inelastic deformations throughout their length as intended in the design. This was confirmed from the surface condition of the SPEA which had flaked in several sections by the end of the loading.
- The post-yielding stiffness of the system increased after the 0.02rad. cycles when the bolts at the connections between the SPEAs and the cover plates started to slip along long slotted holes.
- The base shear resistance of the system is slightly higher when the CORE Damper deformed outward than when it deformed inward. This is due to the difference in boundary conditions in outward and inward deformation modes.
- The preliminary analyses in ABAQUS and OpenSEES predicted well the elastic stiffness and yielding strength of the system.
- The CORE Damper successfully remained below the limit state condition until the end of loading, defined as a physical contact between two SPEAs under the inward deformation mode. The investigation of the components after the test confirmed that damage was concentrated only in the SPEAs.
- The process of reassembling the system by replacing the damaged SPEAs was simple and rapid. This demonstrated the ease of replacement after a significant seismic event.

- The original building with the diagonal cross bracing system suffered from concentrated damage in the first story with the development of a “soft story” due to several large amplitude excursions in the near fault earthquake. Compared to this, the deformation of the building with the CORE Damper system was well distributed along its height and seismic energy was dissipated through the stable inelastic deformation of the CORE Dampers in several stories.
- The example analytical study successfully demonstrated the effectiveness of the seismic upgrading with the application of the CORE Damper bracing system. The performance improvement was achieved through the different shape of the hysteresis behaviour without the increase of strength or stiffness of the building system.

“Narrow Steel Plate Shear Wall with Tension-Only Bracing”

Addition of a properly designed and detailed unstiffened thin steel plate to a steel moment frame can give the system a substantial increase in stiffness, load-carrying capacity, and energy adsorption. In order to utilize a thin steel plate as a supplemental lateral load resisting system for relatively small seismic rehabilitation projects, a geometry where a plate with surrounding boundary elements is installed separately from existing columns is proposed. The proposed geometry intends to minimize installation impact and to reduce the need to strengthen the existing columns. The Vertical Boundary Elements (VBE) which surround the plate need to have significant strength and stiffness overcapacity relative to the infill steel plate, otherwise the thin plate will not resist seismic effectively. This objective was achieved by the use of a relatively weak beam supported by tension-only bracing elements. Installation of a strong beam as a VBE

would require much effort and result in large force demands on the existing beams where the VBE was attached. The main objectives of the study were to provide a prototype geometry and experimental data for the proposed system, named "Narrow Steel Plate Shear Wall with Tension-Only Bracing (NPSW-TB)". The study also provided a design approach and design procedure for the proposed system.

The first task was the development of the prototype NPSW-TB system. This task was accomplished by developing a design approach and design procedure, including a simple and logical design flowchart. For this work, a simplified analysis model was constructed in the OpenSEES platform as a design support tool. A major design constraint for the prototype system is the requirement that yielding of the infill panel should occur prior to yielding of the boundary elements. The Vertical Boundary Elements (VBEs) were also subjected to inelastic deformation late in the load history due to the inward flexural force induced by the tension field developed in the infill panel. The design of the VBE required an iterative procedure since its behavior interacted with the behavior of the tension-only rod and the local geometry of the arm. The tension-only elements were designed to remain elastic until very large deformations. The performance goal of the prototype system was to achieve a total system shear strength which was comparable to the shear force carried by three typical columns in low-to-mid size steel moment resisting frames, with the columns assumed to have fixed-fixed end conditions. The shear strength of the prototype system obtained from a simplified analysis model was close to the shear strength of the infill panel computed by the formula specified in the current seismic codes in U.S. and Canada for steel-plated shear walls. A ½ scale system was also designed for proof-of-concept testing using the proposed design procedure for a

frame. For comparison, nonlinear finite element analyses were conducted for the scaled system as well as the scaled system without tension-only elements. The detailed behavior of the scaled systems were examined using a general-purpose finite element program, ABAQUS, and were compared with the prediction from the preliminary simplified analyses in OpenSEES. The purpose of the FE analyses was to provide an accurate prediction of both global and local behavior for the experimental study and to validate the OpenSEES analyses system.

The second task was to verify the performance of the proposed NSPW-TB system in proof-of-concept testing. This task was accomplished through the performance evaluation of the scaled prototype conducted at Kyoto University, Japan. The test program was embedded into a series of experiments for shear wall type structures planned at the Disaster Prevention Research Institute (DPRI) of Kyoto University, in cooperation with Dr. M. Nakashima. In the experimental program, two shear wall specimens were tested. One was the prototype specimen with tension-only bracing and another was a specimen without tension-only bracing to evaluate the effects of the bracing on the global and local behavior of the prototype. As part of the experimental program, a pre-holed fillet welding method intended for shear walls with light gauge steel plates was proposed collaboratively by the author and a local manufacture. The performance of the welding method was evaluated through preliminary tensile testing of welded thin steel plates. Using the test results, the pitch and the size of holes were determined for the welding of the boundary connection in the shear wall specimens. The performance of the two systems was evaluated through the incremental cyclic loading.

The key findings and conclusions for the study of "Narrow Steel Plate Shear Wall with Tension-Only Bracing" are summarized below:

- The geometry of the prototype selected following the proposed design flowchart successfully meets the target design strength and the primary design constraint, which is the requirement that yielding of the infill panel should occur prior to yielding of the boundary elements. The other design constraint, which is the requirement that the tension-only elements remain elastic until very large deformation, was successfully achieved both in the preliminary analyses and in the physical testing.
- The local and global behavior of the scaled systems obtained using a general-purpose finite element program, ABAQUS, were similar to the prediction from the preliminary simplified analyses in OpenSEES.
- In the FE analyses of the scaled systems, most of the middle part of the infill panel yielded for both cases, but the yielded area was larger with tension-only elements. More notably, most of the VBEs yielded with tension-only elements while, without tension-only elements, damage involving plastic hinge formation was highly concentrated in the area of the HBE-VBE connections.
- For the system without tension-only elements, the HBE-VBE connections located in the extended diagonal suffered from large closing deformation. The closing deformation was more moderate with the presence of tension-only elements. The predicted yield shear strength in both analyses was very close to the design shear strength.

- In the experiental program, both the scaled systems with and without tension-only bracing showed nonlinear hysteresis curves immediately after the loading started. This was mainly caused by the global buckling of the infill plate.
- In the tests, the yield strength and initial secant stiffness were increased by approximately 45% by the addition of tension-only braces. Both systems showed pinched behavior after the second loading cycle at 0.375% story drift. The pinching was severer for the second and/or third cycles of each amplitude. With the presence of the tension-only bracing, the shear strength at the 1% story drift and maximum shear strength increased 67% and 62%, respectively.
- In the experiments, strength started to deteriorate much later with the presence of tension-only bracing. In the case without the tension bracing, the strength started to deteriorate slightly at the 1.5% story drift due to the fractures that propagated at the left bottom of the boundary connections. In the case with the tension bracing, the strength deterioration in the positive loading direction became significant at the 3% story drift, due to the fracture of steel brackets and the development of the yield lines in the flange of the VBEs.
- The ductility of the specimens, defined as the deformation where strength deteriorated to 80% of the maximum strength divided by the deformation at yielding, were roughly estimated as 10 and 14 for specimens with and without tension-only bracing, respectively.
- For both systems, the in-plane deformation shape of the VBE was close to linear until 0.5% story drift. Nonlinearity in the deformed shape became significant after 0.75% story drift. The VBE shape of the system without tension-only

bracing showed kinks under large story deformations. The kinks indicate the formation of plastic hinges in the VBE. The deformed shape of VBEs with tension-only bracing was rather smoooth without severe kinks, indicating the spread inelasticity in the VBE.

- The out-of-deformation of VBEs accumulated under cyclic loading for the system without tension-only bracing while the out-of-deformation did not accumulate and returned to the origin during unloading cycles for the system with tenion-only bracing. The tension-only elements also behaved similar to stability bracings for out-of-deformation.

7.2 Impact of Research

The United Nations noted that we face an urgent need today to realize the freedom of future generations to sustain their lives on this planet. We are failing to provide that freedom. On the contrary, we have been plundering our children's future heritage to pay for environmentally unsustainable practices in the present [United Nations 2000]. The strategies proposed on this thesis should help contribute to realizing sustainable infrastructure systems in our society. They will give an option to building owners and stakeholder for the rehabilitation with low initial cost and thus contribute to sustainable society by providing healthier building stocks.

- The significant contribution of this study is the proposal of the concept for rapid rehabilitation strategies utilizing tension-only design approaches. The proposed strategies showed stable, high physical performance under seismic load with reduced influence on existing framings with replaceable energy dissipating elements. The application of these strategies for rehabilitation should benefit

from reduced installation effort, resulting in minimal environmental impact and social consequences during construction.

- Each component of the proposed systems is light enough to be carried without the help of heavy construction equipment. Also, most components are sized to be transported using existing elevators, which eliminates the use of large cranes. Minimal use of heavy construction equipment may enable overnight or weekend rehabilitations. For instance, if applied to school building, the minimal disruption to classroom activities results in reduced social consequences from rehabilitation. The approach taken for this study can provide a road map for future development of rehabilitation strategies in a sustainable frame work.

- The proof-of-concept testing of the cable bracing system showed that the process of reassembling the system by replacing the damaged SPEAs is simple and rapid. This demonstrated the ease of replacement after a significant seismic event in the adjustable cable bracing geometry. This work provides a unique option to practitioners by adding new bracing geometry with replaceable elements into the lists of exiting bracing system.

- The replacement of slender, tension-only cross bracing systems in traditional steel frames with the proposed cable bracing system could reduce the seismic response of the frames significantly without modifying the strength and stiffness of the original frame. This indicates that seismic responses can be controlled by simply changing hysteresis behavior of the energy dissipating elements with enhanced

ductility, while lateral load resisting path remain the same as was originally designed for in the tension-only cross bracing system.

- The narrow steel plate shear wall system provides a new option for practitioners to utilize thin plate shear wall systems in the situation where exiting columns are not easily accessible or the columns do not possess reserved strength. Also, the experimental study of the narrow shear wall system without tension-only elements provides a much-needed set of experimental data for the infill plates with small aspect ratios.

- Unique welding methods were applied for the narrow steel plate shear wall system. This method is intended for reduced residual stress in the infill panel which may lead to the large reduction of initial stiffness and strength.

7.3 Recommendations for Future Work

Areas in which this study can be extended through additional research are cited below:

- The prototype of the CORE Damper system showed stable performance in analyses and in physical testing but the scalability of the system in terms of strength and stiffness has not yet been explored. These parameters are mainly controlled by the geometry in the CORE Damper and analytical and experimental research on defining the upper limit of the strength and stiffness of the damper should be explored. It is desirable to provide an option to select different performance goals for end users.

- Current design method for the CORE Damper relies on finite element analyses. Simple design formulation to estimate rough geometry of the damper should be developed so that the effort in designing the damper will be significantly reduced.

- The application of the "Cable Bracing-CORE Damper System" for seismic upgrading was explored with only a single building configuration. A series of model buildings with various shapes should be examined for the further understanding of the effectiveness of the proposed system in a general building configuration. A statistical evaluation of the seismic response of these frames under ground motions with various spectral characteristic and at various intensity levels is also desirable for providing the probabilistic information for the performance of the proposed system.

- The proposed cable bracing geometry can be extended to other kinds of structures such as wood frame or concrete frame buildings. The CORE Damper made of other materials, the use of aluminum for the SPEAs and wood for cover palate, cables made with bamboo or synthesis ropes can be used for such rehabilitation projects, possibly outside of the developed countries.

- The impact of the installation of the proposed shear wall systems in existing frames should be quantitatively evaluated and compared with other existing retrofit strategies. A statistical evaluation of the impact of installation for various frame geometries under the earthquake ground motions is also desirable for providing the probabilistic information.

- Cost-benefit analyses of the rehabilitation projects with each proposed systems and other rehabilitation strategies would have larger impact on promoting the proposed strategies. The analyses should include the cost for installation effort and time as well as the amount of saved materials. In addition, limited usage of the heavy construction equipment should have significant advantage in reducing the initial investment.

- Finally, example application of the proposed rapid rehabilitation strategies in the incremental rehabilitation methodology should be demonstrated. The benefit arisen from the use of the rapid rehabilitation strategies into construction management such as flexible scheduling, financial aspect and social consequences.

APPENDIX A

STRUCTURAL COMPONENTS TESTING SETUP AT GEORGIA INSTITUTE OF TECHNOLOGY

A.1 Preliminary Analysis

A new testing setup at the GT structural lab was developed to provide the proof-of-concept data for the proposed seismic rehabilitation systems. The designed testing system was a portal frame with pins at its four corners and is capable of testing sub-assemblages of low-to-mid rise steel buildings under quasi-static earthquake loads. After an overview of previous full-scale tests in steel buildings [Berman *et al*., 2005], the maximum capacity of the testing frame was chosen as 440kips by using two MTS 243.70T hydraulic actuators.

By applying the maximum output force of two actuators, local force demands in all frame elements were examined by pushover analysis of the steel plate shear wall (SPSW). The SPSW was analyzed as a strip model proposed by Thorburn where the number of tension-only strip elements represented a steel infill panel as shown in Figure A.1(a) [Thorburn *et al*., 1983]. Figure A.2(b) and (c) are the results obtained by general purpose structural analysis program, SAP2000. All components of the testing bed were designed to have safety factors larger than 1.3 under the combined shear force and bending moment obtained in the analysis.

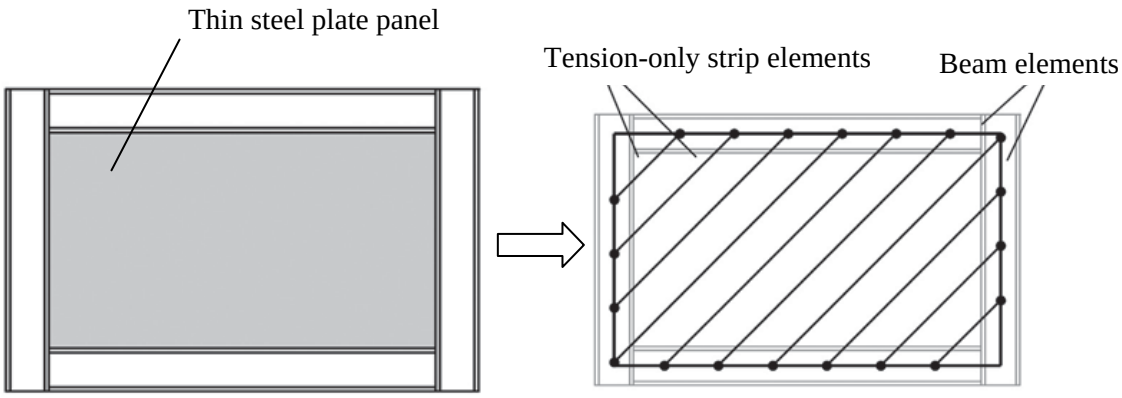

Fig A.1(a):

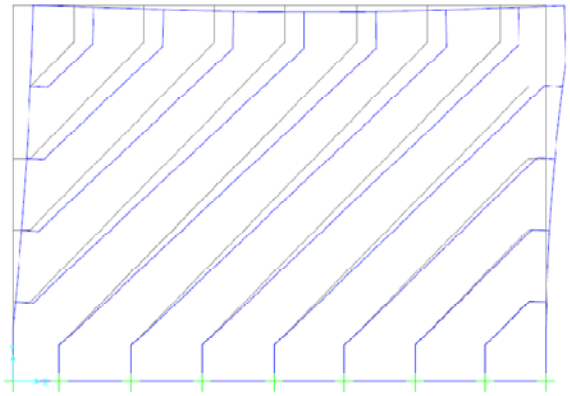

Fig A.1(b):

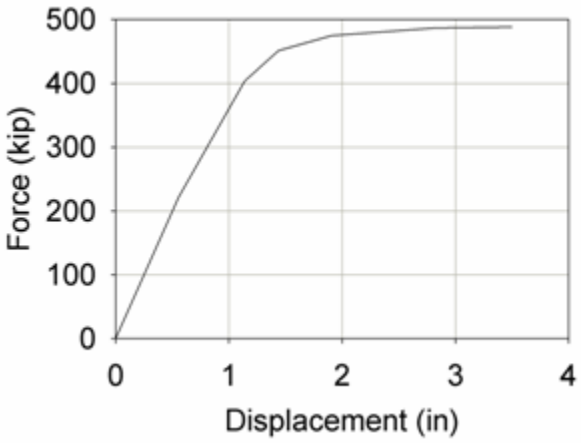

Fig A1.1(c):

Figure A.1: Analysis of testing setup with SPSW (a) strip model [Thorburn *et al.*, 1983]

(b) deformed shape (c) pushover curve

A.2 Geometry of Testing Setup

The main components of the frame are 735mm-W36x160 beams, 457mm-W14x150 columns, and specially assembled frictionless pin clevises. The bottom beam is post tensioned to the strong floor by 24 large diameter DYWIDAG bars. The columns, beams and pins are connected using F1410T super high strength bolts so that the number of the required bolts is reduced. The location of bolt holes at column ends and beam flanges are shown in Figure A.2. An end plate is welded to the left end of the top beam where two diagonal stiffeners are welded to increase strength [Figure A.3(a)]. An "actuator-load end connector" is connected to the left end of the top beam with complete penetrate welding as a primary load transfer system and with 10-M22 high strength bolts as a backup load transfer system [Figure A.3(b)]. An actuator is installed between the "actuator-load end connector" and a "strong wall-actuator connector" [Figure A.3(c)]. These connectors can be used either in single actuator option (1000kN maximum load) or double actuator option (2000kN maximum load).

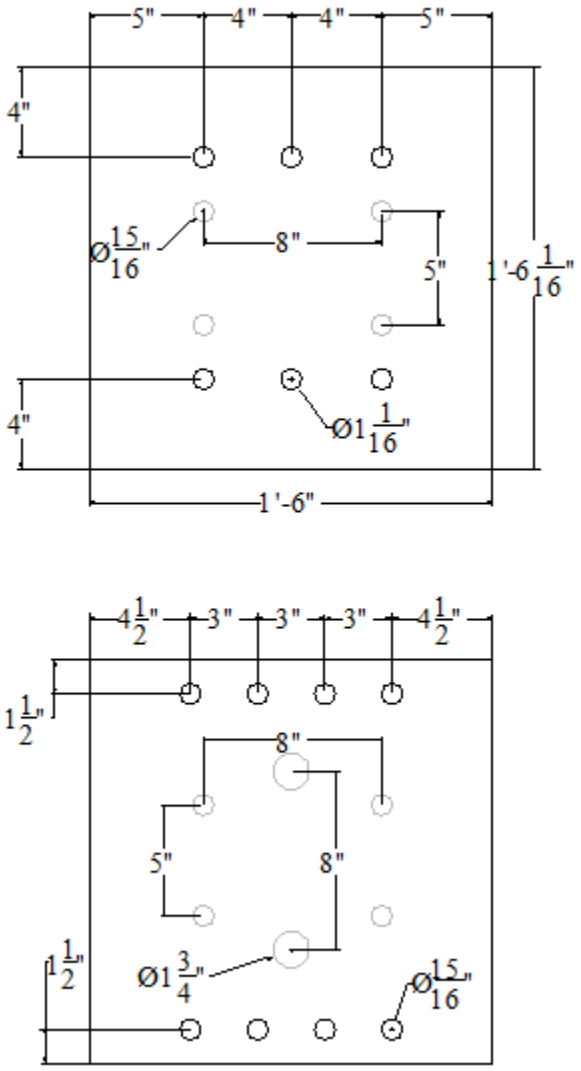
5"
4"
4"
5"
4"
Ø 15/16"
8"
5"
1'-6 1/16"
upper pin side
4"
Ø1 1/16"
1'-6"
4 1/2"
3"
3"
3"
4 1/2"
1 1/2"
8"
5"
8"
lower pin side
1 1/2"
Ø1 3/4"
Ø 15/16"

Fig A.2(a):

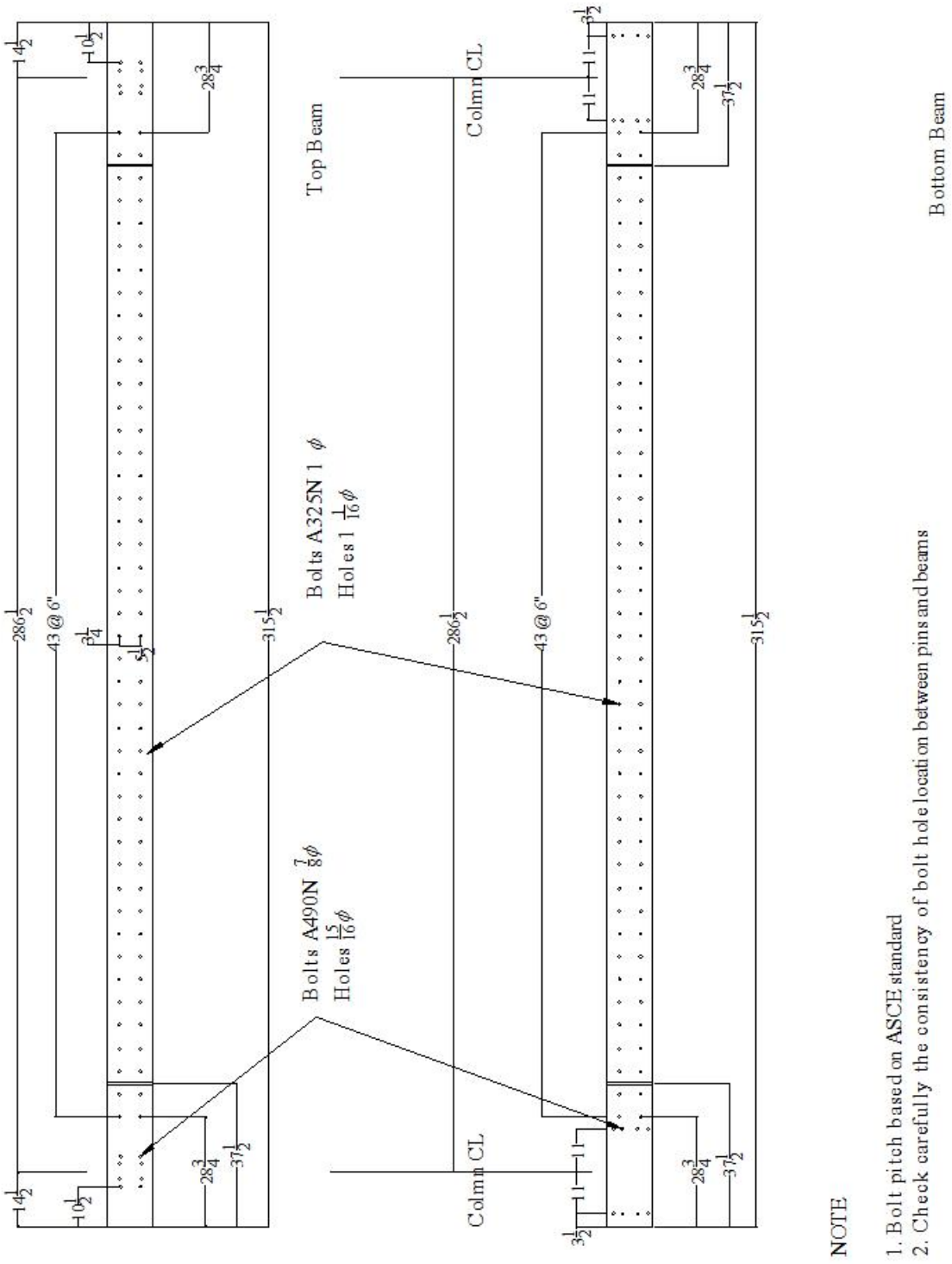

Fig A.2(b):

Figure A.2: Location of bolt holes (a) column end plates (b) beam flanges facing inner side

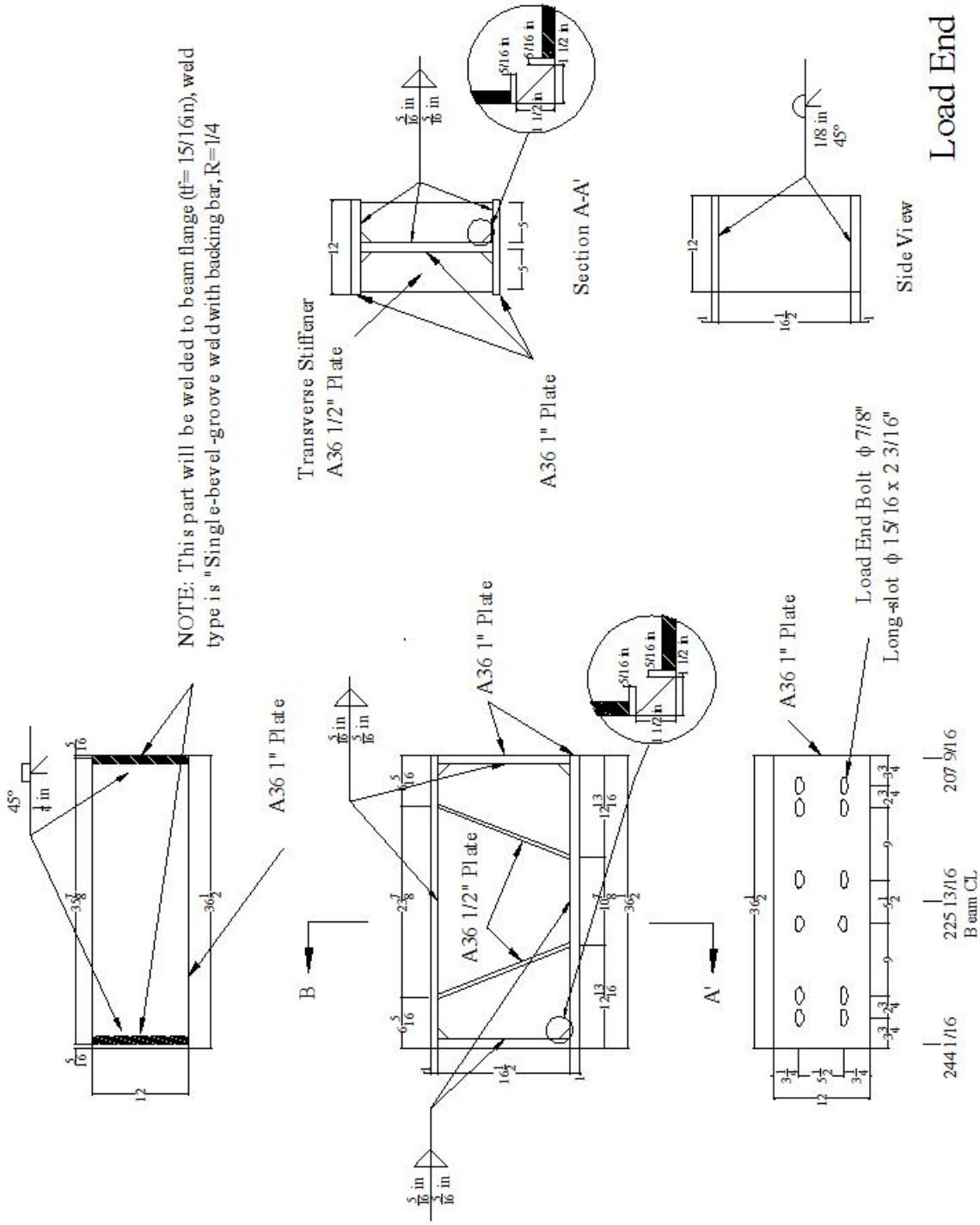
NOTE: This part will be welded to beam flange (tf= 15/16in), weld type is "Single-bevel-groove weld with backing bar, R=1/4
Transverse Stiffener
A36 1/2" Plate
A36 1" Plate
Section A-A'
Side View
Load End
A36 1" Plate
A36 1/2" Plate
A36 1" Plate
Load End Bolt ϕ 7/8"
Long-slot ϕ 15/16 x 2 3/16"
B
A'
Beam CL

Fig A.3(a):

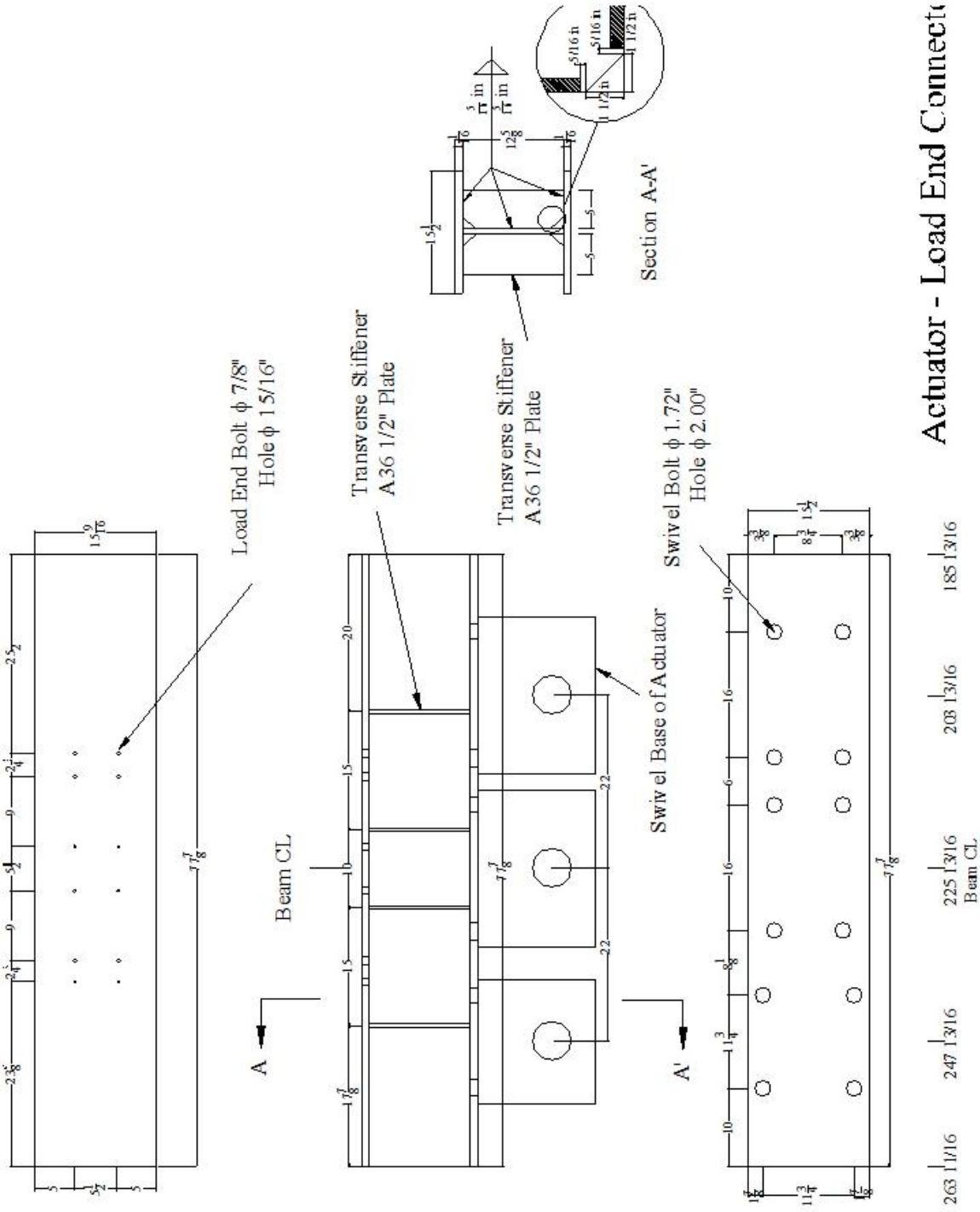
Actuator - Load End Connecti
Load End Bolt ϕ 7/8"
Hole ϕ 15/16"
Transverse Stiffener
A36 1/2" Plate
Transverse Stiffener
A36 1/2" Plate
Swivel Bolt ϕ 1.72"
Hole ϕ 2.00"
Swivel Base of Actuator
Section A-A'
Beam CL
Beam CL
A
A'
263 11/16
247 13/16
225 13/16
208 13/16
185 13/16

Fig A.3(b):

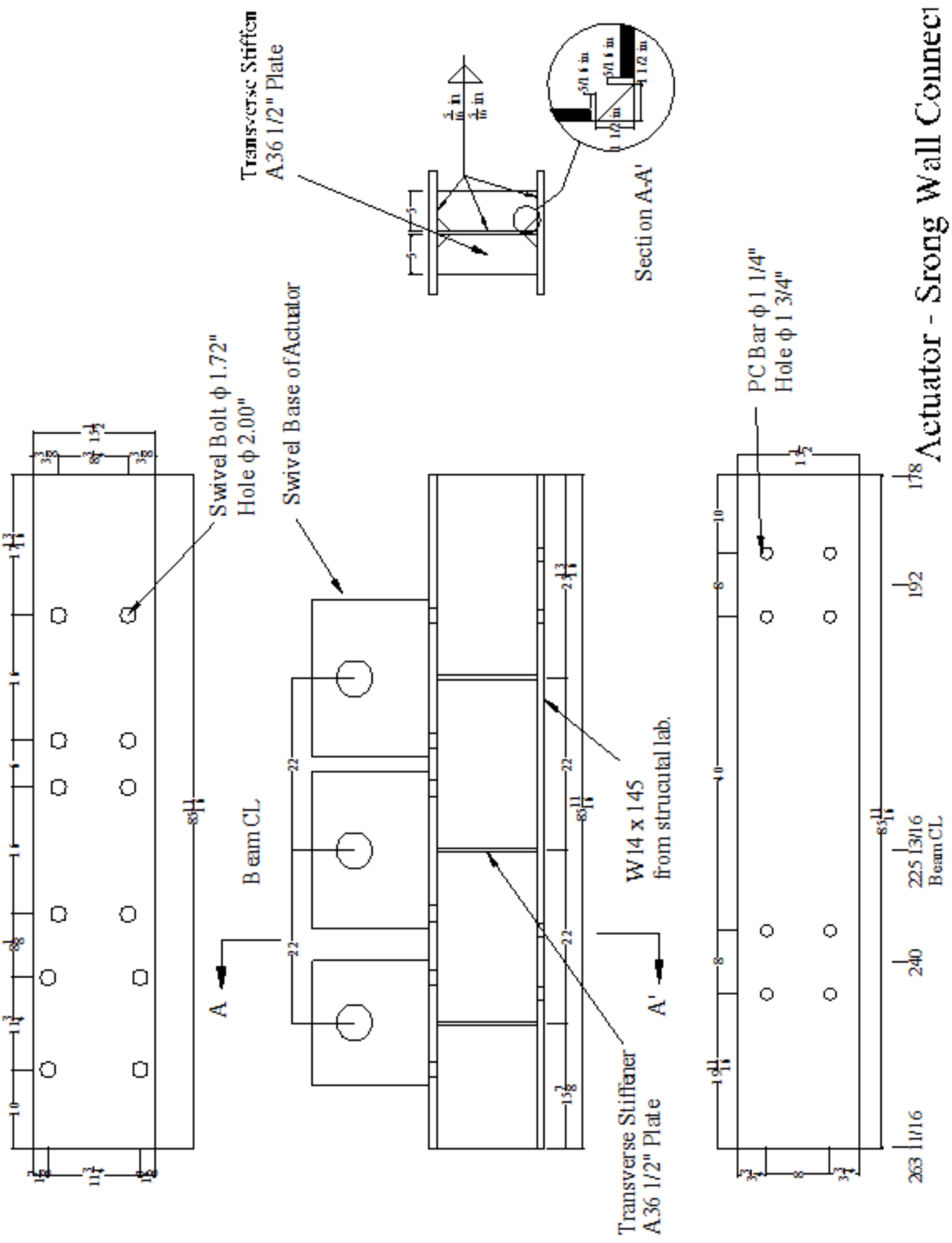

Fig A.3(c):

Figure A.3: Drawing of fixity at loading point

A.3 List of Measurements in CORE Damper Test

The location and properties of the measurements used in the tests are listed in Figure A.4-A.7 and Table A.1-A.3.

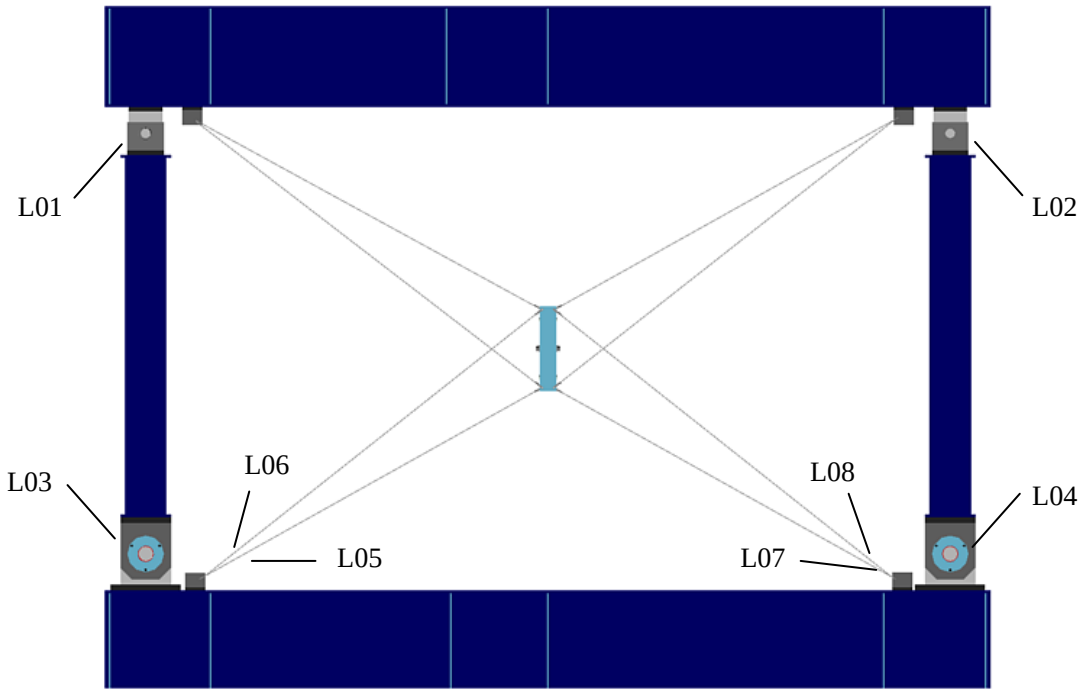

Figure A.4: Location of load measurements

Table A.1: Load measurement plan (terminal SCXI 1314)

Name	*Chan.*	*Capacity*	*Sensitivity*	*Ext*	*Output*	Location
L01	01	160kip	2mV/V	10V	8kip/mV	top left pin
L02	02	160kip	2mV/V	10V	8kip/mV	top right pin
L03	03	330kip	2mV/V	10V	16.5kip/mV	bottom left pin
L04	04	330kip	2mV/V	10V	16.5kip/mV	bottom right pin
L05	05	20kip	82.5lb/mV/V	10V	825lb/mV	left front turnbuckle
L06	06	20kip	86.6lb/mV/V	10V	866lb/mV	left back turnbuckle
L07	07	20kip	82.8lb/mV/V	10V	828lb/mV	right front turnbuckle
L08	08	20kip	83.4lb/mV/V	10V	834lb/mV	right back turnbuckle

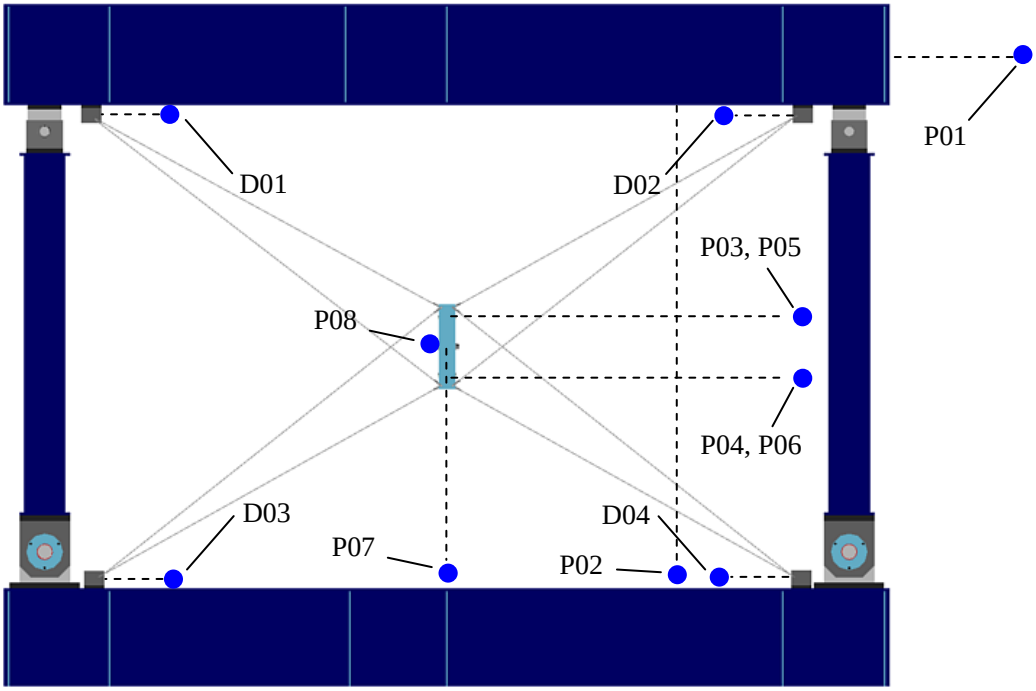

Figure A.5: Location of displacement measurements

Table A.2: Displacement measurement plan (Terminal SCXI 1303)

Name	*Chan.*	*Type*	*Cap*	*Ext*	*Output*	Location
A01	00	Monitor	220kip	10V	22kip/V	actuator
A02	01	Monitor	±10in	10V	1in/V	actuator
P01	02	PA-20	20in	10V	48.0mV/V/in	top beam
P02	03	PA-2	2in	10V	428.6mV/V/in	top beam
P03	04	PA-10	10in	10V	92.5mV/V/in	front cover plate
P04	05	PA-20	20in	10V	48.6mV/V/in	front cover plate
P05	06	PA-10	10in	10V	92.9mV/V/in	back cover plate
P06	07	PA-20	20in	10V	48.1mV/V/in	back cover plate
P07	08	PA-2	2in	10V	488.01mV/V/in	cover plate
P08	09	PT1A-50-UP	50in	10V	18.36mV/V/in	cover plate
D01	11	DCTH500	±0.5in	20V	9.815V/in	left top padeye
D02	12	DCTH500	±0.5in	20V	9.615V/in	right top padeye
D03	13	DCTH500	±0.5in	20V	9.62V/in	left bottom padeye
D04	14	DCTH500	±0.5in	20V	9.76V/in	right top padeye

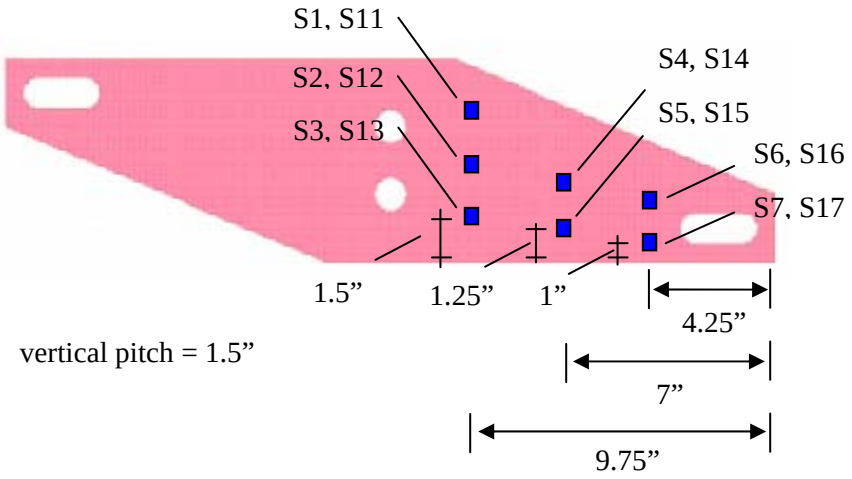

Figure A.6: Location of strain gauges (shown only gauges attached in front surface)

Table A.3: Strain measurement plan (Terminal SCXI 1317)

Name	*Chan.*	*Type*	*Resistance*	*GF*	Location
S1	00	FLA 3-11-3L	120Ω	2.1	front center top
S2	01	FLA 3-11-3L	120Ω	2.1	front center middle
S3	02	FLA 3-11-3L	120Ω	2.1	front center bottom
S4	03	FLA 3-11-3L	120Ω	2.1	front intermediate top
S5	04	FLA 3-11-3L	120Ω	2.1	front intermediate bottom
S6	05	FLA 3-11-3L	120Ω	2.1	front edge top
S7	06	FLA 3-11-3L	120Ω	2.1	front edge bottom
S11	07	FLA 3-11-3L	120Ω	2.1	back center top
S12	08	FLA 3-11-3L	120Ω	2.1	back center middle
S13	09	FLA 3-11-3L	120Ω	2.1	back center bottom
S14	10	FLA 3-11-3L	120Ω	2.1	back intermediate middle
S15	11	FLA 3-11-3L	120Ω	2.1	back intermediate bottom
S16	12	FLA 3-11-3L	120Ω	2.1	back edge top
S17	13	FLA 3-11-3L	120Ω	2.1	back edge bottom

A.4 Load Cell for Cable

Load in the cables mounted in the full scale testing setup was measured using hand-made load cells specially designed for the cables. The load cells were made from ASTM A193 Grade B7 Alloy steel 7/8”-9 threaded rods [Figure A.7]. The unknown cable force was measured by sensing the strain developed in the middle section where surface were grinded to flat. To convert the middle section into a load cell, four uniaxial strain gauges were mounted to the smoothed surface with two opposite gauges in the axial direction and two opposite gauges in the transverse direction as shown in Figure A.8 [Dally and Riley, 1991]. The strain gauge used for the load cell, FLA-2-11-1L, is a general-purpose gauge for mild steel under a room temperature condition (-20 to 80°C) [Tokyo Sokki 2008]. The gauges were bonded to the surface of rods using Cyanoacrylate adhesive, *CN-1*, and coated by Chloroprene rubber, *N-1*, (both are produced by Tokyo Sokki). The four gauges were connected to form the Wheatstone bridge as shown in Figure A.8. As long as strain remains under the proportional limit of a material, the output signal from the bridge is proportional to applied load with a theoretical equation as follows.

$$\frac{\Delta E}{V} = \frac{GF(1+\nu)}{2EA} P \qquad \text{A.1}$$

where ΔE = output signal, V = excitation voltage, GF = gauge factor, E = Young’s modulus, A = area of material, P = applied load

The relationship between load and output signal was calibrated from tensile load tests for each of the manufactured load cells.

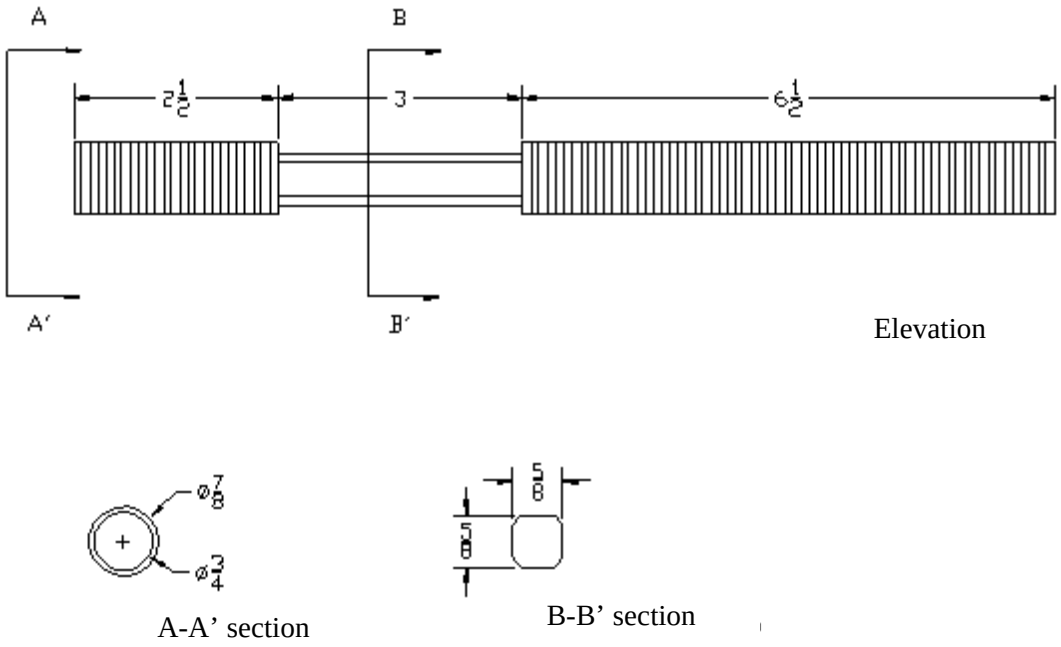

Figure A.7: Dimension of cable load cell

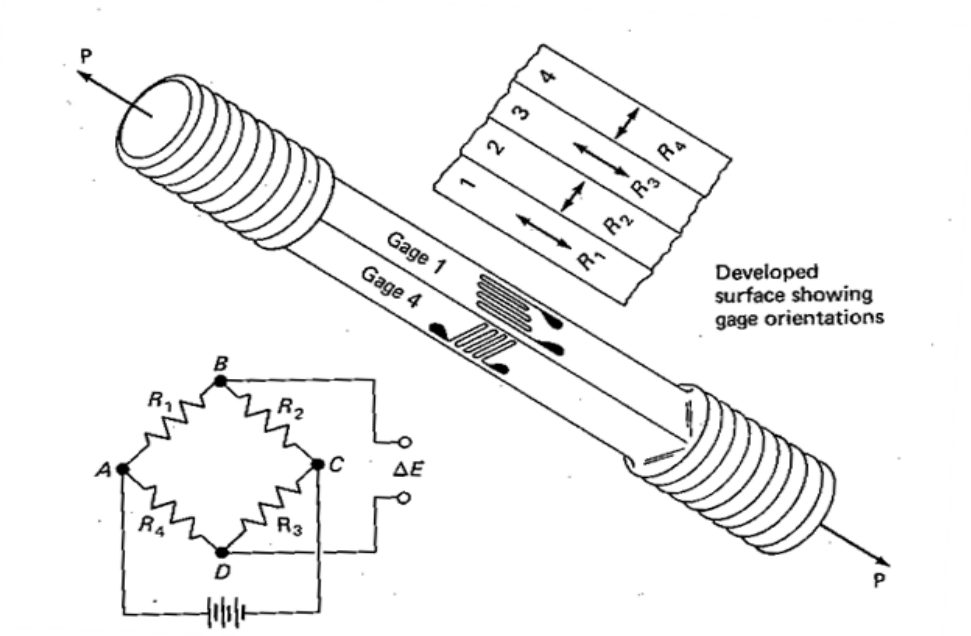

Figure A.8: Strain gauges mounted on a simple tension specimen to produce a load cell

[Dally and Riley, 1991]

APPENDIX B

TESTING SETUP AT DISASTER PREVENTION RESEARCH INSTITUTE IN KYOTO UNIVERSITY

B.1 Test schedule

Table B.1 shows the timeline of the experiments held at the DPRI in Kyoto University.

Table B.1: Timeline of experimental program

Task	Timeline										
	2008								2009		
	5	6	7	8	9	10	11	12	1	2	3
1st planer meeting	x										
2nd planer meeting			x								
3rd planer meeting							x				
Test setup design			←	→							
Test setup fabrication					←	→	→	→	→	→	
Preliminary welding test							←	→			
Specimen design							←	→	→		
Specimen fabrication									←	→	
Testing											x

B.2 Dimension of Components in Test Setup

The dimensions of main components in the test setup constructed in the DPRI are shown in Figure B.1.

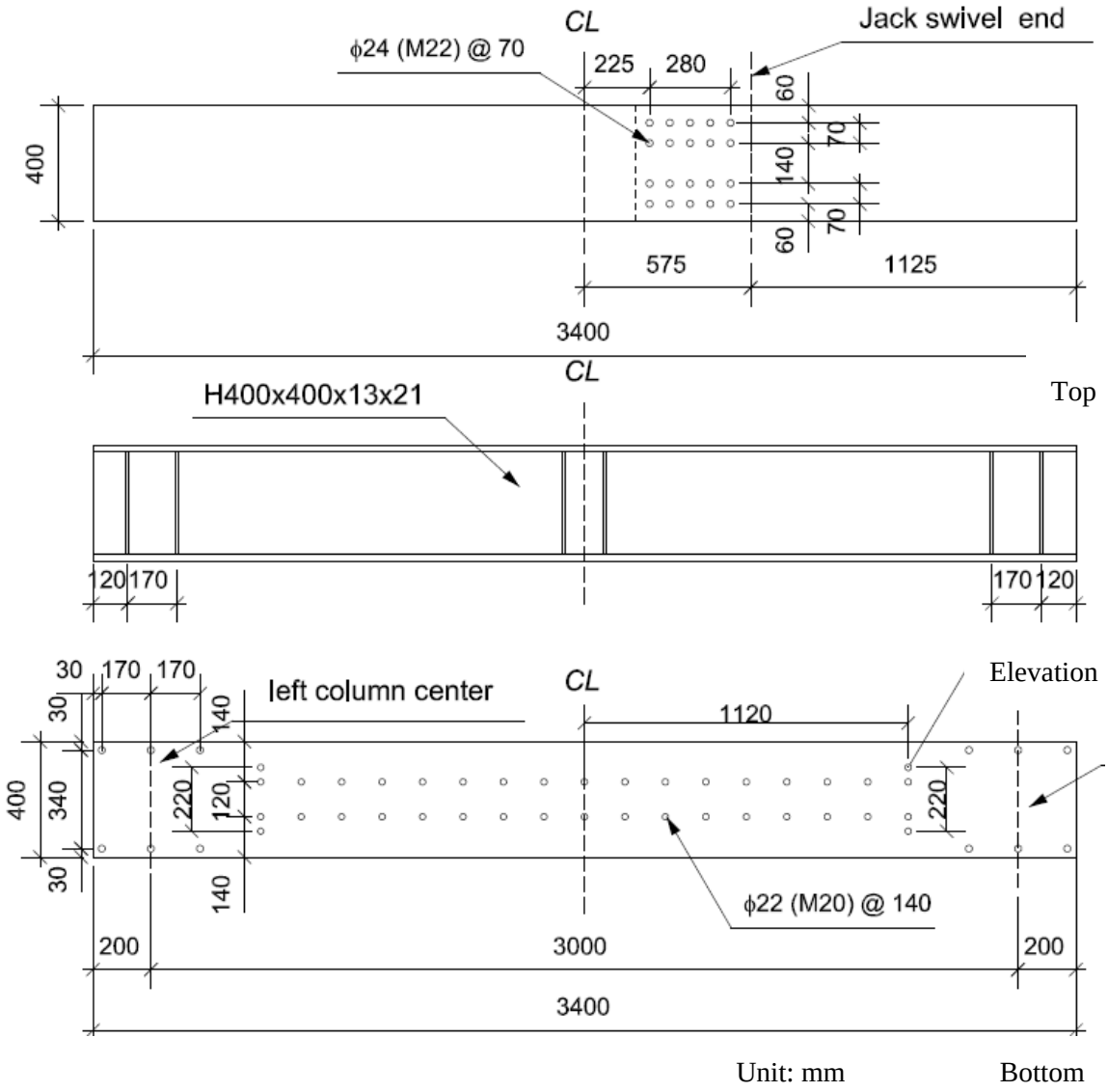

Fig B.1(a):

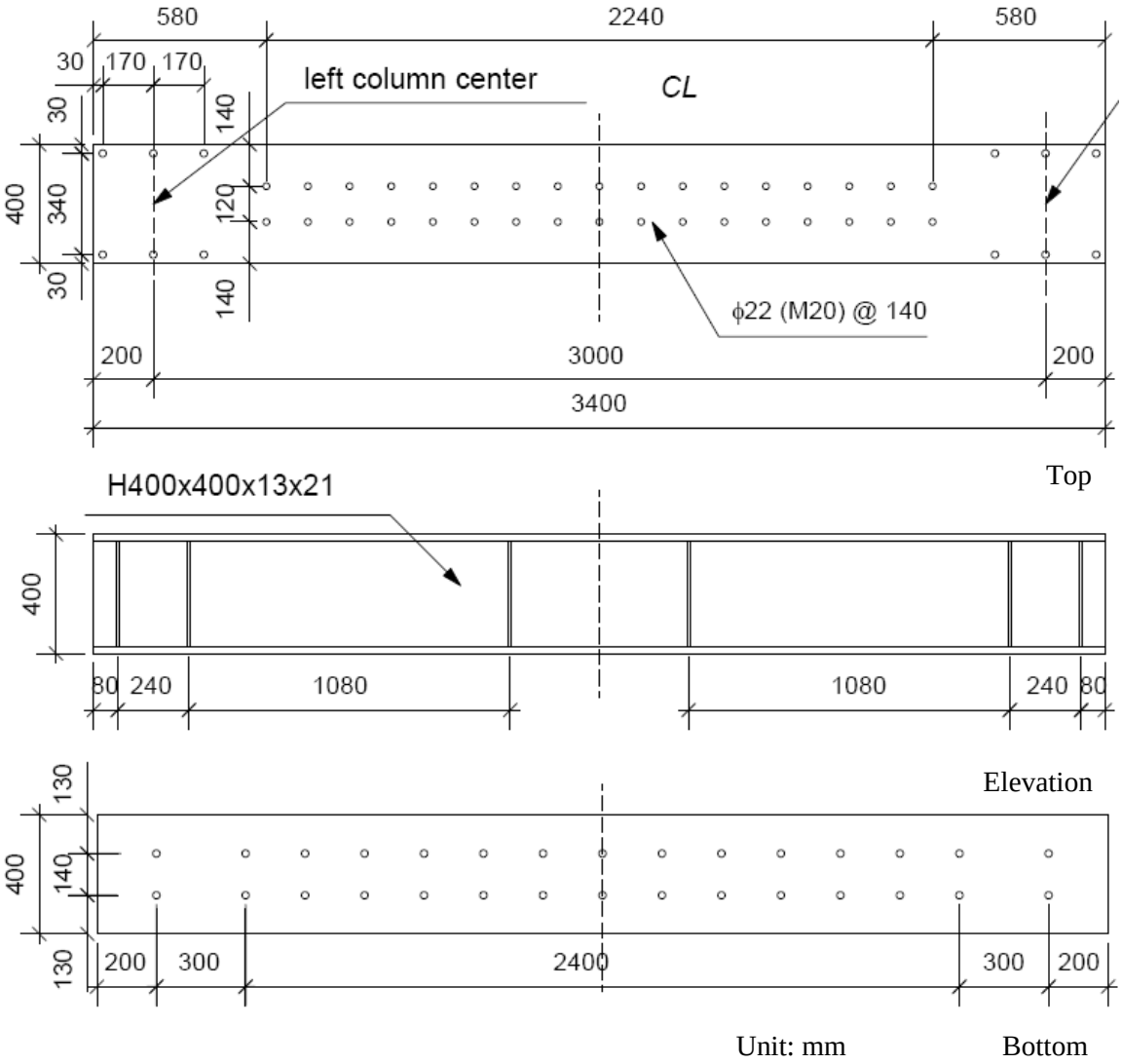
580
2240
580
30
170
170
left column center
CL
30
140
400
340
120
30
140
ϕ22 (M20) @ 140
200
3000
200
3400
Top
H400x400x13x21
400
80
240
1080
1080
240
80
Elevation
130
400
140
130
200
300
2400
300
200
Unit: mm
Bottom

Fig B.1(b):

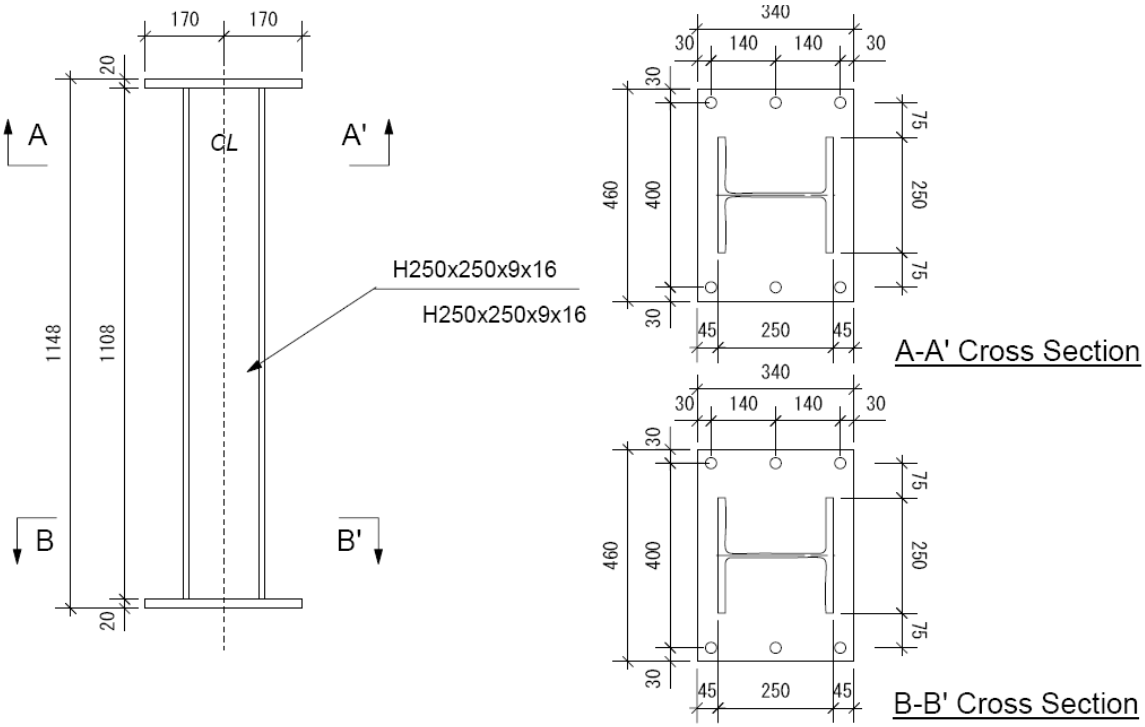

Unit: mm

Fig B.1 (c):

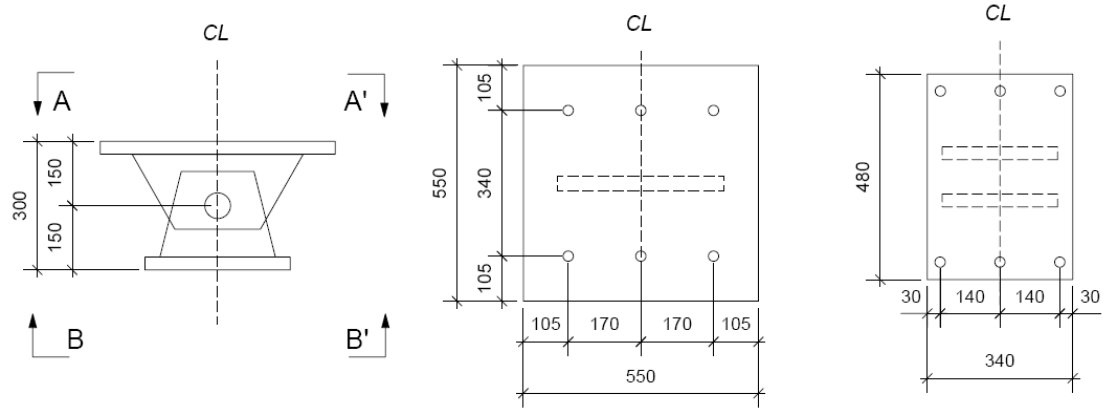

Unit: mm

Fig B.1 (d):

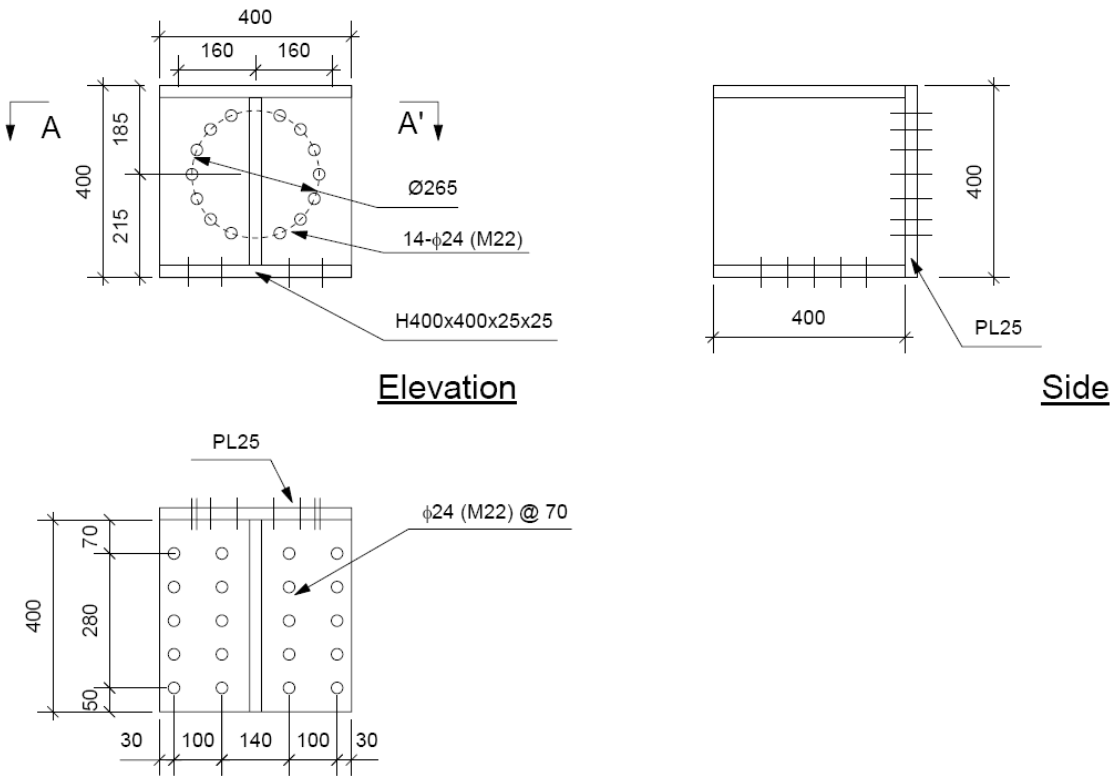

Unit: mm

Fig B.1 (e):

Figure B.1: Components of test setup (a) top beam (b) bottom beam (c) column (d) pin-clevis set (e) fixity to actuator

B.3 Dimension of Components in Specimen

The detailed geometries of the all components in the NSPSW-TB system are shown in Figure B.2.

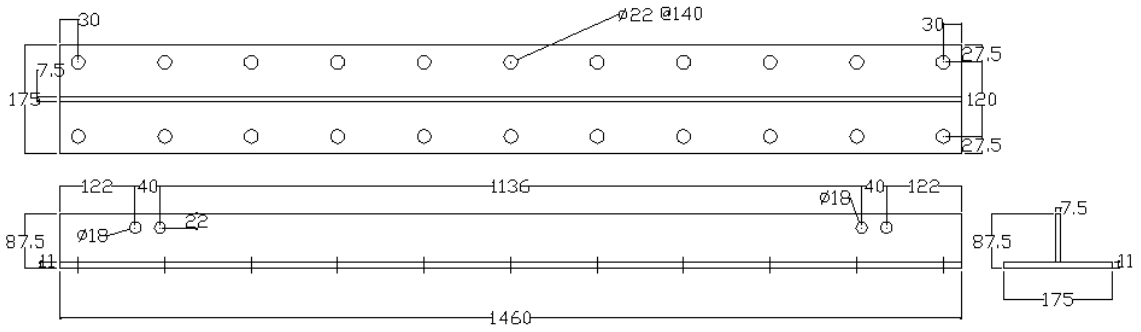

Fig B.2(a):

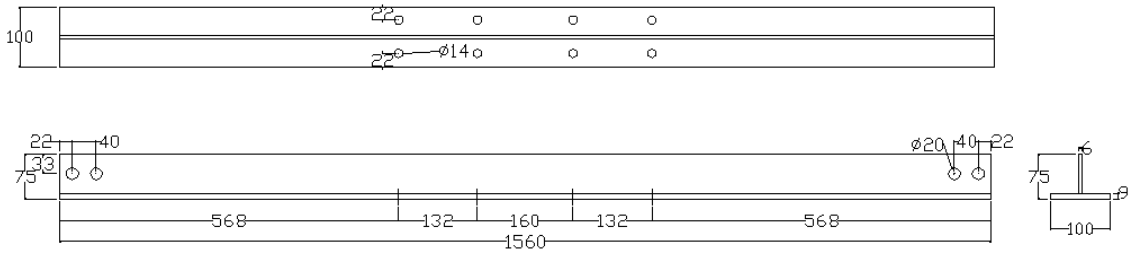

VBE for S1

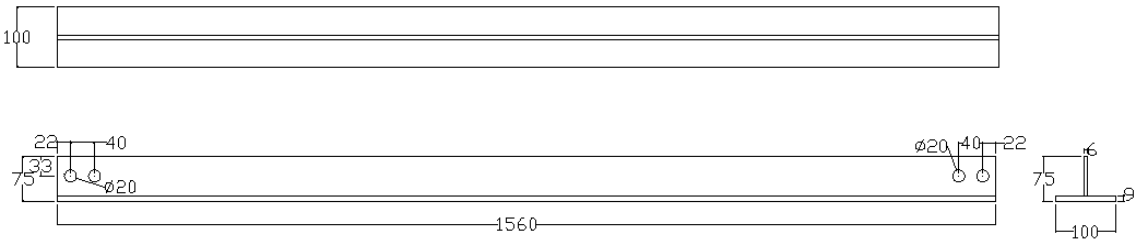

VBE for S2

Fig B.2(b)

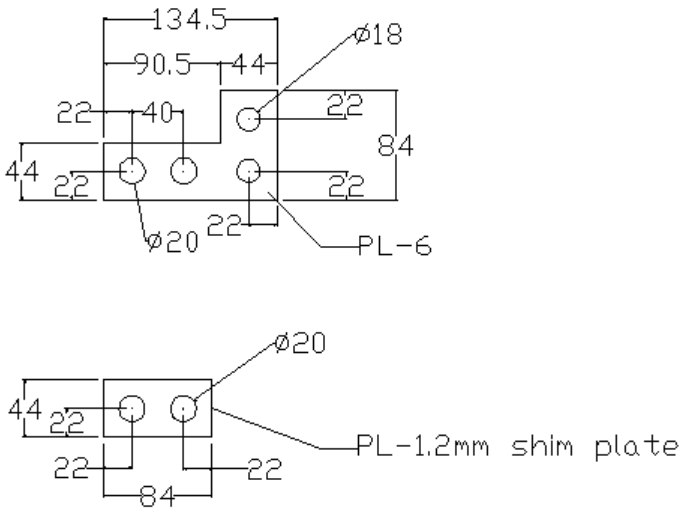

Fig B.2(c):

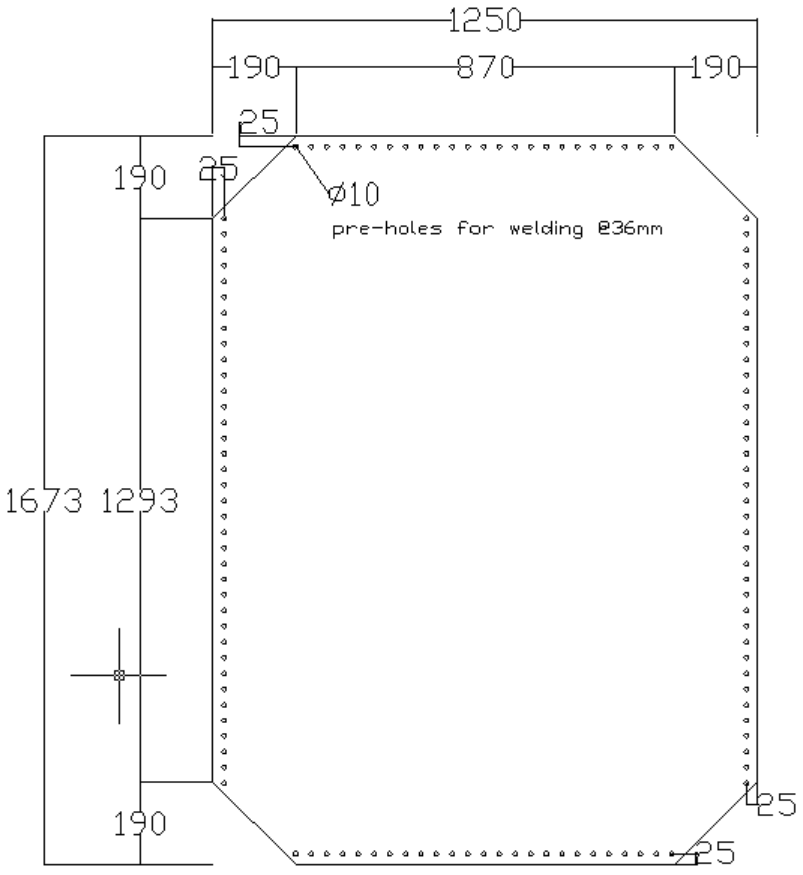

Fig B.2(d):

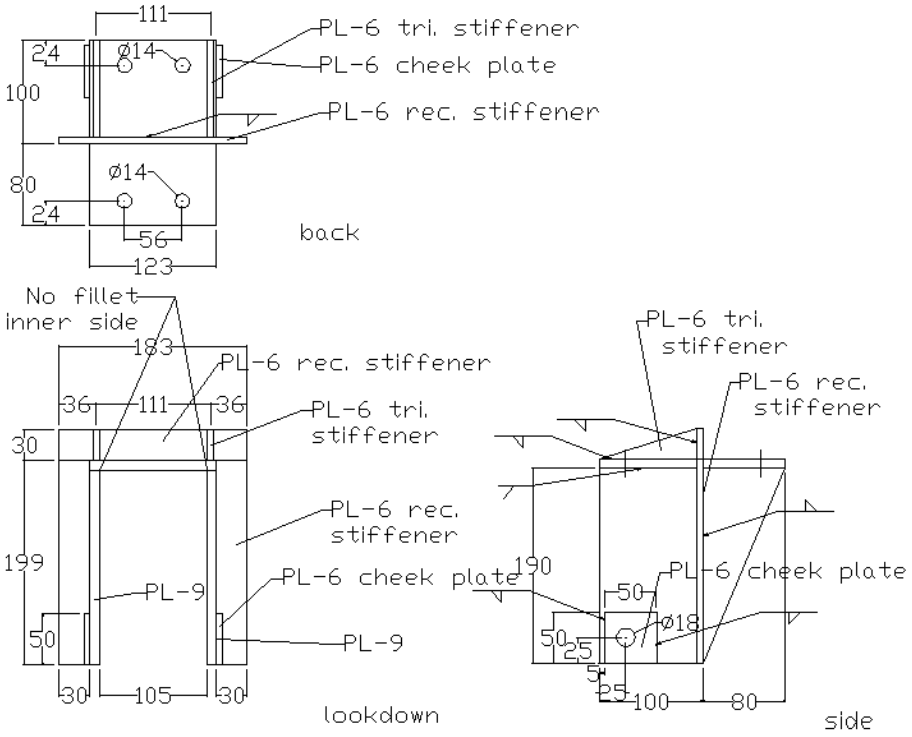

Fig B.2(e):

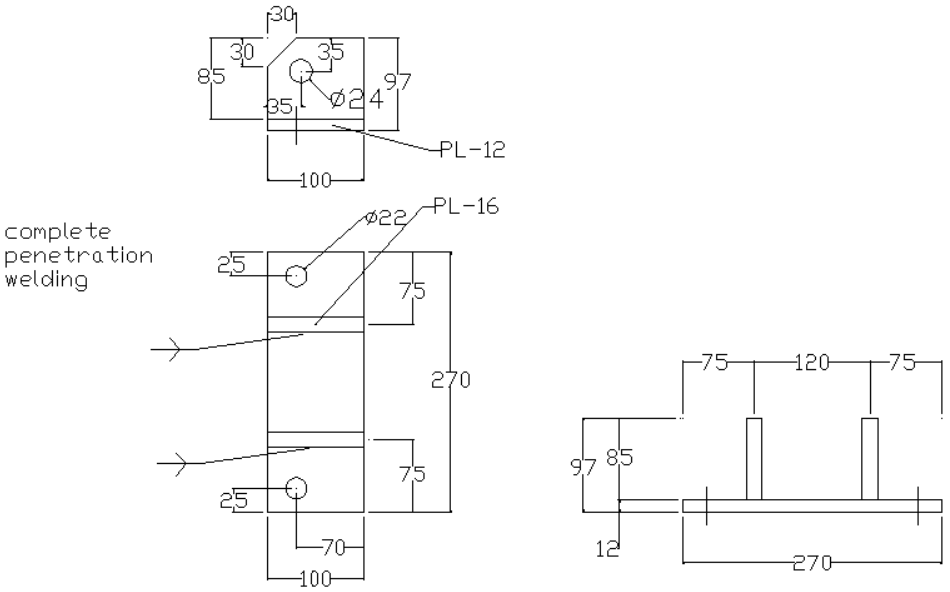

Fig B.2(f):

Figure B.2: Components of specimen (a) horizontal boundary element (HBE) (b) vertical boundary element (VEB) (c) L-shape plate for pin connection at corners of boundary elements (d) infill wall (e) bracket for tension only bracing in S2 (f) padeye in S2

B.4 Out-of-plane Restraining System

The out-of-plane restraining system designed for the test setup constructed at DPRI is presented in Figure B.3(a). The rollers installed between the test setup and the existing load resisting frame is shown in Figure B.3(b).

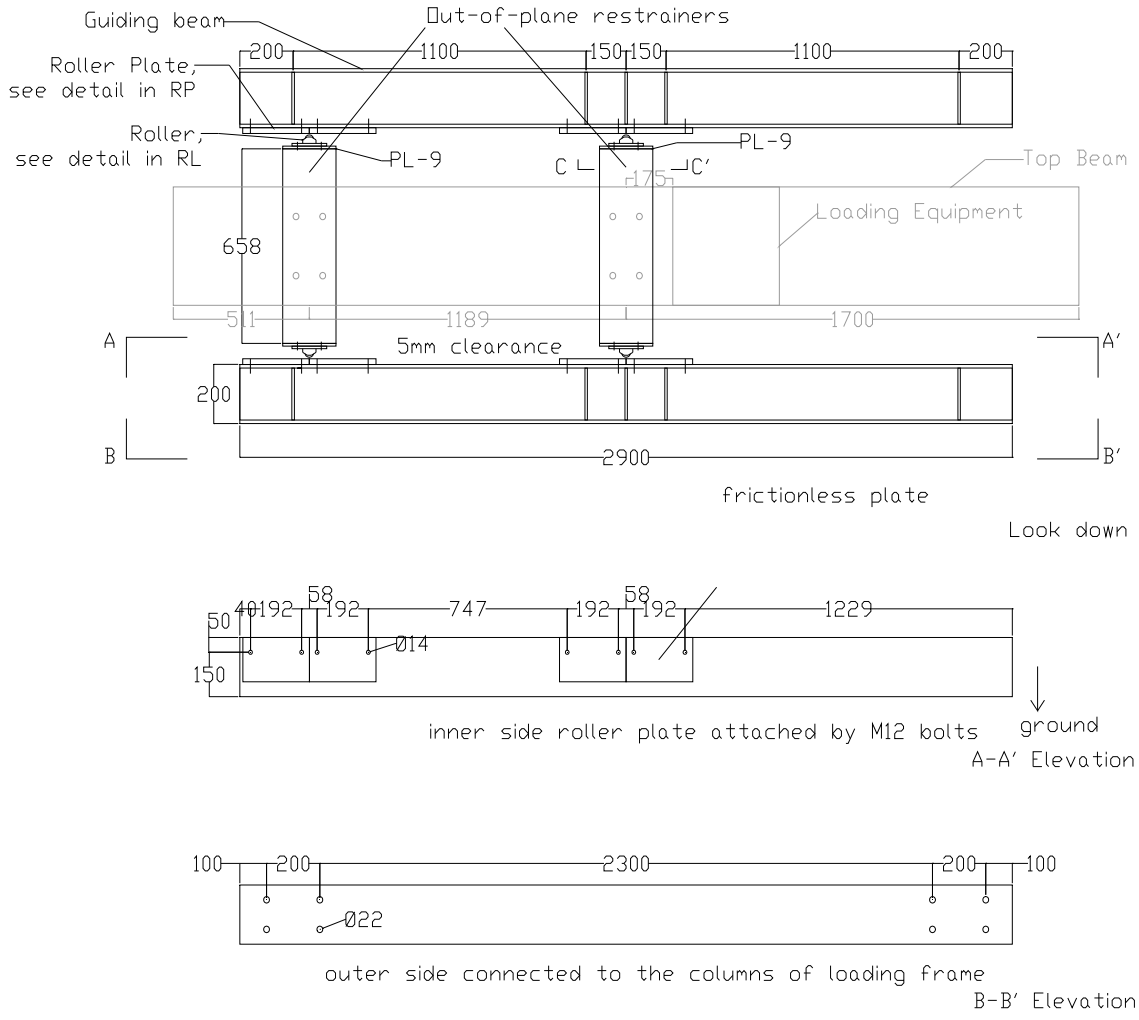

Fig B.3(a):

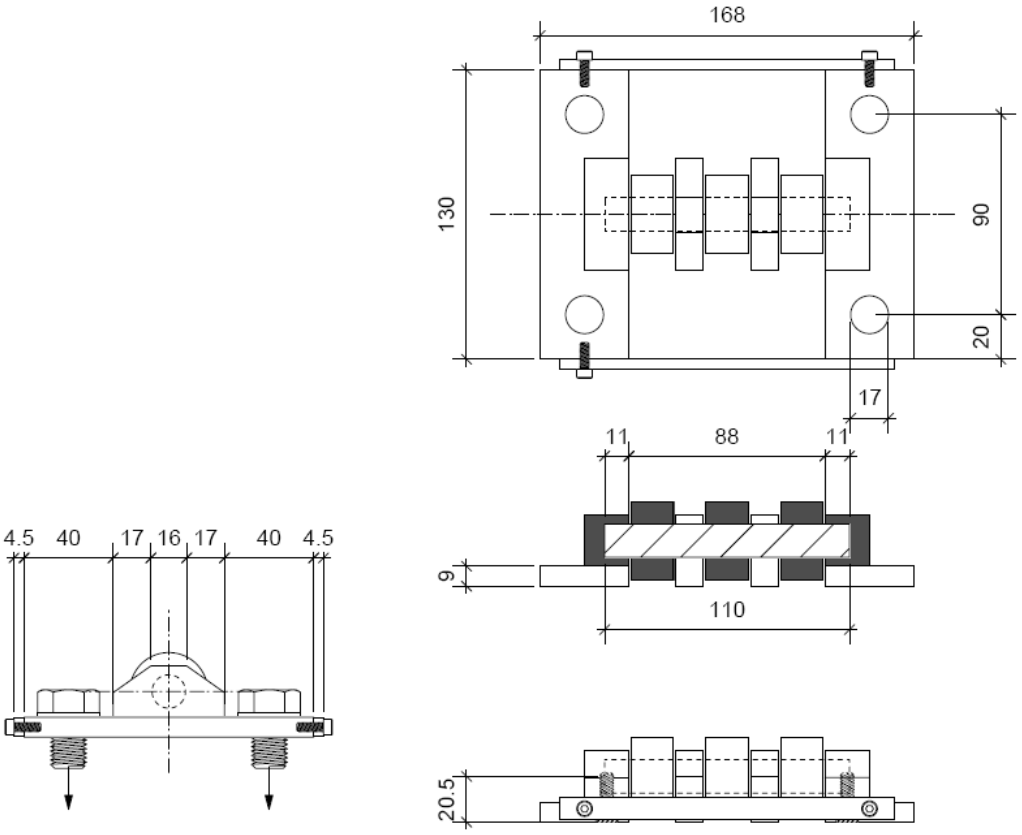

Fig B.3(b):

Figure B.3: Out-of-plane restraining system (a) restrainers and guiding beam (b) roller

B.5 Measurement Channel List

The list of measurement channel used in the tests is shown in Tables B.3 and B.4.

Table B.3: Channel List for Specimen 1

CH	Location	*Type*	Name	*Resolution m/mm*	*Stroke mm*
000	Jack Disp	LVDT			
001	Jack Load	Load Cell			
002	Top Beam H	Potentiometer	DP-500C	10	500
003	LT Ccon H	Potentiometer	SDP-100CT	50	100
004	LB Ccon H	Potentiometer	SDP-100CT	50	100
005	R Ccon H 1	Potentiometer	SDP-100CT	50	100
006	R Ccon H 2	Potentiometer	SDP-100CT	50	100
007	R Ccon H 3	Potentiometer	SDP-100CT	50	100
008	R Ccon H 4	Potentiometer	SDP-50CT	100	50
009	L VBE OOP	Potentiometer	SDP-100CT	50	100
010	R VBE OOP	Potentiometer	SDP-100CT	50	100
011	Top Beam V	Potentiometer	SDP-100CT	50	100
012	Panel LT-RB	Potentiometer	SDP-200R	100	200
013	Panel RT-LB	Potentiometer	SDP-200R	100	200
014	Top HBE H	LVDT	CDP-100	100	100
015	Bottom HBE H	LVDT	CDP-100	100	100
016	Bottom Beam H	LVDT	CDP-100	100	100
017					
018					
019					
020					
021					
022					
023					
024					
025				GF	
026	Wall Middle 1	Rossete Gauge	FRA-5-11-5L	2.1	
027			FRA-5-11-5L	2.1	
028			FRA-5-11-5L	2.1	
029	Wall Middle 2	Rossete Gauge	FRA-5-11-5L	2.1	
030			FRA-5-11-5L	2.1	
031			FRA-5-11-5L	2.1	
032	Wall Middle 3	Rossete Gauge	FRA-5-11-5L	2.1	
033			FRA-5-11-5L	2.1	
034			FRA-5-11-5L	2.1	
035	Wall Middle 4	Rossete Gauge	FRA-5-11-5L	2.1	
036			FRA-5-11-5L	2.1	
037			FRA-5-11-5L	2.1	
038	VBE 1	Uniaxial Gauge	FLA-5-11-5L	2.1	
039	VBE 2	Uniaxial Gauge	FLA-5-11-5L	2.1	
040	VBE 3	Uniaxial Gauge	FLA-5-11-5L	2.1	
041	VBE 4	Uniaxial Gauge	FLA-5-11-5L	2.1	
042	VBE 5	Uniaxial Gauge	FLA-5-11-5L	2.1	
043	VBE 6	Uniaxial Gauge	FLA-5-11-5L	2.1	
044	VBE 7	Uniaxial Gauge	FLA-5-11-5L	2.1	
045	VBE 8	Uniaxial Gauge	FLA-5-11-5L	2.1	
046	VBE 9	Uniaxial Gauge	FLA-5-11-5L	2.1	
047	VBE 10	Uniaxial Gauge	FLA-5-11-5L	2.1	
048	VBE 11	Uniaxial Gauge	FLA-5-11-5L	2.1	
049	VBE 12	Uniaxial Gauge	FLA-5-11-5L	2.1	
050	VBE 13	Uniaxial Gauge	FLA-5-11-5L	2.1	
051	VBE 14	Uniaxial Gauge	FLA-5-11-5L	2.1	
052	VBE 15	Uniaxial Gauge	FLA-5-11-5L	2.1	
053	VBE 16	Uniaxial Gauge	FLA-5-11-5L	2.1	

Table B.4: Channel List for Specimen 2

CH	Location	*Type*	Name	*Resolution m/mm*	*Stroke mm*
000	Jack Disp	LVDT			
001	Jack Load	Load Cell			
002	Top Beam H	Potentiometer	DP-500C	10	500
003	LT Ccon H	Potentiometer	SDP-100CT	50	100
004	LB Ccon H	Potentiometer	SDP-100CT	50	100
005	R Ccon H 1	Potentiometer	SDP-100CT	50	100
006	R Ccon H 2	Potentiometer	SDP-100CT	50	100
007	R Ccon H 3	Potentiometer	SDP-100CT	50	100
008	R Ccon H 4	Potentiometer	SDP-100CT	50	100
009	L VBE OOP	Potentiometer	SDP-100CT	50	100
010	R VBE OOP	Potentiometer	SDP-100CT	50	100
011	Top Beam V	Potentiometer	SDP-50CT	100	50
012	Panel LT-RB	Potentiometer	SDP-200R	100	200
013	Panel RT-LB	Potentiometer	SDP-200R	100	200
014	Top HBE H	LVDT	CDP-100	100	100
015	Bottom HBE H	LVDT	CDP-100	100	100
016	Bottom Beam H	LVDT	CDP-100	100	100
017	LT PadEye	LVDT	CDP-50	200	50
018	RT PadEye	LVDT	CDP-50	200	50
019	LB PadEYE	LVDT	CDP-50	200	50
020	RB PadEye	LVDT	CDP-50	200	50
021					
022					
023					
024					
025					
026	Wall Middle 1	Rossete Gauge	FRA-5-11-5L	2.1	
027			FRA-5-11-5L	2.1	
028			FRA-5-11-5L	2.1	
029	Wall Middle 2	Rossete Gauge	FRA-5-11-5L	2.1	
030			FRA-5-11-5L	2.1	
031			FRA-5-11-5L	2.1	
032	Wall Middle 3	Rossete Gauge	FRA-5-11-5L	2.1	
033			FRA-5-11-5L	2.1	
034			FRA-5-11-5L	2.1	
035	Wall Middle 4	Rossete Gauge	FRA-5-11-5L	2.1	
036			FRA-5-11-5L	2.1	
037			FRA-5-11-5L	2.1	
038	VBE 1	Uniaxial Gauge	FLA-5-11-5L	2.1	
039	VBE 2	Uniaxial Gauge	FLA-5-11-5L	2.1	
040	VBE 3	Uniaxial Gauge	FLA-5-11-5L	2.1	
041	VBE 4	Uniaxial Gauge	FLA-5-11-5L	2.1	
042	VBE 5	Uniaxial Gauge	FLA-5-11-5L	2.1	
043	VBE 6	Uniaxial Gauge	FLA-5-11-5L	2.1	
044	VBE 7	Uniaxial Gauge	FLA-5-11-5L	2.1	
045	VBE 8	Uniaxial Gauge	FLA-5-11-5L	2.1	
046	VBE 9	Uniaxial Gauge	FLA-5-11-5L	2.1	
047	VBE 10	Uniaxial Gauge	FLA-5-11-5L	2.1	
048	VBE 11	Uniaxial Gauge	FLA-5-11-5L	2.1	
049	VBE 12	Uniaxial Gauge	FLA-5-11-5L	2.1	
050	VBE 13	Uniaxial Gauge	FLA-5-11-5L	2.1	
051	VBE 14	Uniaxial Gauge	FLA-5-11-5L	2.1	
060	Turnbuckle 1a	Uniaxial Gauge	FLA-5-11-5L	2.1	
061	Turnbuckle 1b	Uniaxial Gauge	FLA-5-11-5L	2.1	
062	Turnbuckle 2a	Uniaxial Gauge	FLA-5-11-5L	2.1	
063	Turnbuckle 2b	Uniaxial Gauge	FLA-5-11-5L	2.1	
064	Turnbuckle 3a	Uniaxial Gauge	FLA-5-11-5L	2.1	
065	Turnbuckle 3b	Uniaxial Gauge	FLA-5-11-5L	2.1	
066	Turnbuckle 4a	Uniaxial Gauge	FLA-5-11-5L	2.1	
067	Turnbuckle 4b	Uniaxial Gauge	FLA-5-11-5L	2.1	

REFERENCES

AIJ. "*Reconnaissance Report on Damage to Steel Building Structures Observed from the 1995 Hyogoken-Nanbu Earthquake*," Kinki Branch of the Architectural Institute of Japan, Osaka (in Japanese with attached abridged English version), 1995.

AISC. "*Design Guide 15: AISC Rehabilitation and Retrofit Guide-A Reference for Historic Shapes and Specifications*," AISC Manual – 6th Edition, AISC, 1963.

AISC. "Modification of Existing Welded Steel Moment Frames for Seismic Resistance," *AISC Design Guide* 12, American Institute of Steel Construction, Inc., Chicago, 1999.

AISC. "*Seismic Provisions for Structural Steel Buildings*," Chicago, Illinois, American Institute of Steel Construction, INC, 2007.

Anagnostides, G., Hargreaves, A. C., and Wyatt, T. A. "Development and applications of energy absorption devices based on friction," *Journal of Construction Steel Research* 13(4): 317-336, 1989.

Annan, K. N. "*We, the Peoples: the Role of the United Nations in the 21st Century*," United Nations, New York, 2000.

ASCE. "2009 Report Card for America's Infrastructure," Reston, VA, Structuring Engineering Institute, American Society of Civil Engineers, 2009.

ASCE-41. "*Seismic rehabilitation of existing buildings*," Reston, VA, Structuring Engineering Institute, American Society of Civil Engineers, 2006.

ASCE-7. "*Minimum Design Loads for Buildings and Other Structures*," Reston, VA, Structuring Engineering Institute, American Society of Civil Engineers, 2005.

Astaneh-Asl, A. "Seismic Behavior of Steel Plate Shear Walls," *Steel Tips Report*, Structural Steel Education Council, Moraga, California, 2001.

ASTM. "*F1145-92: Standard Specification for Turnbuckles, Swaged, Welded, Forged*," ASTM, West Conshohocken, PA, 1996.

ATC-24. "*Guidelines of Cyclic Seismic Testing on Components for Steel Structures*," Redwood City, California: Applied Technology Council, 1992.

BCJ. "*The Building Standard Law of Japan*," the Building Center of Japan, Tokyo, 2009.

Behbahanifard, M., Grondin. G. Y., *et al*. "Experimental and Numerical Investigation of Steel Plate Shear Walls," *Structural Engineering Report* No. 254, Department of Civil Engineering, University of Alberta, Edmonton, Alberta, Canada, 2003.

Berman, J. W. and Bruneau, M. "Experimental Investigation of Light-Gauge Steel Plate Shear Walls for Seismic Retrofit of Buildings," *Technical Report MCEER-03-0001*, Multidisciplinary Center for Earthquake Engineering Research, Buffalo, New York, 2003a.

Berman, J. W. and Bruneau, M. "Experimental Investigation of Light-Gauge Steel Plate Shear Walls," *Journal of Structural Engineering* 131(2): 259-267, 2005.

Berman, J. W. and Bruneau, M. "Plastic Analysis and Design of Steel Plate Shear Walls," *Journal of Structural Engineering* 129(11): 1148-1156, 2003b.

Bertero, V. V., Anderson, J. C., Krawinkler, H. "Performance of Steel Building Structures During the Northridge Earthquake," *Report No. UCB/EERC-94-09*, University of California at Berkley. The Earthquake Engineering Research Center, 1994.

BIJ. "*Steel Deck 2004*," published by the Building Center of Japan (BCJ), edited by Japan Iron and Steel Federation (JISF), 2004.

Black, C. J., Makris, N., and Aiken, I. "Component Testing, Seismic Evaluation and Characterization of Buckling-Restrained Braces," *Journal of Structural Engineering* 130 (6): 880-894, 2004.

Bruneau, M., *et al*. "A framework to quantitatively assess and enhance the seismic resilience of communities," *Earthquake Spectra* 19(4): 733-752, 2003.

Bruneau, M., Reinhorn, A. "Overview of the Resilience Concept," Proceedings of the 8th U.S. National Conference on Earthquake Engineering, Paper NO. 2040, San Francisco, California, USA, 2006.

Chang, C., Pall, A., and Louie, J. "The Use of Friction Dampers for Seismic Retrofit of the Monterey County Government Center," *Proceeding of 8th U. S. National Conference on Earthquake Engineering*, EERI, Oakland, California, Paper No. 951, 2006.

Christopoulos, C., Tremblay, R., et al. "Self-Centering Energy Dissipative Bracing System for the Seismic Resistance of Structures: Development and Validation," *Journal of Structural Engineering* 134(1): 96-107, 2008.

Constantinou, M. C., and Symans, M. D. "Seismic Response of Structures with Supplemental Damping," Structural Design of Tall Building 2(2):77–92, 1993.

Constantinou, M. C., Soong, T. T., and Dargush, G. F. "Passive Energy Dissipation Systems for Structural Design and Retrofit," MCEER Monograph Series, No. 1, Multidisciplinary Center for Earthquake Engineering Research, Buffalo, N.Y., 1998.

Costello, A., G. "*Theory of Wire Rope*," Springer-Verlag, 1990.

CSA. "*S16-01-CAN/CSA: Limit States Design of Steel Structures-Sixth Edition*," National Standard of Canada, 2006.

Dassault Systems. "*ABAQUS version 6.8 Documentation*," Dassault Systems, Velizy-Villacoublay, France, 2008.

Davidson C., I., *et al*. "Adding Sustainability to the Engineer's Toolbox: A Challenge for Engineering Educators", *Environmental Science & Technology* 41 (14), pp 4847–4849, 2007.

DesRoches, R. "Next Generation Sustainable Urban Infrastructure Systems," *Presentation to GT Alumni Club*, Austin, TX, April 21, 2009.

DesRoches, R., McCormick, J., *et al*. "Cyclic Properties of Superelastic Shape Memory Alloy Wires and Bars," *Journal of Structural Engineering* 130(1): 38-46, 2004.

Disque, R. O. "*Applied Plastic Design in Steel*," Van Nostrand Reinhold Company, New York, 1971.

Driver R. G., Kulak, G. L., Elwi, A. E., Kennedy, D. J. L. "FE and Simplified Model of Plate Shear Wall," *Journal of Structural Engineering* 124(2): 121-130, 1998a.

Driver R. G., Kulak, G. L., Kennedy, D. J. L., Elwi, A. E. "Cyclic Test of Four-Story Steel Plate Shear Wall," *Journal of Structural Engineering* 124(2): 112-120, 1998b.

Elgaaly, M. "Thin Steel Walls Behavior and Analysis," *Thin Walled Structures* 32:151-180, 1998.

Elgaaly, M., Caccese, V., Du, C. "Post Buckling Behavior of Steel-Plate Shear Walls under Cyclic Loads," *Journal of Structural Engineering* 119(2): 588-605, 1993.

Elgaaly, M., Liu, Y. "Analysis of Thin Plate Shear Walls," *Journal of Structural Engineering* 123(11): 1487-1496, 1997.

FED. "*Federal Specification RR-W-410E: Wire Rope and Strand*," Defense Supply Center Richmond, Richmond, VA, 2002.

FEMA. "FEMA 156: Second Edition Typical Costs for Seismic Rehabilitation of Existing Building," *Earthquake Hazards Reduction Series* 39, Federal Emergency Management Agency, 1999.

FEMA. "*Interim Guideline: Evaluation, Repair, Modification and Design of Welded Steel Moment Frame Structures (August 1995),*" plus Interim Guidelines Advisory No.1, Federal Emergency Management Agency, Washington, DC, 1997.

FEMA-351. "*Recommended Seismic Evaluation and Upgrade Criteria for Existing Welded Steel Moment-Frame Buildings*," prepared by SAC Joint Venture for Federal Emergency Management Agency, Washington, DC, 2000.

FEMA-395. "*Incremental Seismic Rehabilitation of School Buildings (K-12).*" prepared for the Federal Emergency Management Agency, Washington, DC, 2002.

FEMA-396. "*Incremental Seismic Rehabilitation of Hospital Buildings*," prepared for the Federal Emergency Management Agency, Washington, DC, 2003.

Fierro, E. A., and Perry, C. L. “San Francisco Retrofit Design Using Added Damping and Stiffness ADAS Elements,” *Proc., ATC-17–1 Seminar on Seismic Isolation, Passive Energy Dissipation, and Active Control*, Vol. 2, ATC, Redwood City, California: 593–603, 1993.

Filiatrault, A., Cherry, S. “Comparative Performance of Friction-Damped Systems and Base Isolation Systems for Earthquake Retrofit and Aseismic Design,” *Earthquake Engineering and structural dynamics* 16(3): 389-416, 1988.

Filiatrault, A., Cherry, S. “Performance Evaluation of Friction Damped Braced Steel Frames under Simulated Earthquake Loads,” *Earthquake Spectra* 3(1), 57-78, 1987.

Filiatrault, A., Tremblay, R. “Design of Tension-Only Concentrically Braced Steel Frames for Seismic Induced Impact Loading,” *Engineering Structure* 20(12): 1087-1096, 1998.

Galambos T. V., Surovek, A. E. “*Structural Stability of Steel: Concepts and Applications for Structural Engineers*,” John Wiley and Sons, NJ, 2008.

Gordon, P., *et al*. “An Integrated Model of Urban Transportation and Production Systems: Toward a General Model of How Losses due to Earthquakes Affect the Spatial Metropolitan Economy,” *Proceedings of the NEHRP Conference and Workshop on Research on the Northridge, California Earthquake of January 17, 1994: Volume IV Social Sciences and Emergency Management*, 102-111, California Universities for Research in Earthquake Engineering, Richmond, California, 1998.

Hitaka, T., Matsui, C. “Experimental Study on Steel Shear Wall with Slits,” *Journal of Structural Engineering* 129(5): 586-595, 2003.

ISDR. “*Disaster Reduction and Sustainable Development*,” International Strategy for Disaster Reduction, United Nations, Geneva, www. unisdr.org, January, 2003.

JIS. “G3136-05: Rolled Steels for Building Structure,” *Japanese Industrial Standards*, 2005.

JSA. “JIS Z2201: Test Pieces for Tensile Test for Metallic Materials,” *Japanese Standard Association*, 1980.

JSA. "JIS G3131: Hot-Rolled Mild Steel Plates, Sheets and Strip," *Japanese Standard Association*, 2005.

Kobe City. "*The Great Hanshin-Awaji Earthquake Statistics and Restoration Progress*," published by City of Kobe, January 1, 2008.

Kouyoumdjian, H. "Renovating Concrete," *Modern Steel Construction*, American Institute of Steel Construction, March, 1999.

Lubell, A., S., H. Prion, G. L. *et al*. "Unstiffened Steel Plate Shear Wall Performance under Cyclic Loading," *Journal of Structural Engineering* 126(4): 453-460, 2000.

Martinez-Rueda, J. E. "On the Evolution of Energy Dissipation Devices for Seismic Design," *Earthquake Spectra* 18(2): 309-346, 2002.

Mazzoni, S., McKenna, F., Scott, M. H., and Fenves, G. L. "*Opensystem for Earthquake Engineering Simulation: User command language manual*," Pacific Earthquake Engineering Research Center, University of California, Berkeley, 2006.

McCormick, J., DesRoches, R., *et al*. "Seismic Assessment of Concentrically Braced Steel Frames with Shape Memory Alloy Braces," *Journal of Structural Engineering* 133(6): 862-870, 2007.

McCormick, J., Tyber, J., *et al*. "Structural Engineering with NiTi. II: Mechanical Behavior and Scaling," *Journal of Engineering Mechanics* 133(9): 1019-1029, 2007.

Mistakidis, E. S., De Matteis, G., *et al*. "Low Yield Metal Shear Panels as an Alternative for the Seismic Upgrading of Concrete Structures," *Advances in Engineering Software* 38(8-9): 626-636 2007.

Mossalam, A. S. "Making the Connection," *Civil Engineering*, April: pp. 57, 1999.

MTS. "*Model 407 Controller Product Manual: Firmware Version 5.3*," MTS Systems Corporation, Eden Prairie, MI, 2000.

Mualla, I. H., Belev B. "Performance of Steel Frames with a New Friction Damper Device under Earthquake Excitation," *Engineering Structures* 24(3): 365-371, 2002.

Munich Re. "Great Natural Catastrophes 1950-2008: Overall and Insured Losses with trend," Munich Re, Geo Risk Research, NatCatSERVICE, http://www.munichre.com/en/homepage/default.aspx, 2008.

Munich Re. "*Topics 2000, Natural Catastrophes- the Current Position*," Munich Re, Munich, 2000.

Nakashima, M., Inoue, K., Tada, M. "Classification of Damage to Steel Buildings Observed in the 1995 Hyogoken-Nanbu earthquakes," *Engineering Structure* 20(4-6):271-281, 1998.

National Instruments. "*LabVIEW: User Manual*," National Instruments, Austin, TX, 2003.

Neaman, A. N. "*Structural Renovation of Buildings: Methods, Details, and Design Examples*," McGraw-Hill, 2001.

NEHRP. "*NEHRP Recommended Provisions for Seismic Regulations for New Buildings and Other Structures (FEMA 450) Part 1: Provisions*," National Earthquake Hazards Reduction Program, Building Seismic Safety Council, National Institute of Building Sciences, Washington, D.C., 2004.

New York Times article, "*China Reports Student Toll for Quake*," by Andrew Jacobs and Edward Wong, 7th May 2009

Newman, A. "*Structural Renovation of Buildings: Methods, Details, and Design Examples*," McGraw-Hill, 2001.

Pall, A. S. "Friction Devices for Aseismic Design of Buildings," *4th Canadian Conference on Earthquake Engineering*: 475-484, 1983.

Pall, A. S., Marsh, C. "Seismic response of friction damped braced frames," *Journal of Structural Division* 108(6): 1313–1323, 1982.

Phocas, M. C., Pochansci, A. P. “Steel Frames with Bracing Mechanism and Hysteretic Dampers,” *Earthquake Engineering & Structural Dynamics* 32(5): 811-825, 2003.

Purba, R. and Bruneau M. “Design Recommendations for Perforated Steel Plate Shear Walls,” *Technical Report* MCEER-07-0011, Multidisciplinary Center for Earthquake Engineering Research, Buffalo, New York, USA, 2007.

Qu, B., Bruneau, M., Lin, C. H., Tsai, K. C. “Testing of Full-Scale Two-Story Steel Plate Shear Wall with Reduced Beam Section Connections and Composite Floors,” *Journal of Structural Engineering* 134(3): 364-373, 2008.

Rezai, M. “Seismic Behavior of Steel Plate Shear Walls by Shake Table Testing,” *PhD Dissertation*, Department of Civil Engineering, University of British Columbia, Vancouver, Canada, 1999.

Ricles, J. M., Sause, R *et al.* “Experimental Evaluation of Earthquake Resistant Posttensioned Steel Connections,” *Journal of Structural Engineering* 128(7): 850-859, 2002.

Roberts, T. M., Lacerte, M., *et al*. “Seismic Response of Multistory Buildings with Self-Centering Energy Dissipative Steel Braces,” *Journal of Structural Engineering* 134(1): 108-120, 2008.

Roberts, T. M., Sabouri-Ghomi, S. “Hysteretic Characteristics of Unstiffened Perforated Steel Plate Shear Panels,” *Thin-Walled Structures* 14:139-151, 1992.

Sabelli, R. and Bruneau, M. “Steel Plate Shear Walls,” *Steel Design Guide* 20, Chicago, Illinois, American Institute of Steel Construction, Inc, 2006.

Sabouri-Ghomi S., Roberts, T. M. “Nonlinear Dynamic Analysis of Steel Plate Shear Walls including Shear and Bending Deformations,” *Engineering Structures* 14(5): 309-317, 1992.

Sabouri-Ghomi S., Ventura, C. E., Mehdi H., K., Kharrazzim H. K. “Shear Analysis and Design of Ductile Steel Plate Walls,” *Journal of Structural Engineering* 131(6): 878-889, 2005.

SAC. “Suites of Earthquake Ground Motions for Analysis of Steel Moment Frame Structures,” http://nisee.berkeley.edu/data/strong_motion/sacsteel/motions/la10in50yr.html, 1997

Satterthwaite, D., *et al*. “Adapting to Climate Change in Urban Areas,” The Possibilities and Constraints in Low- and Middle-Income Nations, *Human Settlements Discussion Paper Series*, Theme: Climate Change and Cities No.1. London, IIED (International Institute for Environment and Development), 2007

SEOAC. “Reflections on the Loma Prieta Earthquake,” Structural Engineers Association of California, Sacrament, California, 1989.

Shinshkin, J. J., Driver, R. G., Grondin, G. Y. “Analysis of Steel Plate Shear Walls using the Modified Strip Model,” *Structural Engineering Report* No. 261, Department of Civil Engineering, University of Alberta, Edmonton, Alberta, Canada, 2005.

Somerville, P.G., Smith, N., Punyamurthula, S., Sun, J. “Development of Ground Motion Time Histories for Phase 2 of the FEMA/SAC Steel Project,” *SAC Background Document, Report* No. SAC/BD 97/04, 1997.

Thouburn, L. J., Kulak, G. L., and Montgomery, C. J. “Analysis of Steel Plate Shear Walls,” *Structural Engineering Report* No.107, Department of Civil Engineering, University of Alberta, Edmonton, Alberta, Canada, 1983.

Timler, P.A. and Kulak, G. L. “Experimental Study of Steel Plate Shear Walls,” *Structural Engineering Report* No.114, Department of Civil Engineering, Universit of Alberta, Edmonton, Alberta, Canada, 1983.

Timler, P.A. and Ventura, C. E., Prion, H., and Anjam, R. “Experimental and Analytical Studies of Steel Plate Shear Walls as Applied to the Design of Tall Buildings,” *Structural Design of Tall Buildings* 7: 233-249, 1998.

Toyoda, T. “Economic loss in earthquake affected areas”, *Yomiuri Online article,* 19th Mar, 2008 (in Japanese)

Tremblay, R., Filiatrault, A. “Seismic Impact Loading in Inelastic Tension-Only Concentrically Braced Steel Frames: Myth or Reality?,” *Earthquake Engineering and Structural Dynamics* 25: 1373- 1389, 1996.

Tremblay, R. “Inelastic seismic response of steel bracing members,” *Journal of Constructional Steel Research* 58: 665–701, 2002.

Tromposch, E. W., and Kulak, G. L. “Cyclic behavior of thin panel steel plate shear walls,” *Structural. Engineering. Report* No. 145, Department of Civil Engineering, University of Alberta, Edmonton, Alberta, Canada, 1987.

Tsai, C. L., Park, S. C., Cheng W. T.”Welding Distortion of a Thin-Plate Panel Structure,” Welding journal 78(55): 157-165, American Welding Society, 1999

Tsai, K. C., Chen, H. W., *et al*. “Design of Steel Triangular Plate Energy Absorbers for Seismic-Resistant Construction,” *Earthquake Spectra* 9(3): 505-528, 1993.

UN/ISDR. “*UN/ISDR 2008/07: Poorly constructed buildings kill people during earthquakes*,” press release, United Nations, International Strategies for Disaster Reduction, Secretariat Geneva, May, 2008

UN-Habitat. “*State of the World’s Cities 2008/2009 - Harmonious Cities*,” first published by Earthscan in the UK and USA in 2008 for and on behalf of the United Nations Human Settlements Programme (UN-HABITAT), 2008

Uriz, P., Filippou, F. C., Mahin, S. A. “Model for Cyclic Inelastic Buckling of Steel Braces,” *Journal of Structural Engineering* 134(4):619-628, 2008.

Vian, D., Bruneau, M. “Steel Plate Shear Walls for Seismic Design and Retrofit of Building Structures,” *Technical Report* MCEER-05-0010, State University of New York, Multidisciplinary Center for Earthquake Engineering Research, University at Buffalo, 2005.

Wakabayashi, M., *et al*. “*Steel Structures*.” Maruzen, Tokyo, (in Japanese), 1992.

Whittaker, A. S., Bertero, V., *et al*. “Seismic Testing of Steel Plate Energy Dissipation Devices,” *Earthquake Spectra* 7(4): 563-604, 1991.

Xia, C., Hanson, R. D. “Influence of ADAS Element Parameters on Building Seismic Response,” *Journal of Structural Engineering*, 118(7):1903–1918, 1992.

Yang, S. Y. “Analytical and Experimental Study of Concentrically Braced Frames with Zipper Struts,” *PhD. Dissertation*, Georgia Institute of Technology, Atlanta, Georgia, 2006.

Yang, S. Y., Leon, R. T., DesRoches, R. “Design and behavior of zipper-braced frames,” *Engineering Structures* 30:1092-1100, 2008.

VITA

Masahiro Kurata

KURATA was born on July 13, 1978 in Osaka, Japan. He graduated from Kyoto University, Japan with his Bachelor's of Engineering in Architecture and continued to graduate school at Kyoto University pursing a Master's in Architectural Engineering. During his graduate study in Kyoto, he completed a one-year Master program of Earthquake Engineering (the ROSE School) at Pavia University, Italy. Masahiro continued his graduate study at the Georgia Institute of Technology pursing a Doctoral Degree in Civil Engineering with a minor in Mathematics.